



(2)

**SYNTHESIS AND STRUCTURAL CHARACTERIZATION OF
NEW LIGHT MOLECULAR WEIGHT INORGANIC OXIDIZERS
AND RELATED DERIVATIVES. VOLUME: II**

Professor G. J. Schrobilgen

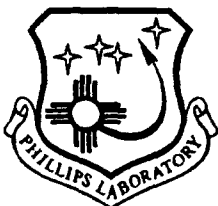
**McMaster University
Department of Chemistry
Hamilton, Ontario L8S 4M1
Canada**

February 1993

Final Report



APPROVED FOR PUBLIC RELEASE; DISTRIBUTION UNLIMITED.



**PHILLIPS LABORATORY
Propulsion Directorate
AIR FORCE MATERIEL COMMAND
EDWARDS AIR FORCE BASE CA 93524-7001**

93-23281



210 pr

96 10 5 030

NOTICE

When U.S. Government drawings, specifications, or other data are used for any purpose other than a definitely related Government procurement operation, the fact that the Government may have formulated, furnished, or in any way supplied the said drawings, specifications, or other data, is not to be regarded by implication or otherwise, or in any way licensing the holder or any other person or corporation, or conveying any rights or permission to manufacture, use or sell any patented invention that may be related thereto.


FOREWORD

This report was prepared by Department of Chemistry, McMaster University, Hamilton - Ontario Canada, under contract F04611-91-K-0004, for Operating Location AC, Phillips Laboratory, Edwards AFB, CA. 93524-7001. Project Manager for Phillips Laboratory was Lt Robert Mantz.

This report has been reviewed and is approved for release and distribution in accordance with the distribution statement on the cover and on the SF Form 298.


ROBERT A. MANTZ, Capt, USAF
Project Manager


STEPHEN L. RODGERS
Chief, Emerging Technologies Branch


LEONARD C. BROLINE, Lt Col, USAF
Director,
Fundamental Technologies Division


RANNEY G. ADAMS
Public Affairs Director

REPORT DOCUMENTATION PAGE

Form Approved
GSA GEN. REG. NO. 27

Public reporting burden for this collection of information is estimated to average 1 hour per response, including the time for reviewing existing data sources, gathering and maintaining the data needed, and completing and reviewing the collection of information. Send comments regarding this burden estimate or any other aspect of this collection of information, including suggestions for reducing this burden, to Washington Headquarters Services, Directorate for Information Operations and Reports, 1215 Jefferson Davis Highway, Suite 1204, Arlington, VA 22202-4302, and to the Office of Management and Budget, Paperwork Project Room (0142-0046) Washington, DC 20503.

1. AGENCY USE ONLY (Leave blank)		2. REPORT DATE February 1993		3. REPORT TYPE AND DATES COVERED Final 1 May 1991 thru 30 April 1992	
4. TITLE AND SUBTITLE Synthesis and Structural Characterization of New Light Molecular Weight Inorganic Oxidizers and Relative Derivatives: Volume II				5. FUNDING NUMBERS C: F04611-91-K-0004 PE: 62302F PR: 5730 TA: 00N2 CC66	
6. AUTHOR(S) Schroibilgen, G. J. Prof					
7. PERFORMING ORGANIZATION NAME(S) AND ADDRESS(ES) McMaster University Department of Chemistry Hamilton, Ontario L8S 4M1 Canada				8. PERFORMING ORGANIZATION REPORT NUMBER	
9. SPONSORING/MONITORING AGENCY NAME(S) AND ADDRESS(ES) Phillips Laboratory OLAC-PL/RKFE Edwards AFB, California 93524-7680				10. SPONSORING/MONITORING AGENCY REPORT NUMBER PL-TR-93-3007 Vol II	
11. SUPPLEMENTARY NOTES COSATI CODES: 07/02					
12a. DISTRIBUTION/AVAILABILITY STATEMENT Approved for Public Release; Distribution is Unlimited				12b. DISTRIBUTION CODE	
13. ABSTRACT (Maximum 200 words) The following annual report encompasses eleven areas of research. The basic philosophy underpinning this work has been to develop the technology for the synthesis, storage, and handling of new high-energy density materials. The importance of performing the "easier" heavy element chemistry as the ground work to synthesizing. The more challenging and potentially more useful lighter analogs has been stressed throughout much of this work. Where possible published or about to be published work is included in this report under each of the appropriate subheadings.					
14. SUBJECT TERMS Crystallography; NMR spectroscopy, synthesis, Raman spectroscopy; High-Valent Oxidants, Xe-N bonded species.				15. NUMBER OF PAGES	
				16. PRICE CODE	
17. SECURITY CLASSIFICATION OF REPORT Unclassified	18. SECURITY CLASSIFICATION OF THIS PAGE Unclassified	19. SECURITY CLASSIFICATION OF ABSTRACT Unclassified	20. LIMITATION OF ABSTRACT SAR		

NSN 7540-01-280-5500

Table of Contents

Part VI

The IOF_6^- Anion: The first example of a Pentagonal Bipyramidal AX_5YX Species	1
Abstract	1
Introduction	3
Experimental Section	4
Results and Discussion	10
Conclusions	24
Acknowledgements	24
Supplementary Material	25
References	26

Part VII

The $\text{F}_6\text{TeC}=\text{N}^-$ Anion and $\text{F}_5\text{TeC}=\text{N}$	I
Abstract	I
Acknowledgement	II
Introduction	1
Goals of the Present Work	11
Experimental Section	13
Results and Discussion	29
Conclusions and Future Work	62
References	64

Part VIII

The PF_4^- Anion and Its Hydrolytic Behavior	1
References	13
References	33

Part IX

Least Coordinating Anions

Introduction	1
Experimental	8
References	82

Part X

^{18}F Exchange Studies of F_2 Activation By Lewis Acids and Hydrogen Fluoride

1

Part XI

Generation of a Microwave-excited Discharge in a Liquid-Nitrogen Cooled Dielectric Tube

1

Background	1
Microwave Generation	2
Excitation Cavity Design and Operation	5

Accession For	
NTIS	CRA&I <input checked="" type="checkbox"/>
DTIC	TAB <input type="checkbox"/>
Unannounced	<input type="checkbox"/>
Justification	
By	
Distribution of	
Availability Codes	
Dist	Avail. and/or Special
A-1	

List of Figures

Part VI

Figure Captions	45
Figure 1:	46
Figure 2:	47
Figure 3:	48
Figure 4:	49
Figure 5	50
Figure 6:	51

Part VII

Figure 1: Geometrics of TeF_7^- , TeF_8^{2-} and $\text{TeF}_6\text{O}^{2-}$	4
Figure 2: Pyrex glass vacuum line; (A) mercury manometer (B) dry N_2 inlet; Liquid N_2 trap.	14
Figure 3: Metal vacuum line components: (A) outlet to liquid nitrogen and charcoal traps followed by a two stage rotary vacuum pump-hard vacuum; (B) outlet to soda lime and liquid nitrogen traps followed by a two stage rotary vacuum pump-rough vacuum; (C) dry nitrogen inlet; (D) fluorine inlet; (E) pressure gauge 0-30 ils/in ² ; (F) pressure transducers 0-1000 Torr; (G) pressure transducer 0-1 Torr; (H) 3/8 in, 316 stainless steel pressure valve (Autoclave Engineers); (I) 316 stainless steel tee; (J) 316 stainless steel cross; (K) 316 stainless steel L-piece; (L) nickel connectors	15
Figure 4: Apparatus for the preparation of HOTeF_5	18
Figure 5: Sublimers for HOTeF_5 purification	20
Figure 6: Purification apparatus used in HOTeF_5 preparation	21
Figure 7: Apparatus used in the preparation of ^{19}F NMR samples of $(\text{C}_2\text{H}_5)_4\text{N}^+\text{Te}(\text{OTeF}_5)_5$	23
Figure 8: Apparatus used in the purification of TeF_5OCF_3	26
Figure 9: Apparatus used in preparation of $(\text{CH}_4)_4\text{N}^+\text{TeF}_6\text{CN}$ and TeF_5CN	28
Figure 10: The ^{19}F NMR spectrum (470.599 MHZ) at -50°C of $\text{Te}(\text{OTeF}_5)_5$ in SO_2ClF . Non-primed letters denote B_4 parts; primed letters denotes A parts. (A) $\text{OTeF}_5(\text{eq})$ in $\text{Te}(\text{OTeF}_5)_5$; (B) $\text{OTeF}_5(\text{eq})$ in $\text{Te}(\text{OTeF}_5)_4$; (C) $\text{OTeF}_5(\text{ax})$ in $\text{Te}(\text{OTeF}_5)_5$. Lower case letters denote ^{125}Te satellites	30

Figure 11: The ^{19}F NMR spectrum (470.599 MHZ) at -50°C of the reaction mixture $(\text{C}_2\text{H}_5)_4\text{N}^+\text{Te}(\text{OTeF}_5)_5 + \text{Xe}(\text{OTeF}_5)_2$ in SO_2ClF after warming to -50°C . The non-primed letters B, C, and D denote B_4 parts; the primed letters B', C', and D' denotes A parts. (A) F-on-Te(IV) in $\text{FTe}(\text{OTeF}_5)_4$, (B) $\text{OTeF}_5(\text{ax})$ in $\text{Te}(\text{OTeF}_5)_5$, (C) $\text{OTeF}_5(\text{eq})$ in $\text{Te}(\text{OTeF}_5)_5$; (D) $\text{Xe}(\text{OTeF}_5)_2$. Lower case letters denote ^{125}Te satellites. 33

Figure 12: The ^{19}F NMR spectrum (470.599 MHZ) at -50°C of the reaction mixture $(\text{C}_2\text{H}_5)_4\text{N}^+\text{Te}(\text{OTeF}_5)_5 + \text{Xe}(\text{OTeF}_5)_2$ in SO_2ClF after warming to -50°C . The non-primed letters B, and C denote B_4 parts; the primed letters B', and C' denotes A parts. (A) F-on-Te(IV) in $\text{FTe}(\text{OTeF}_5)_4$, (B) $\text{OTeF}_5(\text{eq})$ in $\text{FTe}(\text{OTeF}_5)_4$, (C) $\text{Xe}(\text{OTeF}_5)_2$. Lower case letters denote ^{125}Te satellites. 35

Figure 13: The ^{19}F NMR spectrum (470.599 MHZ) at -50°C of the reaction mixture $(\text{C}_2\text{H}_5)_4\text{N}^+\text{Te}(\text{OTeF}_5)_5 + \text{Xe}(\text{OTeF}_5)_2$ in SO_2ClF after warming to 25°C . 38

Figure 14: The F-on-Xe(II) region of the ^{19}F NMR spectrum (470.599 MHZ) at -50°C of the reaction mixture $(\text{C}_2\text{H}_5)_4\text{N}^+\text{Te}(\text{OTeF}_5)_5 + \text{Xe}(\text{OTeF}_5)_2$ in SO_2ClF after warming to 25°C . Asterisks (*) denote ^{129}Xe satellites. 39

Figure 15: The ^{19}F NMR spectrum (470.599 MHZ) at -50°C of the reaction mixture $(\text{C}_2\text{H}_5)_4\text{N}^+\text{Te}(\text{OTeF}_5)_5 + \text{Xe}(\text{OTeF}_5)_2$ in SO_2ClF after warming to -50°C . The non-primed letters A, and B denote B_4 parts; the primed letters A', and B' denotes A parts. (A) $\text{Xe}(\text{OTeF}_5)_2$, (B) $\text{F}_5\text{TeOTeF}_5$; (C) TeF_6 (D) exchanging OTeF_5 . Lower case letters denote ^{125}Te satellites. 40

Figure 16: The ^{19}F NMR spectrum (470.599 MHZ) at -45°C of the products not volatile at -78°C from the reaction mixture $\text{CF}_3\text{OF} + \text{TeF}_4$. 44

Figure 17: The ^{19}F NMR spectrum (470.599 MHZ) at -45°C of the reaction mixture $(\text{CH}_3)_4\text{N}^+\text{TeF}_7^- + (\text{CH}_3)_3\text{SiCN}$ in CH_3CN after warming to -45°C . Asterisks (*) denote ^{125}Te satellites; crosses (†) denotes ^{123}Te satellites. 47

Figure 18: The F-on-Si(IV) region of the ^{19}F NMR spectrum (470.599 MHZ) at -45°C of the reaction mixture $(\text{CH}_3)_4\text{N}^+\text{TeF}_7^- + (\text{CH}_3)_3\text{SiCN}$ in CH_3CN after warming to -45°C . 48

Figure 19: The ^{125}Te NMR spectrum (157.792 MHZ) at -45°C of the reaction mixture $(\text{CH}_3)_4\text{N}^+\text{TeF}_7^- + (\text{CH}_3)_3\text{SiCN}$ in CH_3CN after warming to -45°C . (A) low gain; (B) high gain. Asterisks (*) denote TeF_6CN ; crosses (†) denotes TeF_7 49

Figure 20: The ^{13}C NMR spectrum (125.759 MHZ) at -45°C of the reaction mixture $(\text{CH}_3)_4\text{N}^+\text{TeF}_7^- + (\text{CH}_3)_3\text{SiCN}$ in CH_3CN after warming to -45°C . (A) low gain; (B) high gain. 50

Figure 21: The ^{19}F NMR spectrum (470.599 MHz) at -45°C of the reaction mixture $(\text{CH}_3)_4\text{N}^+\text{TeF}_7^- + (\text{CH}_3)_3\text{SiCN}$ in CH_3CN after warming to -20°C . Asterisks (*) denote ^{125}Te satellites; crosses (†) denotes ^{123}Te satellites.	51
Figure 22: The ^{19}F NMR spectrum (470.599 MHz) at -45°C of the reaction mixture $(\text{CH}_3)_4\text{N}^+\text{TeF}_7^- + (\text{CH}_3)_3\text{SiCN}$ in CH_3CN after warming to -25°C . Asterisks (*) denote ^{125}Te satellites; crosses (†) denotes ^{123}Te satellites	52
Figure 23: Expected geometry of the TeF_6CN^- anion.	54
Figure 24: The ^{19}F NMR spectrum (470.599 MHz) at -45°C of the reaction mixture $\text{TeF}_6 (\text{CH}_3)_3\text{SiCN}$ in CH_3CN after warming to -45°C . Asterisks (*) denote ^{125}Te satellites; crosses (†) denotes ^{123}Te satellites	56
Figure 25: The ^{19}F NMR spectrum (470.599 MHz) at -45°C of the reaction mixture $\text{TeF}_6 (\text{CH}_3)_3\text{SiCN}$ in CH_3CN after warming to -22°C . Asterisks (*) denote ^{125}Te satellites; crosses (†) denotes ^{123}Te satellites	57
Figure 26: The ^{19}F NMR spectrum (470.599 MHz) at -45°C of the reaction mixture $\text{TeF}_6 (\text{CH}_3)_3\text{SiCN}$ in CH_3CN after warming to 0°C . Asterisks (*) denote ^{125}Te satellites; crosses (†) denotes ^{123}Te satellites	58
Figure 27: The ^{19}F NMR spectrum (470.599 MHz) at -45°C of the reaction mixture $\text{TeF}_6 (\text{CH}_3)_3\text{SiCN}$ in CH_3CN after warming to 25°C . Asterisks (*) denote ^{125}Te satellites; crosses (†) denotes ^{123}Te satellites	59
Figure 28: Expected geometry of the TeF_5CN	60

Part VIII

Figure 1: The ^{31}P NMR spectrum (202.459 MHz) at -46°C of $\text{N}(\text{CH}_3)_4^+\text{PF}_4$ in CH_3CN containing a 2.5 molar excess of $\text{N}(\text{CH}_3)_4^+\text{F}$.	2
Figure 2a: Variable temperature ^{31}P NMR spectra (202.459 MHz) at -46°C of $\text{N}(\text{CH}_3)_4^+\text{PF}_4$ in CH_3CN containing a 1.5 molar excess of $\text{N}(\text{CH}_3)_4^+\text{F}$ (A) observed spectra; (B) calculated spectra.	4
Figure 2b: Variable temperature ^{31}P NMR spectra (202.459 MHz) at -46°C of $\text{N}(\text{CH}_3)_4^+\text{PF}_4$ in CH_3CN containing a 1.5 molar excess of $\text{N}(\text{CH}_3)_4^+\text{F}$ (A) observed spectra; (B) calculated spectra.	5

Figure 3: Eyring plot of the exchange rate data extracted from the variable temperature ^{31}P NMR spectra (202.459 MHz) at -46°C of $\text{N}(\text{CH}_3)_4^+\text{PF}_4$ in CH_3CN containing a 1.5 molar excess of $\text{N}(\text{CH}_3)_4^+\text{F}$.	8
Figure 4: The ^{19}F NMR spectrum (470.599 MHz) -46°C of $\text{N}(\text{CH}_3)_4^+\text{PF}_4$ in CH_3CN containing a 1.5 molar excess of $\text{N}(\text{CH}_3)_4^+\text{F}$	10
Figure 5: The ^{31}P NMR spectra (202.459 MHz) of the products from the hydrolysis of $\text{N}(\text{CH}_3)_4^+\text{PF}_4$ with $\text{H}_2^{16,17,18}\text{O}$ in CH_3CN at -45°C	16
Figure 6: The ^{17}O NMR spectrum (67.801 MHz) of the products from the hydrolysis of $\text{N}(\text{CH}_3)_4^+\text{PF}_4$ with $\text{H}_2^{16,17,18}\text{O}$ in CH_3CN at -36°C	17
Figure 7: The ^{31}P NMR spectra (202.459 MHz) of the products from the hydrolysis of $\text{N}(\text{CH}_3)_4^+\text{PF}_4$ with $\text{H}_2^{16,17,18}\text{O}$ in CH_3CN at 30°C	18
Figure 8: The ^{31}P NMR spectra (202.459 MHz) of the products from the hydrolysis of $\text{N}(\text{CH}_3)_4^+\text{PF}_4$ with $\text{H}_2^{16,17,18}\text{O}$ in CH_3CN at 30°C Expansion of the HPO_2F resonance.	19
Figure 9: The ^{17}O NMR spectrum (67.801 MHz) of the products from the hydrolysis of $\text{N}(\text{CH}_3)_4^+\text{PF}_4$ with $\text{H}_2^{16,17,18}\text{O}$ in CH_3CN at 30°C	20
Figure 10: The ^{17}O NMR spectrum (67.801 MHz) of the products from the hydrolysis of $\text{N}(\text{CH}_3)_4^+\text{PF}_4$ with $\text{H}_2^{16,17,18}\text{O}$ in CH_3CN at 30°C . Expansion of the HPO_2F resonance.	21
Figure 11: The ^{31}P NMR spectra (202.459 MHz) of the products from the hydrolysis of $\text{N}(\text{CH}_3)_4^+\text{PF}_4$ with $\text{H}_2^{16,17,18}\text{O}$ in the presence of a 2.5 molar excess of $\text{N}(\text{CH}_3)_4^+\text{F}$ at -45°C .	23
Figure 12: The ^{31}P NMR spectra (202.459 MHz) of the products from the hydrolysis of $\text{N}(\text{CH}_3)_4^+\text{PF}_4$ with $\text{H}_2^{16,17,18}\text{O}$ in the presence of a 2.5 molar excess of $\text{N}(\text{CH}_3)_4^+\text{F}$ at 30°C .	24
Figure 13: The ^{17}O NMR spectrum (67.801 MHz) of the products from the hydrolysis of $\text{N}(\text{CH}_3)_4^+\text{PF}_4$ with $\text{H}_2^{16,17,18}\text{O}$ in the presence of a 2.5 molar excess of $\text{N}(\text{CH}_3)_4^+\text{F}$ in CH_3CN at 30°C .	25
Figure 14: (a) The structural units for $\text{N}(\text{CH}_3)_4^+\text{PF}_4$ and (b) The unit cell of $\text{N}(\text{CH}_3)_4^+\text{PF}_4$	30
Figure 15: View of the PF_4 anion showing the two-fold disorder in the equatorial plane.	31

Part IX

Figure 1: ORTEP view of $\text{N}(\text{CH}_3)_4^+ \text{Bi}(\text{OTeF}_5)_6^-$; thermal ellipsoids are shown at the 50% probability level. 3

Figure 2: ORTEP view of $\text{N}(\text{CH}_3)_4^+ \text{As}(\text{OTeF}_5)_6^-$; thermal ellipsoids are shown at the 30% probability level. 4

Figure 3: Representation of the Sb and N atoms environments in $\text{N}(\text{CH}_3\text{CH}_2)_4^+ \text{Sb}(\text{OTeF}_5)_6^-$; the size of the atoms is arbitrary. 5

Part XI

Figure 1: Half-wave voltage-doubler power-supply circuit used to drive the magnetron. Note that operation of the filament heater is tied to the main circuit. 4

Figure 2: Cross-section of microwave apparatus. The heavy lines indicate the outer conductor and discharge cavity. 6

Figure 3: Equivalent electrical circuit of the microwave apparatus. The quarter-wave shorted stubs are omitted from this schematic because they have no electrical effect. 8

List of Tables

Part IV

Table 1: Summary of Crystal Data and Refinement Results for $\text{N}(\text{CH}_3)_4^+ \text{IOF}_6^-$ at -93°C and -155°C .	31
Table 2: Final Atomic Coordinates ($\times 10^4$), Equivalent Isotropic Displacement Coefficients ($\text{\AA}^2 \times 10^3$) ^a and Site Occupancy Factors For $\text{N}(\text{CH}_3)_4^+ \text{IOF}_6^-$ at -93°C and -155°C .	32
Table 3: Anisotropic Displacement Coefficients ($\text{\AA}^2 \times 10^3$) ^a for $\text{N}(\text{CH}_3)_4^+ \text{IOF}_6^-$ at -93°C and -155°C .	33
Table 4: Bond Lengths, Bond Angles, Average Equatorial Plane Angle and Deviations from the Average O-I-F _{eq} Bond Angle for $\text{N}(\text{CH}_3)_4^+ \text{IOF}_6^-$ at -93°C and -155°C .	34
Table 5: Vibrational Spectra of $\text{N}(\text{CH}_3)_4^+ \text{IOF}_6^-$ and Their Assignments.	35
Table 6: Comparison of Observed and Calculated Frequencies of IOF_6^- , IF_7 and XeF_5^- , Together with Their Approximate Mode Descriptions.	36
Table 7: Observed and Calculated Geometries of IOF_6^- and the closely IF_7 and XeF_5^-	37
Table 8: Symmetry Coordinates and Approximate Mode Descriptions for the Pentagonal Bipyramidal IOF_6^- Anion.	38
Table 9: Symmetry Force Constants ^a of IOF_6^- Calculated from the Scaled ECP Frequencies of Table 6.	40
Table 10: Revised Assignments, ECP Force Field ^a and Potential Energy Distribution ^b for XeF_5^-	41
Table 11: Potential Energy Distribution for IOF_6^-	42
Table 12: Internal Force Constants ^{a,b} (mdyn/ \AA) of IF_7 , IOF_6^- and XeF_5^-	43
Table 13: Atomic Populations (e) in the Valence Electron Orbitals and Total Charge Distributions for XeF_5^- , IF_7 , and IOF_6^-	44

Part VII

Table 1: NMR Properties of Nuclides Relevant to this Work ⁵⁷ .	12
Table 2: Typical Acquisition Parameters for ¹³ C, ¹⁹ F, and ¹²⁵ Te NMR Spectroscopy.	16
Table 3: ¹⁹ F NMR Data for Te(OTeF ₅) ₅ ⁻ in SO ₂ ClF and CH ₂ Cl ₂ Solvents.	31
Table 4: ¹⁹ F NMR Data for Products Observed in the Reaction Between (C ₂ H ₅) ₄ N ⁺ Te(OTeF ₅) ₅ ⁻ and Xe(OTeF ₅) ₂ in SO ₂ ClF Solvent at -50°C.	34
Table 5: ¹⁹ F NMR Data for Products Observed in the Reaction Between (C ₂ H ₅) ₄ N ⁺ Te(OTeF ₅) ₅ ⁻ and Xe(OTeF ₅) ₂ and XeF ₂ in SO ₂ ClF Solvent at -50°C.	36
Table 6: ¹⁹ F NMR Data for Products Observed in the Reaction Between (C ₄ H ₉) ₄ N ⁺ TeF ₅ and Xe(OTeF ₅) ₂ in SO ₂ ClF Solvent at -50°C.	42
Table 7: ¹³ C, ¹⁹ F, and ¹²⁵ Te NMR Data for Products Observed in the Reaction Between (CH ₃) ₄ N ⁺ TeF ₇ and (CH ₃) ₃ SiCN in CH ₃ CN Solvent at -45°C.	46
Table 8: ¹⁹ F NMR Data for Products Observed in the Reaction Between TeF ₆ and (CH ₃) ₃ SiCN in CH ₃ CN Solvent at -45°C.	61

Part VIII

Table 1: Exchange Rate Data Extracted from Variable-Temperature ³¹ P NMR Spectra of N(CH ₃) ₄ ⁺ PF ₄ ⁻ Dissolved in CH ₃ CN Containing a 1.5 Excess of N(CH ₃) ₄ ⁺ F.	7
Table 2: Enthalpies and Entropies of Activation for Intramolecular Exchange in PF ₄ ⁻ and SF ₄ ^a .	9
Table 3: Interatomic distances (Å) and Angles (deg) for N(CH ₃) ₄ ⁺ PF ₄ ⁻ , N(CH ₃) ₄ ⁺ PF ₆ ⁻ , NaPF ₆ H ₂ O and SF ₄	29

Part IX

Table 1: Bond Lengths and Bond Angles in $\text{N}(\text{CH}_3)_4^+ \text{Bi}(\text{OTeF}_5)_6^-$ (1), $\text{N}(\text{CH}_3)_4^+ \text{As}(\text{OTeF}_5)_6^-$ (2) and $\text{N}(\text{CH}_3 \text{ CH}_2)_4^+ \text{Sb}(\text{OTeF}_5)_6^-$ (3). 16

Table 2: Summary of Crystal Data and Refinement Results for $\text{N}(\text{CH}_3)_4^+ \text{Bi}(\text{OTeF}_5)_6^-$ (1), $\text{N}(\text{CH}_3)_4^+ \text{As}(\text{OTeF}_5)_6^-$ (2) and $\text{N}(\text{CH}_3 \text{ CH}_2)_4^+ \text{Sb}(\text{OTeF}_5)_6^-$ (3) 22

PART VI

THE IOF_6^- ANION: THE FIRST EXAMPLE OF A
PENTAGONAL BIPYRAMIDAL AX_5YX SPECIES

*The IOF₆⁻ Anion:
The First Example of a Pentagonal Bipyramidal AX₅YZ Species[†]*

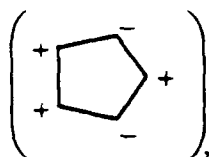
K.O. Christe,^{,1} D.A. Dixon,² A.R. Mahjoub,³ H.P.A. Mercier,⁴ J.C.P. Sanders,⁴
K. Seppelt,^{*,3} G.J. Schrobilgen,^{*,4} and W.W. Wilson¹*

Contribution from Rocketdyne, A Division of Rockwell International, Canoga Park, California 91309, the Department of Chemistry, McMaster University, Hamilton, Ontario L8S 4M1, Canada, the Central Research and Development Department, E.I. du Pont de Nemours and Company, Inc., Experimental Station, Wilmington, Delaware 19880-0328, and the Institut für Anorganische und Analytische Chemie der Freien Universität, Berlin, Germany.

ABSTRACT

The IOF₆⁻ anion, which is the first example of a pentagonal bipyramidal AX₅YZ type species, was prepared in the form of its stable N(CH₃)₄⁺ salt. Its X-ray crystal structure was determined at -93 ° and -155 °C (tetragonal, space group P4/nmm, Z = 2). In addition to two perfectly ordered N(CH₃)₄⁺ cations, the structure contains two IOF₆⁻ anions of approximate C_{5v} symmetry which are subject to a positional four-fold disorder for the equatorial plane. The O-I-F_{ax} angle is constrained by symmetry to be 180°, whereas there are no constraints on the positions of the equatorial fluorines. The I-O bond length indicates substantial double bond character, and the axial I-F bond length is significantly shorter than the five equatorial I-F bond lengths. The mean O-I-F_{eq} bond angle is slightly larger than 90°, due to the doubly bonded oxygen atom being more repulsive than the singly bonded axial fluorine ligand. The equatorial IF₅ plane is puckered to alleviate its congestion. In contrast to the highly fluxional, free IF₇ molecule, in which the equatorial fluorines undergo a very rapid, dynamic, pseudorotational ring puckering and a slower intramolecular equatorial-axial ligand exchange, the puckering of the IOF₆⁻ anion in its N(CH₃)₄⁺ salt is frozen out due to anion-cation interactions, and the equatorial-axial ligand exchange is precluded by the more repulsive oxygen ligand which occupies exclusively axial positions. Therefore, the IOF₆⁻ anion is ideally suited for studying the nature of the equatorial puckering in species of five-fold symmetry. The puckering in IOF₆⁻ is of the C_s symmetry-type

[†] Dedicated to Professor Jean'ne Shreeve on the occasion of her sixtieth birthday.



, and the deviations from the ideal equatorial plane are relatively small and decrease with decreasing temperature. Furthermore, the axial I-O bond length decreases and the mean O-I-F_{eq} bond angle increases with decreasing temperature. These findings demonstrate that, in agreement with our results from *ab initio* calculations and contrary to the VSEPR concept of repelling points on a sphere, the minimum energy structures of these main group heptacoordinated fluorides or oxyfluorides are those of pentagonal bipyramids with an unpuckered equatorial plane and not those of either monocapped octahedra or monocapped trigonal prisms. Whereas in solid N(CH₃)₄⁺IOF₆⁻ the equatorial ring puckering of IOF₆⁻ is frozen out, in the dissolved free ion this puckering becomes dynamic, as demonstrated by ¹⁹F NMR spectroscopy which shows five equivalent equatorial fluorine ligands. Contrary to IF₇ and TeF₇⁻, the IOF₆⁻ anion does not undergo an intramolecular equatorial-axial ligand exchange on the NMR time scale because of the more repulsive, doubly bonded oxygen. The vibrational spectra of N(CH₃)₄⁺IOF₆⁻ in both the solid state and CH₃CN solution were recorded and assigned with the help of *ab initio* calculations on IOF₆⁻ using effective core potentials and local density functional theory. Normal coordinate analyses were carried out for the pentagonal bipyramidal series IF₇, IOF₆⁻, XeF₅⁻ which show that the equatorial, in-plane deformation force constants (*f*_α) are a good measure for the degree of congestion in the equatorial plane. Puckering increases with decreasing bond lengths, increasing ligand and decreasing central atom sizes, and increasing temperature. The pentagonal bipyramidal structures of these molecules and the coplanarity of their equatorial ligands, which are found for their minimum energy structures, are explained by a bonding scheme involving delocalized p_{xy} hybrid orbitals of the central atom for the formation of a coplanar, semi-ionic, 6-center 10-electron bond system for the five equatorial bonds and of an sp_z hybrid orbital for the formation of two, more covalent, colinear, axial bonds. This bonding scheme can account for all the observed structural features and also the bond length differences.

INTRODUCTION

In main group element chemistry, coordination numbers in excess of six are relatively rare, but are of considerable interest due to special features caused by steric crowding of the ligands, free valence electron pairs being sterically either active or inactive, and the propensity of the molecules to exhibit fluxionality. Of particular interest are heptacoordinated species which could exist either as a monocapped octahedron, a monocapped trigonal prism, or a pentagonal bipyramid.⁵ According to the VSEPR model of "repelling points on a sphere",⁵ the preferred structures should be the monocapped octahedron or trigonal prism. However, for main group elements and relatively low repulsive forces, the pentagonal bipyramid is favored⁶ and has been found for species such as IF_7 ^{7,8} or TeF_7^- .⁹⁻¹¹ In pentagonal bipyramidal structures, the pentagonal equatorial plane is highly congested which results in increased repulsion among the equatorial ligands and, as a result, in increased bond lengths and usually some kind of puckering.⁵⁻⁸ In the case of five-fold symmetry, this puckering presents a special problem. The odd number of ligands does not allow for a highly symmetric arrangement in which all five equatorial ligands can be placed into equivalent positions, i.e. with identical displacements alternately above and below the equatorial plane. One way to achieve equivalency of the equatorial ligands is a fast, dynamic, pseudorotational ring puckering, as found for IF_7 ,^{7,8} which results in a highly fluxional molecule. In addition, the pentagonal bipyramidal XF_7 molecules generally exhibit a second kind of fluxionality, i.e. a slower, intramolecular, axial-equatorial ligand exchange.⁸ The combination of these two types of fluxionality makes it experimentally very difficult to characterize and describe the structures of these molecules. Many of the difficulties with the fluxionality of the XF_7 species might be overcome by studying ionic XOF_6^{n-} salts. The presence of one doubly bonded oxygen which is more repulsive than the fluorine ligands should preempt a facile axial-equatorial ligand exchange, and the dynamic puckering of the equatorial plane could be frozen out by anion-cation interactions. Therefore, an effort was undertaken to prepare and characterize a salt containing an XOF_6^- anion. Examples of pentagonal bipyramidal

XOF₆ species had previously been unknown and only recently been reported^{10,11} in two separate preliminary notes from our laboratories. In this paper, a full account and analysis of our work on the IOF₆⁻ anion is given.

EXPERIMENTAL SECTION

Caution: IOF₅ is a strong oxidizer, and its combination with organic materials, such as CH₃CN or N(CH₃)₄⁺ salts, could be potentially hazardous. Although no difficulties were encountered in the present study, appropriate safety precautions and shielding should be used, particularly when working on a larger scale with these materials.

Materials. The CH₃CN (Baker, Bio-analyzed, having a water content of 40 ppm) was treated with P₂O₅ and freshly distilled prior to use, thereby reducing its water content to <4 ppm. Literature methods were used for the syntheses of IOF₅¹²⁻¹⁴ and anhydrous N(CH₃)₄⁺F⁻.¹⁵

Synthesis of N(CH₃)₄⁺IOF₆⁻. The salt N(CH₃)₄⁺IOF₆⁻ was prepared by condensing gaseous IOF₅ (6.40 mmol) from the calibrated volume of a nickel and stainless steel vacuum line at room temperature onto anhydrous N(CH₃)₄⁺F⁻ (0.4473 g., 5.779 mmol) in 8 mL of dry CH₃CN at -196°C. The mixture was warmed to and allowed to react, with frequent agitation, at -35°C for 30 minutes. The solvent and unreacted IOF₅ were pumped off at -35°C leaving behind N(CH₃)₄⁺IOF₆⁻ as a very pale yellow crystalline solid in essentially quantitative yield (1.8298 g., 5.772 mmol). Anal. Calc. for C₄H₁₂F₆IO: C, 14.50; H, 3.63; F, 33.00; I, 38.35; N, 4.23. Found: C, 14.62; H, 3.66; F, 32.4; I, 38.51; N, 4.33.

Vibrational Spectroscopy. Raman spectra were recorded on either a Cary Model 83 or a Spex Model 1403 spectrophotometer using the 488-nm exciting line of an Ar ion or the 647.1-nm line of a Kr ion laser, respectively. Baked-out Pyrex melting point capillaries or thin-walled Kel-F tubes were used as sample containers. A previously described¹⁶ device was used for recording the low-temperature spectra.

Infrared spectra were recorded by using either AgCl or AgBr disks on a Perkin-Elmer Model 283 spectrophotometer. The finely powdered samples were sandwiched between two thin disks and pressed together in a Wilks minipress inside the dry box.

Nuclear Magnetic Resonance Spectroscopy. The ^{19}F NMR spectra were recorded at McMaster University unlocked (field drift $< 0.1 \text{ Hz h}^{-1}$) on a Bruker AM-500 spectrometer equipped with an 11.744 T cryomagnet and an Aspect 3000 computer. The spectra were obtained using a 5-mm combination $^1\text{H}/^{19}\text{F}$ probe operating at 470.599 MHz. The spectra were recorded in a 32 K memory. A spectral width setting of 62.500 Hz was employed, yielding a data point resolution of 3.8 Hz/data point and an acquisition time of 0.262 s. No relaxation delays were applied. Typically, 40,000 transients were accumulated. The pulse width corresponding to a bulk magnetization tip angle, θ , of approximately 90° was equal to 1 μs . Line broadening parameters used in the exponential multiplication of the free induction decays were 3 - 4 Hz.

The low temperature study was carried out by the use of a Bruker temperature controller. The temperature was measured with a copper-constantan thermocouple inserted directly into the sample region of the probe and was accurate to $\pm 1^\circ\text{C}$.

The spectra were referenced to a neat external sample of CFCl_3 . The chemical shift convention used is that a positive (negative) sign signifies a chemical shift to high (low) frequency of the reference compound.¹⁷

Computational Methods. The electronic structure calculations were done at the ab initio molecular orbital level using either local density function (LDF) theory¹⁸⁻²¹ or effective core potentials (ECP). The LDF calculations were carried out with the program system DMol,²² as previously described,⁸ with a double-numerical basis set augmented by d polarization functions. This can be considered in terms of size as a polarized double- ζ basis set. However, because exact numerical solutions are employed for the atom, this basis set is of significantly higher quality than a normal molecular orbital polarized double- ζ basis set. The fitting functions have an angular

momentum number one greater than that of the polarization function, resulting in a value of $l = 3$ for the fitting functions.

The ECP calculations were done with all electrons on the F and O and with an effective core potential replacing all of the *core electrons* on the I. The valence basis set is of polarized double zeta quality. The fluorine and oxygen basis set is from Dunning and Hay,²³ and the ECP from Hay and Wadt²⁴ including relativistic corrections. The valence basis set of Hay and Wadt²⁴ was used augmented by a d function on I with an exponent of 0.266.²⁵ The geometries were optimized by using gradient techniques,²⁶ and the force fields were calculated analytically.^{27,28} The ab initio MO calculations were done with the program GRADSCF,²⁹ as implemented on a Cray YMP computer system.

Crystal Structure Determinations of $N(CH_3)_4^+IOF_6^-$. Two independent crystal structure determinations were carried out for this compound at McMaster University and the Freie Universität Berlin, respectively.

At McMaster, only one type of crystal was observed, tetragonal $P4/nmm$ crystals which have IOF_6^- with a positional four-fold disorder for the puckered equatorial plane. The structure of one of these crystals was determined at $-93^\circ C$ and is given in this paper.

At Berlin, originally a very similar, orthorhombic crystal was studied at $-163^\circ C$, and the data were refined either in $P4/nmm$ with four-fold disorder or $Pmmn$ with systematic twinning; however, no puckering of the equatorial plane was observed.¹¹ In repeat experiments, exclusively crystals identical to those found at McMaster were obtained. The structure of one of these crystals was determined at $-155^\circ C$ and is given in this paper.

Single crystals of $N(CH_3)_4^+IOF_6^-$ were grown by making a saturated solution of $N(CH_3)_4^+IOF_6^-$ in CH_3CN in a Teflon-FEP tube at room temperature and warming it to $45^\circ C$ whereupon it completely dissolved to give a pale yellow solution. The sample tube was then

positioned horizontally above a dewar containing water at 60 °C, covered with aluminum foil and slowly allowed to cool overnight. This resulted in the growth of transparent crystals which could be described as tetragonal prisms. At McMaster, the crystals were sealed in Lindemann quartz capillaries and centered on a Siemens R3m/v diffractometer. Accurate cell dimensions were determined at $T = -93\text{ }^{\circ}\text{C}$ from a least-squares refinement of the setting angles (χ , ϕ and 2θ) obtained from 25 accurately centered reflections (with $34.71^{\circ} \leq 2\theta \leq 38.05^{\circ}$) chosen from a variety of points in reciprocal space. Examination of the peak profiles revealed that they were single.³⁰ Integrated diffraction intensities were collected using a $\theta - 2\theta$ scan technique with scan rates varying from 1.5 to 14.65°/min (in 2θ) and a scan range of $\pm 0.6^{\circ}$, so that the weaker reflections were examined slowly to minimize counting errors. Data were collected in four steps since the crystal was diffracting very strongly. In the first step, the data were collected with $-15 \leq h \leq 15$, $0 \leq k \leq 15$ and $0 \leq l \leq 11$ and with $3^{\circ} \leq 2\theta \leq 60^{\circ}$, using silver radiation monochromatized with a graphite crystal ($\lambda = 0.56087\text{ \AA}$). During data collection, the intensities of three standard reflections were monitored every 97 reflections to check for crystal stability and alignment. A total of 1583 reflections were collected out of which 16 were standard reflections. At this stage, the distribution of the reflections in the reciprocal space indicated that the crystal was diffracting at relatively high angles, consequently a second data set was recorded with $45^{\circ} \leq 2\theta \leq 55^{\circ}$. This time a total of 1163 reflections were collected out of which 12 were standard reflections. Finally, a third data set was recorded with $55^{\circ} \leq 2\theta \leq 60^{\circ}$ giving rise to 712 reflections out of which 8 were standard reflections. These data sets were recorded with the maximum intensity (i.e. 1.5 kW Ag X-rays), without attenuation, and as a consequence, the strongest reflections at very low angles were not recorded. In order to record these missing reflections, the power had to be decreased to 750 W. Another set of data was collected with $-3 \leq h \leq 3$, $0 \leq k \leq 3$ and $0 \leq l \leq 2$. A total of 31 reflections were collected, out of which 6 were standard reflections. No crystal decay was observed. In total, 3328 reflections were collected and 876 unique reflections remained after averaging of equivalent reflections. A total of 780 reflections, satisfying the condition $I \geq 3\sigma(I)$, were used for the structure solution. These reflections exhibited systematic absences for $hk0$: $h +$

$k = 2n$ and $h00: h = 2n$. Corrections were made for Lorentz and polarization effects. Absorption corrections were applied by using the program DIFABS.³¹ The transmission factors ranged from 0.728 to 1.117.

The XPREP program was used to determine the correct cell and space group. It confirmed that the original cell was correct and that the lattice was tetragonal primitive ($R_{int} = 0.028$). The structure was shown to be centrosymmetric by an examination of the E-statistics (calc: 0.616; theor: 0.736). The two space groups which were consistent with the systematic absences (n -glide and C_2) were the centrosymmetric $P4/n$ and $P4/nmm$ space groups.

A first solution was obtained without absorption corrections; it was achieved in the space group $P4/nmm$ (129) by conventional heavy-atom Patterson methods which located the positions of the iodine, nitrogen and carbon atoms on special positions (i.e. $4mm$, $-4m2$, $..m$). The full matrix least-squares refinement of their positions and isotropic thermal parameters gave a conventional agreement index $R = (\sum |F_o| - |F_c|) / \sum |F_o|$ of 0.12. A subsequent difference Fourier synthesis revealed the positions of two atoms located on special positions, above and below the iodine. It was possible to distinguish a fluorine from an oxygen atom from the difference in bond lengths (i.e., 1.83 Å and 1.74 Å). The introduction of these positions gave a residual factor R of 0.10. A further difference Fourier synthesis clearly showed the presence of three atoms in the equatorial environment of the iodine. Two of these atoms were positioned on general positions, while the third one was positioned on a special position ($..m$). Consequently, the model implied a four-fold disorder in the "pseudo" equatorial plane consisting of a superposition of four molecules with identical I, axial F and O positions. Consequently, the site occupancy factors of the equatorial fluorine atoms were set equal to 0.25 and 0.125 (general and special positions, respectively) instead of 1.00 and 0.5. The introduction of these positions and isotropic thermal parameters for the equatorial F atoms (all set equal), resulted in a drop of the residual factor R to 0.057. Another improvement of the structure was achieved by introducing anisotropic thermal parameters for the I, N, C, F_{ax} and O atoms (the F_{eq} were kept isotropic because of the presence of the four-fold

disorder), and the positions of the hydrogen atoms located from a difference Fourier map ($U(H)$ fixed to 0.08 \AA^2), as well as a weighting factor ($w = 1/\sigma^2(F) - 0.0003F^2$), dropping the R-factor to 0.044 ($R_w = 0.041$).

The structure was solved a second time using data that had been corrected for absorption. The initial model used the atomic coordinates and isotropic thermal parameters defined previously for all the atoms. The solution obtained ($R = 0.043$) indicated a slight improvement over that obtained without absorption corrections ($R = 0.057$). The final refinement was obtained by introducing anisotropic thermal parameters for the I, F_{ax}, O, N and C atoms and a weighting factor ($w = 1/\sigma^2(F) + 0.0000F^2$), and gave rise to a residual R of 0.0375 ($R_w = 0.035$). In the final difference Fourier map, the maximum and the minimum electron densities were 1.5 and -1.6 \AA^3 .

All calculations were performed using the SHELXTL PLUS³² determination package for structure determination molecular graphics.

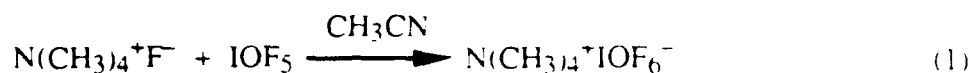
At Berlin, the crystal was mounted, with the help of a special apparatus,³³ on an Enraf Nonius CAD 4 diffractometer at -155 °C. Oscillating crystal photographs were used to check the reflection quality. There were 25 reflections in the ϑ range 12 - 25° that were used to obtain the orientation matrix and lattice constants. Space group determination: The lattice constants indicated no deviation from tetragonal symmetry. Reflection intensities obeyed the rules $F(hkl) = F(\bar{h}kl) = F(kh\bar{l})$ with $R_{int} = 0.0204$. Extinction of $hk0 \neq 2n$ left only space group $P4/nmm$ (no. 129), which enforces the four-fold disorder model. Calculations in orthorhombic space groups $Pmmn$ (no. 59) or $P2_1 mn$ (No. 31) generated the same disorder of the equatorial fluorine atoms. Three reflections were used to check for crystal decay and standard reflections orientation. Further details of the measurement routine are given in Tables 1 and S1. After applying Lorentz and polarization corrections, the data were used for refinement of the previously published¹¹ model with the program SHELXS 76.³⁴ Atomic form factors were taken from the Kynoch Tables.³⁵ The atoms I, O, F(1), N, and C were refined anisotropically, and F(2)-F(4)

isotropically which resulted in $R = 0.045$. Absorption correction was introduced at this stage. Optical measurements were not possible because of the embedding of the colorless crystal in paraffin oil. The psi scan method gave no better results. Finally the method DIFABS³¹ was used. Maximal and minimal corrections of 1.28 and 0.85 were applied. At this stage, hydrogen atoms were found in difference Fourier maps and refined with fixed isotropic U . This model refined to $R = 0.0291$ and $R_w = 0.0255$ (see Table 1). The four-fold disordered atoms F(2)-F(4) were then treated anisotropically. This resulted in $R = 0.020$, and $R_w = 0.0171$. The F(2), F(3), and F(4) atoms became quite disk-like, with a considerable bond shrinkage effect. Since it is unclear whether or not it is advisable to refine these four-fold disordered atoms anisotropically because of overlap of these atoms with each other, the calculation with isotropic F(2), F(3), F(4) atoms is regarded as the best solution.

Summaries of the data collection parameters and other crystallographic information for both data sets are given in Table 1. The final atomic coordinates, the thermal parameters, interatomic distances, bond angles and deviations from the average O-I-Feq angles are listed in Tables 2-4. Summaries of the structure determinations and the observed and calculated structure factors are given in Tables S1-S3 (supplementary material).

RESULTS AND DISCUSSION

Synthesis and Properties of $N(CH_3)_4^+IOF_6^-$. In a previous study,³⁶ it was shown that, at room temperature, CsF does not react with a large excess of IOF₅, while at higher temperatures it tends to undergo deoxygenation. In the same paper it was speculated that the failure to observe fluorine-oxygen exchange in the IF₇-CsNO₃ system might be due to the lack of formation of an intermediate IOF₆⁻ salt. The present study clearly demonstrates that under suitable reaction conditions, i.e. using a soluble anhydrous fluoride of a large cation in a compatible solvent, IOF₆⁻ salts are readily formed according to:



The resulting $\text{N(CH}_3)_4^+\text{IOF}_6^-$ is a very pale yellow solid which is thermally stable up to about 137 °C where it starts to decompose to IOF_4^- , CF_4 and COF_2 as the major products. It was characterized by elemental analysis, a crystal structure determination, and vibrational and ^{19}F NMR spectroscopy (see below).

X-Ray Crystal Structure of $\text{N(CH}_3)_4^+\text{IOF}_6^-$. The crystal structure of $\text{N(CH}_3)_4^+\text{IOF}_6^-$ at -93 °C was determined at McMaster University and confirmed at the Freie Universität Berlin for a crystal kept at -155 °C. Although the gross features of both structures are very similar, they exhibit an extremely interesting temperature dependence of the degree of puckering and, therefore, both data sets are given in full detail.

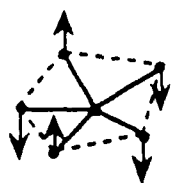
The crystal structure of $\text{N(CH}_3)_4^+\text{IOF}_6^-$ consists of well separated $\text{N(CH}_3)_4^+$ and IOF_6^- ions. The packing of the ions (see Figure 1) can be described as a cubic close packing of alternating layers of IOF_6^- anions and $\text{N(CH}_3)_4^+$ cations in which the alternating orientation of the tetrahedral cations results in a cuboctahedral³⁷ unit cell with $Z = 2$. While the cation is perfectly ordered with the expected bond lengths, the IOF_6^- anion is subject to a positional four-fold disorder in the equatorial plane. The model results from the superposition of four anions in which the central I atom and the axial O and F(1) atoms occupy identical positions. One of these anions is shown in Figure 2. There are no significant contacts to iodine other than the directly bonded oxygen and six fluorine ligands, and the anion exhibits a gross pentagonal bipyramidal geometry. The O-I-F_{ax} angle is constrained by symmetry to be 180°, while there are no constraints on the positions of the equatorial fluorines. The equatorial fluorines are bent away from the axial oxygen ligand, as expected for a doubly bonded oxygen being more repulsive than a singly bonded fluorine ligand.⁵

The I-O bond length (1.75-1.77 Å) indicates significant double bond character for the I-O bond.³⁸⁻⁴³ Its temperature dependence will be discussed below. The greater I-O bond length in IOF_6^- , when compared with that in IOF_5 (1.715(4) Å),³⁸ is consistent with the placement of some of the negative charge on oxygen, thereby increasing the polarity and decreasing the bond order of the I-O bond. The axial I-F bond (1.823(3) Å) is, within experimental error ($\pm 3\sigma$), significantly shorter than all of the equatorial I-F bonds (average 1.88 Å), and both types of I-F bonds in IOF_6^- are significantly longer than the corresponding bonds in IF_7 (1.786(7) Å and 1.81(1) Å, respectively)⁷. These differences can be attributed again to the formal negative charge on IOF_6^- , which leads to greater $\overset{\delta+}{\text{I}} - \overset{\delta-}{\text{F}}$ bond polarities and consequently longer bonds. The greater length of the equatorial bonds in IOF_6^- and IF_7 relative to their axial ones is due to the increased mutual repulsion of the fluorine ligands in the highly congested equatorial plane and their higher ionicity (see below).

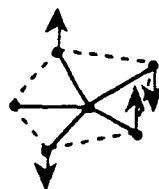
Nature and Temperature Dependence of the Equatorial Puckering in IOF_6^- .

As mentioned above, the equatorial fluorine atoms in IOF_6^- are bent away from the doubly bonded oxygen atom by about 5°. Furthermore, the plane of the equatorial fluorine atoms is puckered and its I-F bonds are elongated in order to lessen the high degree of ligand-ligand repulsion encountered for these fluorines. Contrary to the rapid dynamic puckering in free, pentagonal-bipyramidal molecules, such as IF_7 ,⁸ the puckering in solid $\text{N}(\text{CH}_3)_4^+ \text{IOF}_6^-$ is frozen out by hydrogen...fluorine bridging between the two F(2) atoms of IOF_6^- and hydrogen atoms from two different cations. This bridging results in two close F...C contacts of 3.175(9) Å and 3.271(9) Å, while the remaining closest F...C contacts occur at 3.317(9), 3.473(9) and 3.416(9) Å and are very close to the accepted sum of the van der Waals radii of CH_3 (2.00 Å)⁴⁴ and F (1.35-1.40 Å)^{44,45} which is 3.35-3.40 Å.

A pentagonal plane can be puckered in two ways resulting in structures of either C_s or C_2 symmetry, respectively.

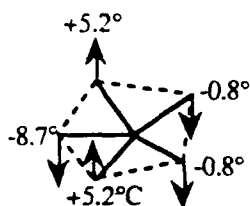


C_s

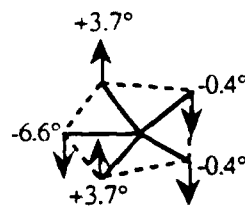


C_2

As mentioned above, the doubly bonded, axial oxygen ligand in IOF_6^- is more repulsive than the singly bonded, axial fluorine ligand. Therefore, the average equatorial plane, which can be defined as a plane perpendicular to the O-I-F_{ax} axis containing all five equatorial fluorine ligands at the averaged $\text{F}_{\text{eq-I-O}}$ bond angle, drops below the center of the iodine atom. As can be seen from Table 4 and Figure 2, the puckered plane of IOF_6^- definitely exhibits C_s symmetry. Furthermore, the relative displacements of the equatorial fluorine ligands from the average equatorial plane decrease with decreasing temperature, i.e. *the degree of puckering decreases with decreasing temperature*.

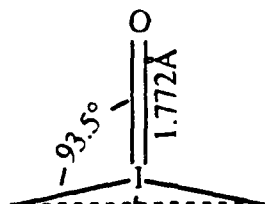


-93 °C

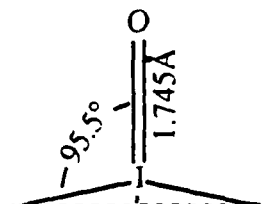


-155 °C

This decrease in the degree of puckering at lower temperatures causes additional important structural changes. Thus, the I-O bond length is significantly shortened and the angle between the oxygen ligand and the average equatorial plane is increased.



-93 °C



-155 °C

These temperature effects can be explained by a decreasing population of the higher vibrational states of the ring puckering motion which, due to its low frequency of about 141 cm^{-1} , is, even at low-temperatures, still highly populated. The resulting decrease in the thermal motion of the equatorial fluorines diminishes their mutual repulsion and allows the equatorial fluorines to become more coplanar and less repulsive which, in turn, results in a shortening of the I-O bond length. It would therefore, be of great interest to determine the crystal structure of $\text{N}(\text{CH}_3)_4^+\text{IOF}_6^-$ at a very low temperature at which the puckering motion is completely frozen out and to compare the resulting structure with those of the present study. Such a study could establish beyond a doubt that in their minimum energy structures these normally puckered, pentagonal bipyramidal molecules indeed possess unpuckered equatorial planes.

^{19}F NMR Spectrum of the IOF_6^- Anion. The ^{19}F NMR spectrum (obtained at McMaster University) of $\text{N}(\text{CH}_3)_4^+\text{IOF}_6^-$ was recorded at -40°C in CH_3CN solution and is in agreement with a pentagonal bipyramidal structure for the IOF_6^- anion. This structure is expected to have an average C_{5v} point group symmetry with the oxygen in the axial position. Accordingly, the ^{19}F NMR spectrum (Figure 3) displays a broad doublet ($\Delta\nu_{1/2} \approx 170\text{ Hz}$) at 166.0 ppm , assigned to the equatorial fluorines, and a broad binomial sextet ($\Delta\nu_{1/2} \approx 360\text{ Hz}$) at 111.1 ppm , assigned to the axial fluorine *trans* to oxygen. The weak triplet observed at 114.5 ppm [$^2J(\text{F}_{\text{eq}}-\text{F}_{\text{ax}}) = 200\text{ Hz}$] is attributed to the F-*trans*-to-O environment of $\text{cis-IO}_2\text{F}_4^-$ ⁴⁶ which probably arose from adventitious hydrolysis of IOF_6^- in its synthesis or during the NMR sample preparation. The observation of separate ^{19}F resonances for the axial and equatorial ligand environments of IOF_6^- is unusual for a pentagonal bipyramidal species and demonstrates that the IOF_6^- anion does not undergo intramolecular ligand exchange (i.e., pseudorotation) in solution, in contrast with the related TeF_7^- anion^{10,11} and IF_7 molecule.⁴⁷ This is not surprising because any plausible intermediate in the pseudorotation process for IOF_6^- would require the doubly bonded oxygen ligand to move into an equatorial position. The greater space requirement of the oxygen double bond domain, compared with that of a fluorine single bond domain, would render the

placement of the oxygen ligand in the more sterically crowded equatorial position energetically unfavorable, thereby creating a high activation barrier for the process. Although the X-ray crystal structure reveals that, in the solid state, the equatorial fluorine ligands of the IOF_6^- anion are unevenly puckered, only a single resonance is observed for these ligands in the ^{19}F NMR spectrum of the solution. Clearly, the puckering, which is frozen out in the solid state, becomes a dynamic process in solution which is fast on the NMR time scale.

It is of interest to compare the ^{19}F chemical shifts of IOF_6^- with those of other related iodine(VII) oxofluoro-species. The ^{19}F chemical shifts of the F-*trans*-to-F environments in *trans*- IO_2F_4^- , *cis*- IO_2F_4^- ⁴⁶ and IOF_5 ⁴⁷ occur in a specific region at 65.1, 66.0 and 68 ppm, respectively. Similarly, the ^{19}F chemical shifts of the F-*trans*-to-O environments in *cis*- IO_2F_4^- and IOF_5 also occur in a distinct region at 112.8⁴⁶ and 107 ppm,⁴⁸ respectively. In the IOF_6^- anion it can be seen that the F-*trans*-to-O environment (111.1 ppm) also resonates in this region but that the resonance of the five equatorial fluorines (166.0 ppm) is strongly deshielded (i.e., by ca. 100 ppm) from the F-*trans*-to-F environments of IOF_5 and *cis*/*trans*- IO_2F_4^- . This phenomenon has also been noted for the XeF_5^- anion in which the fluorines in the pentagonal plane resonate 56.8 ppm to high frequency of the fluorine ligands in square planar XeF_4 .⁴⁹ In the cases of the pentagonal bipyramidal TeF_7^- anion and IF_7 molecule, even at low temperature^{10,11,47} only average ^{19}F chemical shifts can be obtained owing to their fluxional behavior. Nevertheless, the fact that these average chemical shifts occur at significantly higher frequency than those of the related octahedral TeF_6 ⁵⁰ and IF_6^+ ⁵¹ species indicates that the five equatorial fluorines have a higher frequency ^{19}F chemical shift than the two axial fluorine ligands, since the former will contribute the largest weighting to the average chemical shift.

The large chemical shift differences between fluorine ligands in a square plane and those in a pentagonal plane in the aforementioned species are indicative of the dominance of the paramagnetic contribution to the ^{19}F shielding constant. In the theory developed by Pople and Karplus,⁵² the

paramagnetic contribution to the shielding constant of an atom A bonded to another atom B is given by equation (2)

$$\sigma_p^A = \frac{-e^2\hbar^2\langle r^{-3} \rangle_{2p}}{2m^2c^2\Delta E} \left[Q_{AA} + \sum_{B \neq A} Q_{AB} \right] \quad (2)$$

where $\langle r^{-3} \rangle_{2p}$ is the mean inverse cube of the 2p-orbital radial function on atom A; Q_{AA} is the charge density term for atom A; Q_{AB} is the bond order term for the A-B bond and ΔE is the mean excitation energy.

Compared with the bonds in the corresponding octahedral or pseudo-octahedral precursors, MO_yF_x^n , those in the $\text{MO}_y\text{F}_{x+1}^{n-1}$ species, which contain a pentagonal plane of M-F bonds (where $M = \text{Xe}, \text{I}, \text{Te}$), exhibit greater ionic character, as indicated by their longer bond lengths and lower vibrational stretching frequencies. This greater ionic character would be expected to bring about a decrease in the $\langle r^{-3} \rangle_{2p}$ and charge density-bond order terms of Equation (2). This would result in a decrease in σ_p and a more shielded chemical shift and does not account for the experimentally observed trend. Consequently, it would appear that the origin of the observed deshielding most likely lies in the ΔE term. Unfortunately, the nature of the excited states is unknown at present, however it is interesting to note that comparison of the HOMO energies in XeF_4 and XeF_5^- ⁴⁹ as well as IOF_5 and IOF_6^- reveals that the anions have significantly lower values than the neutral molecules and may facilitate excitation to a higher excited state, i.e., ΔE is smaller for XeF_5^- and IOF_6^- than for XeF_4 and IOF_5 .

The two-bond fluorine-fluorine scalar coupling $^2J(^{19}\text{F}_{\text{ax}}-^{19}\text{F}_{\text{eq}})$ in IOF_6^- has a value of 205 Hz and is almost identical in magnitude to that measured previously for *cis*- IO_2F_4^- in CH_3CN [$^2J(^{19}\text{F}_{\text{ax}}-^{19}\text{F}_{\text{eq}}) = 204 \text{ Hz}$].⁴⁶ The couplings in both anions are smaller than the corresponding coupling in the related IOF_5 molecule [$^2J(^{19}\text{F}_{\text{ax}}-^{19}\text{F}_{\text{eq}}) = 271 - 280 \text{ Hz}$],⁵³ which may reflect the anticipated greater ionic character in the bonds of the anionic species.⁵⁴ In the ^{19}F NMR spectrum of IOF_6^- , both the doublet and sextet are significantly broadened owing to partially collapsed scalar

coupling to the quadrupolar ^{127}I ($I = 5/2$) nucleus. The ^{19}F NMR spectra of $\text{cis-IO}_2\text{F}_4^-$ ⁴⁶ and IOF_5 ^{47a} also show broadening attributed to the same cause. Interestingly, the line width of the sextet of IOF_6^- is substantially broader than that of the doublet, indicating that $^1J(^{19}\text{F}_{\text{ax}}-^{127}\text{I})$ is larger than $^1J(^{19}\text{F}_{\text{eq}}-^{127}\text{I})$ and therefore less quadrupole collapsed. If it is assumed that the Fermi-contact mechanism provides the dominant coupling contribution, then this observation is consistent with the relatively more covalent (i.e., greater s-character) bond between iodine and the axial fluorine as compared with those between iodine and the equatorial fluorines.⁵⁴ The X-ray crystallographic data and vibrational spectra for $\text{N}(\text{CH}_3)_4^+\text{IOF}_6^-$ support this idea in that the I-F_{ax} bond distance is shorter than the average I-F_{eq} bond distance and the I-F_{ax} force constant is larger than the I-F_{eq} one (see below).

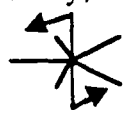
Vibrational Spectra. The infrared and Raman spectra of solid $\text{N}(\text{CH}_3)_4^+\text{IOF}_6^-$ and the Raman spectra of its CH_3CN solution were recorded and are shown in Figure 4. The observed frequencies, together with their assignments, are summarized in Table 5. A comparison of the observed and calculated (see below) frequencies of IOF_6^- with those of the closely related pentagonal IF_7 molecule⁸ and XeF_5^- anion,⁴⁹ together with their approximate mode descriptions, are given in Table 6. After subtraction of the well known^{15,55} bands of the $\text{N}(\text{CH}_3)_4^+$ cation (see Table 5), the remaining bands, which are due to IOF_6^- , can be readily assigned based on the data given in Table 6. Since the vibrational spectra of IOF_6^- in solid $\text{N}(\text{CH}_3)_4^+\text{IOF}_6^-$ do not appear to be noticeably affected by the slight equatorial puckering, they were assigned (see Table 6) in point group C_{5v} which is the lowest energy structure of the free anion (see below).

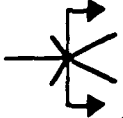
Ab-initio Calculations and Normal Coordinate Analyses. The electronic structure of IOF_6^- was calculated at the ab initio level by using both local density functional (LDF) theory and molecular orbital theory with an effective core potential (ECP) for the core electrons of iodine. Both types of calculations resulted in minimum energy structures of C_{5v} symmetry with the ECP calculations duplicating the experimentally observed geometry (see Table 7) and vibrational frequencies (see Table 6) much better than the LDF calculations. In view of the superiority of the

ECP calculations, we have also recalculated the structure of the closely related XeF_5^- anion, for which previously⁴⁹ only LDF values had been available. As can be seen from Tables 6 and 7, the ECP calculations are in excellent agreement with the observed values, after scaling of the calculated frequencies by empirical factors to maximize their fit with the experimental data, and therefore, are invaluable for the correct assignments of the vibrational spectra. For XeF_5^- , for example, they clearly indicate that the previous assignments⁴⁹ for $\nu_2(A_2'') = 274 \text{ cm}^{-1}$ and $\nu_4(E_1') = 290 \text{ cm}^{-1}$ should be reversed. In view of the closeness of these two frequencies, the reversal of their assignments has very little or no impact on the conclusions previously reached⁴⁹ for XeF_5^- .

The eleven fundamental vibrations of a pentagonal bipyramidal AX_5YZ species in point group C_{5v} can be classified as $\Gamma = 4A_1(\text{IR}, \text{Ra}) + 4E_1(\text{IR}, \text{Ra}) + 3E_2(\text{Ra})$. The internal coordinates, symmetry coordinates and approximate mode descriptions for IOF_6^- are summarized in Figure 5 and Table 8, respectively. The tentative assignments given in our preliminary communication¹⁰ for IOF_6^- and IF_7 have been significantly improved resulting in revised assignments for ν_6, ν_7, ν_8 , and ν_{10} of IOF_6^- and for ν_9 and ν_{10} of IF_7 .

By the use of the scaled ECP frequencies, force fields were calculated for IOF_6^- (see Table 9) and XeF_5^- (see Table 10). The potential energy distribution (PED) for IOF_6^- is given in Table 11. As can be seen from Table 11, the IF_5 in-plane deformation motions, due to their high frequencies, mix considerably with some of the other symmetry coordinates, and the $\nu_7(E_1)$ and $\nu_8(E_1)$ modes are antisymmetric and symmetric combinations, respectively, of S_7 and S_8 .

Consequently, ν_7 and ν_8 are better described as an O-I- F_{ax} rocking motion, , and an O-I-

F_{ax} scissoring motion, , respectively, than as separated I=O and I- F_{ax} wagging motions. The only deficiency of the ECP calculation for IOF_6^- was the low frequency value and resulting force constant for the scaled I-O stretching mode, $\nu_1(A_1)$. Consequently, we prefer to use for this mode the unscaled value of 860 cm^{-1} which is in much better agreement with the observed value of

873 cm^{-1} . The low value calculated for this stretching frequency is surprising as the calculated I-O bond length is shorter than the experimental value. Due to the larger number of symmetry species for XeF_5^- , its PED (see Table 10) is highly characteristic and requires no further comment. It should be noted, however, that the symmetry coordinates and internal force constants, previously published⁴⁹ for XeF_5^- , contained two typographical errors. S_{5b} should read $\sqrt{\frac{2}{5}} [\sin 2\alpha (\Delta r_2 - \Delta r_5) - \sin \alpha (\Delta r_3 - \Delta r_4)]$, and subscripts had been omitted from the last two internal force constants in Table VIII which should read $f_{\gamma\gamma} - f_{\gamma\gamma'}$ and $f_{\gamma} - f_{\gamma\gamma}$, respectively.

The internal force constants of greatest interest are those involving the stretching of the axial and the equatorial fluorine bonds and the equatorial in-plane deformation constants. These data are summarized for the IF_7 , IOF_6^- , XeF_5^- series in Table 12. As can be seen from this Table, the X-F_{ax} bonds are considerably stronger than the X-F_{eq} ones for a given compound, as expected from the bonding scheme proposed below. Furthermore, the stretching force constants decrease significantly on going from IF_7 to IOF_6^- and XeF_5^- , as expected from an increasing ionicity of the X-F bonds caused by the formal negative charge in the anions and the reduction in the formal oxidation state of the central atom from +VII in IF_7 and IOF_6^- to +IV in XeF_5^- . The large increase in the value of $f_{\pi\pi'}$, the coupling to opposite bonds, from IOF_6^- to XeF_5^- is analogous to those previously observed⁴⁷ for going from either *trans*- IO_2F_4^- ($f_{\pi\pi'} = 0.27 \text{ mdyn/\AA}$) to IOF_4^- ($f_{\pi\pi'} = 0.45 \text{ mdyn/\AA}$) and IF_4^- ($f_{\pi\pi'} = 0.47 \text{ mdyn/\AA}$) or IOF_5 ($f_{\pi\pi'} = 0.18 \text{ mdyn/\AA}$) to IF_5 ($f_{\pi\pi'} = 0.38 \text{ mdyn/\AA}$) and, hence, appears to be associated with the introduction of a sterically active, free valence electron pair into the ligand sphere around the central atom.

The in-plane deformation constants, f_{α} , are a measure for the strength of the mutual repulsion of the equatorial ligands and hence, for the degree of congestion in this plane which, in turn, is responsible for the puckering. As can be seen from Table 12, the value of f_{α} decreases markedly on going from IF_7 to IOF_6^- and XeF_5^- . In IF_7 , the in-plane deformation constant, f_{α} , is about five times larger than the out-of-plane deformation constant, f_{β} , and accounts for the

puckering of the equatorial plane in IF_7 . On the other hand, in XeF_5^- the f_α value has become much smaller and approaches the range of values expected for the out-of-plane deformation constants, f_β . This is in good agreement with the x-ray crystal structure of $\text{N}(\text{CH}_3)_4^+\text{XeF}_5^-$ which showed⁴⁹ that XeF_5^- is planar and not puckered. Hence, it appears that the value of the in-plane deformation force constant, f_α , is a useful parameter for measuring the degree of congestion and the likely occurrence of puckering in the equatorial ligand plane.

It must be pointed out that the problem of calculating the internal deformation constants from the corresponding symmetry force constants is underdetermined (more unknowns than available equations) and, hence, requires additional assumptions. For the calculation of f_α in our compounds, the pure vibrational force field⁵⁶ condition of Kuczera, adapted to five-fold symmetry, $f_\alpha + 2f_{\alpha\alpha} + 2f_{\alpha\alpha'} \equiv 0$, was used. Since for f_β , the case is even more complex, no explicit values were calculated for f_β of IOF_6^- and XeF_5^- , however we estimate f_β of IOF_6^- to be slightly larger than and that of XeF_5^- to be similar to that of IF_7 .

Structure and Bonding in IOF_6^- and Related Molecules and Ions. The pentagonal bipyramidal structure and the co-planarity of the equatorial ligands in the minimum energy configuration of IOF_6^- , which cannot be accounted for by either "repelling points on a sphere" VSEPR arguments⁵ or classical, directionally localized molecular orbitals, can be rationalized in terms of a bonding scheme, first noticed⁴⁹ for XeF_5^- and elaborated on in more detail⁸ for IF_7 . In this scheme, the structure and bonding of XeF_5^- are explained by a simple model derived from XeF_4 . The bonding in the square-planar XeF_4 can be described by two semi-ionic, 3-center 4-electron (3c-4e) bonds⁵⁷ for the four Xe-F bonds and two lone valence electron pairs on Xe ($s^2p_z^2$ hybrids). The 3c-4e bonds involve the p_x^2 and p_y^2 orbitals of xenon. Addition of an F^- ion to the equatorial plane in XeF_4 results in pentagonal-planar XeF_5^- and the formation of a semi-ionic, 6-center 10-electron (6c-10e) bond involving the delocalized $p_x^2p_y^2$ hybrid orbitals of Xe and 6 electrons on the 5 F ligands.⁴⁹ The two lone valence electron pairs on Xe in XeF_5^- are analogous to those in XeF_4 .

Now let us consider the bonding in IF_7 and IOF_6^- . Their planar IF_5 fragments have essentially the same bonding as XeF_5^- , as shown by the atomic population calculations given in Table 13. As expected for the replacement of two free valence electron pairs on the central atom by two bonded ligands, each of which contributes one electron to its bond, the population of the s^2 and p_z^2 orbitals of I in IF_7 and IOF_6^- has decreased by about two electrons, compared to XeF_4 and XeF_5^- . The higher oxidation state of the central atoms in IF_7 and IOF_6^- (+VII) results in I having a higher positive charge than Xe (+IV) in XeF_5^- . This causes the effective electronegativity differences between the central atoms and the ligands in IF_7 and IOF_6^- to be smaller than those in XeF_4 and XeF_5^- and results in an increased covalency and a shortening of the central atom-fluorine bonds. Furthermore, the axial fluorine ligands in IF_7 and IOF_6^- carry less of a negative charge than the equatorial ones which accounts for the axial I-F bonds to be more covalent and, hence, shorter than the equatorial ones. The total charge distributions in IF_7 and IOF_6^- (see Table 13) also demonstrate the effect of replacing an F ligand in IF_7 by an O^- ligand. The oxygen substitution results in the release of electron density into the IF_6 part of the molecule which increases the negative charges on the six fluorines and weakens the I-F bonds in IOF_6^- relative to those in IF_7 .

Of course, the above model does not account for the fact that the electrons will try to minimize their mutual repulsions and occupy all of the available orbitals to do so. This results in the participation of some d functions. Although we are not proposing a d hybridization model, the population in the d orbitals does suggest a redistribution into these orbitals beyond that expected if the d orbitals were to act solely as polarization functions.

The above atomic population and total charge distribution analysis qualitatively confirms our simple bonding model for pentagonal-bipyramidal molecules. This model involves the use of delocalized p_x^2 and p_y^2 hybrid orbitals of the central atom for the formation of a semi-ionic, 6c-10e bond with the five equatorial ligands and of an sp_z hybrid orbital for the formation of two, more covalent, axial bonds. This bonding scheme can account for all the observed structural features

and also the observed bond length differences. The planarity of the p_x^2 and p_y^2 hybrid orbitals of the central atom also provides the explanation why these heptacoordinated main group fluorides and oxyfluorides prefer pentagonal-bipyramidal structures and not the monocapped octahedral or trigonal prismatic ones expected from VSEPR arguments.

As far as the puckering of the equatorial plane in pentagonal bipyramidal molecules is concerned, the data given above for IF_6O^- strongly suggest that the congestion in its equatorial plane and hence the driving force towards puckering is intermediate between those of puckered IF_7 and planar XeF_5^- . Therefore, it might be possible that, by a reduction of the thermal motion of the ligands, the mutual repulsion among the equatorial ligands will be sufficiently diminished to allow for the observation of a temperature dependent transition from a puckered to a planar configuration. Our two crystal structure determinations of $\text{N}(\text{CH}_3)_4^+\text{IOF}_6^-$ at different temperatures clearly demonstrate such a temperature dependency of the degree of puckering, and the ab-initio calculations point to a minimum energy structure with co-planar equatorial ligands.

A comparison of the structure of IOF_6^- with those^{7,38,58-61} of other hexa- and heptacoordinated iodine fluoride and oxyfluorides is shown in Figure 6 and suggests the following general effects: (i) If the central iodine atom possesses a free valence electron pair, this pair seeks high s -character, i.e. sp^n hybridization. If the number of ligands is larger than four, then as many F ligands form semi-ionic, 3-center 4-electron (3c-4e)⁵⁷ or similar multi-center bonds as are required to allow the free electron pairs to form an sp^n hybrid with any remaining ligands. The resulting semi-ionic, multi-center bonds are considerably longer than the more covalent sp^n hybrid bonds.⁶² This effect accounts for the long equatorial I-F bonds in IF_4^- ,⁵⁸ IOF_4^- ,⁵⁹ and IF_5 ,⁶⁰ and the short axial I-F bond in IF_5 .⁶⁰ (ii) If the central atom does not possess any free valence electron pair, the ionicity of the bonds and, as a result, their lengths are influenced by the following secondary effects: (a) An increase in the oxidation state of the central atom generally increases its effective electronegativity and results in increased covalency and, hence, shorter bonds. It must be

kept in mind, however, that the addition of two fluorine ligands results in a considerably stronger electron density withdrawal from the central atom than that caused by the addition of one doubly bonded oxygen ligand. Thus, for extremely electronegative central atoms, such as chlorine in ClF_2^+ or ClF_4^- , the addition of an oxygen ligand may even result in the reverse effect, i.e. the release of electron density to the central atom.^{62,63} (b) In the case of coordination number (CN) seven, steric crowding and, hence, repulsion effects, also become important. The increased congestion in the equatorial planes of IF_7 and IOF_6^- , for example, results in increased mutual repulsion and increased lengths of the equatorial bonds. Thus, the nearest-neighbor $\text{F}_{\text{eq}}\dots\text{F}_{\text{eq}}$ contacts in the IOF_6^- anion at -93°C are $2.090(16) - 2.362(12)\text{\AA}$ and are significantly less than twice the nominal van der Waals radius for fluorine, i.e., $2.70 - 2.80\text{\AA}$,^{44,45} while in hexacoordinated IF_5 ³⁸ the nearest neighbor $\text{F}_{\text{eq}}\dots\text{F}_{\text{eq}}$ contacts are 2.571\AA and are still at the limit of the sum of the fluorine van der Waals radii. Similarly, the increased repulsion from the sterically active, free valence electron pair on iodine in heptacoordinated IF_6^- causes an elongation of the three neighboring I-F bonds.⁶¹ (c) A formal negative charge, as found in an anion, enhances the $\overset{\delta-}{\text{F}} - \overset{\delta+}{\text{I}}$ bond polarity and hence the ionicity of a bond and, thereby, increases the bond lengths.⁶²

The combination of these effects can explain the features of the compounds shown in Figure 6. For IOF_6^- , the relative length of equatorial I-F bonds can be explained by semi-ionic, multi-center bonding, which is enhanced by the formal negative charge and the repulsion effects caused by the steric crowding in the equatorial plane, while the lengthening of the I-O bond is attributed mainly to the formal negative charge and the repulsion effects. There is one piece of data in Figure 6, however, which does not fit the overall picture. This is the axial I-F bond length in IOF_5 . The published³⁸ value of 1.863\AA appears too long and, based on the fact that the axial IF stretching force constant in IOF_5 is larger than the equatorial one⁶⁴ and by analogy with the isoelectronic TeOF_5^- anion ($\text{Te-F}_{\text{ax}} = 1.854\text{\AA}$, $\text{Te-F}_{\text{eq}} = 1.853\text{\AA}$),⁶⁵ the axial bond distance in IOF_5 should be similar to or shorter than the equatorial ones. A cursory examination⁶⁶ of the

experimental data^{38,64,67-69} available for IOF₅ revealed that these bond distances are not well determined and are very sensitive to the choice of the O-I-F_{eq} bond angle. Thus, a decreasing angle lengthens the I-O and shortens the I-F_{ax} bond. Furthermore, a lengthening of the I-F_{eq} bond distance results in a shortening of the I-F_{ax} bond distance. Obviously, additional experimental data are required for a more precise structure determination of IOF₅.

Conclusions. The IOF₆⁻ anion provides unique information on the nature of heptacoordinated molecules. The high degree of fluxionality, which is normally encountered for free heptacoordinated molecules, is absent. Dynamic puckering of the equatorial ligand plane is frozen out by crystal forces, and axial-equatorial ligand exchange is precluded by the incorporation of the more repulsive, axial oxygen ligand. It is shown that the statically puckered, equatorial fluorine plane exhibits C_s symmetry in the crystal. Furthermore, it is demonstrated by ab initio calculations and the crystal structure of XeF₅⁻ that the lowest energy structures of these molecules are pentagonal bipyramids with co-planar equatorial ligands. This co-planarity is explained by a bonding scheme involving delocalized, planar p_x²-p_y² hybrid orbitals of the central atom for the formation of a semi-ionic, 6-center 10-electron system for the five I-F_{eq} bonds which also accounts for their increased lengths. The degree of puckering of the equatorial ligand plane increases with increasing mutual repulsion of the equatorial ligands and, therefore, is temperature dependent as demonstrated for IOF₆⁻.

Acknowledgements. The work at Rocketdyne was financially supported by the U.S. Air Force Phillips Laboratory and the U.S. Army Research Office, that at McMaster University by the U.S. Air Force Phillips Laboratory and the Natural Sciences and Engineering Research Council of Canada, and that at Freie Universität Berlin by the Deutsche Forschungsgemeinschaft.. We also wish to thank Professor Neil Bartlett, Dr. A.J. Arduengo and Dr. C.J. Schack and Mr. R.D. Wilson for helpful discussions and to Professor S. Kukolich for the calculations on the structure of IOF₅.

Supplementary Material. A structure determination summary (Table S1, 2 pages);
tabulation of calculated and observed structure factor amplitudes (Tables S2 and S3, 16 pages).
Ordering information is given on any current masthead page.

REFERENCES

- (1) Rockwell International, Rocketdyne Division.
- (2) E.I. du Pont de Nemours and Company, Inc.
- (3) Freie Universität, Berlin.
- (4) McMaster University.
- (5) Gillespie, R.J.; Hargittai, I. in "The VSEPR Model of Molecular Geometry," Allyn and Bacon, A Division of Simon & Schuster, Inc. Needham Heights, MA (1991), p58.
- (6) Thompson, H.B.; Bartell, L.S. *Inorg. Chem.* **1968**, *7*, 488.
- (7) Adams, W.J.; Thompson, H.B.; Bartell, L.S. *J. Chem. Phys.* **1970**, *53*, 4040.
- (8) Christe, K.O.; Curtis, E.C.; Dixon, D.A. *J. Am. Chem. Soc.* in press.
- (9) Selig, H.; Sarig, S.; Abramowitz, S. *Inorg. Chem.* **1974**, *13*, 1508.
- (10) Christe, K.O.; Sanders, J.C.P.; Schrobilgen, G.J.; Wilson, W.W. *J. Chem. Soc. Chem. Commun.* **1991**, 837.
- (11) Mahjoub, A.R.; Seppelt, K. *J. Chem. Soc. Chem. Commun.* **1991**, 840.
- (12) Holloway, J.H.; Selig, H.; Claassen, H.H. *J. Chem. Phys.* **1971**, *54*, 4305.
- (13) Schack, C.J.; Pilipovich, D.; Cohz, S.N.; Sheehan, D.F. *J. Phys. Chem.* **1968**, *72*, 4697.
- (14) Schack, C.J.; Christe, K.O. *J. Fluor. Chem.* **1990**, *49*, 167.
- (15) Christe, K.O.; Wilson, W.W.; Wilson R.D.; Bau, R.; Feng, J. *J. Am. Chem. Soc.* **1990**, *112*, 7619.
- (16) Miller, F.A.; Harney, B.M. *Appl. Spectrosc.* **1969**, *23*, 8.
- (17) *Pure Appl. Chem.* **1972**, *29*, 627; **1976**, *45*, 217.
- (18) Parr, R.G.; Yang, W. *Density Functional Theory of Atoms and Molecules*; Oxford University Press: New York, **1989**.
- (19) Salahub, D.R. in *Ab Initio Methods in Quantum Methods in Quantum Chemistry*, 2nd ed.; Lawley, K.P., Ed.; J. Wiley & Sons: New York, **1987**, p447.

- (20) (a) Wimmer, E.; Freeman, A.J.; Fu, C.-L.; Cao, P.-L.; Chou, S.-H.; Delley, B. in *Supercomputer Research in Chemistry and Chemical Engineering*; Jensen, K.F., Truhlar, D.G., Eds.; ACS Symposium Series: American Chemical Society: Washington, DC, 1987, p49. (b) Dixon, D.A.; Andzelm, J.; Fitzgerald, G.; Wimmer, E.; Delley, B. in *Science and Engineering on Cray Supercomputers. Proceedings of the Fifth International Symposium*; Cray Research: Minneapolis, MN, 1990; p285.
- (21) Jones, R.O.; Gunnarsson, O. *Rev. Mod. Phys.* **1989**, *61*, 689.
- (22) Delley, B. *J. Chem. Phys.* **1990**, *92*, 508. DMol is available commercially from BIOSYM Technologies, San Diego, California.
- (23) Dunning, T.H., Jr.; Hay, P.J. in "*Methods of Electronic Structure Theory*," Schaefer, H.F., III, Ed., Plenum Press: New York, 1977, Ch. 1.
- (24) Hay, P.J.; Wadt, W.R. *J. Chem. Phys.* **1985**, *82*, 299.
- (25) Huzinaga, S.; Andzelm, J.; Klobukowski, M.; Radzio, E.; Sakai, Y.; Tatasaki, H. "*Gaussian Basis Sets of Molecular Calculations*", Elsevier: Amsterdam, 1984.
- (26) (a) Komornicki, A.; Ishida, K.; Morokuma, K.; Ditchfield, R.; Conrad, M. *Chem. Phys. Lett.* **1977**, *45*, 595. (b) McIver, J.W., Jr.; Komornicki, A. *Chem. Phys. Lett.* **1971**, *10*, 202. (c) Pulay, P. in "*Applications of Electronic Structure Theory*", Schaefer, H.F. III, Ed.; Plenum Press: New York, 1977, p153.
- (27) (a) King, H.F.; Komornicki, A. *J. Chem Phys.* **1986**, *84*, 5465. (b) King, H.F.; Komornicki, A. in "*Geometrical Derivatives of Energy Surfaces and Molecular Properties*" Jorgenson, P.; Simons, J. Eds. NATO ASI Series C. Vol. 166, D. Reidel: Dordrecht 1986, p207.
- (28) Breidung, J.; Thiel, W.; Komornicki, A. *Chem. Phys. Lett.* **1988**, *153*, 76.
- (29) GRADSCF is an ab initio program system designed and written by A. Komornicki at Polyatomics Research.

- (30) Despite the fact that all the peaks proved to be single, the possibility of twinning was checked by verifying that the hkl values associated with the very weak and very strong reflections at low $\sin\theta/\lambda$ refined using the same orientation matrix.
- (32) Walker, N.; Stuart, D. *Acta Crystallogr.* **1983**, A39, 158.
- (32) Sheldrick, G.M. (1990); SHELXTL PLUS™ Release 4.21/V. Siemens Analytical X-Ray Instruments, Inc., Madison, Wisconsin.
- (33) Keith, M.; Bärnighausen, H.A. *Kristallogr.* **1985**, 170, 5. Schumann, H.; Genthe, W.; Hahn, F.; Hossein, M.B.; d. Helin, D.V. *Organomet. Chem.* **1986**, 229, 67.
- (34) Sheldrick, G.M. *Program for Crystal Structure Determination*, Göttingen, 1976.
- (35) Internat. Tables for X-ray Crystallography, Vol. III, The Kynoch Press, Birmingham 1968.
- (36) Christe, K.O.; Wilson, W.W.; Wilson, R.D. *Inorg. Chem.* **1989**, 28, 904.
- (37) Hyde, B.G.; Anderson, S. "Inorganic Crystal Structures," John Wiley & Sons, New York, **1989**, p7.
- (38) Bartell, L.S.; Clippard, F.B. Jacob, J.E. *Inorg. Chem.* **1976**, 15, 3009.
- (39) Smart, L.E. *J. Chem. Soc., Chem. Commun.* **1977**, 519.
- (40) Selte, K.; Kjekshus, A. *Acta Chem. Scand.* **1970**, 24, 1912.
- (41) Kálmán, K.; Cruickshank, D.W.J. *Acta Crystallogr.* **1970** B26, 1782.
- (42) Feikeman, Y.D. *Acta Crystallogr.* **1961**, 14, 315.
- (43) Feikeman, Y.D. *Acta Crystallogr.* **1966**, 20, 765.
- (44) Pauling, L. *The Nature of the Chemical Bond*, 3rd ed.; Cornell University Press: Ithaca, New York, **1960**, p260.
- (45) Bondi, A. *J. Phys. Chem.* **1964**, 68, 441.
- (46) Christe, K.O.; Wilson, R.D.; Schack, C.J. *Inorg. Chem.* **1981**, 20, 2104.
- (47) (a) Gillespie, R.J.; Quail, J.W. *Can. J. Chem.*, **1964**, 42, 2671. (b) Bartlett, N.; Beaton, S.; Reeves, L.W.; Wells, E.J. *Can. J. Chem.* **1964**, 42, 2531. (c) Alexakos, L.G.; Cornwell, C.D.; Pierce, St. B. *Proc. Chem. Soc.* **1964**, 86, 293. (e) Gutowski, H.S.; Hoffmann, C.F. *J. Chem. Phys.* **1951**, 19, 1259.

- (48) Remeasured for this work in CH₃CN at -40 °C.
- (49) Christe, K.O.; Curtis, E.C.; Dixon, D.A.; Mercier, H.P.; Sanders, J.C.P.; Schrobilgen, G.J. *J. Am. Chem. Soc.* **1991**, *113*, 3351.
- (50) This work; chemical shift determined as $\delta = -51.3$ ppm for TeF₆ in CH₃CN at -40 °C.
- (51) Brownstein, M.; Selig, H. *Inorg. Chem.* **1972**, *11*, 656.
- (52) Karplus, M.; Pople, J.A. *J. Chem. Phys.* **1963**, *38*, 2803.
- (53) Brownstein, M.; Gillespie, R.J.; Krasznai, J.P. *Can. J. Chem.* **1978**, *56*, 2253.
- (54) Jameson, C.J. in "Multinuclear NMR"; Mason, J., Ed.; Plenum Press: New York, **1987**, Chapter 4, pp 97-101.
- (55) Christe, K.O.; Wilson, W.W.; Bau, R.; Bunte, S.W. *J. Am. Chem. Soc.* **1992**, *114*, 3411, and references cited therein.
- (56) (a) Kuczera, K.; Czerminski, R. *J. Mol. Struct.* **1983**, *105*, 269. (b) Kuczera, K. *J. Mol. Struct.* **1987**, *160*, 159.
- (57) Pimentel, G.C. *J. Chem. Phys.* **1951**, *10*, 446. Hach, R.J.; Rundle, R.E. *J. Am. Chem. Soc.* **1951**, *73*, 4321. Rundle, R.E. *J. Am. Chem. Soc.* **1963**, *85*, 112.
- (58) The bond length in IF₄⁻ is a value estimated from a normal coordinate analysis by Christe, K.O.; Naumann, D. *Inorg. Chem.* **1973**, *12*, 59.
- (59) Ryan, R.R.; Asprey, L.B. *Acta Crystallogr. Part B* **1972**, *B28*, 979.
- (60) Balikci, B.; Brier, P.N. *J. Mol. Spectrosc.* **1981**, *89*, 254.
- (61) Majhoub, A.R.; Seppelt, K. *Angew. Chem. Int. Ed. Engl.* **1991**, *30*, 323.
- (62) Christe, K.O.; Schack, C.J. *Adv. Inorg. Chem. Radiochem.* **1976**, *18*, 331.
- (63) Christe, K.O.; Curtis, E.C. *Inorg. Chem.* **1972**, *11*, 2209.
- (64) Smith, D.F.; Begun, G.M. *J. Chem. Phys.* **1965**, *43*, 2001, Holloway, J.H.; Selig, H.; Claassen, H.H. *J. Chem. Phys.* **1971**, *54*, 4305.
- (65) Miller, P.K.; Abney, K.D.; Rappé, A.K.; Anderson, O.P.; Strauss, S.H. *Inorg. Chem.* **1988**, *27*, 2255.
- (66) Kukolich, S.G. private communication of unpublished results.

- (67) Brier, P.N. *J. Mol. Spectrosc.* **1987**, *125*, 233.
- (68) Brier, P.N.; Winrow, M.J. *J. Mol. Spectrosc.* **1984**, *107*, 21.
- (69) Pierce, S.B.; Cornwell, C.D. *J. Chem. Phys.* **1967**, *47*, 1731.

Table 1. Summary of Crystal Data and Refinement Results for
 $N(CH_3)_4^+IOF_6^-$ at -93 °C and -155 °C

T (°C)	-93 °C	-155 °C
space group	P4/nmm (tetragonal)	
a (Å)	8.8590(10)	8.8151(10)
c (Å)	6.3690(10)	6.3213(12)
V (Å ³)	499.85(11)	491.20(10)
molecules/unit cell	2	
molecular weight	331.0	
crystal dimensions (mm)	0.4 x 0.5 x 0.2	0.4 x 0.4 x 0.4
calculated density (g cm ⁻³)	2.199	2.238
color	very faintly yellow	
crystal decay (%)	no	no
absorption coefficient (mm ⁻¹)	3.259	3.326
wavelength (Å) used for data collection	0.56086	0.71069
sin θ/λ limit (Å ⁻¹)	0.8915	0.9045
total number of reflections measured	3136	3489
number of independent reflections	876	887
number of reflections used in structural analysis, I > 3σ (I)	780	885
number of variable parameters	28	34
final agreement factors,	R	0.0291
	Rw	0.0255

Table 2. Final Atomic Coordinates ($\times 10^4$), Equivalent Isotropic Displacement Coefficients ($\text{\AA}^2 \times 10^3$) and Site Occupancy Factors for $\text{N}(\text{CH}_3)_4^+ \text{IOF}_6^-$ at -93° and -155°C

-93°C

	x	y	z	U(eq)	s.o.f.
I	2500	2500	1018(1)	28(1)	0.125
F(1)	2500	2500	-1843(10)	72(2)	0.125
O	2500	2500	3801(12)	74(2)	0.125
F(2)	2927(8)	405(10)	794(12)	59(1)	0.250
F(4)	3967(11)	3967(11)	395(22)	59(1)	0.125
F(3)	4253(11)	1362(10)	1104(12)	59(1)	0.250
N	2500	7500	5000	33(1)	0.125
C	1124(5)	7500	3676(7)	54(1)	0.500
H(1)	286	7500	4729	80	0.500
H(2)	1075	6667	2733	80	1.000

-155°C

I	2500	2500	1029(0)	19(0)	0.125
F(1)	2500	2500	-1850(5)	51(2)	0.125
O	2500	2500	3786(6)	50(2)	0.125
F(2)	2087(6)	393(6)	723(7)	43(1)	0.250
F(4)	3973(8)	3973(8)	408(15)	49(2)	0.125
F(3)	4321(8)	1400(8)	938(9)	54(1)	0.250
N	2500	7500	5000	24(1)	0.125
C	1116(3)	7500	3633(4)	39(2)	0.500
H(1)	284(35)	7500	4490(38)	40	0.500
H(2)	1096(23)	6559(24)	2699(27)	40	1.000

(a) Equivalent isotropic U defined as one third of the trace of orthogonalized U_{ij} tensor. One orientation of the anion IOF_6^- is obtained by application of the symmetry y, x, z. The cation is obtained by application of 0.5 -x, y, z; -y, -x, -z; -y, 0.5 + x, -z.

Table 3. *Anisotropic Displacement Coefficients ($\text{\AA}^2 \times 10^3$)^a
for $\text{N}(\text{CH}_3)_4^+ \text{IOF}_6^-$ at -93° and -155°C*

-93°C

	U_{11}	U_{22}	U_{33}	U_{12}	U_{13}	U_{23}
I	28(1)	28(1)	29(1)	0	0	0
F(1)	94(3)	94(3)	28(2)	0	0	0
O	91(4)	91(4)	40(4)	0	0	0
N	34(1)	34(1)	32(2)	0	0	0
C	44(2)	61(2)	57(3)	0	-14(2)	0

-155°C

I	19.1(1)	19.1(1)	19.4(1)	0	0	0
F(1)	63(2)	63(2)	23(2)	0	0	0
O	64(2)	64(2)	22(2)	0	0	0
N	23(1)	23(1)	26(2)	0	0	0
C	30(1)	44(2)	40(2)	0	-9(1)	0
F(2) ^b	177	19	46	7	26	-5
F(3) ^b	74	146	142	11	93	21
F(4) ^b	143	143	60	-5	-32	-5

-
- (a) The anisotropic displacement exponent takes the form: $-2\pi^2(h^2a^{*2}U_{11} + \dots + 2hka^*b^*U_{12})$.
 (b) In the final structure, the atoms F(2), F(3), and F(4) were treated isotropically because of the fourfold disorder.

Table 4. Bond Lengths, Bond Angles, Average Equatorial Plane Angle and Deviations from the Average O—I—F_{eq} Bond Angle for N(CH₃)₄⁺IOF₆⁻ at -93 ° and -155 °C

	Bond Lengths (Å)		Deviations (deg) from the Mean O—I—F _{eq} Bond Angle	
	-93 °C	-155 °C	-93 °C	-155 °C
I—O	1.772(8)	1.745(4)		
I—F(1)	1.822(5)	1.823(3)		
I—F(2)	1.899(9)	1.894(5)	-0.8(2)	-0.4(1)
I—F(3)	1.852(10)	1.868(7)	5.2(2)	3.7(2)
I—F(4)	1.880(14)	1.868(9)	-8.7(4)	-6.6(3)
N—C	1.483(4)	1.491(3)		

	Bond Angles (deg)				
	-93 °C	-155 °C		-93 °C	-155 °C
O—I—F(2)	94.3(2)	95.9(1)	F(1)—I—F(4)	77.8(4)	77.9(3)
O—I—F(3)	88.3(2)	91.8(2)	F(3)—I—F(2e)	68.7(4)	69.9(3)
O—I—F(4)	102.4(4)	102.1(3)	F(4)—I—F(3)	78.6(3)	76.1(2)
F(1)—I—F(2)	85.7(2)	84.1(1)	F(2c)—I—F(2e)	66.8(5)	67.5(3)
F(1)—I—F(3)	91.7(2)	88.2(2)	Mean O—I—F _{eq}	93.5(3)	95.5(2)
			Mean pucker angle ^a	4.14(30)	2.96(20)

(a) Mean deviation of the equatorial fluorine ligands from the mean O—I—F_{eq} angle.

Table 5. Vibrational Spectra of $N(CH_3)_4^+IOF_6^-$ and Their Assignment

IR 25 °C	obsd freq, cm-1 (rel intens)			assignments, (point group)	
	Ra			N(CH ₃) ₄ ⁺ (T _d)	IOF ₆ ⁻ (C _{5v})
	solid		CH ₃ CN sol 25 °C		
	25 °C	-150 °C			
3045 mw	3043(20)	3045(5)		v ₅ (E)	
	2996(13)			v ₁₄ (F ₂)	
2970 w	2965(13)	2970(4)		v ₁ (A ₁)	
	2927(6)			+ combin. bands	
	2819(5)				
1489 vs				v ₁₅ (F ₂)	
	1464(46)	1466(15)		v ₂ (A ₁), v ₆ (E)	
1418 m	1417(6)	1416(3)		v ₁₆ (F ₂)	
1285 mw	1288(3)			v ₁₇ (F ₂)	
	1173(6)	1174(4)		v ₇ (E)	
949 vs	948(41)	949(28)		v ₁₈ (F ₂)	
873 vs	874(53)	873(37)	880(50)p		v ₁ (A ₁)
	752(45)	753(15)			
	740 sh	742 sh		v ₃ (A ₁)	
649 s	649(88)	658(57)	656(75)p		v ₂ (A ₁)
585 vs					v ₅ (E ₁)
	578(100)	584(100)	581(100)p		v ₃ (A ₁)
535 w,sh	530(4)	530(3)			v ₉ (E ₂)
490 m		466(15)			
475 sh				v ₁₉ (F ₂)	
	457(49)	456(23)	457(20)dp		v ₁₀ (E ₂)
405 vs					v ₆ (E ₁)
	373 sh	377(5)		v ₈ (E)	
359 s		354(4)			v ₄ (A ₁)
	341(62)	344(52)			v ₇ (E ₁)
		335(5)		v ₁₂ (F ₁)	
255 s	260(2)	260(2)			v ₈ (E ₁)

Table 6. Comparison of Observed and Calculated Frequencies of IOF_6^- , IF_7 and XeF_5^- , Together with Their Approximate Mode Descriptions

$\text{IOF}_6^-(\text{C}_{5v})$					$\text{IF}_7(\text{D}_{3h})^c$					$\text{XeF}_5^-(\text{D}_{3h})$				
assign- ment	approximate mode description	obsd freq, cm^{-1} , int (IR, Ra)	calcd freq, cm^{-1}	LDF	assign- ment	approximate mode description	obsd freq, cm^{-1} , int (IR, Ra)	calcd freq, cm^{-1}	LDF	assign- ment	approximate mode description	obsd freq, cm^{-1} , int (IR, Ra) ^d	calcd freq, cm^{-1}	LDF
A ₁ v ₁	v l=O	873 (vs, 53p)	860 ^b	870	v ₃ (A ₂ '')	v as IF _{2ax}	746 (s, -)	753	710	—	—	—	—	—
v ₂	v lF _{ax}	649 (s, 88p)	625	599	v ₁ (A ₁ ')	v sym IF _{2ax}	676 (-, 20p)	673	630	—	—	—	—	—
v ₃	v sym IF ₅	584 (vs, 100p)	566	537	v ₂ (A ₁ ')	v sym IF ₅	635 (-, 100p)	644	598	v ₁ (A ₁ ')	v sym XeF ₅	502 (-, 100)	498	467
v ₄	δ umbrella IF ₅	359 (s, 4)	371	314	v ₄ (A ₂ '')	δ umbrella IF ₅	365 (s, -)	368	304	v ₂ (A ₂ '')	δ umbrella XeF ₅	290 (m, sh, -)	301	270
E ₁ v ₅	v as IF ₅	585 (vs, v ₃)	583	568	v ₅ (E ₁ ')	v as IF ₅	670 (vs, -)	681	647	v ₃ (E ₁ ')	v as XeF ₅	450 (vs, -)	449	502
v ₆	δ as IF ₅ in plane	405 (vs, -)	415	365	v ₆ (E ₁ ')	δ as IF ₅ in plane	425 (vs, -)	441	377	v ₄ (E ₁)	δ as XeF ₅ in plane	274 (s, -)	273	248
v ₇	δ rock O=l-F _{ax}	341 (-, 62)	340	292	v ₈ (E ₁ '')	δ rock IF _{2ax}	319 (-, 6)	320	259					
v ₈	δ sciss O=l-F _{ax}	260 (s, 2)	273	233	v ₇ (E ₁ ')	δ sciss IF _{2ax}	257 (w, -)	265	213					
E ₂ v ₉	δ sciss IF ₅ in plane	530 (-, 4)	530	486	v ₉ (E ₂ ')	mixture of δ sciss in-plane and v as IF ₅	596 (-, 2)	605	561	v ₅ (E ₂)	v as XeF ₅	423 (-, 16)	420	413
v ₁₀	v as IF ₅	457 (-, 49)	446	421	v ₁₀ (E ₂ '')		510 (-, 17)	515	467	v ₆ (E ₂)	δ sciss XeF ₅ in-plane	377 (-, 23)	373	375
v ₁₁	δ pucker IF ₅	n. obsd	141	111	v ₁₁ (E ₂ '')	δ pucker IF ₅	[68]	59	50 ^e	v ₇ (E ₂ '')	δ pucker XeF ₅	n. obsd	105	79

(a) Frequency values were scaled by an empirical factor of 0.9038. (b) Unscaled frequency value; scaled frequency value is 789 cm^{-1} . (c) Frequency values were scaled by an empirical factor of 0.932. (d) Frequency values were scaled by an empirical factor of 0.8618. (3) Data from ref. 8. (f) Data from ref. 49.

Table 7. Observed and Calculated Geometries of IOF_6^- and the Closely Related IF_7 and XeF_5^-

IOF_6^-				IF_7			XeF_5^-		
	exp ^a	calcd ^a		exp ^b	calcd ^c		exp ^d	calcd	
		ECP	LDF		ECP	LDF		ECP	LDF
r I-O(Å)	1.75-1.77	1.7255	1.791	r I-F _{ax}	1.781	1.7705	r Xe-F _{eq}	2.012	1.9924
r I-F _{ax} (Å)	1.82	1.8087	1.913	r I-F _{eq}	1.857	1.8333		2.077	
r I-F _{eq} (Å)	1.88	1.8819	1.969	∠ F _{ax} -I-F _{eq}	90	90			
∠ O-I-F _{ax} (deg)	94-96	95.76	96.0						

(a) Data from this study. (b) Data from ref. 7. (c) Data from ref. 8. (d) Data from ref. 49.

Table 8. Symmetry Coordinates and Approximate Mode Descriptions for the Pentagonal Bipyramidal IOF_6^- Anion

A ₁	$S_1 = \Delta S$	I=O stretch
	$S_2 = \Delta R$	I-F _{ax} stretch
	$S_3 = \frac{1}{\sqrt{5}} (\Delta r_1 + \Delta r_2 + \Delta r_3 + \Delta r_4 + \Delta r_5)$	IF ₅ sym stretch
	$S_4 = \frac{1}{\sqrt{10}} \left[\sum_{i=1}^5 (\Delta \beta_{i7} - \Delta \gamma_{i6}) \right]$	IF ₅ umbrella deformation
E ₁	$S_{5a} = \sqrt{\frac{2}{5}} [\Delta r_1 + \cos \alpha (\Delta r_2 + \Delta r_5) + \cos 2\alpha (\Delta r_3 + \Delta r_4)]$	IF ₅ asym stretch
	$S_{5b} = \sqrt{\frac{2}{5}} [\sin \alpha (\Delta r_2 - \Delta r_5) + \sin 2\alpha (\Delta r_3 - \Delta r_4)]$	
	$S_{6a} = \sqrt{\frac{2}{5}} [\Delta \alpha_{34} + \cos \alpha (\Delta \alpha_{45} + \Delta \alpha_{23}) + \cos 2\alpha (\Delta \alpha_{15} + \Delta \alpha_{12})]$	IF ₅ in-plane deformation
	$S_{6b} = \sqrt{\frac{2}{5}} [\sin \alpha (\Delta \alpha_{45} - \Delta \alpha_{23}) + \sin 2\alpha (\Delta \alpha_{15} - \Delta \alpha_{12})]$	
	$S_{7a} = \frac{1}{\sqrt{5}} [\Delta \beta_{17} + \cos \alpha (\Delta \beta_{27} + \Delta \beta_{57}) + \cos 2\alpha (\Delta \beta_{37} + \Delta \beta_{47})]$	I-F _{ax} δ wag
	$S_{7b} = \frac{1}{\sqrt{5}} [\sin \alpha (\Delta \beta_{27} - \Delta \beta_{57}) + \sin 2\alpha (\Delta \beta_{37} - \Delta \beta_{47})]$	
	$S_{8a} = \frac{1}{\sqrt{5}} [\Delta \gamma_{16} + \cos \alpha (\Delta \gamma_{26} + \Delta \gamma_{56}) + \cos 2\alpha (\Delta \gamma_{36} + \Delta \gamma_{46})]$	I=O δ wag
	$S_{8b} = \frac{1}{\sqrt{5}} [\sin \alpha (\Delta \gamma_{26} - \Delta \gamma_{56}) + \sin 2\alpha (\Delta \gamma_{36} - \Delta \gamma_{46})]$	
E ₂	$S_{9a} = \sqrt{\frac{2}{5}} [\Delta \alpha_{34} + \cos 2\alpha (\Delta \alpha_{45} + \Delta \alpha_{23}) + \cos \alpha (\Delta \alpha_{15} + \Delta \alpha_{12})]$	IF ₅ in-plane (scissor) deformation
	$S_{9b} = \sqrt{\frac{2}{5}} [\sin 2\alpha (\Delta \alpha_{45} - \Delta \alpha_{23}) - \sin \alpha (\Delta \alpha_{15} - \Delta \alpha_{12})]$	
	$S_{10a} = \sqrt{\frac{2}{5}} [\Delta r_1 + \cos 2\alpha (\Delta r_2 + \Delta r_5) + \cos \alpha (\Delta r_3 + \Delta r_4)]$	IF ₅ asym stretch
	$S_{10b} = \sqrt{\frac{2}{5}} [\sin 2\alpha (\Delta r_2 - \Delta r_5) - \sin \alpha (\Delta r_3 - \Delta r_4)]$	
	$S_{11a} = \frac{1}{\sqrt{5}} [\Delta \beta_{17} - \Delta \gamma_{16}) + \cos 2\alpha (\Delta \beta_{27} - \Delta \gamma_{26} + \Delta \beta_{57} - \Delta \gamma_{56}) + \cos \alpha (\Delta \beta_{37} - \Delta \gamma_{36} + \Delta \beta_{47} - \Delta \gamma_{46})]$	IF ₅ asym out-of-plane deformation (pucker)
	$S_{11b} = \frac{1}{\sqrt{5}} [\sin 2\alpha (\Delta \beta_{27} - \Delta \gamma_{26} - \Delta \beta_{57} + \Delta \gamma_{56}) - \sin \alpha (\Delta \beta_{37} - \Delta \gamma_{36} - \Delta \beta_{47} + \Delta \gamma_{46})]$	

Table 8. *Symmetry Coordinates and Approximate Mode Descriptions for the Pentagonal Bipyramidal IOF_6^- Anion (Continued)*

Redundant Coordinates

$$S_1^0 = \frac{1}{\sqrt{5}} \{ \Delta\alpha_{12} + \Delta\alpha_{23} + \Delta\alpha_{34} + \Delta\alpha_{45} + \Delta\alpha_{51} \} \equiv 0$$

$$S_2^0 = \frac{1}{\sqrt{10}} \left[\sum_{i=1}^5 (\Delta\beta_{i7} + \Delta\gamma_{i6}) \right] \equiv 0$$

$$S_3^0 = \frac{1}{\sqrt{5}} [(\Delta\beta_{17} + \Delta\gamma_{16}) + \cos 2\alpha (\Delta\beta_{27} + \Delta\gamma_{26} + \Delta\beta_{57} + \Delta\gamma_{56}) + \cos \alpha (\Delta\beta_{37} + \Delta\gamma_{36} + \Delta\beta_{47} + \Delta\gamma_{46})] \equiv 0$$

$$S_4^0 = \frac{1}{\sqrt{5}} [\sin 2\alpha (\Delta\beta_{27} + \Delta\gamma_{26} - \Delta\beta_{57} - \Delta\gamma_{56}) - \sin \alpha (\Delta\beta_{37} + \Delta\gamma_{36} - \Delta\beta_{47} - \Delta\gamma_{46})] \equiv 0$$

Table 9. Symmetry Force Constants^a of IOF_6^- Calculated from the Scaled ECP Frequencies of Table 6

A ₁	F ₁₁	F ₂₂	F ₃₃	F ₄₄
	F ₁₁			
	6.077 ^b			
	(4.967) ^c			
	F ₂₂	3.899		
	F ₃₃	0.169	3.656	
	F ₄₄	0.332	0.078	1.725
E ₁	F ₅₅	F ₆₆	F ₇₇	F ₈₈
	F ₅₅			
	3.040			
	F ₆₆	3.246		
	F ₇₇	-0.234	1.087	
	F ₈₈	-0.271	0.085	0.891
E ₂	F ₉₉	F _{10,10}	F _{11,11}	
	F ₉₉			
	2.844			
	F _{10,10}	2.478		
	F _{11,11}	-0.064	0.395	

(a) Stretching constants in mdyne/Å, deformation constants in mdyne Å/rad², and stretch-bend interaction constants in mdyne/rad. (b) Unscaled value (see text). (c) Scaled value.

*Table 10. Revised Assignments, ECP Force Field^a and
Potential Energy Distribution^b for XeF₅⁻*

assignment	approx mode description	freq cm ⁻¹		symmetry force constants	PED
		calcd (ECP)	obsd ^c		
A ₁ v ₁	v sym XeF ₅	498	502	F ₁₁ = 2.775	100(1)
A ₂ " v ₂	δ umbrella	301	290	F ₂₂ = 1.191	100(2)
E ₁ ' v ₃	v asym XeF ₅	449	450	F ₃₃ = 1.6714 F ₃₄ = -0.193	97(3) + 3(4)
	v ₄ δ asym in plane	273	274	F ₄₄ = 1.940	99(4) + 1(3)
E ₂ ' v ₅	v asym XeF ₅	420	423	F ₅₅ = 1.938 F ₅₆ = 0.1191	92(5) + 8(6)
	v ₆ δ in-plane	373	377	F ₆₆ = 1.7505	91(6) + 9(5)
E ₂ " v ₇	δ pucker	105	—	F ₇₇ = 0.2498	100(7)

(a) Force constants calculated with the ECP frequencies; stretching constants in mdyne/Å, deformation constants in mdyne Å/rad², and stretch-bend interaction constants in mdyne/rad. (b) PED in percent. (c) Data from ref. 49.

Table 11. Potential Energy Distribution for IOF_6^-

		freq cm^{-1}	PED (%)
A_1	ν_1	860	87(1) + 7(2) + 5(4)
	ν_2	625	83(2) + 10(3) + 4(1) + 2(4)
	ν_3	566	88(3) + 12(2)
	ν_4	371	100(4)
E_1	ν_5	583	97(5) + 2(8)
	ν_6	415	44(6) + 26(8) + 25(7) + 5(5)
	ν_7	340	58(8) + 42(7)
	ν_8	273	43(8) + 40(7) + 16(6)
E_2	ν_9	530	73(9) + 27(10)
	ν_{10}	446	72(10) + 28(9)
	ν_{11}	141	100(11)

Table 12. Internal Force Constants^{a,b} (mdyn/Å) of IF₇, IOF₆⁻ and XeF₅⁻

	IF ₇	IOF ₆ ⁻	XeF ₅ ⁻
f_R	5.005	3.897	—
f_r	3.947	2.938	2.062
f_π	0.326	0.306	0.198
$f_{\pi'}$	0.0265	0.0536	0.317
f_α	0.847	0.690	0.364
$f_{\alpha\alpha}$	-0.183	-0.147	-0.081
$f_{\alpha\alpha'}$	-0.240	-0.198	-0.102
f_β	0.163		

(a) The deformation constants have been normalized for the following bond distances: IF₇, $r_{I-F_{eq}} = 1.857 \text{ \AA}$; IOF₆⁻, $r_{I-F_{eq}} = 1.877 \text{ \AA}$; XeF₅⁻, $r_{Xe-F} = 2.0124 \text{ \AA}$. (b) f_π and $f_{\pi'}$ denote coupling to adjacent and opposite bonds, respectively, and f_α and $f_{\alpha\alpha'}$ coupling to adjacent and opposite bond angles, respectively.

Table 13. Atomic Populations (*e*) in the Valence Electron Orbitals and
Total Charge Distributions for XeF_5^- , IF_7 and IOF_6^-

Central Atom		XeF_5^-	IF_7	IOF_6^-	
s		2.22	1.35	1.43	
$p_x = p_y$		0.61	0.64	0.64	
p_z		2.02	0.60	0.71	
d_z^2		0.03	0.11	0.14	
$d_x^2 = d_y^2$		0.06	0.12	0.09	
d_{xy}		0.14	0.20	0.16	
$d_{xz} = d_{yz}$		0.04	0.14	0.15	
d total		0.37	0.83	0.78	
Equatorial Fluorines					
s		1.98	1.93	1.94	
p bond		1.70	1.57	1.64	
p in plane		1.98	1.96	1.97	
p_z		1.97	1.94	1.95	
d		0	0.03	0.02	
Axial Fluorines and Oxygens				F	O
s	—		1.92	1.92	1.86
p_z	—		1.54	1.57	1.16
$p_x = p_y$	—		1.94	1.95	1.83
d	—		0.04	0.03	0.04
Total Charges					
Central Atom		2.25	2.94	2.71	
F_{eq}		-0.63	-0.43	-0.53	
F_{ax}		—	-0.39	-0.44	
O_{ax}		—	—	-0.74	

Figure Captions

Figure 1. Packing diagram of $\text{N}(\text{CH}_3)_4^+\text{IOF}_6^-$ viewed along the c -axis.

Figure 2. The structure of the IOF_6^- anion showing the puckering pattern of the equatorial fluorine ligands.

Figure 3. The ^{19}F NMR spectrum (470.599 MHz) of a saturated solution of $\text{N}(\text{CH}_3)_4^+\text{IOF}_6^-$ in CH_3CN at -40°C . (A) F_{eq} environment of IOF_6^- ; (B) F_{ax} environment of IOF_6^- ; (C) F-trans-to-O environment of $\text{cis-IO}_2\text{F}_4^-$ impurity.

Figure 4. Vibrational spectra of $\text{N}(\text{CH}_3)_4^+\text{IOF}_6^-$. Trace A, infrared spectrum of the solid as an AgBr disk; traces B and C, Raman spectra of the solid at 25 and -146°C ; traces D and E, Raman spectra of the CH_3CN solution with parallel and perpendicular polarization, respectively.

Figure 5. Internal Coordinates for IOF_6^- .

Figure 6. A comparison of the structure of IOF_6^- with those of closely related hexa- and hepta-coordinated iodine fluorides and oxyfluorides.

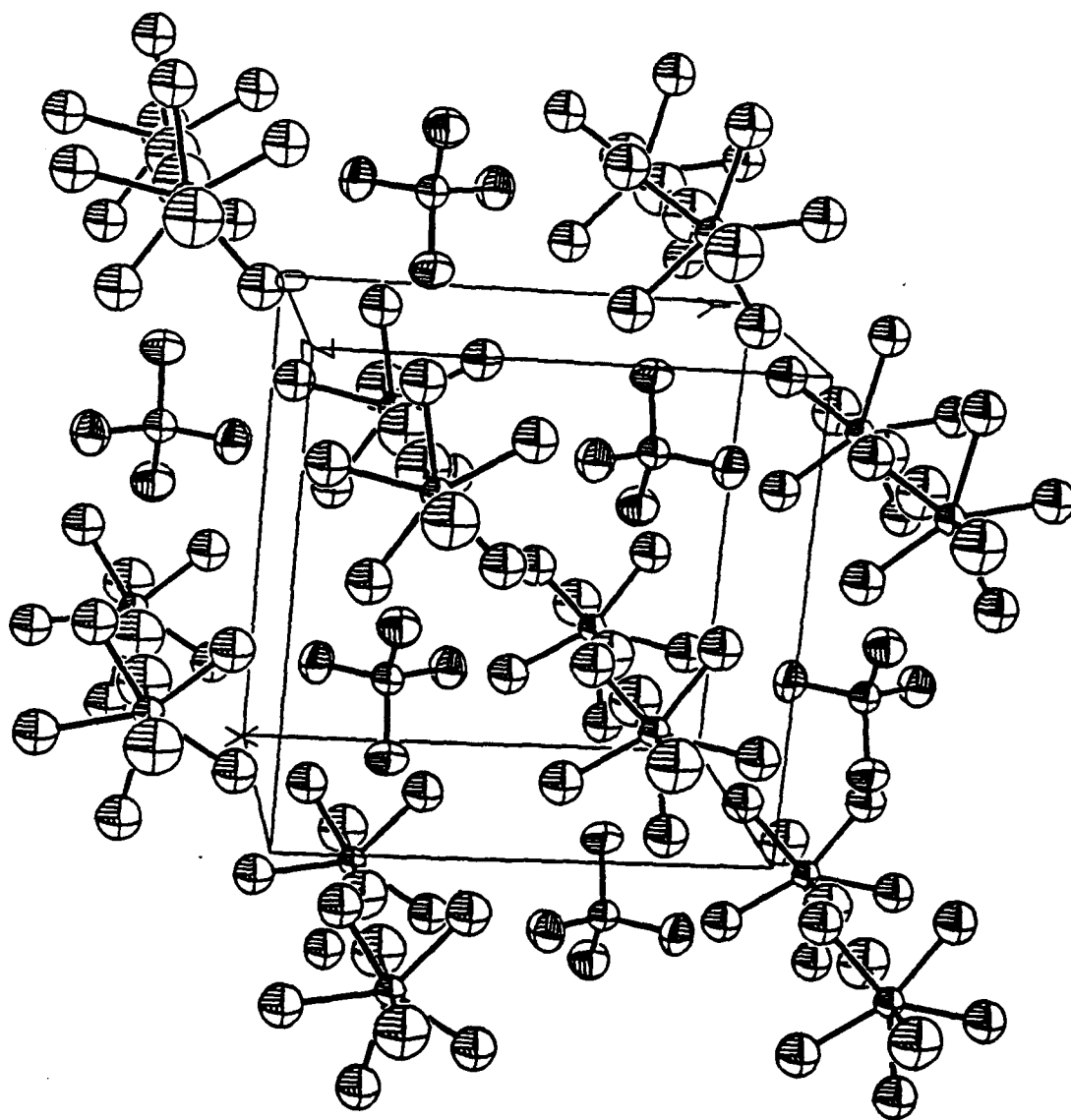


Figure 1.

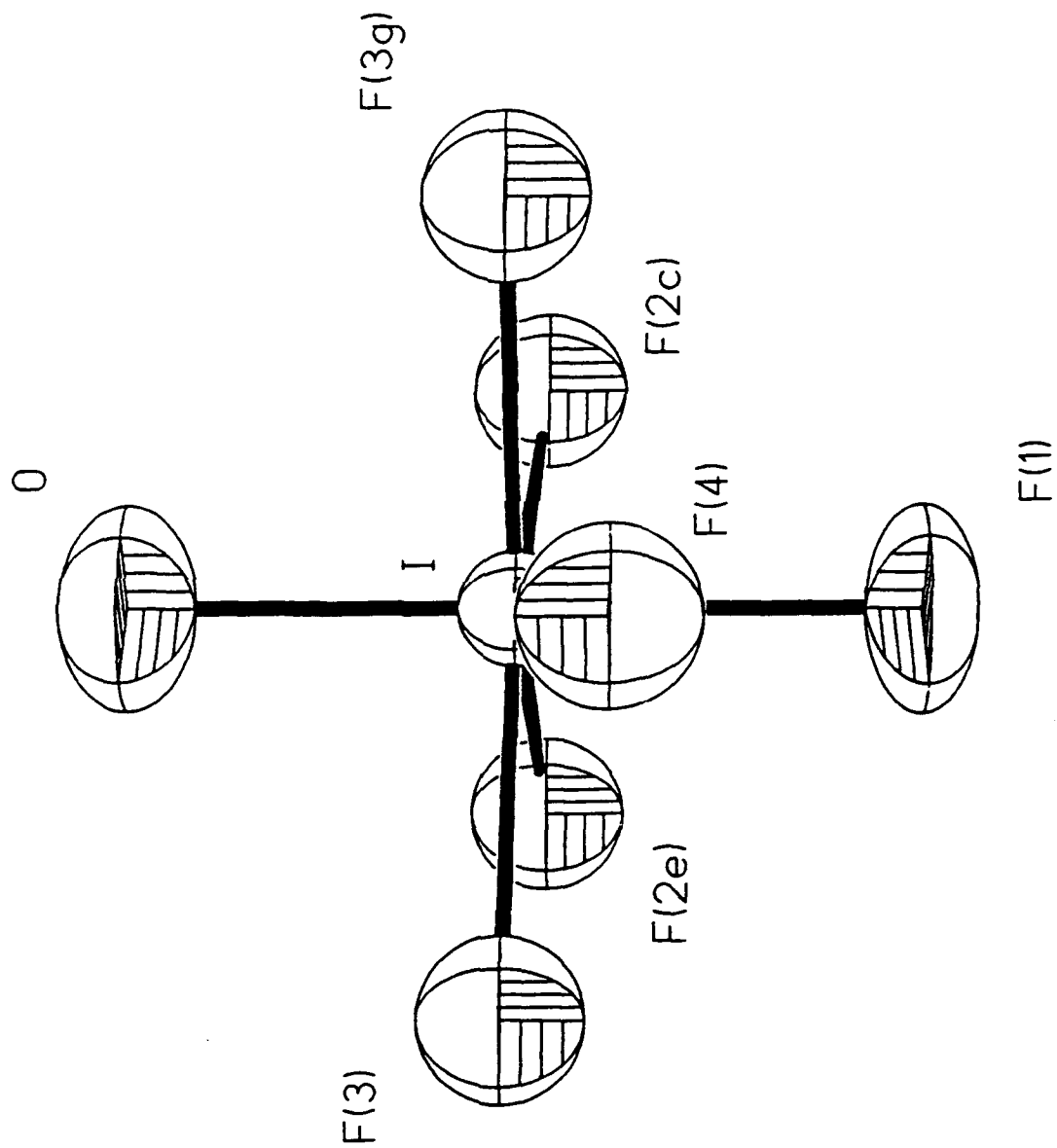


Figure 2.

A

5000 Hz

1000 Hz

B

C

170

160

150

140

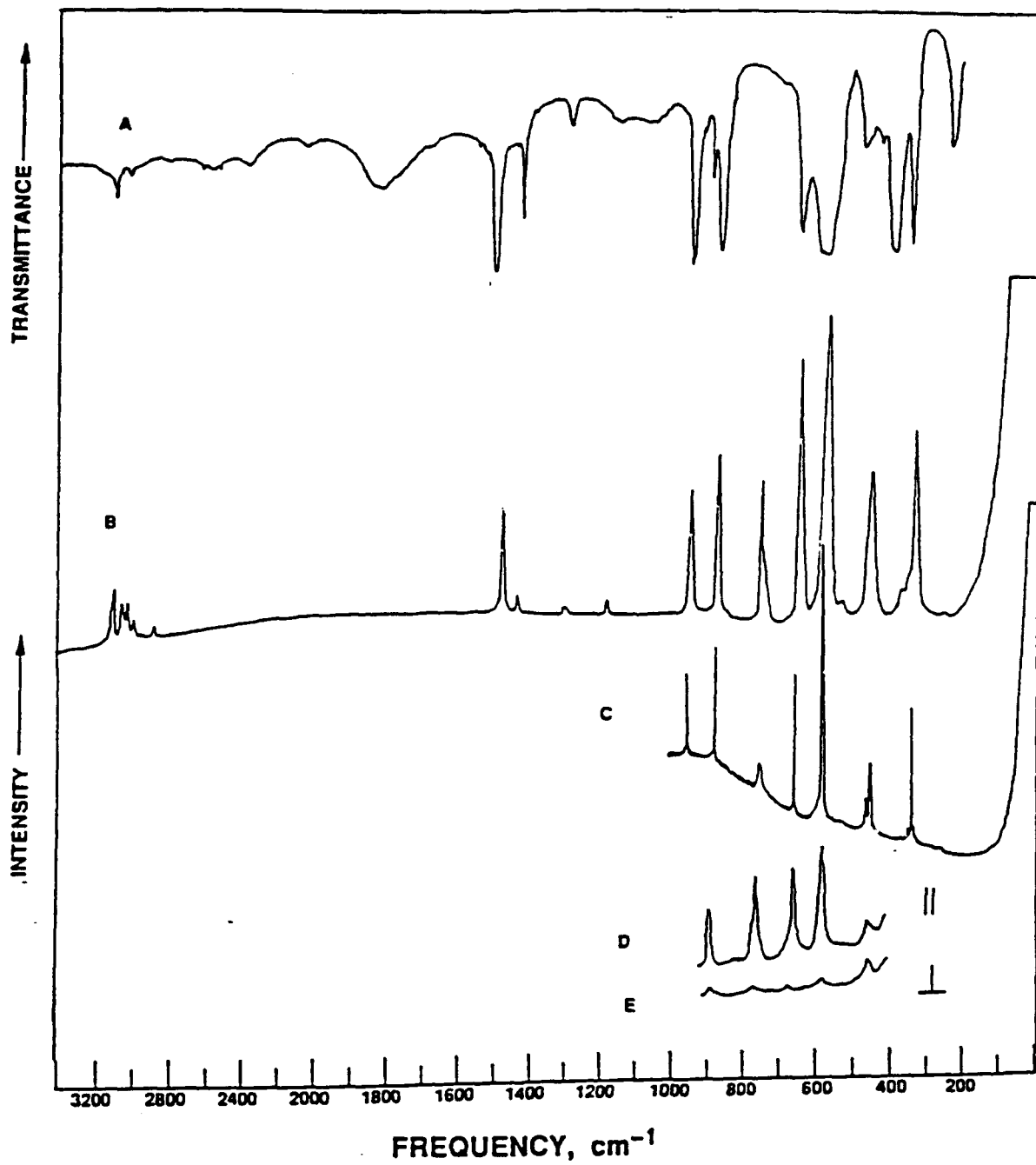
130

120

110

 $\delta_{^{19}\text{F}}$ (ppm from CFCl_3)

Figure 3.



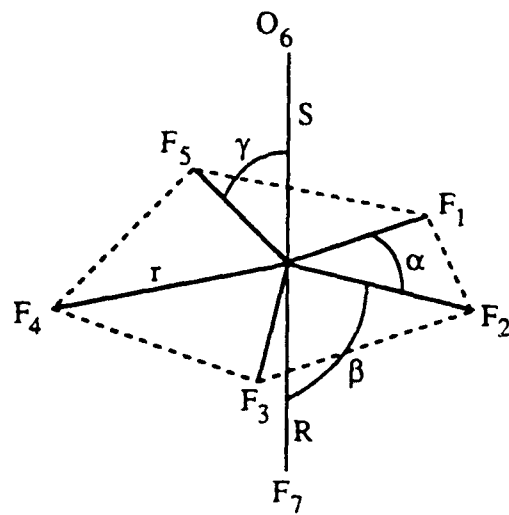
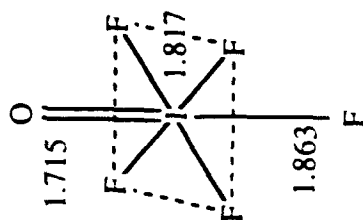
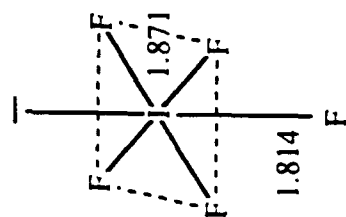
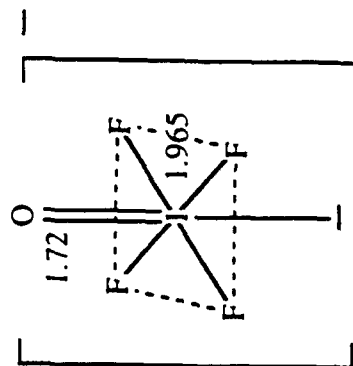
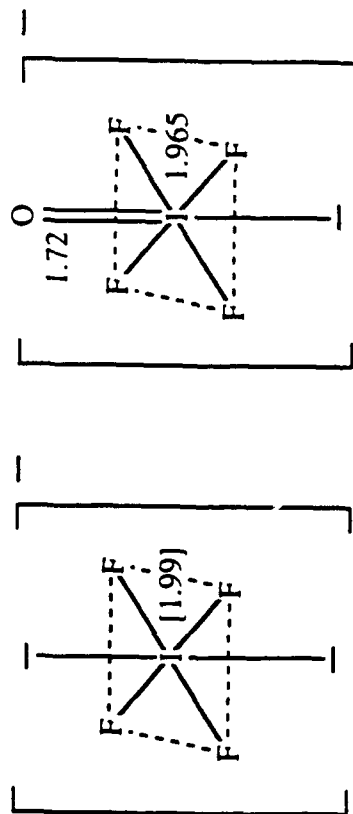
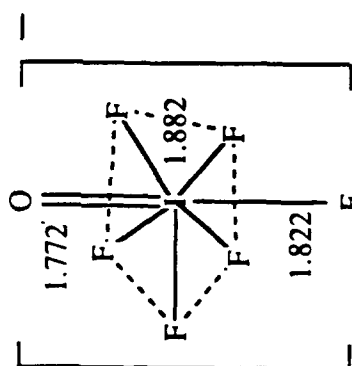
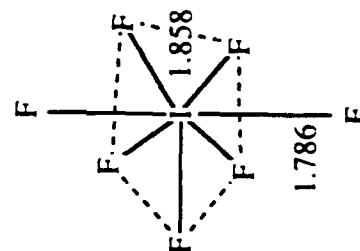
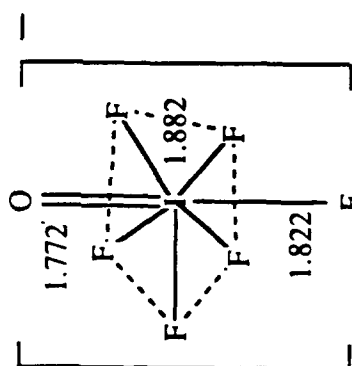
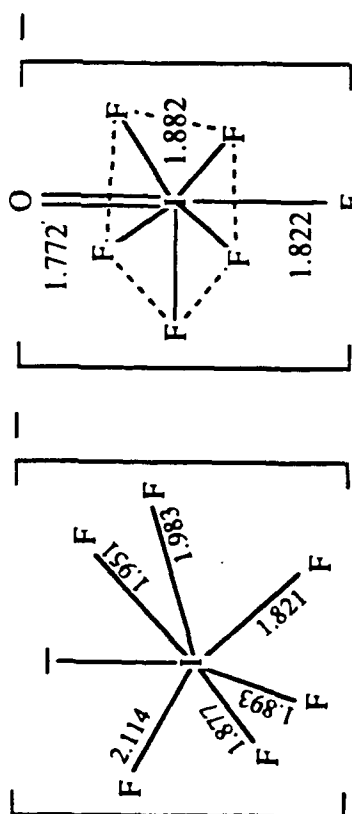


Figure 5.



CN6



CN7

Figure 6.

PART VII
THE $\text{F}_6\text{TeC}\equiv\text{N}^-$ ANION AND $\text{F}_5\text{TeC}\equiv\text{N}$

ABSTRACT

The recent synthesis of truly anhydrous $N(CH_3)_4F$ has facilitated the synthesis of high-coordination, high-oxidation state main-group anions. Heptacoordinated and octacoordinated $Te(VI)$ anions have been reported recently, including TeF_7^- , TeF_8^{2-} and TeF_6O^{2-} . These anions exhibit D_{3h} , D_{4d} and C_{3v} symmetry, respectively.

The preparation of three different substituted analogs of TeF_7^- was attempted by using the electronegative $OTeF_5$, OCF_3 and CN ligands to replace the fluorine ligands.

The preparation of $OTeF_5$ substituted analogs of TeF_7^- , namely $TeF_{7-x}(OTeF_5)_x$ ($x = 0, 2, 5$), was attempted by oxidative addition of F or $OTeF_5$ ligands to pentacoordinated $Te(IV)$ precursors in SO_2ClF solvent. Fluorine-19 NMR spectroscopy indicated negative results in each attempt.

The preparation of $TeF_6OCF_3^-$ was attempted but abandoned due to insufficient yields in the preparation of the $Te(VI)$ precursor TeF_5OCF_3 . Two attempts were made at preparing TeF_5OCF_3 , including its preparation by reacting TeF_4 with CF_3OF , but both were unsuccessful.

The preparation of the monocyano-substituted analog of TeF_7^- , namely TeF_6CN^- anion, was achieved in a non-oxidative ligand transfer process. In CH_3CN solvent, TeF_7^- reacted with $(CH_3)_3SiCN$ at $-45^\circ C$ to produce a 3.5 % yield of TeF_6CN^- . The product began to decompose into $Te(VI)$ and $Te(IV)$ species at $-22^\circ C$; the decomposition was complete at room temperature. In order to attain a higher yield of TeF_6CN^- , the preparation of its logical precursor, namely TeF_5CN , was attempted, and preliminary evidence indicates the experiment was successful. In CH_3CN solvent, TeF_6 and $(CH_3)_3SiCN$ were combined at $-20^\circ C$ to produce a ca. 8 % yield of TeF_5CN . This product was stable at room temperature.

ACKNOWLEDGEMENTS

I would like to thank my supervisor, Dr. Gary Schrobilgen, for his extensive assistance in both researching and preparing this work. His guidance and support often extended beyond what was required.

I would like to give equal thanks to Dr. Jeremy Sanders, who helped to guide me through my research with his experimental expertise. Were it not for his assistance, and good humour for that matter, my thesis work would not have been accomplished.

I also wish to thank my coworkers in the laboratory, Dr. Adel Emara, Dr. Helene Mercier, Ayaaz Pirani, Scott Tsai, Marc Whalen, and especially Mark Adams, who doubled as my chauffeur.

INTRODUCTION

CONTRASTS BETWEEN THE CHEMISTRY OF Te(VI) FLUORO- AND OXOFLUORO- DERIVATIVES AND THOSE OF S(VI) AND Se(VI); A BRIEF SURVEY

Tellurium is a fifth row element which exhibits a chemistry that is, in several aspects, distinct from that of the lighter chalcogens. For the chalcogen group in general, as the atomic radius increases there is an increase in the metallic character of the element, an increase in the tendency to form anionic compounds such as SeCl_6^{2-} , TeBr_6^{2-} , and PoI_6^{2-} , and a decrease in the stability of its compounds in high formal oxidation states.¹

The compounds SF_6 , SeF_6 and TeF_6 are octahedrally coordinated, but due to the different sizes of the central chalcogen atoms, their chemical properties are significantly different. Sulfur hexafluoride, for example, is inert to attack by bases owing to the lack of available d-orbitals to provide an opportunity for expansion of the valence shell upon coordination of a seventh ligand such as OH or H_2O . In contrast to SF_6 , both SeF_6 and TeF_6 are susceptible to attack by bases, forming heptacoordinated intermediate species. In the case of Te(VI), hepta- and octacoordinate species have been isolated.^{2,3}

The pentafluorooxochalcogen(VI) acids are virtually spherical with the thermal stabilities of the acids HOXF_5 varying considerably.⁴ The acid, HOSF_5 , is stable to reduction of coordination only up to -60°C because of the high bond energy of HF and the favourable formation of pentacoordinate SOF_4 , while HOSeF_5 is stable to reduction of coordination up to 290°C .⁴ Since Te(VI) is the most stable hexavalent state among the chalcogens, the acid HOTeF_5 is, not surprisingly, the most stable of the three acids. The acids HOSeF_5 and HOTeF_5 can be converted into salts, with HOTeF_5 being more easily converted than HOSeF_5 due to the lower oxidizing power of Te(VI).

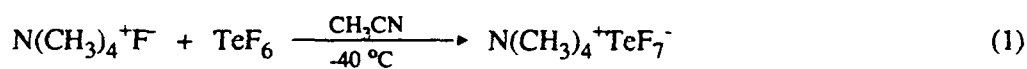
A characteristic property of neutral Te(VI) compounds is their strong preference for octahedral coordination,⁵ whereas tetra- and hexacoordinate sulfur and selenium compounds are both prevalent.⁶ The Te(VI) compounds are, in general, thermodynamically stable with high vapour pressures. Interestingly, double bonds to Te(VI) do not occur, including $\text{Te}=\text{O}$, owing to the propensity of Te(VI) to increase its coordination number and hence become octahedrally coordinated.⁶ This tendency is clearly illustrated by the hydrolytic behaviour of TeF_6 where pentacoordinate $\text{O}=\text{TeF}_4$ might be expected as a product,⁷⁻⁸ or by the HF solvolysis of $\text{Te}(\text{OH})_6$, in which almost all of the pseudo-octahedral $(\text{HO})_x\text{TeF}_{6-x}$ ($x = 0 - 5$) intermediates have been detected.⁸⁻¹¹ The monomer, $\text{O}=\text{TeF}_4$, has not been observed, but is always found as the oxygen bridged dimer

(F₄TeO)₂ in which the Te atoms are octahedrally coordinated.^{12,13} In contrast, SOF₄ and SeOF₄ exist as trigonal bipyramidal monomers having O=X bonds, although above -100 °C SeOF₄ dimerizes to form (F₄SeO)₂.^{13,14}

TELLURIUM(VI) AT THE LIMITS OF COORDINATION; THE TeF₇⁻, TeF₈²⁻ AND TeOF₆²⁻ ANIONS

The recent syntheses of novel seven and eight coordinate Te(VI), I(VII) and Xe(VI) fluoro- and oxofluoro-anions have been facilitated by the development of a preparative scale synthesis of truly anhydrous N(CH₃)₄⁺F⁻ by Christie and coworkers.¹⁵ This salt has proven to be an excellent source of naked F⁻ ion as well as a very effective reagent in preparing high-oxidation state fluoro- and oxofluoro-anions. It not only functions as an excellent fluoride ion source, but the complex anions that are formed are stabilized by the large oxidatively resistant N(CH₃)₄⁺ cation. Owing to the relatively high solubilities of N(CH₃)₄⁺ salts in solvents such as CH₃CN and CHF₃,² NMR and vibrational structural studies can be performed as well as X-ray structural determinations on single crystals. Another important discovery was that CH₃CN and CHF₃, along with the N(CH₃)₄⁺ cation, have good kinetic stability toward strong oxidizers such as I(VII) and Xe(VI) compounds.^{2,16}

Recently, there have been several studies reporting the formation of high-valent, high coordination number fluoro- and oxofluoro-anions of the main-group elements. The TeF₇⁻ anion, which was first isolated as N(CH₃)₄⁺TeF₇⁻, has a pentagonal bipyramidal D_{5h} structure, as predicted by the VSEPR model.² The reaction proceeds quantitatively in CH₃CN at -40 °C



After removal of the solvent *in vacuo*, the product was isolated as a stable white crystalline solid at room temperature.² The room temperature ¹²⁵Te NMR spectrum of this salt in CH₃CN showed a binomial octet arising from the one-bond spin-spin coupling between the central ¹²⁵Te and seven chemically equivalent ¹⁹F ligands, and established that all seven fluoride ligands are rendered equivalent on the NMR time scale by means of a facile intramolecular exchange process. The ¹⁹F NMR spectrum of TeF₇⁻ is also consistent with a fluxional process in which the axial and equatorial fluorine environments are rendered equivalent, and consists of a singlet with ¹²⁵Te satellites. The fluxional behavior of the TeF₇⁻ anion is therefore consistent with that of the isoelectronic IF₇ molecule, which also exhibits a single fluorine resonance in its ¹⁹F NMR spectrum.¹⁷

The fluxional behaviour of the isoelectronic IF₇ and TeF₇⁻ species, which are both AX₇ species in the

VSEPR notation, probably results from the fact that AX_7 species can adopt one of three geometries: pentagonal bipyramidal, capped octahedral, or capped trigonal prismatic.¹⁸ The energy differences among these three geometries are quite small, and it is hypothesized that there could be facile interconversion between these three geometries on account of these small energy separations. The vibrational spectra of TeF_7^- have been assigned, and are in agreement with the pentagonal bipyramidal D_{5h} geometry. Since the vibrational time scale is approximately 10^6 times faster than the NMR time scale, the pentagonal bipyramidal geometry appears to be the energetically favoured structure.

The octacoordinated TeF_8^{2-} anion, as well as the isostructural IF_8^- anion, could adopt one of three structures: a cube of symmetry O_h , which is unlikely due to steric interactions; a dodecahedron of symmetry D_{2d} ; or a square antiprism of symmetry D_{4d} .² Due to the low solubility of this anion in CH_3CN solvent, ^{19}F NMR characterization has not been possible. Vibrational spectroscopy indicates that both anions possess D_{4d} symmetry.

The TcF_6O^{2-} anion has a distorted pentagonal bipyramidal structure, possessing C_{5v} symmetry; the Raman and infrared spectra of $[N(CH_3)_4^+]_2TeF_6O^{2-}$ indicate that the oxygen is in an axial position, resulting in two types of fluorine ligand.¹⁶ This anion has not been observed in solution by ^{19}F NMR spectroscopy due to its low solubility and tendency to dissociate into F^- and $OTeF_5^-$. Presumably, the five equatorial fluorine ligands should not be coplanar with the central tellurium atom, but rather slightly displaced away from the apical oxygen atom (see below for a discussion of IOF_6^-).¹⁶

The geometries of TeF_7^- , TeF_8^{2-} and TeF_6O^{2-} are given in Figure 1.

OTHER HYPERVALENT, HIGH-COORDINATION NUMBER FLUORO- AND OXOFLUORO-MAIN GROUP ANIONS

The ClF_6^- , BrF_6^- , IF_6^- , XeF_5^- , IOF_6^- , XeF_7^- , IF_8^- , and XeF_8^{2-} anions have all been synthesized recently as their $N(CH_3)_4^+$ salts, using $N(CH_3)_4^+F^-$ as the source of fluoride ion.^{13,16,19-24}

Raman spectroscopy has shown both ClF_6^- and BrF_6^- , which are AX_6E species in the VSEPR notation, to be octahedral in structure exhibiting negligible symmetry distortion,²⁰⁻²² thereby contradicting the VSEPR model in that the non-bonding electron pair in each molecule is not sterically active.²⁵ The X-ray crystal

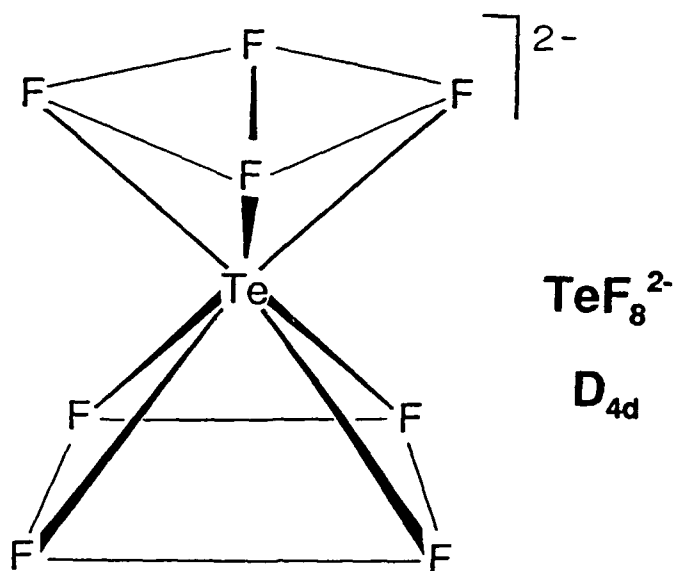
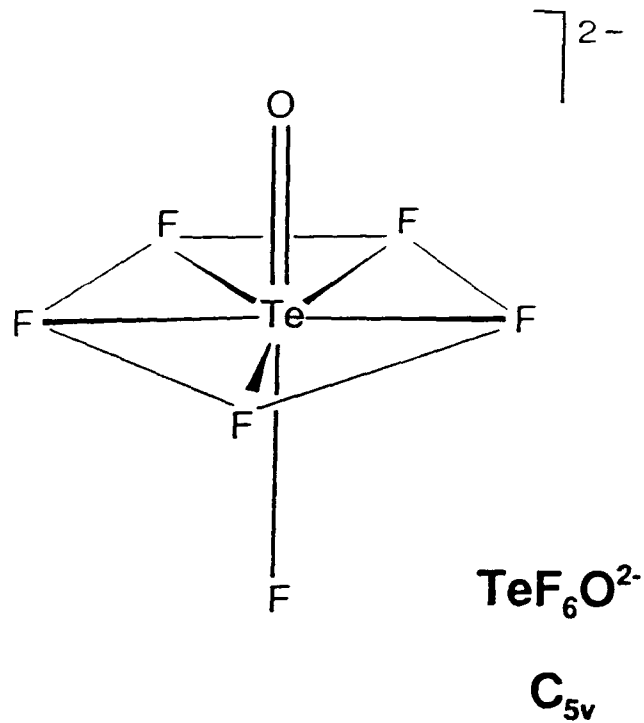
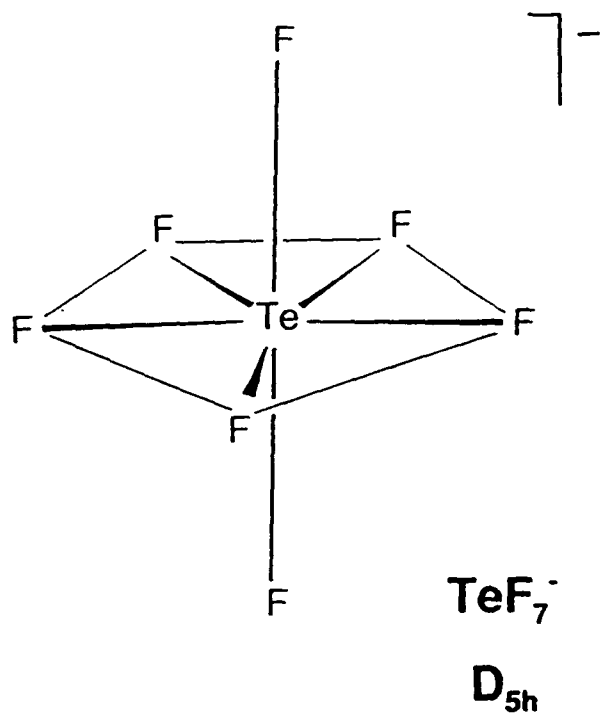


Figure 1. Geometries of TeF_7^- , TeF_8^{2-} and $\text{TeF}_6\text{O}^{2-}$.

structure of CsBrF_6 also shows that the anion exists as an almost perfect octahedron. Although BrF_6^- was found to be octahedral on the vibrational time scale, it appears to be fluxional on the NMR time scale, displaying only a singlet in the ^{19}F NMR spectrum of the anion,^{21,22} which can only be explained if dissociative fluoride ligand exchange is taking place. These studies suggest that chlorine and bromine cannot accommodate more than six electron pairs in their valence shells. Thus, the stereochemical inactivity of the lone pair in both ClF_6^- and BrF_6^- results from crowding in their respective valence shells.

In contrast, the solution Raman spectrum of IF_6^- indicates that this anion is a distorted octahedron having an electron pair that is stereochemically active on the vibrational time scale.²² The ^{19}F NMR spectrum consists of a singlet suggesting a fluxional process on the NMR time scale; the lack of observable I-F spin-spin coupling indicates the lack of a rigid octahedral structure or dissociative fluoride exchange.²² The crystal structure of the NO^+ salt consists of a fluoride-bridged tetramer, while the low-temperature crystal structure of the $\text{N}(\text{CH}_3)_4^+$ salt was obtained from a twinned crystal.²³ The structure of IF_6^- in $\text{N}(\text{CH}_3)_4^+\text{IF}_6^-$ differs from those of ClF_6^- in $\text{N}(\text{CH}_3)_4^+\text{ClF}_6^-$ and BrF_6^- in $\text{N}(\text{CH}_3)_4^+\text{BrF}_6^-$ by having a sterically active free valence electron pair which produces a distorted octahedral geometry around I of near C_{3v} symmetry.

The XeF_5^- and IOF_6^- anions have been shown by X-ray crystallography, vibrational spectroscopy and NMR spectroscopy to have pentagonal planar and pentagonal bipyramidal geometries, respectively,^{2,16} with XeF_5^- providing the first example of an AX_5E_2 geometry. The ^{129}Xe NMR spectrum of XeF_5^- consists of a binomial sextet, while the ^{19}F NMR spectrum consists of a singlet, indicating five equivalent fluorine ligands.¹⁶ The crystal structure of $\text{N}(\text{CH}_3)_4^+\text{XeF}_5^-$ shows that the anion has D_{5h} symmetry. Interestingly, there appears to be no puckering of the five equatorial fluorine ligands, although puckering is observed in the seven coordinate IF_7 molecule, which also possesses five equatorial fluorine ligands.^{2,17} The lack of fluxional behaviour in XeF_5^- can be attributed to the presence of two axial electron lone pairs, which exert a larger repulsive force as compared with axial fluorine ligands. The steric crowding of the planar fluorine ligands is also alleviated by the more polar, and therefore elongated, Xe-F bond length (2.012 Å), as compared with the Xe-F bond length in XeF_4 (1.953 Å).²⁶ This is attributable to the formal negative charge in the XeF_5^- anion.¹⁶ The IOF_6^- anion is isostructural and isoelectronic with the $\text{TeF}_6\text{O}^{2-}$ anion, and therefore possesses C_{5v} symmetry. The ^{19}F NMR spectrum of IOF_6^- consists of a binomial doublet and a sextet, indicating an oxygen in the axial position.^{2,3} Thus, unlike TeF_7^- and IF_7 , IOF_6^- does not undergo intramolecular ligand exchange on the NMR time scale.

The X-ray crystal structure of the $\text{N}(\text{CH}_3)_4^+$ salt shows that the five equatorial fluorine atoms are not coplanar with the central iodine atom, rather they are slightly displaced away from the oxygen atom and towards the axial fluorine ligand.³ Initially it was thought that the equatorial fluorine ligands were not puckered, but recent work has shown that the equatorial ligands are indeed puckered; the most recent X-ray data suggests that there are, in fact, three different $\text{F}_{\text{eq}}\text{-I-O}$ bond angles, not one as previously thought.²⁷

Unlike ClF_6^- and BrF_6^- , the XeF_7^- anion has a non-bonding electron pair that appears to be stereochemically active in the valence shell.¹⁹ Raman spectroscopy indicates that this anion has a structure based on a square antiprismatic geometry (C_{2v} symmetry) with the lone pair replacing the eighth ligand.¹⁹ The ^{129}Xe NMR spectrum shows Xe coupled to seven equivalent fluorine ligands. Thus, like IF_7 and TeF_7^- , this anion is also fluxional on the NMR time scale.²⁷

The crystal structure of $(\text{NO}^+)_2\text{XeF}_8^{2-}$ shows that the XeF_8^{2-} anion possesses an almost perfect square antiprismatic geometry, having D_{4d} symmetry.²⁸ The anion exhibits a stereochemically inactive valence lone pair, which is supported by Raman spectroscopy.¹⁹ This inactivity is due to steric limitations in the eight-coordinate valence shell, analogous to the situation in the BrF_6^- anion.

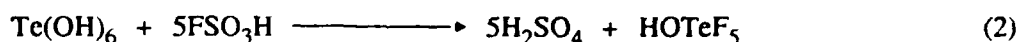
The IF_8^- anion, as previously mentioned, exhibits D_{4d} symmetry according to Raman and infrared spectroscopy. The crystal structure of the $[\text{NO}(\text{NOF}_2)]^+$ salt shows that the anion has square antiprismatic geometry, which is consistent with the vibrational data.²³

THE CHEMISTRY OF THE OTeF_5 LIGAND

The most ubiquitous Te(VI) ligand is the univalent OTeF_5 group, systematically called pentafluorooxotellurate(VI). The ligand is large, oxidatively resistant, and very weakly basic.⁶ Main-group elements from every period are known to form derivatives containing the OTeF_5 ligand.⁶ In particular, the usefulness of this ligand stems from its ability to stabilize high-oxidation state compounds, which is unsurpassed by any other polyatomic ligand.⁶ The effective group electronegativity of OTeF_5 on the Pauling scale is 3.88, and is therefore just slightly smaller than that of fluorine itself, which has an electronegativity of 4.00.²⁹ The high effective electronegativity of the OTeF_5 group results from the inductive effect of five electronegative fluorines withdrawing electron density from the central tellurium atom, which in turn withdraws electron density from the oxygen by means of backbonding to tellurium. The formation of xenon derivatives is testimony to the

high effective electronegativity of the OTeF_5 group, and is evidenced by the resistance of OTeF_5 to oxidative attack by xenon in the neutral compounds $\text{Xe}(\text{OTeF}_5)_2$, $\text{Xe}(\text{OTeF}_5)_4$ and $\text{O}=\text{Xe}(\text{OTeF}_5)_4$.³⁰⁻³² The OTeF_5 group forms the only known analogs of XeF_4 , XeOF_4 , KrF_2 and the most stable analog of XeF_2 .⁶

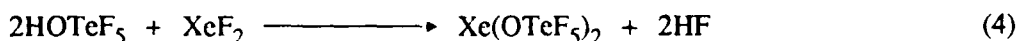
The precursor to the OTeF_5 ligand is pentafluorooorthotelluric acid, HOTeF_5 , which is a moderately strong monoprotic acid ($\text{pK}_a = 9.2$)³³. The acid strength of HOTeF_5 in glacial acetic acid is between HCl and HNO_3 , and is indicative of the strong inductive effect of the five fluorine ligands attached to the tellurium atom.³⁴ It is prepared under anhydrous conditions according to equation (2).³⁵



As has already been noted, the structure of this acid is pseudo-octahedral.⁶ The acid has a high melting point and a significant vapour pressure at room temperature, which is consistent with its near spherical shape. Above 310°C , HOTeF_5 decomposes to HF and a number of $\text{Te}(\text{IV})$ and $\text{Te}(\text{VI})$ species, including $(\text{TeOF}_4)_n$, TeF_6 and TeF_4 .¹³ The ^{19}F NMR spectrum of HOTeF_5 consists of an AB_4 spin system, indicating that the $\text{Te}-\text{O}$ bond rotates freely on the NMR time scale. Thus, there is no evidence for $\text{H}-\text{F}$ intramolecular bridging arising from the short equatorial fluorine-hydrogen distance (238 pm) on the NMR time scale.⁶

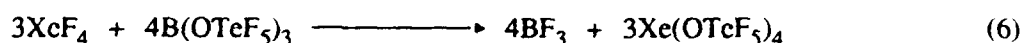
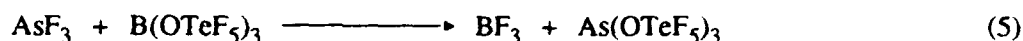
The distinguishing feature between F and OTeF_5 ligand chemistry is that OTeF_5 ligands rarely form bridges, while F ligands often do; this characteristic is due to the large ligand size and to the internal bonding of the OTeF_5 ligand, which renders it weakly coordinating.⁶ These characteristics are evidenced by the fact that the majority of the covalent $\text{Te}(\text{VI})$ and OTeF_5 derivatives are molecular and have high vapour pressures which allow them to be readily sublimed.

There are a variety of methods which can be used to prepare OTeF_5 derivatives. The precursor for the synthesis of all OTeF_5 derivatives is HOTeF_5 . A common route to the preparation of OTeF_5 derivatives involves displacement of a hydrogen halide³⁶⁻³⁹



The products of the above reactions are themselves useful as OTeF_5 ligand transfer reagents and also provide

two important pathways for introducing an OTeF_5 ligand into a compound. Pentafluorooxotellurate(VI) can be introduced non-oxidatively by reaction of an element fluoride with $\text{B}(\text{OTeF}_5)_3$, the most widely used and convenient OTeF_5 transfer reagent; for example^{31,40}



The use of $\text{B}(\text{OTeF}_5)_3$ as a transfer reagent is particularly effective in that volatile BF_3 is produced as a product of the OTeF_5 group transfer, and is easily removed under vacuum. Pentafluorooxotellurate(VI) can also be introduced oxidatively, and this is most easily accomplished by using a noble gas-containing oxidizer such as $\text{Xe}(\text{OTeF}_5)_2$.^{5,41}



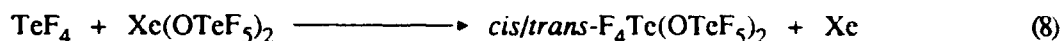
This type of reaction also produces xenon gas, which is volatile and easily removed under vacuum, and thus provides another clean synthetic route.

TELLURIUM DERIVATIVES CONTAINING THE OTeF_5 LIGAND

The tetrakis OTeF_5 derivative of TeF_4 has a pseudo-trigonal bipyramidal (disphenoidal) structure,⁴² in which the axial and equatorial OTeF_5 groups undergo rapid intramolecular exchange between the axial and equatorial sites.⁴³ The ^{125}Te NMR spectrum of $\text{Te}(\text{OTeF}_5)_4$ in both CH_3CN and SO_2ClF solvents at room temperature consists of a doublet of quintets in the Te(VI) region, resulting from Te-F_{ax} and Te-F_{eq} coupling in the exchange-averaged axial and equatorial OTeF_5 ligands.⁴³ The ^{125}Te NMR spectrum also shows only one Te(VI)-Te(IV) coupling at room temperature, and therefore indicates the presence of four equivalent rapidly exchanging OTeF_5 groups. Upon cooling to -127°C in SO_2ClF , the rapid intramolecular exchange is slowed sufficiently for the two Te(VI) environments to be observed in the ^{19}F and ^{125}Te NMR spectra.⁴³

The mixed F/ OTeF_5 derivatives, $\text{TeF}_{4-x}(\text{OTeF}_5)_x$ ($x = 1 - 3$), resulting from ligand redistribution among TeF_4 and $\text{Te}(\text{OTeF}_5)_4$ also exhibit rapid intramolecular exchange at room temperature, which cannot be slowed down even upon cooling to the freezing point of the solvent SO_2ClF .⁴³ The ^{125}Te NMR spectra of these

compounds show, in the Te(IV) region, a singlet for $\text{Te}(\text{OTeF}_5)_4$, a doublet for $\text{TeF}(\text{OTeF}_5)_3$, and a binomial triplet for $\text{TeF}_2(\text{OTeF}_5)_2$.⁴³ A mixture of *cis/trans*- $\text{F}_4\text{Te}(\text{OTeF}_5)_2$ is produced by oxidative addition of $\text{Xe}(\text{OTeF}_5)_2$ to TeF_4 at 110 °C.⁵



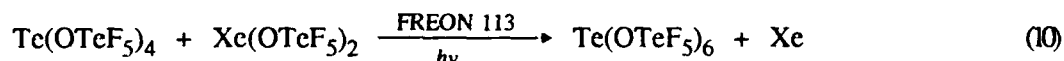
It can be assumed that this reaction proceeds through the formation of OTeF_5 radicals, which oxidize TeF_4 to the hexavalent state.⁵ The ^{19}F NMR spectrum of the *cis*-isomer shows partly overlapping A_2B_2 and AB_4 patterns; the A_2B_2 pattern results from two pairs of non-equivalent fluorines bonded to the tellurium, while the AB_4 pattern results from the axial and equatorial fluorine ligands of the equivalent OTeF_5 groups.⁵

The tetrakis- OTeF_5 derivatives of TeF_6 are synthesized in Freon 113 at -10 °C.⁵



The ^{19}F NMR spectrum of *cis*- $\text{F}_2\text{Te}(\text{OTeF}_5)_4$ shows two distinct AB_4 patterns, indicating two non-equivalent OTeF_5 groups, while the ^{19}F NMR spectrum of *trans*- $\text{F}_2\text{Te}(\text{OTeF}_5)_4$ shows only one AB_4 pattern, indicative of four equivalent OTeF_5 ligands whose oxygens are coplanar. There is no evidence of isomerization between the *cis*- and *trans*-isomers.⁵ The *mer*- $\text{F}_3\text{Te}(\text{OTeF}_5)_3$ isomer is also present as a product in the mixture derived from reaction (9); the characteristic AB_2 pattern of this molecule is observed in the ^{19}F NMR spectrum. When $\text{Te}(\text{OTeF}_5)_4$ is allowed to react with XeF_2 instead of F_2 , inexplicably the major product is $\text{FTe}(\text{OTeF}_5)_5$ with some *cis*- $\text{F}_2\text{Te}(\text{OTeF}_5)_4$, but none of the *trans*-isomer.⁵ The ^{19}F NMR spectrum of $\text{FTe}(\text{OTeF}_5)_5$ shows two different AB_4 patterns in a 1:4 ratio, as well as a singlet from the fluorine ligand attached to the central tellurium.⁵

The fully substituted compound, $\text{Te}(\text{OTeF}_5)_6$, is easily produced in Freon 113 solvent at room temperature upon irradiation of the solution with a 500-W high pressure mercury lamp⁵

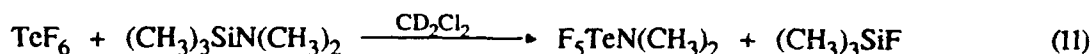


The reaction can also be effected thermally. The central tellurium in $\text{Te}(\text{OTeF}_5)_6$ is bonded octahedrally to the six oxygen atoms of the $-\text{OTeF}_5$ ligands, which are themselves almost octahedral in shape.

OTHER TELLURIUM(VI) DERIVATIVES

Compounds of the general formula TeF_5X are known where X is OH ,^{8,11,44} OCl ,⁴⁵ OCF_3 ,⁴⁶ OCH_3 ,^{47,48} OF ,⁴⁹ NCO ,⁵⁰ Cl ,⁵¹ Br ,⁵² NH_2 ,⁵³ N_3 ,⁵⁴ $\text{N}(\text{CH}_3)_2$,⁵⁴ and a variety of other highly substituted alkoxy species.^{48,55}

The reaction of TeF_6 and $(\text{CH}_3)_3\text{SiN}(\text{CH}_3)_2$ is easily facilitated at 0°C in anhydrous CD_2Cl_2 , producing compounds of the series $\text{TeF}_x[\text{N}(\text{CH}_3)_2]_{6-x}$ ($x = 1 - 5$) in small quantities;⁵⁴ for the product series $\text{TeF}_x[\text{N}(\text{CH}_3)_2]_{6-x}$, which were identified using ^{19}F NMR spectroscopy, the value of x depends on the molar ratio of $\text{TeF}_6 : (\text{CH}_3)_3\text{SiN}(\text{CH}_3)_2$.⁵⁴ For a 1 : 1 reaction mixture, $x = 1$



The reaction of TeF_6 with $(\text{CH}_3)_3\text{SiN}_3$ in a 2 : 1 molar ratio proceeds partially to give a 1 : 1 product ratio of TeF_5N_3 and *cis*- $\text{TeF}_4(\text{N}_3)_2$ after a one day reaction period. The reaction of TeF_6 with $(\text{CH}_3)_3\text{SiN}_3$ in a 1:4 molar ratio gives all members of the series $\text{TeF}_x\text{X}_{6-x}$ ($x = 1 - 5$) except *mer*- TeF_3X_3 ; the TeF_6 is completely consumed.⁵⁴ With the N_3 ligand, reduction over time occurs to give a hitherto unidentifiable $\text{Te}(\text{IV})$ species, while the products of $\text{X} = \text{N}(\text{CH}_3)_2$ decomposed to a grey powder after several hours of reaction above 0°C .⁵⁴

Pentafluorotellurium hypochlorite, ClOTeF_5 , is efficiently produced according to reaction (12)⁵⁶



The low temperature reaction of ClOTeF_5 with the fluorocarbon iodides, CF_3I , $\text{C}_2\text{F}_5\text{I}$, and *n*- $\text{C}_3\text{F}_7\text{I}$ results in the formation of $\text{RI}(\text{OTeF}_5)_2$ in high yield.⁴⁶ The latter two are stable, while the trifluoromethyl derivative decomposes above -78°C to give a 17 % yield of CF_3OTeF_5 .⁴⁶ The perfluoroethyl and perfluoro-*n*-propyl compounds decompose at 120°C , or under UV radiation, to give $\text{C}_2\text{F}_5\text{OTeF}_5$ and *n*- $\text{C}_3\text{F}_7\text{OTeF}_5$, respectively.⁴⁶

NUCLEAR MAGNETIC RESONANCE SPECTROSCOPY

Nuclear Magnetic Resonance spectroscopy is one of the most useful techniques for gathering structural information on fluoro-tellurium (main-group) species. This technique is especially useful for low-temperature structural determinations on fluoro-tellurium compounds, many of which are labile at ambient temperature. The presence of several naturally occurring spin $\frac{1}{2}$ isotopes, such as ^{125}Te , ^{19}F , and ^{13}C , facilitates a thorough analysis of the products of reactions between fluoro-tellurium and carbon-containing species.

From NMR spectra, one can use data pertaining to chemical shifts and coupling constants, which can traverse a number of bonds in some cases, to arrive at the gross molecular structure. The NMR-active isotopes which are relevant to this work, and some of their properties, are listed in Table 1.⁵⁷

GOALS OF THE PRESENT WORK

The main goal of this research is to explore the limits of the coordination ability of Te(VI), namely, to produce the heptacoordinated Te(VI) anionic analogs of TeF_7^- , which, in the main, are derivatives of the OTeF_5 group. Three attempts to prepare heptacoordinated analogs of TeF_7^- will be attempted, each with a different ligand; namely OTeF_5 , OCF_3 , and CN .

The syntheses of the novel heptacoordinated Te(VI) anions $\text{TeF}_n(\text{OTeF}_5)_{7-n}^-$, ($n = 0, 2, 7$), will be attempted in oxidative-addition ligand-transfer reactions using the pentacoordinated Te(IV) precursors $\text{N}(\text{C}_2\text{H}_5)_4^+\text{Te}(\text{OTeF}_5)_5^-$ or $\text{N}(\text{C}_4\text{H}_9)_4^+\text{TeF}_5^-$, as the Te(IV) source, in order to verify the capability of the large, highly electronegative OTeF_5 ligand to participate in heptacoordination to Te(VI). The respective neutral analogs of the above heptacoordinated anions, namely $\text{TeF}_2(\text{OTeF}_5)_4$, $\text{TeF}_4(\text{OTeF}_5)_2$, and $\text{Te}(\text{OTeF}_5)_6$ are well characterized and stable. The syntheses of anions related to those above have been attempted previously by Seppelt,⁵⁸ but in a non-oxidative manner, and were not successful.

The syntheses of the novel heptacoordinated Te(VI) anions $\text{F}_6\text{TeOCF}_3^-$ and F_6TeCN^- will be attempted in non-oxidative ligand-transfer reactions with Te(VI) precursors, again in order to determine the ability of the OCF_3 and CN ligands to participate in heptacoordination to Te(VI). The Te(VI) precursor to $\text{TeF}_6\text{OCF}_3^-$, TeF_5OCF_3 , has been prepared previously in low yield (ca. 17 %)⁴⁶ and characterized by infrared and ^{19}F NMR spectroscopy, while the obvious Te(VI) precursor to TeF_6CN^- , namely TeF_5CN , is not known; thus, its preparation will also be attempted.

Table 1. NMR Properties of Nuclides Relevant to This Work⁵⁷

<u>ISOTOPE</u>	<u>SPIN</u>	<u>N.A., %^a</u>	<u>Ξ, MHz^b</u>	<u>γ, 10⁷rad/sT^c</u>
¹ H	$\frac{1}{2}$	99.985	100.00	26.7522
¹³ C	$\frac{1}{2}$	1.108	25.145	6.7283
¹⁹ F	$\frac{1}{2}$	100.00	94.094	25.1815
²⁹ Si	$\frac{1}{2}$	4.70	19.867	-5.3190
¹²³ Tc	$\frac{1}{2}$	0.87	26.170	-7.0576
¹²⁵ Tc	$\frac{1}{2}$	6.99	31.550	-8.5087

a Natural abundance.

b Frequencies are relative to the protons of Si(CH₃)₄, which resonate at exactly 100 MHz ($B_0 = 2.349$ T).

c Magnetogyric ratio.

EXPERIMENTAL SECTION

MATERIALS The solvents CH_3CN (HPLC Grade Caledon Laboratories), CH_2Cl_2 (Caledon Laboratories), and SO_2ClF (Columbia Organic Chemicals) were purified and dried according to the literature methods.⁵⁹⁻⁶¹ The reagents XeF_2 ,⁶² $(\text{C}_2\text{H}_5)_4\text{N}^+\text{OTeF}_5^-$,⁶³ TeF_4 ,⁶⁴ ClF ,⁶⁵ TeF_6 ,⁶⁶ $(\text{C}_2\text{H}_5)_4\text{N}^+\text{Te}(\text{OTeF}_5)_5^-$,⁶³ $(\text{C}_4\text{H}_9)_4\text{N}^+\text{TeF}_5^-$ ⁶⁷ and $(\text{CH}_3)_4\text{N}^+\text{TeF}_7^-$ ² were prepared according to the literature methods. Other reagents used were F_2 (Air Products), $\text{Te}(\text{OH})_6$ (BDH), HSO_3F (Allied Chemical), BCl_3 (Matheson), COF_2 (Matheson), CF_3I (K & K), CsF (Merck) and $(\text{CH}_3)_3\text{SiCN}$ (Aldrich). The CsF was dried by fusion in a platinum crucible at red heat, immediately placed in the dry box port and evacuated while cooling, and ground in the dry box.

APPARATUS The air- and moisture-sensitive natures of the precursors and products required that all manipulations be carried out under anhydrous conditions. Nonvolatile materials were handled in the dry atmosphere of a dry box (Vacuum Atmospheres Model DLX) equipped with cryogenic wells, as previously described.^{68,69} Volatile materials were handled in glass (Pyrex) and metal (316 stainless steel/nickel, fluoroplastic, FEP, and Kel-F) vacuum lines (Figures 2 and 3). Pressures were measured at ambient temperature on the glass vacuum line using a mercury manometer. Pressures were measured at ambient temperature on the metal vacuum line using an MKS Model PDR-5B digital readout with pressure transducers having wetted inconel surfaces.

NUCLEAR MAGNETIC RESONANCE SPECTROSCOPY The ^{19}F NMR spectra were recorded unlocked (field drift, 0.1 Hz h^{-1}) with a Bruker AM-500 spectrometer equipped with a 11.744-T cryomagnet and an Aspect 3000 computer. The ^{19}F NMR spectra were obtained by using a 5-mm combination $^1\text{H}/^{19}\text{F}$ probe operating at 470.599 MHz. Typical parameters for the acquisition of the ^{19}F NMR spectra are given in Table 2.

The ^{13}C and ^{125}Te NMR spectra were obtained using a broad-band VSP probe tunable over the range of 23-202 MHz. The ^{13}C spectra were recorded at 125.759 MHz while the ^{125}Te NMR spectra were recorded at 157.792 MHz. Typical acquisition parameters for these two nuclides are listed in Table 2.

The ^{19}F NMR spectra were referenced to a neat external sample of CFCl_3 at ambient temperature; the

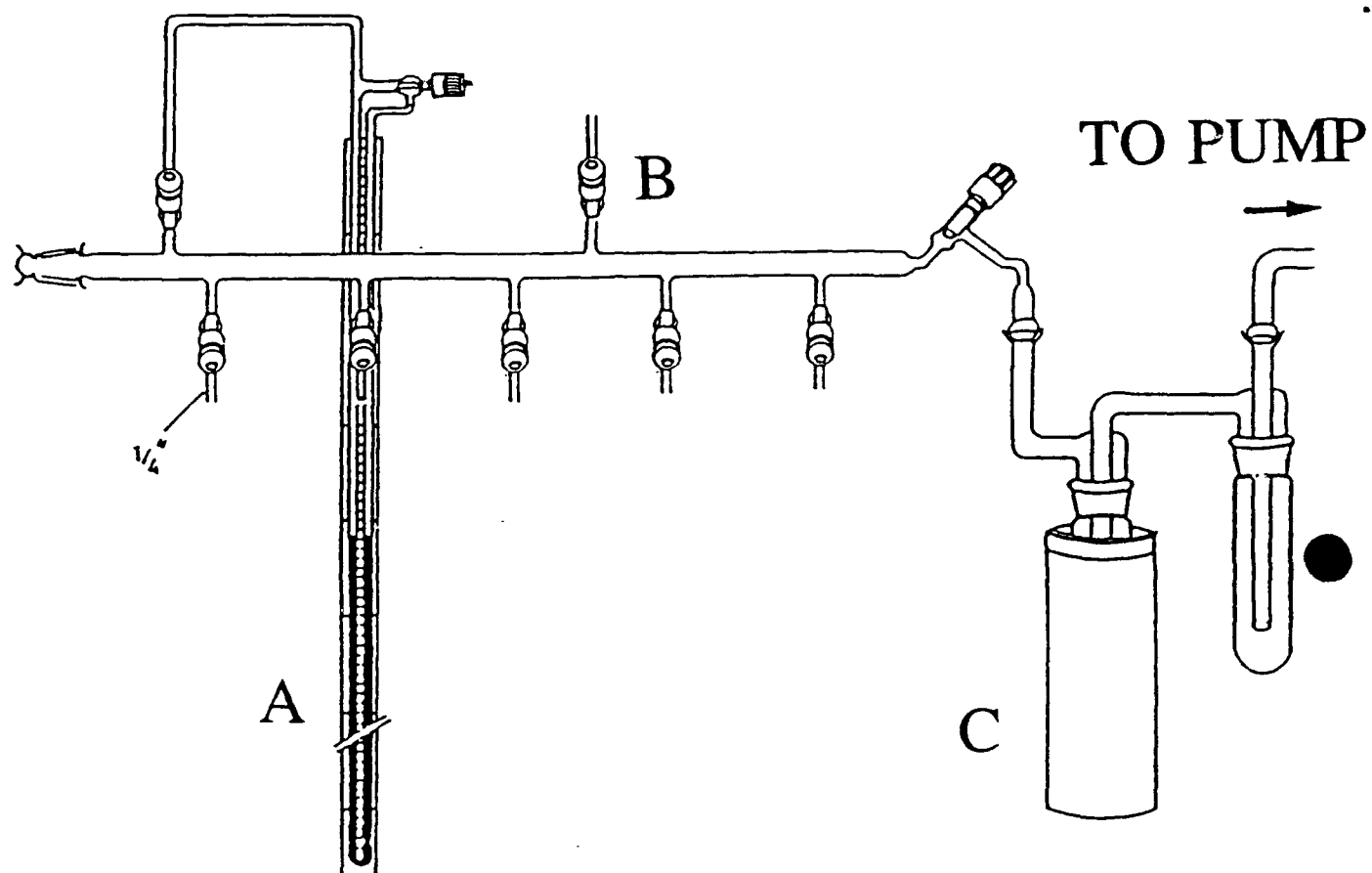


Figure 2. Pyrex glass vacuum line; (A) mercury manometer; (B) dry N₂ inlet; (C) liquid N₂ trap.

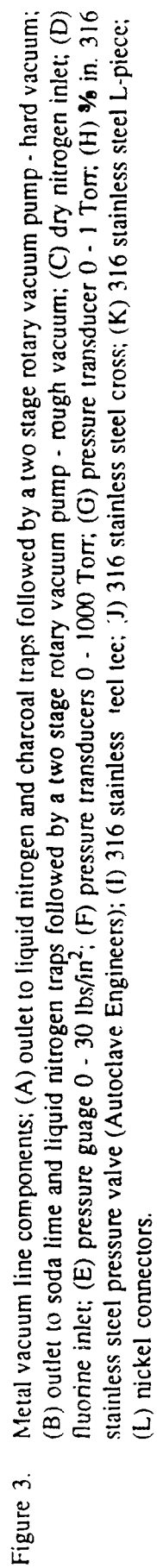


Table 2. Typical Acquisition Parameters for ^{13}C , ^{19}F and ^{125}Te NMR Spectroscopy

<u>ACQUISITION PARAMETER</u>	<u>^{13}C</u>	<u>^{19}F</u>	<u>^{125}Te</u>
1) Reference standard	$\text{Si}(\text{CH}_3)_4$	CFCl_3	$\text{Te}(\text{CH}_3)_2$
2) Spectrometer frequency ^a (MHz)	125.759	470.599	157.792
3) Data point resolution (Hz/d.p.)	3.6	1.79 - 3.05	6.1
4) Spectral width (kHz)	30	30 - 50	100
5) Memory size (Kb)	16	32	32
6) Pulse width (μs)	6.4	1.00	18.0
7) Line Broadening (Hz)	2	0	6
8) Number of transients	20,000	1000 - 5000	50,000
9) Acquisition Time (s)	0.278	0.557-0.327	0.166

a At a field strength of 11.744 T frequencies are relative to the protons of $\text{Si}(\text{CH}_3)_4$, which resonate at 500.137 MHz.

^{125}Te spectra were referenced similarly to $\text{Te}(\text{CH}_3)_2$ at ambient temperature, and the ^{13}C spectra were referenced to a neat sample of $\text{Si}(\text{CH}_3)_4$. The chemical shift convention used is that a positive sign signifies a chemical shift to high frequency of the reference compound.

Fluorine-19 and ^{13}C NMR samples were prepared in ca. 30 cm lengths of AWG 9 (ca. 4-mm o.d., 0.8-mm wall) FEP plastic tubing, which was heat sealed at one end with an open end flared (45° SAE) and joined, by means of a compression fitting, to a Kel-F valve. The NMR samples for ^{125}Te NMR spectroscopy were prepared similarly to the ^{19}F NMR samples, except that 9-mm o.d. (1.5-mm wall) FEP plastic tubing was used instead. The 9-mm NMR sample tubes were made by molding 10-mm o.d. FEP tubing into 9-mm o.d. tubing using a heated brass mold. The NMR samples were placed in Wilmad glass tubes (5-mm o.d. thin wall for ^{19}F ; 10-mm o.d. precision thin wall for ^{125}Te) for insertion into the NMR probes.

For low temperature NMR measurements, samples were usually warmed only sufficiently to liquify and solubilize the reagents. Samples were precooled to the approximate temperature of the NMR probe, inserted into the probe and allowed to equilibrate while spinning prior to data acquisition.

PREPARATION OF HOTeF_5 ³⁵ Finely ground $(\text{HO})_6\text{Te}$ (72.05 g, 313.8 mmol) was loaded into the reaction bulb (Figure 4); the entry point to the bulb (A) was sealed with a B-19 glass cap using halocarbon wax. The apparatus was attached to a glass vacuum line and evacuated for 24 hours. The apparatus was pressurized with 1 atm. N_2 , removed from the glass vacuum line, and placed in a fumehood. In a glove bag with a N_2 atmosphere, 130 ml (2.27 mmol) of crude HSO_3F was measured into a weight buret. The buret was removed from the glove bag and attached to the reaction bulb via a side outlet. The reaction bulb was immersed in a dry ice/acetone bath, and the HSO_3F added slowly in a dropwise manner with constant stirring of the resultant mixture. Upon completion of the HSO_3F addition, the reaction bulb was removed from the bath and allowed to warm to room temperature. At this point the reaction mixture was a thick opaque white liquid suspension.

The upper glass cup of the reaction apparatus (B) was filled with a dry ice/acetone slush, and the condenser (C) covered with a J-cloth cooled with liquid N_2 . The reaction flask was heated gently using a heating mantle. As the reaction mixture refluxed, the solution became clear. The first fraction distilled at 30°C , and was condensed by cooling the J-cloth using liquid N_2 . When a sufficient amount of HOTeF_5 had accumulated, the J-cloth was removed and the condenser gently warmed in order to melt product so that it could flow into the receiving

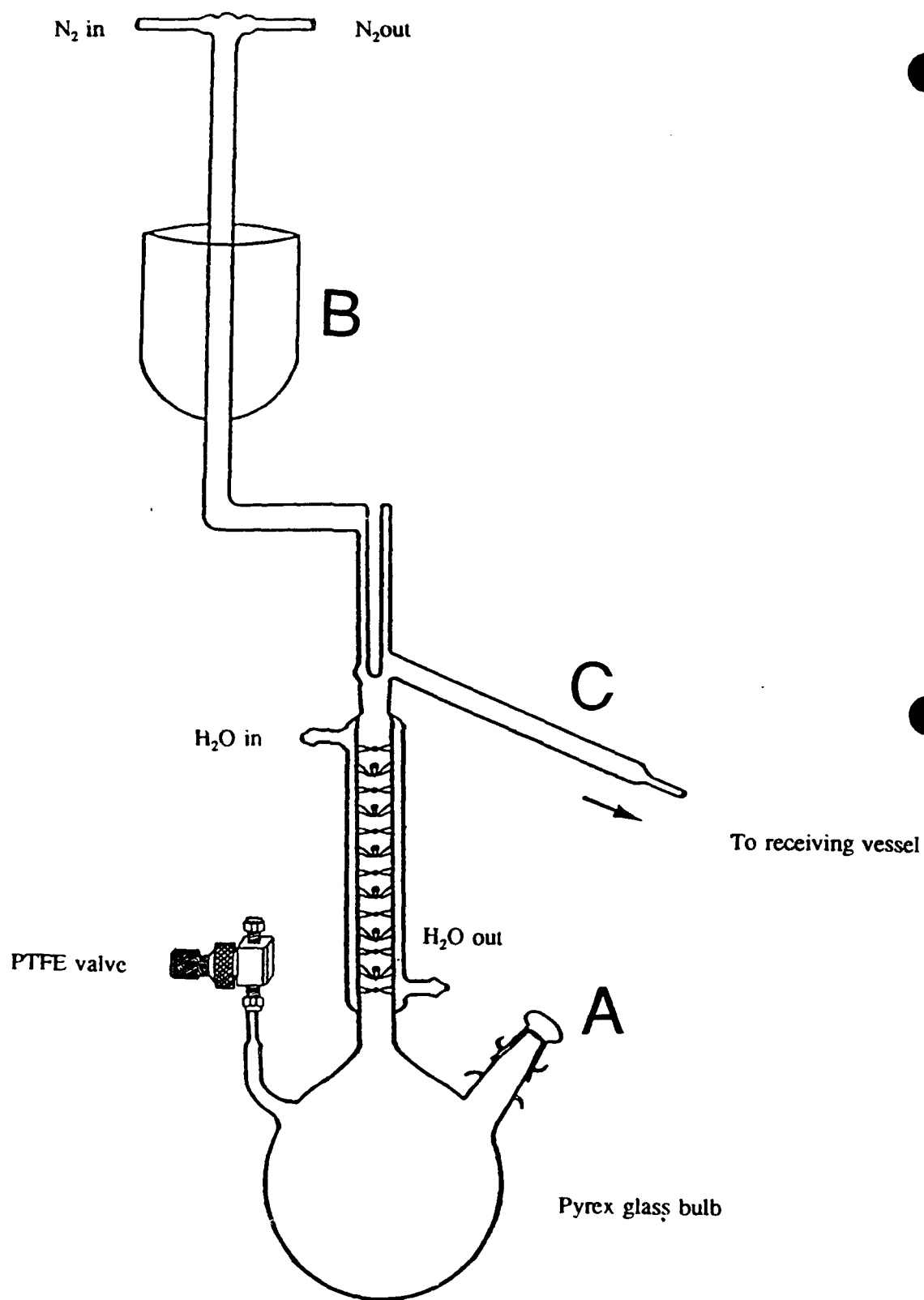


Figure 4. Apparatus for the preparation of HOTeF_5 .

vessel. This process was repeated until the vapour temperature reached 95 °C, at which point the distillation was halted.

The crude HOTeF_5 was distilled *in vacuo* at -196 °C from the receiving vessel into a sublimator (Figure 5) containing concentrated H_2SO_4 (125 ml). A portion of previously prepared impure HOTeF_5 was added to this sample, by vacuum distillation on the glass vacuum line, for purification purposes. The sublimator was removed from the vacuum line to the fume hood, and immersed in a hot oil bath. The cold finger of the sublimator was cooled by passing cold water through it. The sublimation was performed overnight at 100 - 145 °C. The sublimator was attached to the glass vacuum line, and the HOTeF_5 was distilled into a pre-weighed FEP tube equipped with a Kel-F valve. The resultant solid white product displayed premelting on warming to room temperature, and was therefore judged to be impure.

A purification apparatus was constructed (Figure 6) in order to remove the liquid impurity, using $\text{Et}_4\text{N}^+\text{OTeF}_5^-$ as the purification reagent. The crude HOTeF_5 was vacuum distilled on to the solid $\text{Et}_4\text{N}^+\text{OTeF}_5^-$ in (a) at -196 °C. After warming to room temperature, the resulting clear liquid was allowed to react for ca. 24 hours. The repurified HOTeF_5 was vacuum distilled into the same pre-weighed FEP tube. Some premelting was still apparent in the sample.

Owing to the addition of extra crude HOTeF_5 from a previous preparation at the purification stage, no true yield could be reported. The FEP tube was pressurized with dry N_2 and stored at room temperature until used.

PREPARATION OF $\text{B}(\text{OTeF}_5)_3$ ^{36,37} Pentafluorooxotelluric acid (57.67 g, 240.7 mmol) was distilled *in vacuo* into a reaction vessel constructed from a 500 mL Schott Pyrex glass bulb and equipped with a glass/Teflon Rotoflo stopcock at -196 °C. In order to prevent any of the premelted HOTeF_5 from transferring during the distillation, the bottom of the FEP tube containing the HOTeF_5 was immersed in an ice/water bath. Redistilled BCl_3 was condensed *in vacuo* in three aliquots (9.411 g, 80.32 mmol) into a 3 mL graduated glass tube. Each aliquot was prepared by distilling ca. 3 mL of BCl_3 into the preweighed graduated glass tube at -78 °C. The graduated tube was weighed (after BCl_3 had been distilled into it) and then attached to a Y-piece connecting the reaction vessel containing the HOTeF_5 to the vacuum line. The BCl_3 was vacuum distilled on to the HOTeF_5 at -196 °C. Upon completion of each of the three BCl_3 transfers, the reaction vessel was slowly allowed to warm to room temperature. Gaseous HCl was evolved as the reactants were allowed to warm. The

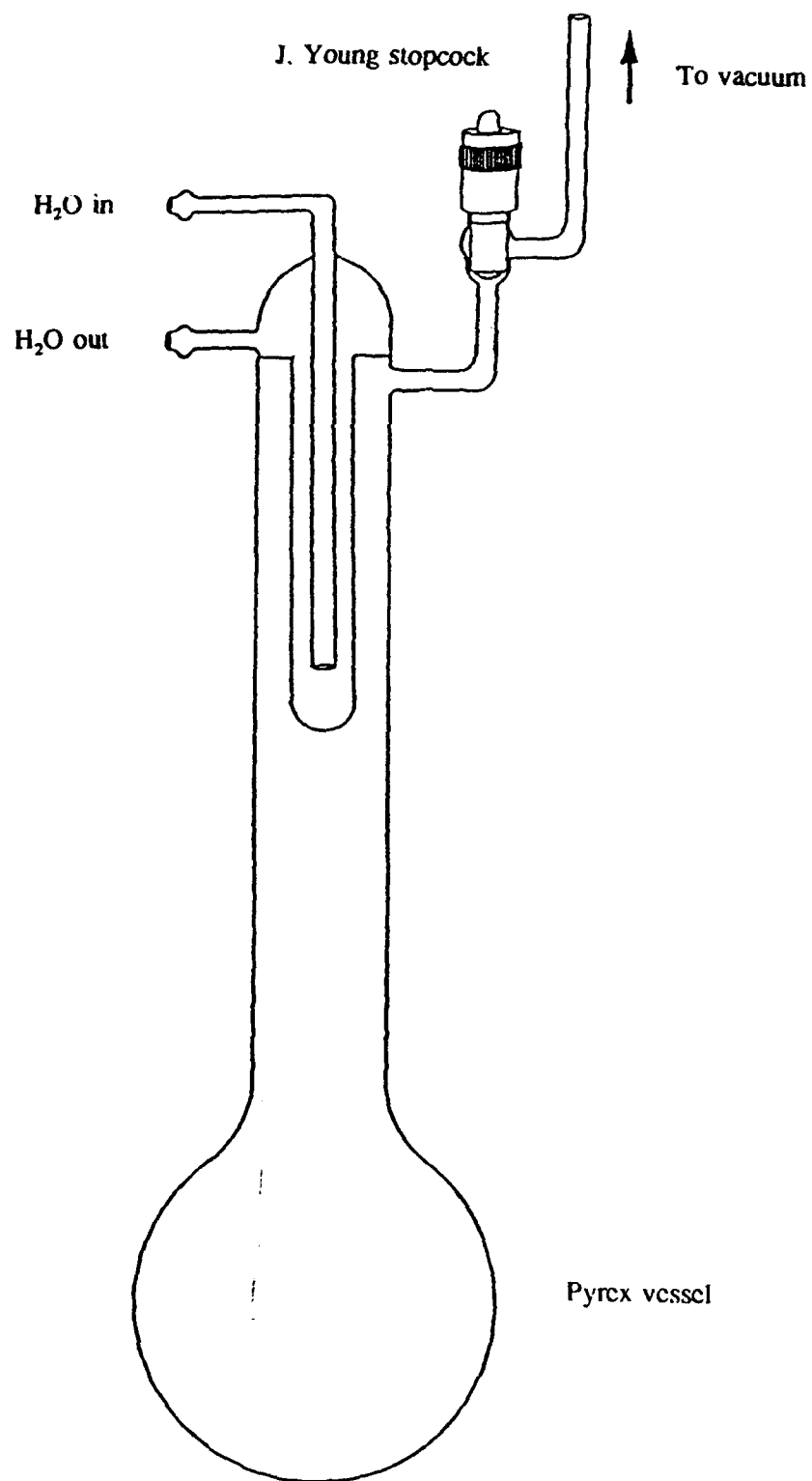


Figure 5. Sublimier for HOTeF₅ purification.

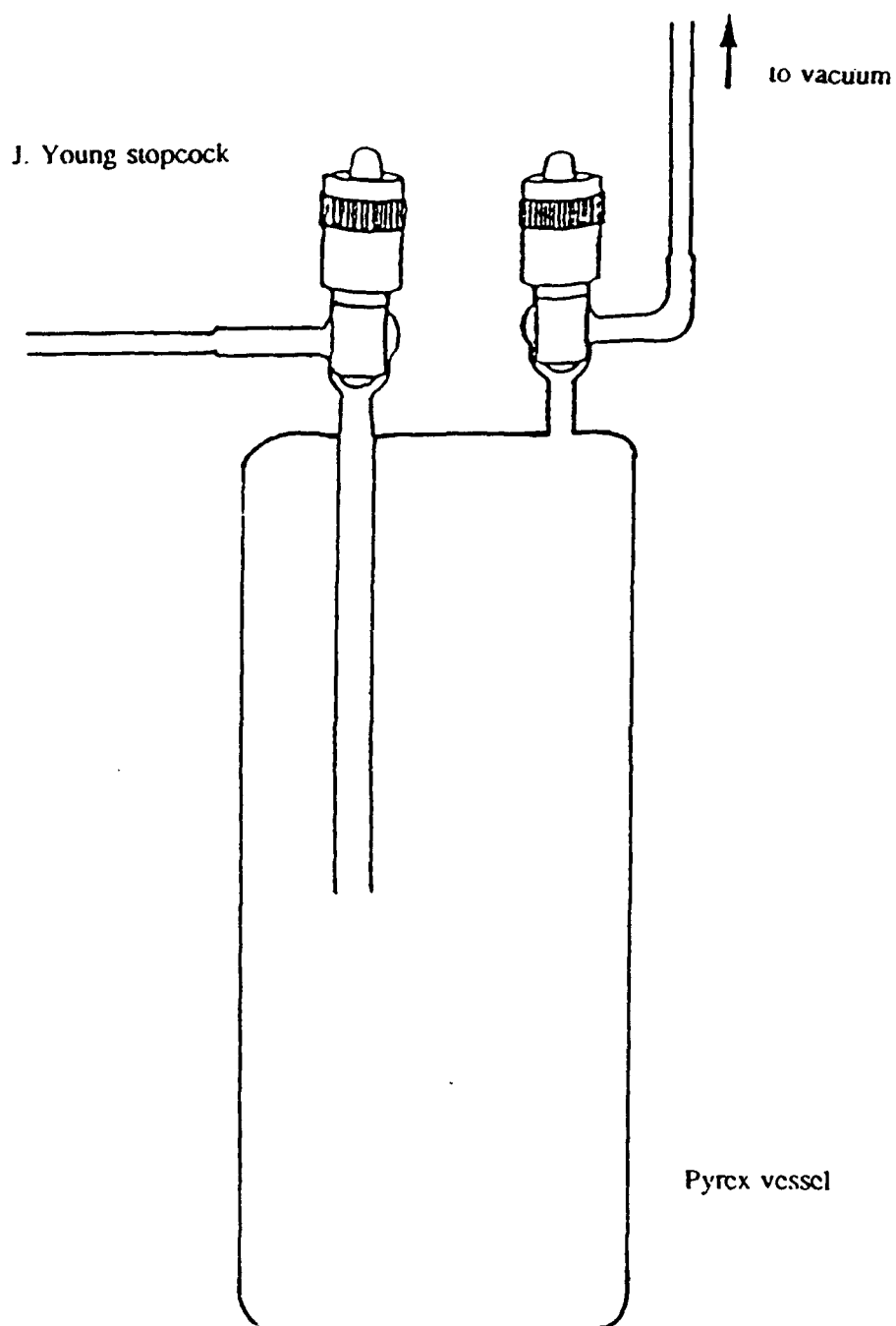


Figure 6. Purification apparatus used in HOTeF_5 preparation.

reaction mixture was melted with tepid water to ensure thorough mixing of the reagents. The mixture was then cooled to -78°C and the HCl pumped off.

The final product (yield 57.60 g, 99.97 %) was free of visible contamination and showed no pre-melting. The product was stored at room temperature in the dry box in its glass reaction bulb until required.

PREPARATION OF $\text{Xe}(\text{OTeF}_5)_2$ Boron tris[pentafluorooxotellurate(VI)] (10.6631 g, 14.68 mmol) was loaded into a dry $\frac{1}{2}$ " FEP tube in the dry box. The tube was then placed into a cold-well, located inside the dry box and cooled to -196°C . Xenon difluoride (3.7482 g, 22.14 mmol) was added to the cold $\text{B}(\text{OTeF}_5)_3$. The FEP tube was kept cold and fitted with a Kel-F valve before removal from the dry box. The cold tube was attached to a glass vacuum line and Freon 114 (ca. 6 cm depth) distilled on to the solid reagents at -196°C . The tube was placed in a -78°C cold bath, attached to a metal vacuum line and the open tube and vacuum manifold were pressurized to 1 atmosphere with dry N_2 . The reaction mixture was further warmed to -8°C over the period of 1 hour. During this time, BF_3 slowly evolved and was periodically pumped away in order to maintain the pressure in the manifold and reaction tube at ca. 1 atmosphere. As the reaction rate slowed, the tube was allowed to warm to room temperature in order to complete the reaction. When no further pressure increase was noted the solvent was slowly pumped away, leaving a very pale yellow microcrystalline powder in essentially quantitative yield (13.2162 g, 98.1 %). The tube was pressurized with dry N_2 and stored at -78°C until required.

PREPARATION OF SAMPLES OF $(\text{C}_2\text{H}_5)_4\text{N}^+\text{Te}(\text{OTeF}_5)_5^-$ IN SO_2ClF AND CH_2Cl_2 FOR ^{19}F NMR SPECTROSCOPY

In the dry box $(\text{C}_2\text{H}_5)_4\text{N}^+\text{Te}(\text{OTeF}_5)_5^-$ (tube A: 3.4691 mg, 2.391 mmol; tube B: 2.8849 mg, 1.988 mmol) was weighed into two predried 4-mm o.d. FEP NMR tubes. The tubes were removed from the drybox and attached to a glass vacuum line. The solvent CH_2Cl_2 (ca. 4 cm depth) was vacuum distilled on to the solid in tube A at -196°C (Figure 7). The tube was heat-sealed under vacuum at -196°C . A similar quantity of SO_2ClF was distilled into tube B, which was then heat-sealed. The samples both formed clear colourless solutions at -45°C . Both samples were stored at -196°C until their NMR spectra could be recorded.

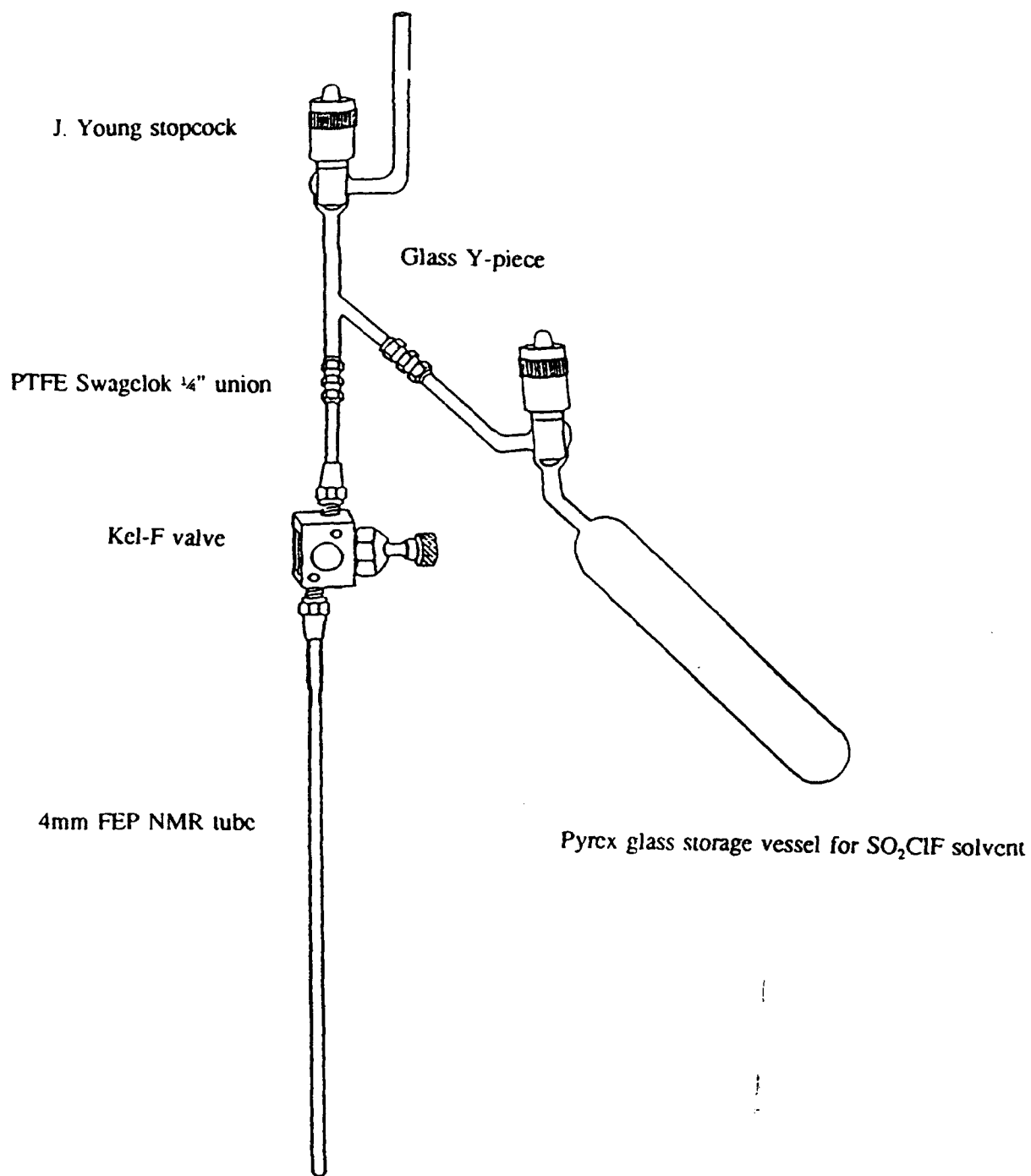


Figure 7. Apparatus used in the preparation of ^{19}F NMR samples of $(\text{C}_2\text{H}_5)_4\text{N}^+\text{Te}(\text{OTeF}_5)_5^-$

ATTEMPTED PREPARATION OF $(C_2H_5)_4N^+Te(OTeF_5)_7^-$ In the drybox, $(C_2H_5)_4N^+Te(OTeF_5)_5^-$ (0.0734 g, 0.0506 mmol) was weighed into a predried 4-mm FEP tube. The tube was cooled to $-196^\circ C$ and $Xe(OTeF_5)_2$ (0.0312 g, 0.0513 mmol) added. The tube was fitted with a Kel-F valve, removed cold from the dry box, and attached to the glass vacuum line. Approximately 4 cm (depth) of SO_2ClF was vacuum distilled on to the solids at $-196^\circ C$. The tube was heat-sealed under vacuum and stored at $-196^\circ C$ until its NMR spectrum could be recorded.

ATTEMPTED PREPARATION OF $(C_2H_5)_4N^+TeF_2(OTeF_5)_5^-$ In an manner analogous to the attempted preparation of $(C_2H_5)_4N^+Te(OTeF_5)_7^-$, $(C_2H_5)_4N^+Te(OTeF_5)_5^-$ (0.0659 g, 0.0454 mmol) and excess XeF_2 (0.0117 g, 0.0691 mmol) were added to a 4-mm FEP NMR tube at $-196^\circ C$ and ca. 4 cm (depth) of SO_2ClF distilled on to the solids at $-196^\circ C$. The tube was heat-sealed under vacuum and stored at $-196^\circ C$ until its NMR spectrum could be recorded.

ATTEMPTED PREPARATION OF $(C_4H_9)_4N^+TeF_5(OTeF_5)_2^-$ In an analogous manner to the attempted preparation of $(C_2H_5)_4N^+Te(OTeF_5)_7^-$, $(C_4H_9)_4N^+TeF_5^-$ (0.0385 g, 0.0827 mmol) and $Xe(OTeF_5)_2$ (0.0755 g, 0.1241 mmol), in a 50 % molar excess, were added to a 4-mm FEP NMR tube at $-196^\circ C$ and ca. 4 cm (depth) of SO_2ClF distilled on to the solids at $-196^\circ C$. The tube was heat-sealed under vacuum and stored at $-196^\circ C$ until its NMR spectrum could be recorded.

PREPARATION OF CF_3OF ⁷⁰ In a drybox, finely ground CsF (9.04 g, 59.5 mmol) was transferred into a prefluorinated 75 ml Whitey 304 stainless steel cylinder equipped with a Whitey ORM2 316 stainless steel valve. The cylinder was attached to a metal vacuum line, evacuated, cooled to $-196^\circ C$ and COF_2 (27.54 mmol) was condensed in. After pumping away any non-condensibles at $-196^\circ C$, F_2 (29.02 mmol) was condensed into the cylinder at $-196^\circ C$. The cylinder was placed in a $-78^\circ C$ bath and allowed to warm slowly to room temperature over a 24 hour period. The yield of CF_3OF was 2.7991 g (97.7 %).

PREPARATION OF $ClOTeF_5$ ⁴⁵ Boron tris[pentafluorooxotellurate(VI)] (5.5893 g, 7.6948 mmol) was melted into a 40 mL Whitey 304 stainless steel cylinder and fitted with a Whitey ORM2 316 stainless steel valve in the

dry box. The cylinder was attached to the metal vacuum line, which had been seasoned with F_2 , then ClF . The ClF (23.885 mmol) was metered out at $-78\text{ }^\circ\text{C}$, in order to avoid contamination with Cl_2 , and condensed on to the $B(OTeF_5)_3$ in the cylinder at $-196\text{ }^\circ\text{C}$. The valve on the cylinder was closed and the cylinder surrounded by a dry ice/acetone bath. The reaction was allowed to proceed at $-78\text{ }^\circ\text{C}$ for 20 hours. The cylinder was warmed to $0\text{ }^\circ\text{C}$ for ca. 20 minutes, and cooled to $-105\text{ }^\circ\text{C}$ in a CS_2 /liquid N_2 slush. The gaseous product BF_3 and excess ClF were pumped off under vacuum at $-105\text{ }^\circ\text{C}$. The can was allowed to warm to room temperature and the contents vacuum distilled into a pre-fluorinated $\frac{1}{4}$ " FEP storage tube equipped with a Kel-F valve. The product was a bright yellow liquid. The tube was pressurized to 1.5 atmospheres with dry N_2 at $-78\text{ }^\circ\text{C}$ and stored at room temperature in a fumehood. The yield was 6.2768 g (99.2 %).

ATTEMPTED PREPARATION OF TcF_5OCF_3

Method one: In a dry box, finely ground TeF_4 (1.9125 g, 9.394 mmol) was transferred into a 40 mL prefluorinated Whitey 304 stainless steel cylinder equipped with a Whitey ORM2 316 stainless steel valve. The cylinder was removed from the dry box, attached to a metal vacuum line, and evacuated. A total of ten aliquots of CF_3OF (9.911 mmol) were distilled into the metal cylinder at $-196\text{ }^\circ\text{C}$, providing a 5.5 % molar excess. The cylinder was allowed to warm to room temperature over a 24 hour period. The cylinder was placed in a furnace at $100\text{ }^\circ\text{C}$ and allowed to react for another 24 hours. A sample was removed in order to check the gas phase IR spectrum, which showed that the reaction was incomplete; thus, the cylinder was warmed at $150\text{ }^\circ\text{C}$ for a further 24 hours. The IR spectrum of the products volatile at $-78\text{ }^\circ\text{C}$ showed the presence of unreacted CF_3OF as well as COF_2 . The volatile product at room temperature was distilled into an NMR tube for ^{19}F NMR study, which was stored at $-196\text{ }^\circ\text{C}$ until its spectrum could be recorded.

Method two:⁴⁶ On the metal vacuum line, CF_3I (5.222 mmol) was condensed into a pre-fluorinated 20 mL Monel cannister equipped with a Hoke stainless steel valve at $-196\text{ }^\circ\text{C}$. The $ClOTeF_5$ (10.402 mmol) was condensed on to solid CF_3I at $-196\text{ }^\circ\text{C}$. The valve on the cannister was closed and the cannister surrounded by a dry ice/acetone bath. The reaction was allowed to proceed at $-78\text{ }^\circ\text{C}$ for four days, with periodic removal of the evolved Cl_2 gas at $-78\text{ }^\circ\text{C}$. After four days, the cannister was attached to two U-traps cooled to $-78\text{ }^\circ\text{C}$ and $-126\text{ }^\circ\text{C}$, respectively (Figure 8), and the contents distilled under dynamic vacuum. After a 15 minute distillation

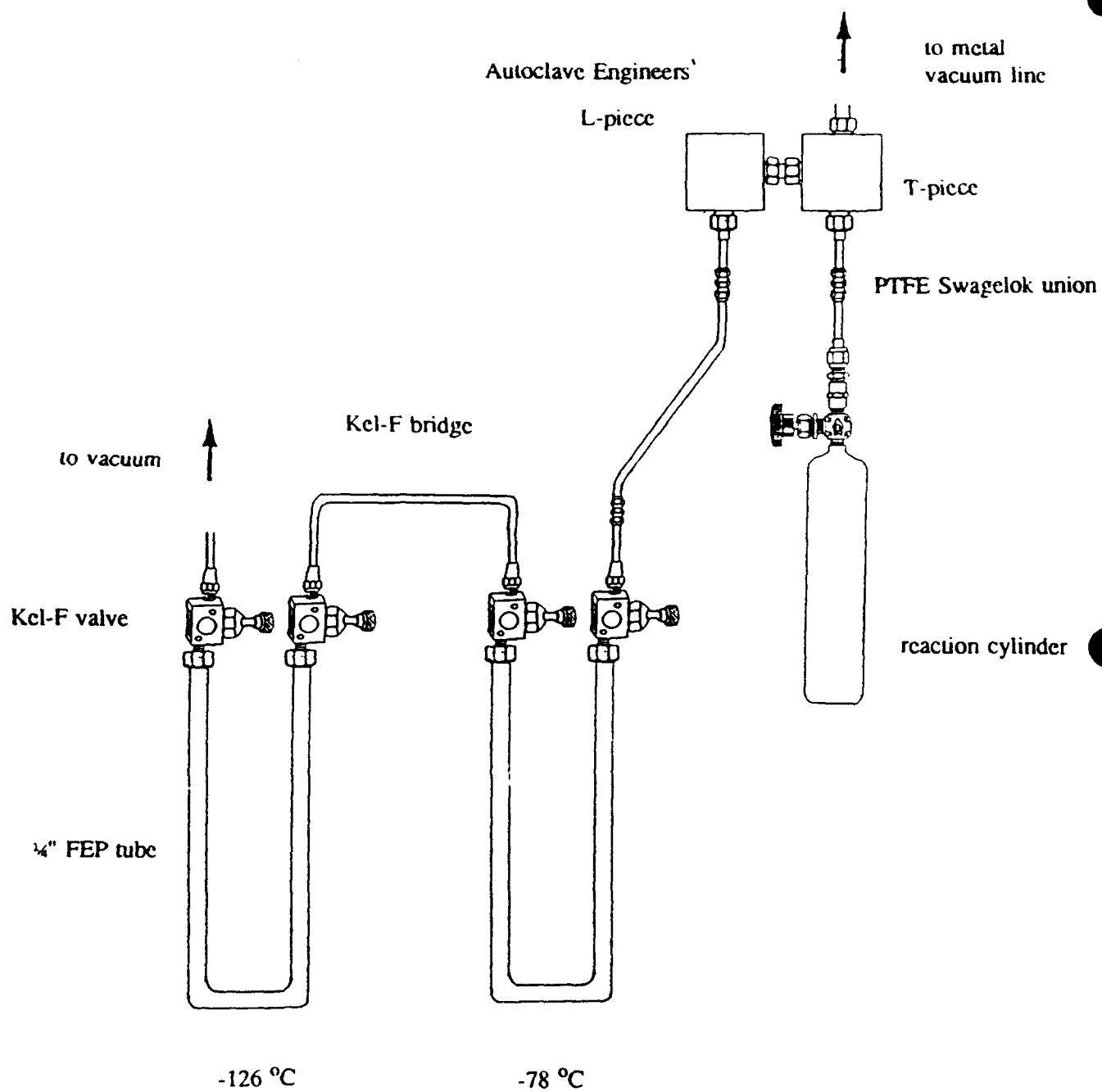


Figure 8. Apparatus used in the purification of TeF_5OCF_3

period, there was an accumulation of brown non-volatile material in the -78°C trap, and an accumulation of yellow volatile material in the -126°C trap. The contents of the trap at -126°C were distilled into a $\frac{1}{4}$ " FEP tube and warmed to room temperature. At room temperature there was only a small amount of the expected clear-coloured TeF_5OCF_3 product, and thus, further attempts to prepare TeF_6OCF_3 were abandoned.

PREPARATION OF $(\text{CH}_3)_4\text{N}^+\text{TeF}_6\text{CN}^-$ In the dry box, $(\text{CH}_3)_4\text{N}^+\text{TeF}_7^-$ (0.0516 g, 0.1609 mmol) was transferred in to a 4-mm o.d. FEP NMR tube. The tube was fitted with a Kel-F valve, attached to a glass vacuum line and CH_3CN (ca. 3.5 cm depth) vacuum distilled into the tube.

The requisite amount of $(\text{CH}_3)_3\text{SiCN}$ (0.01470 g, 0.1482 mmol) was vacuum distilled into a small glass weighing tube equipped with a J. Young stopcock (Figure 9). The weighing tube was reattached to the vacuum line and the $(\text{CH}_3)_3\text{SiCN}$ vacuum distilled into the NMR tube. The tube was heat-sealed and stored at -196°C until its NMR spectrum could be recorded.

In a manner analogous to the preparation of the ^{19}F NMR sample, a sample was prepared for ^{125}Te NMR characterization using a 9-mm o.d. FEP NMR tube and the following quantities of reagents: $(\text{CH}_3)_3\text{SiCN}$ (0.0807 g, 0.8135 mmol) and $\text{N}(\text{CH}_3)_4^+\text{TeF}_7^-$ (0.2723 g, 0.8490 mmol).

PREPARATION OF TeF_5CN In a typical experiment ca. 3.5 cm (height) of CH_3CN solvent was transferred on a glass vacuum line into a dry 4 mm-FEP NMR fitted with a Kel-F valve. As described for the previous preparation, $(\text{CH}_3)_3\text{SiCN}$ (0.1531 mmol) was condensed into the FEP tube at -196°C . The FEP tube was attached to a metal vacuum line where TeF_6 (0.1540 mmol) was condensed into the 4 mm FEP tube at -196°C . The tube was heat-sealed, and stored at -196°C .

In an analogous manner to the preparation of the ^{19}F NMR sample, a sample for ^{125}Te NMR characterization was prepared, using a 9-mm o.d. FEP NMR tube and the following quantities: $(\text{CH}_3)_3\text{SiCN}$ (0.1563 g, 1.576 mmol) and $\text{N}(\text{CH}_3)_4^+\text{TeF}_7^-$ (0.4027 g, 1.667 mmol).

Both ^{19}F and ^{125}Te NMR samples were analogously prepared using SO_2ClF solvent instead of CH_3CN solvent.

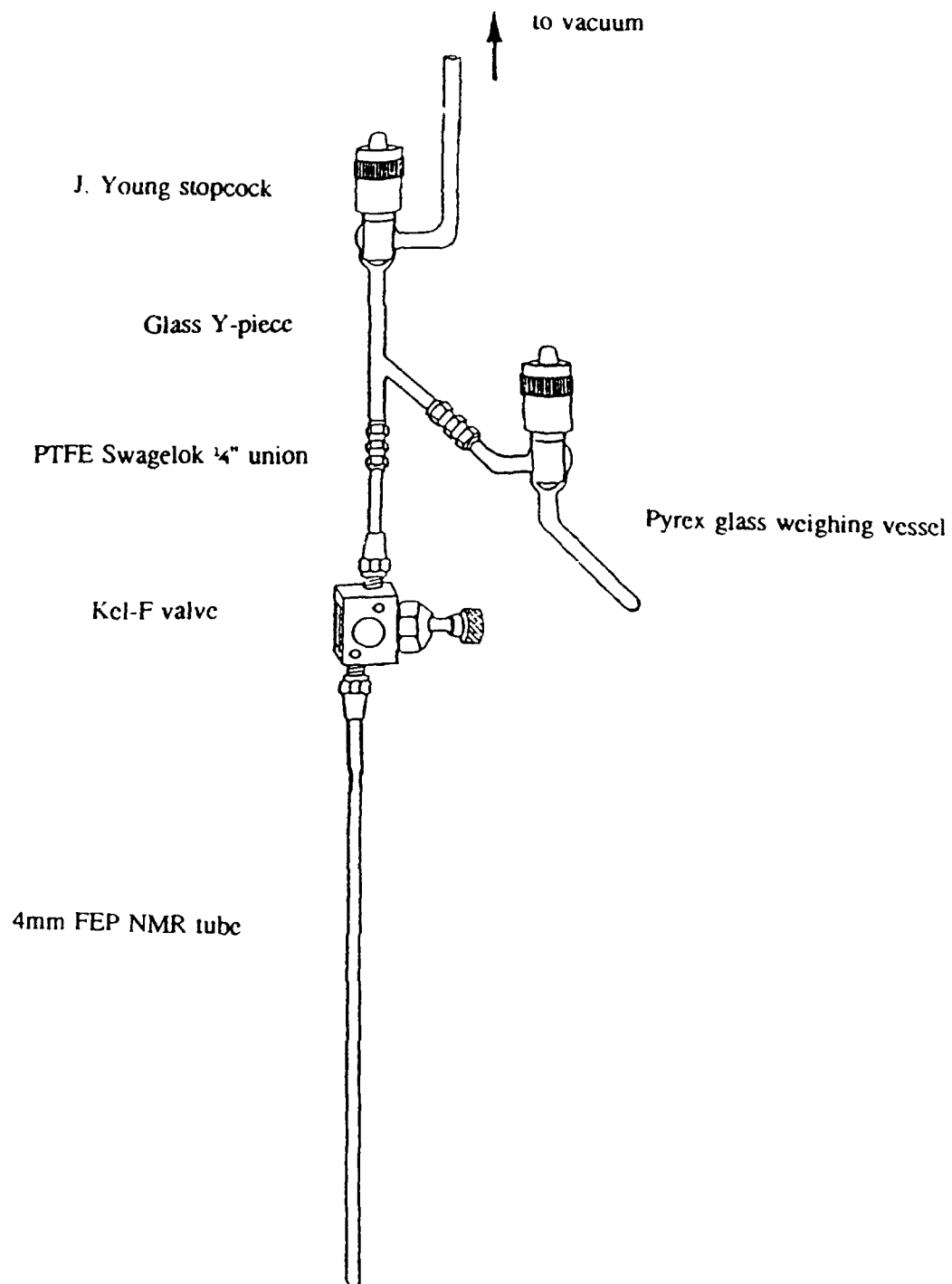


Figure 9. Apparatus used in the preparation of $(\text{CH}_3)_4\text{NTeF}_6\text{CN}^-$ and TeF_5CN .

RESULTS AND DISCUSSION

^{19}F NMR SPECTROSCOPIC CHARACTERIZATION OF $(\text{C}_2\text{H}_5)_4\text{N}^+\text{Te}(\text{OTeF}_5)_5^-$ IN SO_2ClF AND CH_2Cl_2

The ^{19}F NMR spectrum of $(\text{C}_2\text{H}_5)_4\text{N}^+\text{Te}(\text{OTeF}_5)_5^-$ in SO_2ClF solvent at -50°C , showed three AB_4 spin patterns and one singlet (Figure 10). The two AB_4 patterns in a 1 : 4 ratio were attributed, respectively, to the one axial and four equatorial OTeF_5 ligands of the square pyramidal $\text{Te}(\text{OTeF}_5)_5^-$ anion. The chemical shifts and coupling constants for this species are summarized in Table 3. The singlet at -15.3 ppm was attributed to the F-on-Te(IV) environment in the $\text{FTe}(\text{OTeF}_5)_4^-$ anion based on recent results in our laboratory.⁶³ This anion is an impurity arising from the original preparation of the $(\text{C}_2\text{H}_5)_4\text{N}^+\text{Te}(\text{OTeF}_5)_5^-$ salt. The AB_4 spin pattern of the four equivalent equatorial OTeF_5 ligands of $\text{FTe}(\text{OTeF}_5)_4^-$ partially overlaps with the AB_4 spin pattern of the equatorial OTeF_5 ligands of the $\text{Te}(\text{OTeF}_5)_5^-$ anion. The singlet at -28.7 ppm arises from an unidentified oxidatively inert impurity in the SO_2ClF solvent, while the resonance at ca. -25 ppm is a solvent fold-in.

The ^{19}F NMR spectrum of $(\text{C}_2\text{H}_5)_4\text{N}^+\text{Te}(\text{OTeF}_5)_5^-$ in CH_2Cl_2 solvent at -50°C , showed two AB_4 spin patterns in the range of -30 to -43 ppm, which were not well resolved. The AB_4 pattern of the equatorial OTeF_5 ligands in $\text{FTe}(\text{OTeF}_5)_4^-$ overlaps almost completely with the AB_4 pattern of the equatorial OTeF_5 ligands in $\text{Te}(\text{OTeF}_5)_5^-$ in this solvent, and thus, the chemical shifts and coupling constants could not be accurately determined.

Because of the stability of SO_2ClF towards the oxidizers XeF_2 and $\text{Xe}(\text{OTeF}_5)_2$,⁷¹ and because the ^{19}F resonances of $\text{Te}(\text{OTeF}_5)_5^-$ and $\text{FTe}(\text{OTeF}_5)_4^-$ are better dispersed in SO_2ClF solvent compared with CH_2Cl_2 solvent, all subsequent syntheses were carried out in SO_2ClF solvent.

ATTEMPTED PREPARATION OF $(\text{C}_2\text{H}_5)_4\text{N}^+\text{Te}(\text{OTeF}_5)_7^-$

The ^{19}F NMR spectra of the products of the reaction between $(\text{C}_2\text{H}_5)_4\text{N}^+\text{Te}(\text{OTeF}_5)_5^-$ and $\text{Xe}(\text{OTeF}_5)_2$ in SO_2ClF solvent were initially recorded after warming to -50°C , and then again after 5 minutes at 0°C . There was no apparent reaction after either warming, nor after 15 minutes at room temperature, nor was gas evolution observed. After each warming, the spectra were run at -50°C .

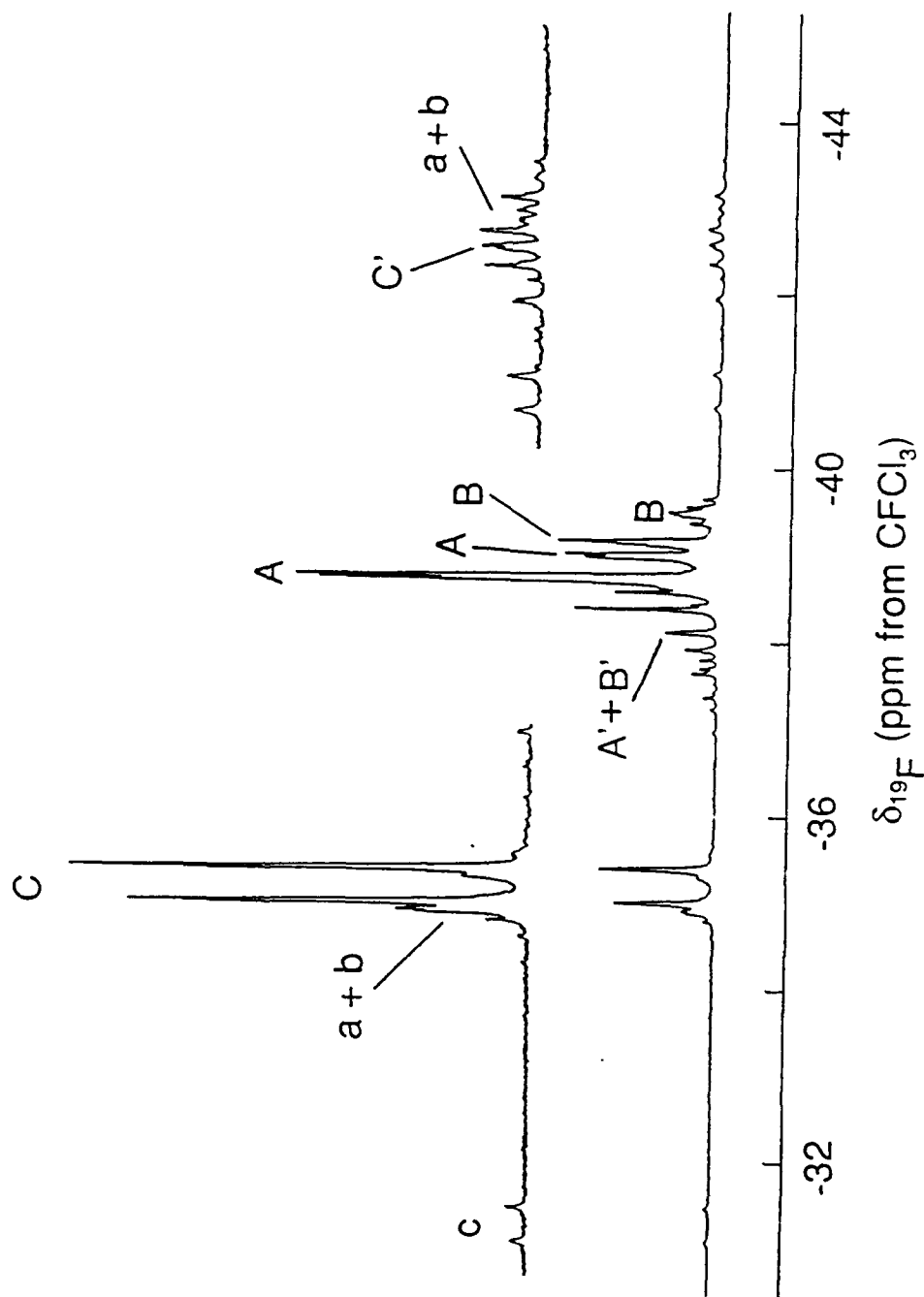


Figure 10. The ^{19}F NMR spectrum (470.599 MHz) at -50°C of $\text{Te}(\text{OTeF}_5)_3$ in SO_2ClF . Non-primed letters denote B_4 parts; primed letters denote A parts. (A) OTeF_5 in $\text{Te}(\text{OTeF}_5)_3$; (B) OTeF_5 in $\text{FTe}(\text{OTeF}_5)_4$; (C) OTeF_5 in $\text{Te}(\text{OTeF}_5)_3$. Lower case letters denote ^{125}Te satellites.

Table 3. ^{19}F NMR Data for $\text{Te}(\text{OTeF}_5)_5^-$ in SO_2ClF and CH_2Cl_2 Solvents

	$\delta(\text{A}), \text{ppm}$	$\delta(\text{B}_4), \text{ppm}$	$^1\text{J}(^{19}\text{F}_{\text{eq}}-^{125}\text{Te}), \text{Hz}$	$^2\text{J}(^{19}\text{F}_{\text{ax}}-^{19}\text{F}_{\text{eq}}), \text{Hz}$
<u>SO_2ClF Solvent</u>				
$(\text{OTeF}_5)_{\text{ax}}$	-42.8	-35.2	3685	173
$(\text{OTeF}_5)_{\text{eq}}$	-37.9	-38.8	3697	173
<u>CH_2Cl_2 Solvent</u>				
$(\text{OTeF}_5)_{\text{ax}}$	- ^a	- ^a	3699 ^b	188 ^b
$(\text{OTeF}_5)_{\text{eq}}$	- ^a	- ^a	3690 ^b	177 ^b

a Owing to the superposition of the A and B_4 resonances from $\text{Te}(\text{OTeF}_5)_5^-$ and $\text{FTe}(\text{OTeF}_5)_4^-$, the chemical shifts could not be accurately determined.

b Approximate values.

At -50 °C, the spectrum (Figure 11) consisted of a singlet and four overlapping AB₄ spin patterns. The singlet at -15.3 ppm results from the F-on-Te(IV) environment in the FTe(OTeF₅)₄⁻ anion, which, as mentioned previously, is an impurity from the original preparation of (C₂H₅)₄N⁺Te(OTeF₅)₅⁻. The two AB₄ spin patterns arising from the equatorial OTeF₅ ligands of both Te(OTeF₅)₅⁻ and FTe(OTeF₅)₄⁻ were located as described above, as was the resonance for the equatorial OTeF₅ ligand of the Te(OTeF₅)₅⁻ anion. The fourth AB₄ pattern, which partially overlaps with the A part of the axial OTeF₅ ligand of Te(OTeF₅)₅⁻, resulted from the presence of unreacted Xe(OTeF₅)₂; the chemical shift and coupling constant for Xe(OTeF₅)₂ agreed with literature values.⁷² The chemical shifts and coupling constants for these species are summarized in Table 4.

There was no apparent change in the ¹⁹F NMR spectrum of the sample upon warming the NMR tube to 0 °C for ca. 5 minutes.

ATTEMPTED PREPARATION OF (C₂H₅)₄N⁺TeF₂(OTeF₅)₅⁻

The ¹⁹F NMR spectra of the products of the reaction between (C₂H₅)₄N⁺Te(OTeF₅)₅⁻ and a 50 % molar excess of XeF₂ in SO₂ClF solvent, were recorded initially after warming the sample from -196 °C to -50 °C then after a 15 minute warming at 25 °C. There was no observed gas evolution at either temperature. The probe temperature was maintained at -50 °C.

The ¹⁹F NMR spectrum of the reaction products at -50 °C exhibited two singlets and two AB₄ spin patterns (Figure 12). The two AB₄ spin patterns attributed to the Te(OTeF₅)₅⁻ anion were no longer present. The more intense singlet at -15.3 ppm was attributed to the F-on-Te(IV) environment of FTe(OTeF₅)₄⁻, and was much more intense in comparison with the corresponding resonance of the same anion as an impurity in the ¹⁹F NMR spectrum of Te(OTeF₅)₅⁻. The less intense singlet at -176.8 ppm was attributed to XeF₂,^{73,74} and was due to the ca. 50 % molar excess of XeF₂ relative to Te(OTeF₅)₅⁻. The most intense AB₄ spin pattern corresponded to the equatorial OTeF₅ ligands of FTe(OTeF₅)₄⁻, while the less intense of the two AB₄ spin patterns, which were also observed in the Te(OTeF₅)₅⁻/Xe(OTeF₅)₂ system (*vide supra*), was assigned to Xe(OTeF₅)₂. The chemical shifts and coupling constants for the observed species are summarized in Table 5.

Since the concentration of Te(OTeF₅)₅⁻ was essentially the same for both this and the Te(OTeF₅)₅⁻/Xe(OTeF₅)₂ system, a comparison between the two spectra could be made using the resonance at -15.3 ppm. The increase in intensity in the F-on-Te(IV) resonance at -15.3 ppm in this spectrum, after taking into

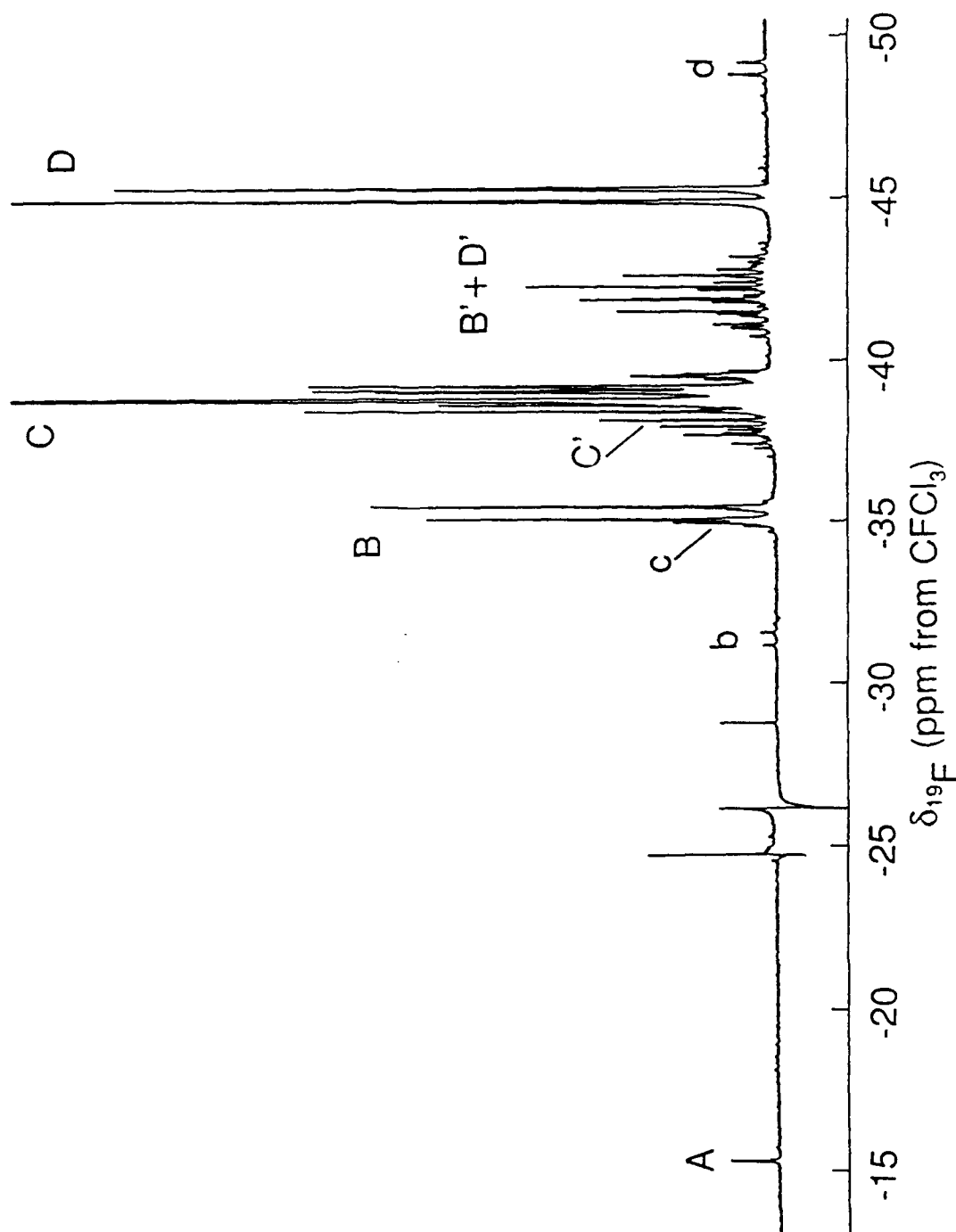


Figure 11. The ^{19}F NMR spectrum (470.599 MHz) at -50°C of the reaction mixture $(\text{C}_2\text{H}_5)_4\text{N}^+\text{Te}(\text{OTeF}_3)_5^- + \text{Xe}(\text{OTeF}_3)_2$ in SO_2ClF after warming to -50°C . The non-primed letters B, C and D denote B_4 parts; the primed letters B', C' and D' denote A parts. (A) F-on-Te(IV) in $\text{FTe}(\text{OTeF}_3)_4^-$; (B) $\text{OTeF}_3(\text{eq})$ in $\text{Te}(\text{OTeF}_3)_5$; (C) $\text{OTeF}_3(\text{eq})$ in $\text{Te}(\text{OTeF}_3)_5$; (D) $\text{Xe}(\text{OTeF}_3)_2$. Lower case letters denote ^{125}Te satellites.

Table 4. ^{19}F NMR Data for Products Observed in the Reaction Between $(\text{C}_2\text{H}_5)_4\text{N}^+\text{Te}(\text{OTeF}_5)_5^-$ and $\text{Xe}(\text{OTeF}_5)_2$ in SO_2ClF Solvent at -50°C

F-on-Tc(VI) Environments:

	<u>$\delta(\text{A}), \text{ppm}$</u>	<u>$\delta(\text{B}_4), \text{ppm}$</u>	<u>$^1\text{J}(^{19}\text{F}_{\text{eq}}-^{125}\text{Te}), \text{Hz}$</u>	<u>$^2\text{J}(^{19}\text{F}_{\text{ax}}-^{19}\text{F}_{\text{eq}}), \text{Hz}$</u>
$[\text{Te}(\text{OTeF}_5)_5]^-$				
$(\text{OTeF}_5)_{\text{ax}}$	-42.8	-35.2	3684	175
$(\text{OTeF}_5)_{\text{eq}}$	-37.9	-38.8	3710	182
$\text{FTe}(\text{OTeF}_5)_4^-$	-37.8	-39.4	3578	170
$\text{Xe}(\text{OTeF}_5)_2$	-42.0	-45.1	3645	175

F-on-Tc(IV) Environment:

	<u>δ, ppm</u>	<u>$^1\text{J}(^{19}\text{F}_{\text{eq}}-^{125}\text{Te}), \text{Hz}$</u>
$\text{FTe}(\text{OTeF}_5)_4^-$	-15.3	- ^a

a Owing to the poor signal-to-noise ratio, this coupling could not be resolved from the baseline noise.

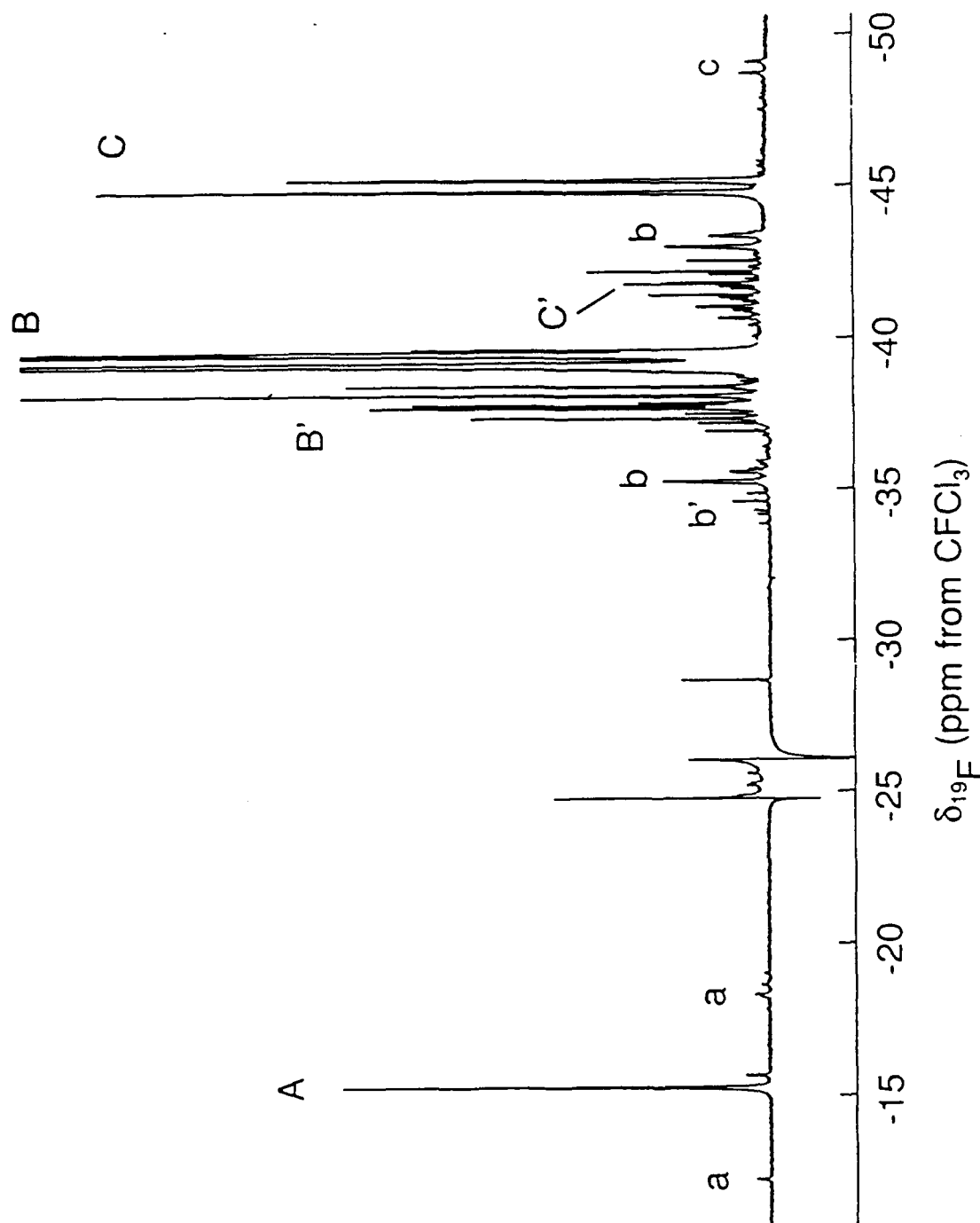


Figure 12. The ^{19}F NMR spectrum (470.599 MHz) at -50°C of the reaction mixture $(\text{C}_2\text{H}_5)_4\text{N}^+\text{Te}(\text{OTeF}_5)_5^- + \text{XeF}_2$ in SO_2/ClF after warming to -50°C . The non-primed letters B and C denote B_4 parts; the primed letters B' and C' denote A parts. (A) F-on-Te(IV) in $\text{FTe}(\text{OTeF}_5)_4$; (B) OTeF_5 in $\text{FTe}(\text{OTeF}_5)_4$; (C) $\text{Xe}(\text{OTeF}_5)_2$. Lower case letters denote ^{125}Te satellites.

Table 5. ^{19}F NMR Data for Products Observed in the Reaction Between $(\text{C}_2\text{H}_5)_4\text{N}^+\text{Te}(\text{OTeF}_5)_5^-$ and XeF_2 in SO_2ClF Solvent at -50°C

F-on-Tc(VI) Environments:

	$\delta(\text{A}), (\text{ppm})$	$\delta(\text{B}_4), (\text{ppm})$	$^1\text{J}(^{19}\text{F}_{\text{eq}}-^{125}\text{Te}), \text{Hz}$	$^2\text{J}(^{19}\text{F}_{\text{ax}}-^{19}\text{F}_{\text{eq}}), \text{Hz}$
$\text{FTc}(\text{OTeF}_5)_4^-$	-37.8	-39.4	3647	177
$\text{Xe}(\text{OTeF}_5)_2$	-41.9	-45.0	3649	176
FXcOTeF_5	^a	-46.3	3621	179

F-on-Tc(IV) Environment:

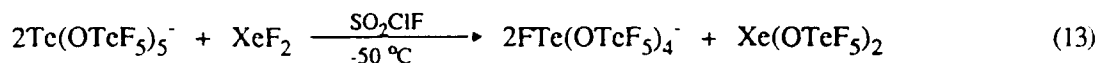
	δ, ppm	$^1\text{J}(^{19}\text{F}_{\text{eq}}-^{125}\text{Te}), \text{Hz}$
$\text{FTc}(\text{OTeF}_5)_4^-$	-15.3	2874

F-on-Xe(II) Environments:

	δ, ppm	$^1\text{J}(^{19}\text{F}-^{129}\text{Xe}), \text{Hz}$
XeF_2	-176.8	5607
FXcOTeF_5	-151.0	5729

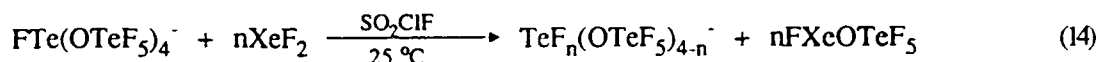
a Obscured owing to overlap with other resonances.

consideration the intensity of the corresponding impurity resonance resulting from the attempted preparation of the $\text{Te}(\text{OTeF}_5)_7^-$ anion, an intensity approximately $\frac{1}{4}$ that of the resonance attributed to $\text{Xe}(\text{OTeF}_5)_2$ was observed in this preparative attempt. Thus, at -50°C , there appears to have been simple ligand exchange according to reaction (13)



Upon warming the NMR tube to 25°C and re-running the spectrum at -50°C , the singlet and AB_4 spin pattern attributed to $\text{FTe}(\text{OTeF}_5)_4^-$ disappeared, while the resonance attributed to $\text{Xe}(\text{OTeF}_5)_2$ increased greatly in intensity (Figure 13). A resonance attributed to FXeOTeF_5 was also noted, which agreed with the published data,⁷⁵ although only the B_4 resonance could be discerned for this species; the A resonance was obscured under the spin patterns of the mixed $\text{TeF}_n(\text{OTeF}_5)_{5-n}$ ($n = 2 - 5$) species, while the F-on-Xe(II) singlet of FXeOTeF_5 was located at -151.0 ppm (Figure 14).

Therefore, warming to 25°C did not effect oxidative addition of OTeF_5 ligands to any Te(IV) species to form heptacoordinate Te(VI) anions. Rather, further ligand exchange occurred, consuming all of the $\text{FTe}(\text{OTeF}_5)_4^-$ anion present, and producing the series of mixed F/ OTeF_5 substituted pentacoordinated Te(IV) anions, $\text{TeF}_n(\text{OTeF}_5)_{5-n}^-$ ($n = 2 - 5$)⁶³ according to equation (14). These anions gave a complex series of overlapping resonances in the range of -33 to -43 ppm.



ATTEMPTED PREPARATION OF $(\text{C}_4\text{H}_9)_4\text{N}^+\text{TeF}_5(\text{OTeF}_5)_2^-$

The ^{19}F NMR spectra of the products of the reaction between $(\text{C}_4\text{H}_9)_4\text{N}^+\text{TeF}_5^-$ and a 50 % molar excess of $\text{Xe}(\text{OTeF}_5)_2$, in SO_2ClF solvent, were recorded initially after warming the sample from -196°C to -50°C , and then after 15 minutes at 0°C . At -50°C gas evolution was observed. The probe temperature was maintained at -50°C .

The ^{19}F NMR spectra were identical after warming at both temperatures. The spectra exhibited two AB_4 spin patterns, one sharp singlet, and one broad resonance (Figure 15). All the resonances were in the F-on-

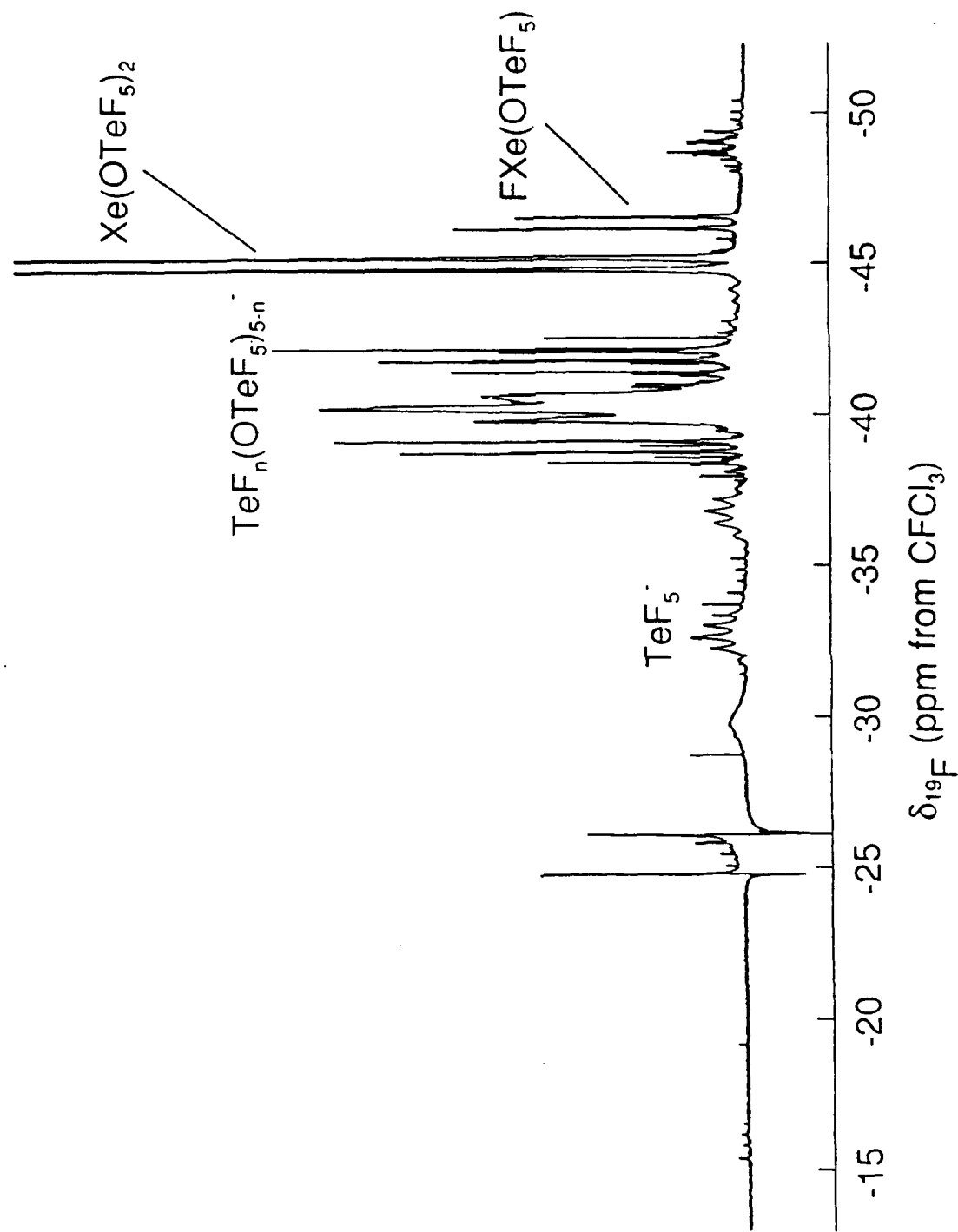


Figure 13. The ^{19}F NMR spectrum (470.599 MHz) at -50°C of the reaction mixture $(\text{C}_2\text{H}_5)_4\text{N}^+\text{Te}(\text{OTeF}_5)_3^-$ + XeF_2 in SO_2ClF after warming to 25°C .

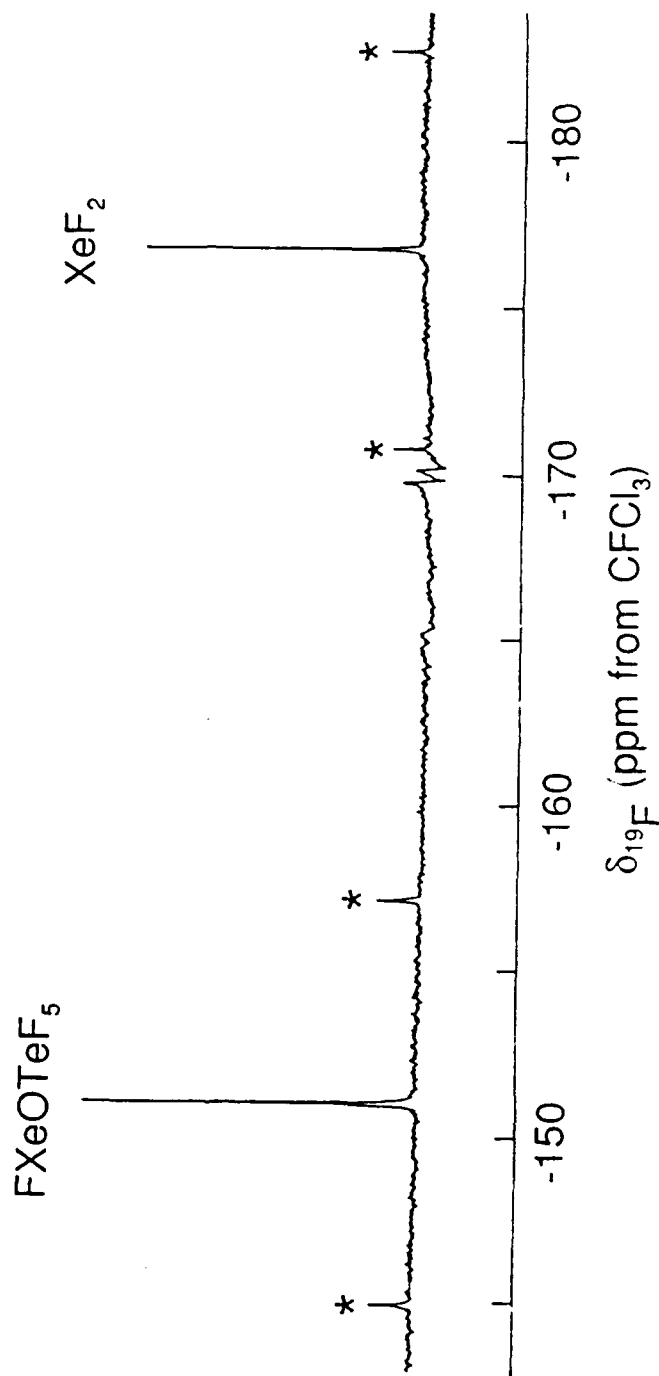


Figure 14. The F-on-Xe(II) region of the ^{19}F NMR spectrum (470.599 MHz) at -50°C of the reaction mixture $(\text{C}_2\text{H}_5)_4\text{N}^+\text{Te}(\text{OTeF}_5)_5^- + \text{XeF}_2$ in SO_2ClF after warming to 25°C . Asterisks (*) denote ^{129}Xe satellites.

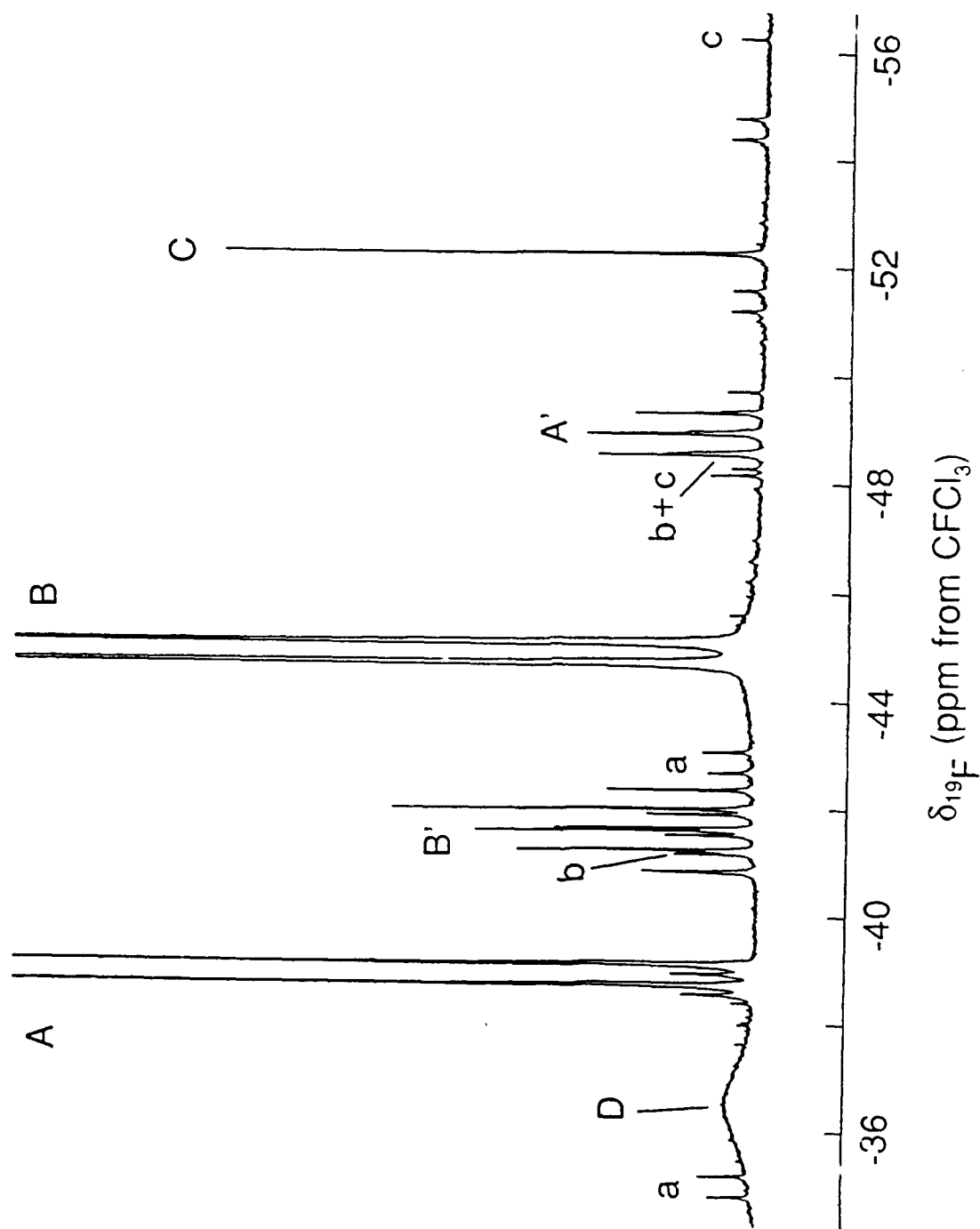
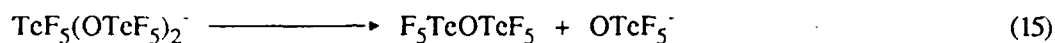


Figure 15. The ^{19}F NMR spectrum (470.599 MHz) at -50°C of the reaction mixture $(\text{C}_4\text{H}_9)_4\text{N}^+\text{TeF}_6^- + \text{Xe}(\text{OTeF}_5)_2$ in SO_2ClF after warming to -50°C . The non-primed letters A and B denote B_4 parts; the primed letters A' and B' denote A parts. (A) $\text{Xe}(\text{OTeF}_5)_2$; (B) $\text{F}_3\text{TeOTeF}_5$; (C) TeF_6 ; (D) exchanging OTeF_5 . Lower case letters denote ^{125}Te satellites.

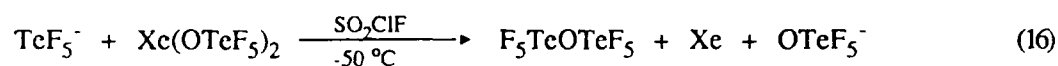
Te(VI) region. The singlet displaying satellites, at -52.3, was attributed to TeF_6 , and is believed to be the product of a side reaction. By comparison with the data obtained for previous samples, one AB_4 spin pattern was attributed to the reactant $\text{Xe}(\text{OTeF}_5)_2$, while the other AB_4 spin pattern was attributed to $\text{F}_5\text{TeOTeF}_5$, in agreement with the literature values.⁷⁶ The chemical shifts and coupling constants for both of these species are listed in Table 6.

The broad resonance centered at ~ 36.5 ppm most likely arises from exchanging OTeF_5^- . Presumably, the OTeF_5^- anion is produced from the decomposition of a labile heptacoordinated Te(VI) intermediate, probably $\text{TeF}_5(\text{OTeF}_5)_2^-$, which is the product of an oxidative-addition reaction between $\text{Xe}(\text{OTeF}_5)_2$ and TeF_5^- . The labile intermediate decomposes according to equation (15)



The oxidative addition of two OTeF_5 groups to TeF_5^- would result, initially, in axially substituted OTeF_5 ligands, forming an anion with distorted pentagonal bipyramidal geometry. As a heptacoordinated analog of TeF_7^- , $\text{TeF}_5(\text{OTeF}_5)_2^-$ would be expected to exhibit fluxional behaviour on the NMR time scale, and it is thought that upon pseudorotation of the OTeF_5 ligands into the equatorial plane, the configuration would become sterically unfavourable and hence labile.

Therefore, these results indicate that an oxidation did indeed occur in this reaction in which the TeF_5^- was oxidized by $\text{Xe}(\text{OTeF}_5)_2$ to produce $\text{F}_5\text{TeOTeF}_5$, OTeF_5^- and Xe as end products according to equation (16)



Heptacoordinated Te(VI) anions exhibit a characteristic high frequency shift relative to octahedrally coordinated Te(VI) species,⁷⁷ and since no resonances were observed in the presently known heptacoordinated F-on-Te(VI) region (10 - 40 ppm), it appears that no stable heptacoordinated Te(VI) anions with OTeF_5 substitution were produced.

ATTEMPTED PREPARATION OF TeF_5OCF_3

Two attempts were made at preparing the title compound in order to use it as a precursor in the preparation of $\text{TeF}_6\text{OCF}_3^-$. Both methods were oxidative-addition processes. Cady had successfully prepared SF_5OCF_3

Table 6. ^{19}F NMR Data for Products Observed for the Reaction Between $(\text{C}_4\text{H}_9)_4\text{N}^+\text{TeF}_5^-$ and $\text{Xe}(\text{OTeF}_5)_2$ in SO_2ClF Solvent at -50°C

F-on-Te(VI) Environments:

	<u>$\delta(\text{A})$, ppm</u>	<u>$\delta(\text{B}_4)$, ppm</u>	<u>$^1\text{J}(\text{}^{19}\text{F}_{\text{eq}}-\text{}^{125}\text{Te})$, Hz</u>	<u>$^2\text{J}(\text{}^{19}\text{F}_{\text{ax}}-\text{}^{19}\text{F}_{\text{eq}})$, Hz</u>
$\text{F}_5\text{TeOTeF}_5$	-41.6	-39.0	3704	182
$\text{Xe}(\text{OTeF}_5)_2$	-41.9	-45.0	3745	177

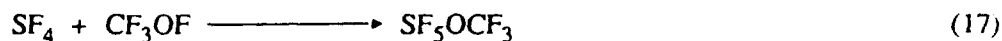
	<u>δ, ppm</u>	<u>$^1\text{J}(\text{}^{19}\text{F}_{\text{eq}}-\text{}^{125}\text{Te})$, Hz</u>	<u>$^1\text{J}(\text{}^{19}\text{F}_{\text{eq}}-\text{}^{123}\text{Te})$, Hz</u>
TeF_6	-52.3	3800	^b

	<u>δ, ppm</u>	<u>$^1\text{J}(\text{}^{19}\text{F}_{\text{eq}}-\text{}^{125}\text{Te})$, Hz</u>
F_5TeO^-	-36.5	^a

a Not observed due to exchange.

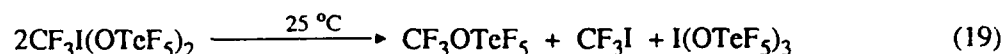
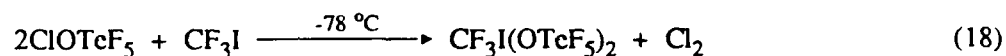
b Owing to the poor signal-to-noise ratio, this coupling could not be resolved from the baseline noise.

according to equation (17),⁷⁸ and thus, the preparation of the tellurium analog was attempted in the same manner.



In the first preparative attempt, the ^{19}F NMR spectrum was recorded of the products of the reaction between TeF_4 and CF_3OF at 150°C , which were not volatile at -78°C , in SO_2ClF solvent. The ^{19}F NMR spectrum at -50°C (Figure 16) exhibited only a singlet flanked by satellites at -52.7 ppm [$^1J(^{19}\text{F}-^{125}\text{Te}) = 3742$ Hz; $^1J(^{19}\text{F}-^{123}\text{Te}) = 3104$ Hz] in the F-on-octahedral Te(VI) region, which was assigned to TeF_6 . Thus, it appears that TeF_5OCF_3 cannot be prepared by oxidative addition of CF_3OF to TeF_4 .

The second preparative attempt proceeded according to the previous preparation of TeF_5OCF_3 , by Christie and coworkers, reactions (18) and (19), in which CF_3I reacted with ClOTeF_5 to produce TeF_5OCF_3 in an approximate yield of only 17 %.⁴⁶ Attempts to duplicate these results proved unsuccessful, and further attempts to prepare TeF_6OCF_3 were abandoned.



PREPARATION OF $(\text{CH}_3)_4\text{N}^+\text{TeF}_6\text{CN}^-$

The ^{19}F NMR spectra of the products of the reaction between $(\text{CH}_3)_4\text{N}^+\text{TeF}_7^-$ and $(\text{CH}_3)_3\text{SiCN}$, in CH_3CN solvent, were recorded after warming the sample from -196 to -45 , -20 , 0°C , and finally to room temperature. After each warming the sample was cooled to -45°C , and the spectra run at -45°C . The ^{13}C and ^{125}Te NMR spectra were recorded only after warming to -45°C . In every instance, the solution colour became, initially, faint pink upon warming to -45°C , and darkened with time. Upon warming to -20°C the solution colour became light orange, while warming to 0°C and above produced a turbid, brown coloured solution.

The ^{19}F NMR spectra of the reaction products after warming to -45°C (Figure 17) showed two singlets with satellites, in the F-on-heptacoordinated Te(VI) region, and a decet in the F-on-Si(IV) region. The more intense singlet at 16.2 ppm, showing both ^{125}Te and ^{123}Te satellites, was attributed to the TeF_7^- anion, in good agreement with previously obtained data,² while the weaker singlet at 34.7 ppm was attributed to the new monocyano-substituted TeF_6CN^- anion. The decet centered at -156.7 ppm, with ^{29}Si satellites, was attributed to $(\text{CH}_3)_3\text{SiF}$ (Figure 18).⁷⁹ The chemical shifts and coupling constants for all the observed species are listed

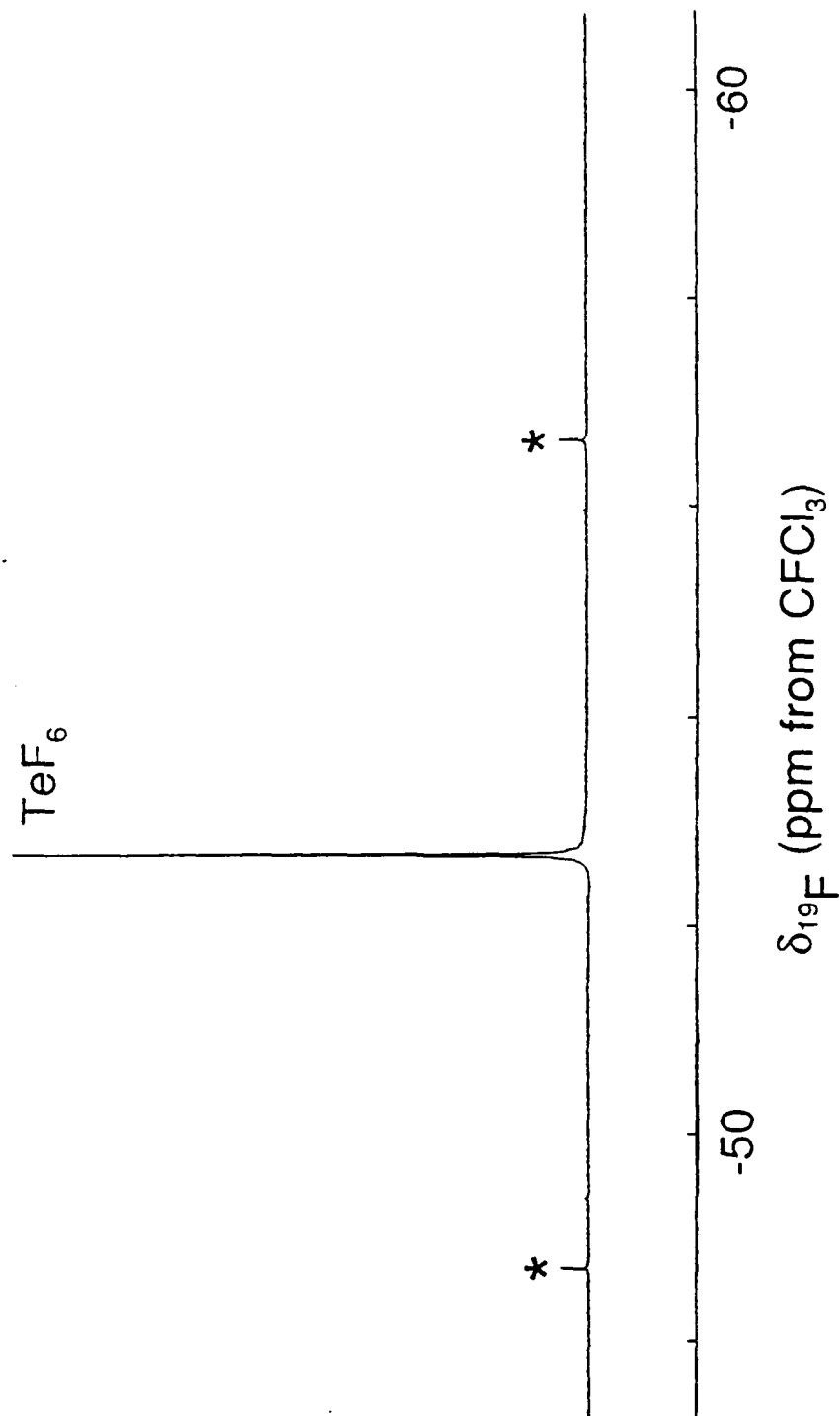
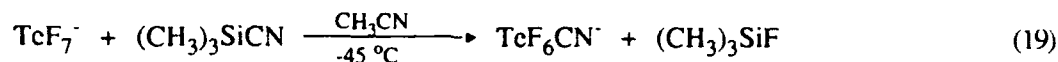


Figure 16. The ^{19}F NMR spectrum (470.599 MHz) at -45°C of the products not volatile at -78°C from the reaction mixture $\text{CF}_3\text{OF} + \text{TeF}_4$.

in Table 7. The reaction to form TeF_6CN^- proceeded according to equation (20)



According to ^{19}F NMR data, the heptacoordinated TeF_6CN^- anion was produced in ca. 3.5 % yield at $-45\text{ }^\circ\text{C}$.

The ^{125}Te NMR spectrum of the reaction products after warming to $-45\text{ }^\circ\text{C}$ showed a binomial octet and a binomial septet in the heptacoordinated Te(VI) region (Figure 19). The intense binomial octet at 326.1 ppm was attributed to TeF_7^- , in accordance with the published data², while the weak septet at 300.0 ppm was attributed to TeF_6CN^- . The one-bond ^{19}F - ^{125}Te coupling constants for both of these species (Table 7), are in good agreement with those found in the ^{19}F spectrum, and are ca. 1000 Hz smaller than those found for octahedrally coordinated Te(VI) species.

The natural abundance ^{13}C NMR spectrum at $-45\text{ }^\circ\text{C}$ (Figure 20) supports the formation of $(\text{CH}_3)_3\text{SiF}$ as a reaction product. Two overlapping quartets were observed at ~ 2 ppm; the less intense quartet of doublets at -0.2 ppm was attributed to $(\text{CH}_3)_3\text{SiF}$, while the more intense quartet at 1.9 ppm was attributed to the methyl carbon of the solvent CH_3CN . The singlet at 119 ppm was attributed to the cyano carbon of the solvent CH_3CN . The quartet at 56 ppm was assigned to the $(\text{CH}_3)_4\text{N}^+$ cation. All these chemical shifts are in good agreement with the literature values.^{80,81} There was also a weak unassigned resonance at 96 ppm, while the resonance for $(\text{CH}_3)_3\text{SiCN}$ could not be discerned. Owing to the low yield of TeF_6CN^- , the weak resonance expected for the CN environment in TeF_6CN^- could not be assigned unequivocally; a ^{13}C enriched sample would be required to do this. The ^{13}C chemical shifts and coupling constants for the above species are given in Table 7.

The ^{19}F NMR spectra of the reaction products after warming to $-20\text{ }^\circ\text{C}$ (Figure 21) were not identical to those at $-45\text{ }^\circ\text{C}$. The peak assigned to TeF_6CN^- was marginally more intense in comparison with the ^{125}Te satellite peaks of TeF_7^- , and there was a new AX_4 multiplet of weak intensity in the pentacoordinated Te(IV) region, which was attributed to the square pyramidal TeF_5^- anion by comparison with literature data.⁸² The ^{19}F NMR spectra of the reaction products after warming to $0\text{ }^\circ\text{C}$ showed an increase in the intensity of the multiplet assigned to TeF_5^- , and a decrease in intensity of the resonance assigned to TeF_6CN^- . After warming the sample to room temperature (Figure 22), the peak assigned to TeF_6CN^- had totally disappeared, while those assigned to TeF_5^- and TeF_7^- had increased in intensity.

The production of TeF_5^- and TeF_7^- anions upon warming of the sample, combined with the disappearance

Table 7. ^{13}C , ^{19}F , and ^{125}Te NMR Data for Products Observed in the Reaction Between $(\text{CH}_3)_4\text{N}^+\text{TeF}_7^-$ and $(\text{CH}_3)_3\text{SiCN}$ in CH_3CN Solvent at -45°C

Heptacoordinated-Te(VI) Environments:

	<u>Nucleus</u>	<u>δ, ppm</u>	<u>$^1\text{J}(^{19}\text{F}-^{125}\text{Te})$, Hz</u>	<u>$^1\text{J}(^{19}\text{F}-^{123}\text{Te})$, Hz</u>
TeF_7^-	^{19}F	16.2	2883	2390
TeF_6CN^-	^{19}F	34.7	2896	- ^a
TeF_7^-	^{125}Te	326.1	2882	
TeF_6CN^-	^{125}Te	300.0	2890	

Pentacoordinated-Te(IV) Environments:

	<u>Nucleus</u>	<u>$\delta(\text{A})$, ppm</u>	<u>$\delta(\text{X}_4)$, ppm</u>	<u>$^2\text{J}(^{19}\text{F}_{\text{ax}}-^{19}\text{F}_{\text{eq}})$, Hz</u>
TeF_5^-	^{19}F	-18.8	-36.9	170

F-on-Si(IV) Environment:

	<u>Nucleus</u>	<u>δ, ppm</u>	<u>$^1\text{J}(^{19}\text{F}-^{29}\text{Si})$, Hz</u>	<u>$^3\text{J}(^1\text{H}-^{19}\text{F})$, Hz</u>
$(\text{CH}_3)_3\text{SiF}$	^{19}F	-156.7	268	6.0

^{13}C Environments:

	<u>Nucleus</u>	<u>δ, ppm</u>	<u>$^1\text{J}(^1\text{H}-^{13}\text{C})$, Hz</u>	<u>$^2\text{J}(^{13}\text{C}-^{19}\text{F})$, Hz</u>
$(\text{CH}_3)_3\text{SiF}$	^{13}C	-0.2	120	12.9
$(\text{CH}_3)_3\text{SiCN}$	^{13}C	- ^a	- ^a	
CH_3CN	^{13}C	1.9	136	
CH_3CN	^{13}C	118.7	- ^b	
$(\text{CH}_3)_4\text{N}^+$	^{13}C	55.5	144	

a Not observed due to low intensity of signal.

b Too small to be resolved.

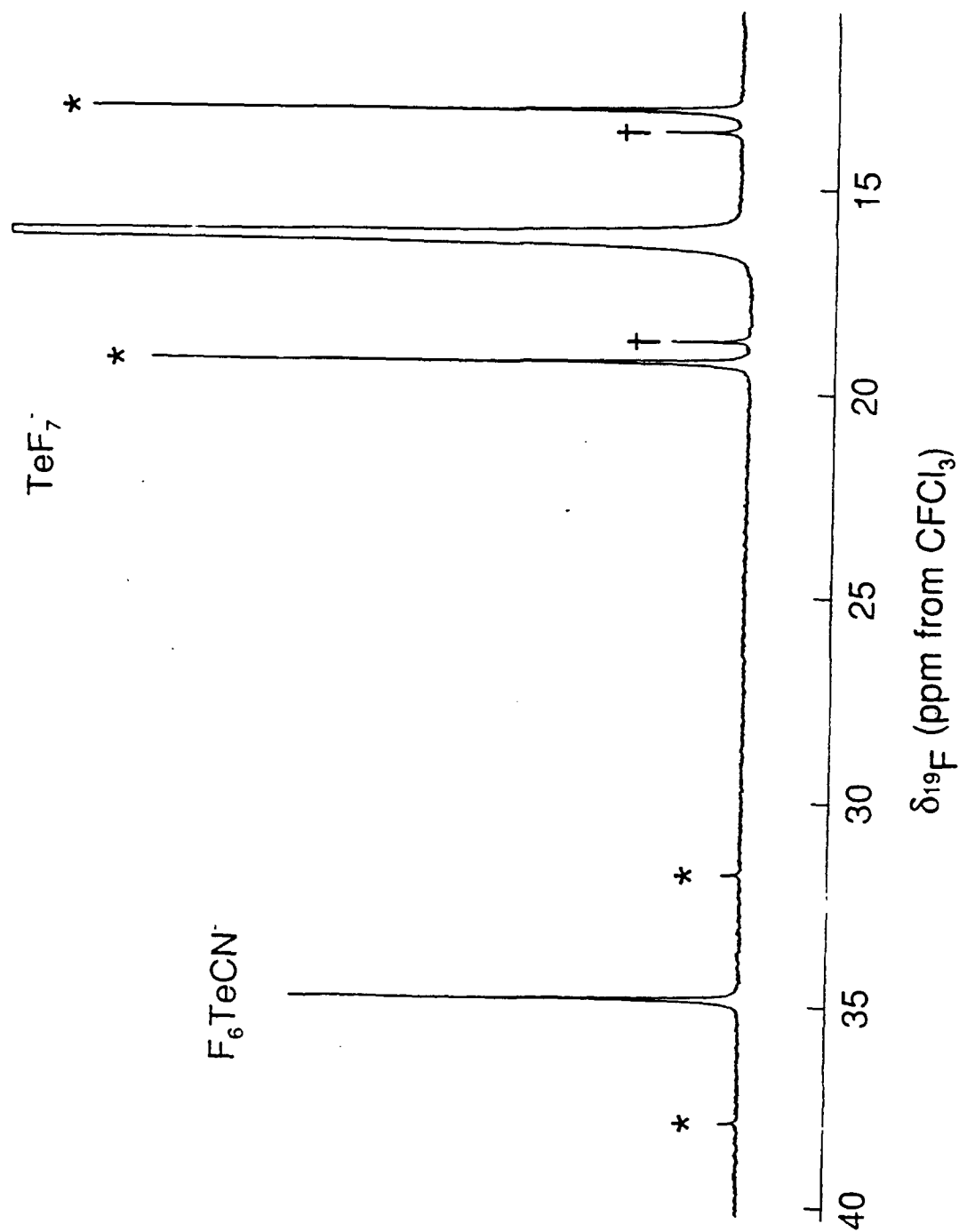


Figure 17. The ^{19}F NMR spectrum (470.599 MHz) at -45°C of the reaction mixture $(\text{CH}_3)_4\text{N}^+\text{TeF}_7^- + (\text{CH}_3)_3\text{SiCN}$ in CH_3CN after warming to -45°C . Asterisks (*) denote ^{125}Te satellites; crosses (†) denote ^{123}Te satellites.

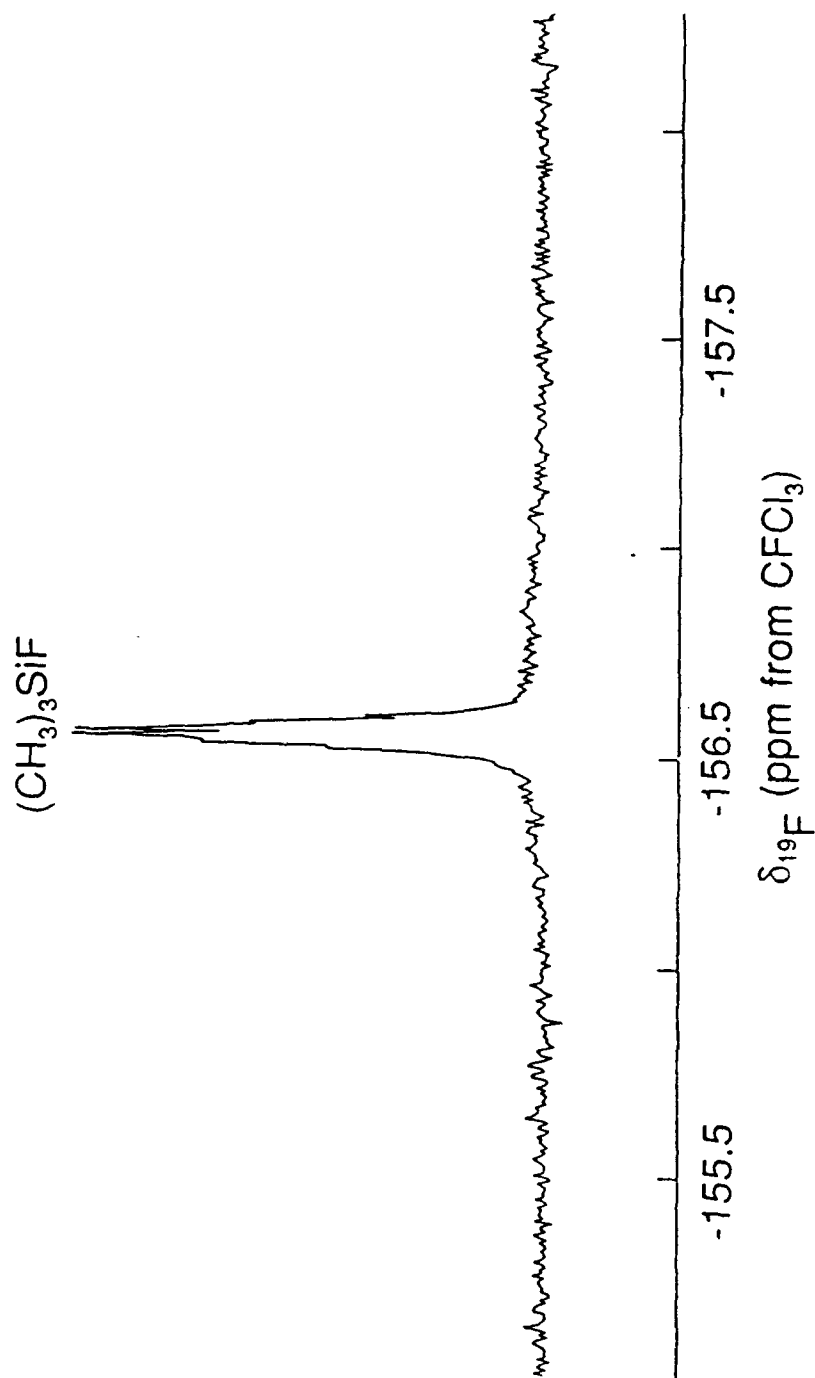
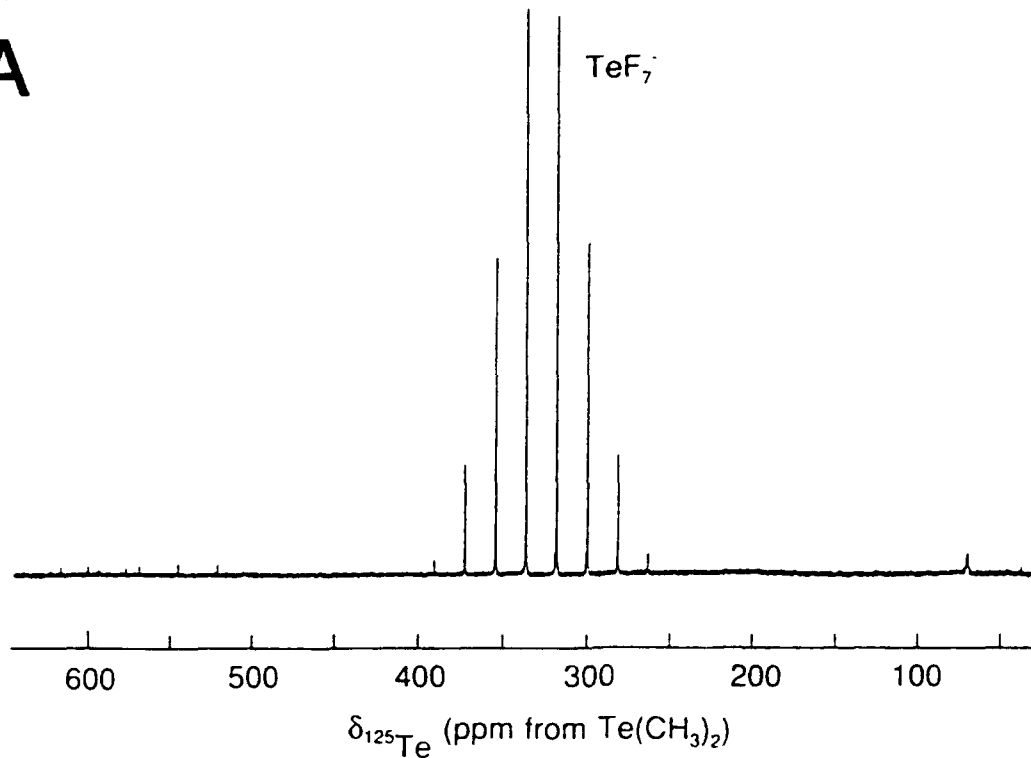


Figure 18. The F-on-Si(IV) region of the ^{19}F NMR spectrum (470.599 MHz) at -45°C of the reaction mixture $(\text{CH}_3)_4\text{N}^+\text{TeF}_6^- + (\text{CH}_3)_3\text{SiCN}$ in CH_3CN after warming to -45°C .

A

49



B

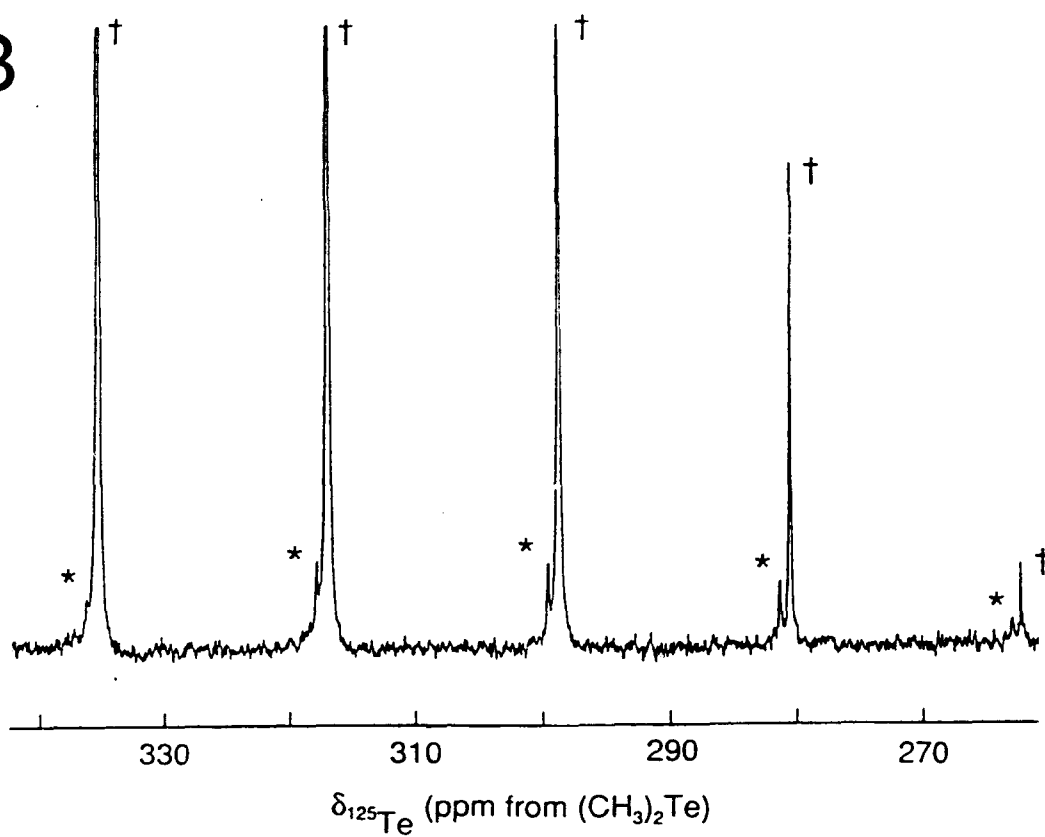


Figure 19. The ^{125}Te NMR spectrum (157.792 MHz) at -45°C of the reaction mixture $(\text{CH}_3)_4\text{N}^+\text{TeF}_7^-$ + $(\text{CH}_3)_3\text{SiCN}$ in CH_3CN after warming to -45°C . (A) low gain; (B) high gain. Asterisks (*) denote TeF_6CN^- ; crosses (†) denote TeF_7^- .

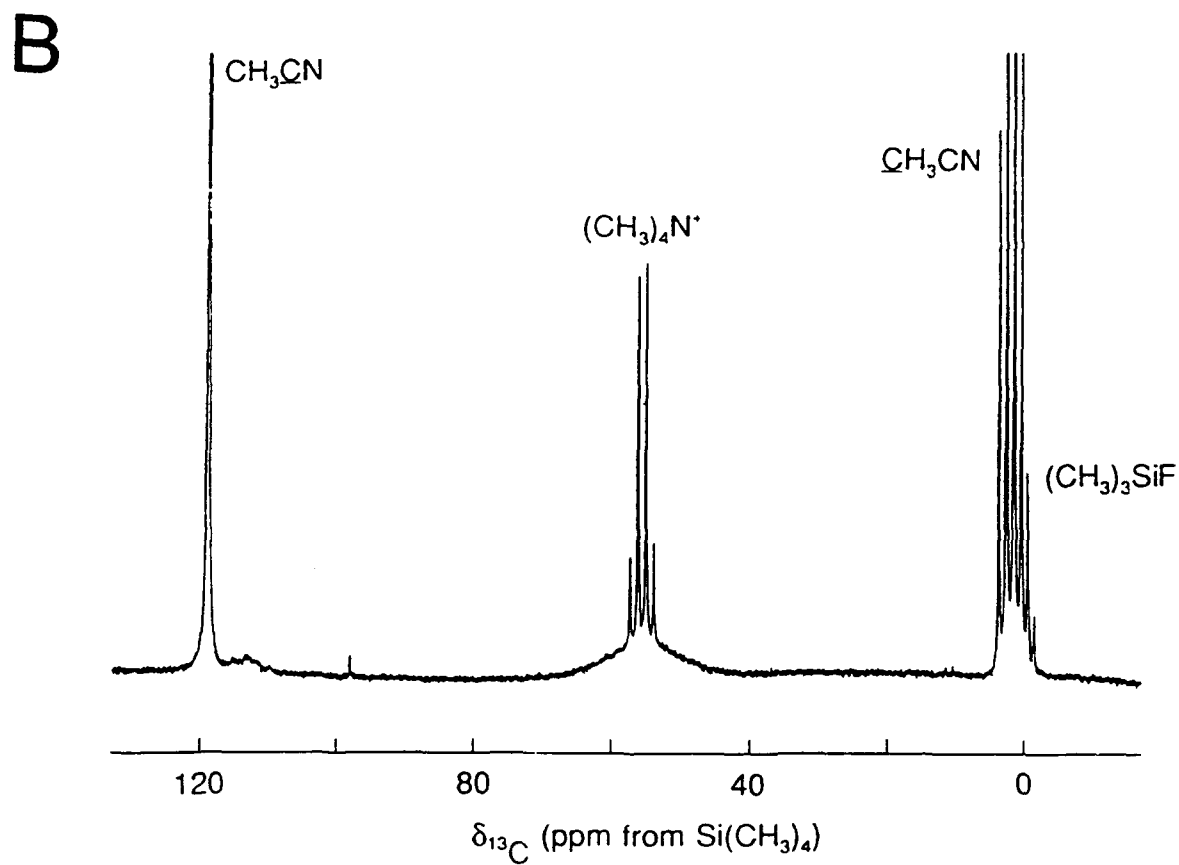
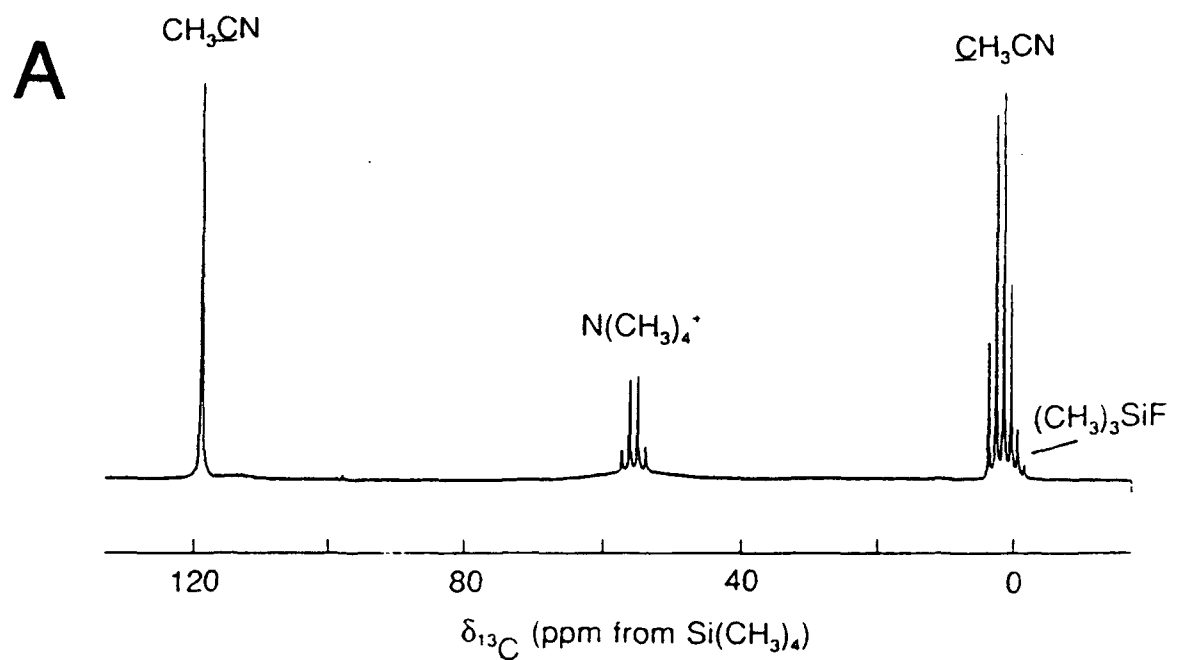


Figure 20. The ^{13}C NMR spectrum (125.759 MHz) at -45°C of the reaction mixture $(\text{CH}_3)_4\text{N}^+\text{TeF}_7^-$ + $(\text{CH}_3)_3\text{SiCN}$ in CH_3CN after warming to -45°C . (A) low gain; (B) high gain.

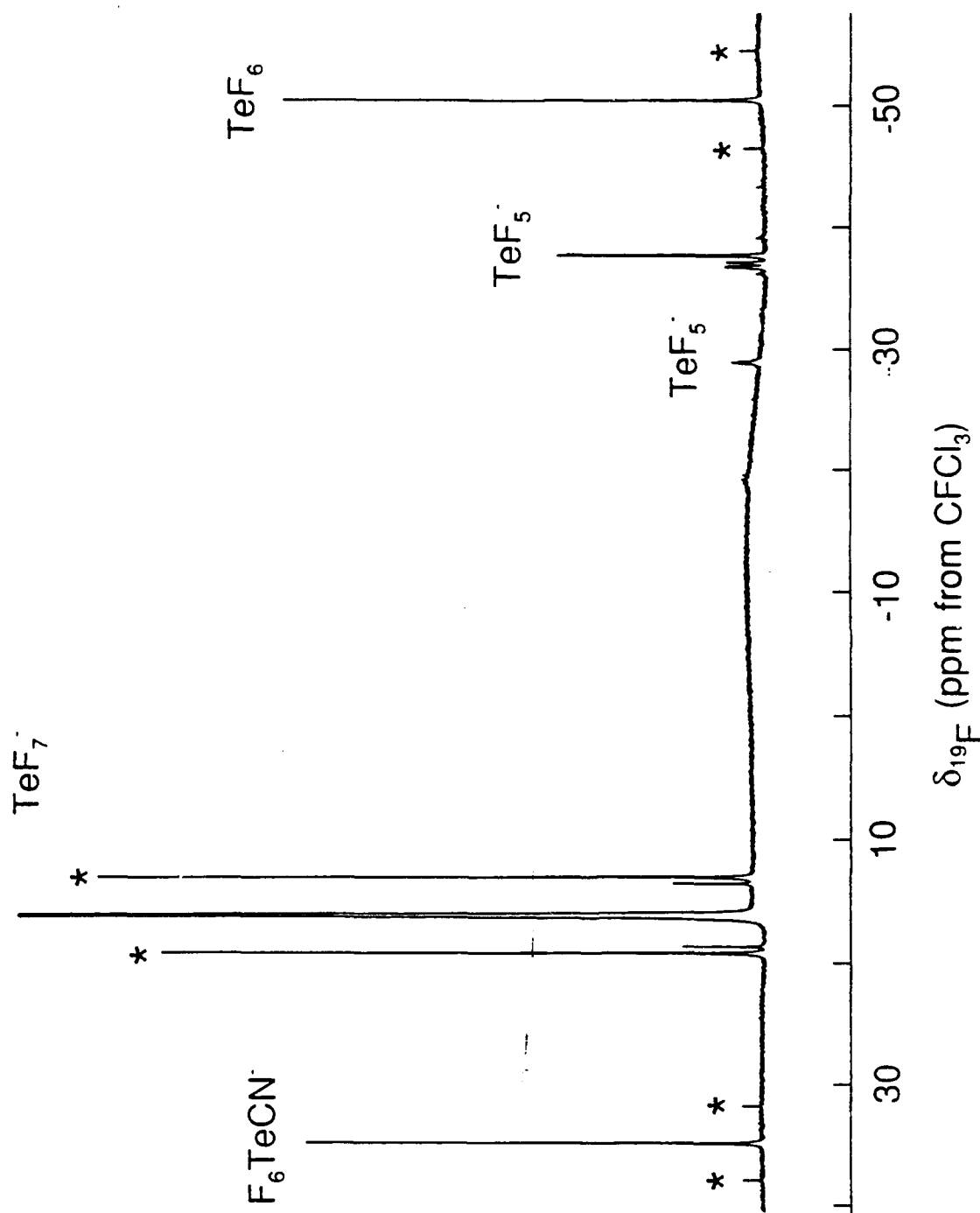


Figure 21. The ^{19}F NMR spectrum (470.599 MHz) at -45°C of the reaction mixture $(\text{CH}_3)_4\text{N}^+\text{TeF}_7^- + (\text{CH}_3)_3\text{SiCN}$ in CH_3CN after warming to -20°C . Asterisks (*) denote ^{125}Te satellites; crosses (†) denote ^{123}Te satellites.

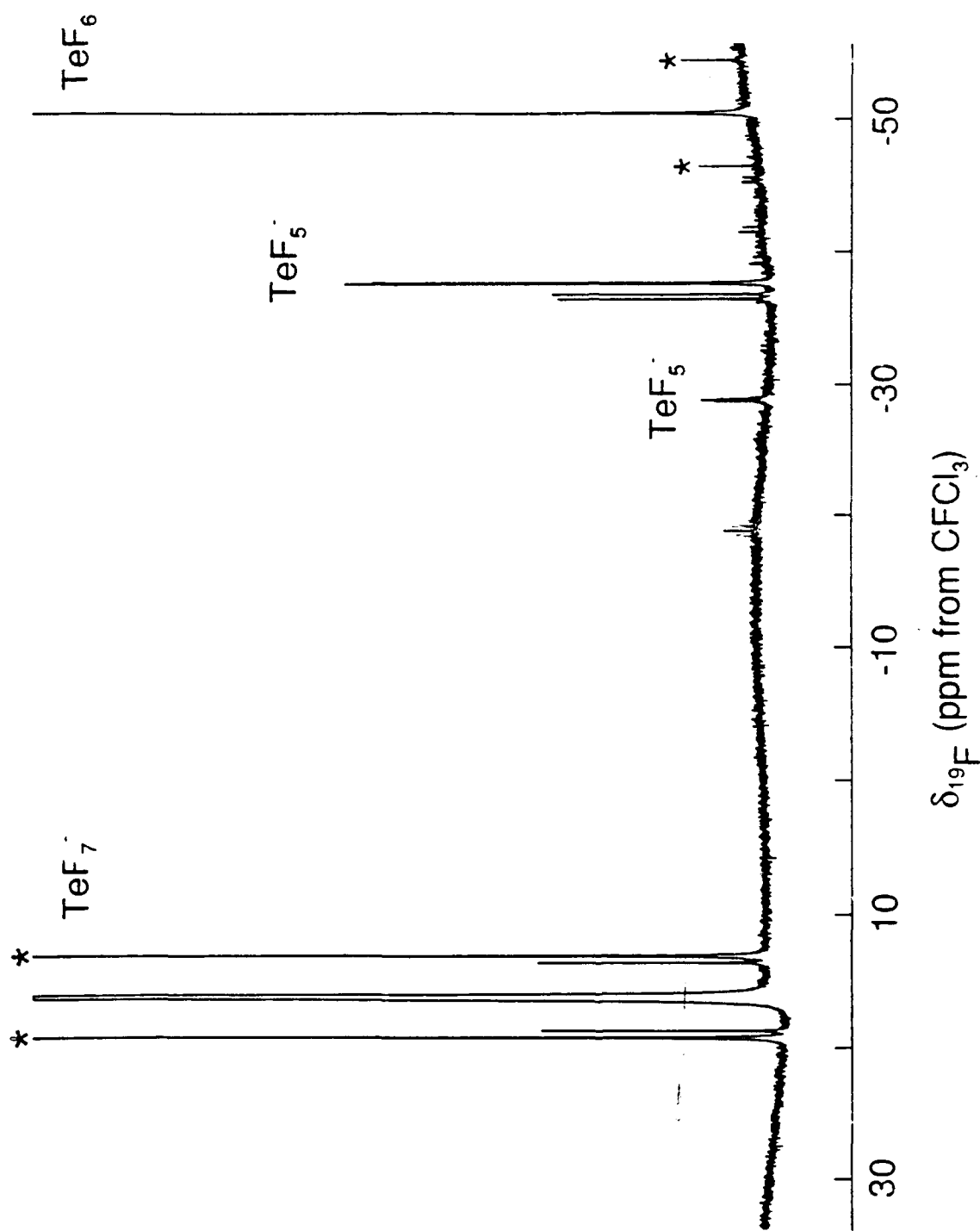
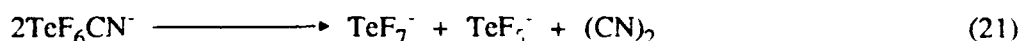


Figure 22. The ^{19}F NMR spectrum (470.599 MHz) at -45°C of the reaction mixture $(\text{CH}_3)_4\text{N}^+\text{TeF}_7^- + (\text{CH}_3)_3\text{SiCN}$ in CH_3CN after warming to 25°C . Asterisks (*) denote ^{125}Te satellites; crosses (x) denote ^{123}Te satellites.

of the TeF_6CN^- anion, suggests that TeF_6CN^- is not thermally stable, and that it readily decomposes above -20°C . The Te-CN bond is believed to be relatively weak due to the large ionic character of the bond. The CN ligand is readily oxidizable to the parent pseudohalogen cyanogen, and thus, there can be electron transfer from Te(VI) to the CN ligand. The decomposition of the TeF_6CN^- anion is believed to proceed according to equation (21), although the observation of cyanogen, which would confirm this pathway, would probably require ^{13}C enrichment and subsequent ^{13}C NMR characterization since no unequivocal assignment of cyanogen could be made in the natural abundance ^{13}C spectrum.



The observation of a binomial septet in the ^{125}Te NMR spectrum suggests that, by analogy with the TeF_7^- anion, the TeF_6CN^- anion is also fluxional on the NMR time scale. The expected geometry of TeF_6CN^- is given in Figure 23.

PREPARATION OF TeF_5CN

Although TeF_5CN had not been reported, it was thought that this species might be a useful precursor in a higher yield preparation of the TeF_6CN^- anion. The first chalcogen to form a stable MF_5CN compound was sulfur, with SF_5CN being prepared in 1989,⁸³ while the selenium analog is still unknown. Pentafluorosulfur cyanide was prepared, in a 5 % yield, by fluorinating $(\text{SCN})_2$ in $\text{Cl}_2\text{FCClF}_2$ with dilute F_2 ($\text{F}_2 : \text{N}_2 = 1 : 10$) at -20°C to produce a product mixture which was then condensed into a 2 M KOH solution at room temperature in order to separate the desired product.

The ^{19}F NMR spectra of the products of the reaction between TeF_6 and $(\text{CH}_3)_3\text{SiCN}$ were recorded in both CH_3CN and SO_2ClF solvents, while the ^{125}Te NMR spectra were recorded only in SO_2ClF solvent. The ^{19}F NMR spectra of the reaction products in CH_3CN solvent were recorded after warming the sample successively from -196 to -45 , -22°C , and finally to room temperature, while the spectra of the reaction products in SO_2ClF solvent were initially warmed to -45°C and then to room temperature. The ^{125}Te NMR sample was treated similarly. After each warming, the sample was cooled to -45°C , and the spectra run at -45°C . Samples using SO_2ClF as the solvent showed no colour changes upon warming from -196°C to room temperature; similarly the CH_3CN samples were also colourless throughout the series of warmings.

The ^{19}F NMR spectra of the reaction products, in CH_3CN solvent, after warming to -45°C showed only

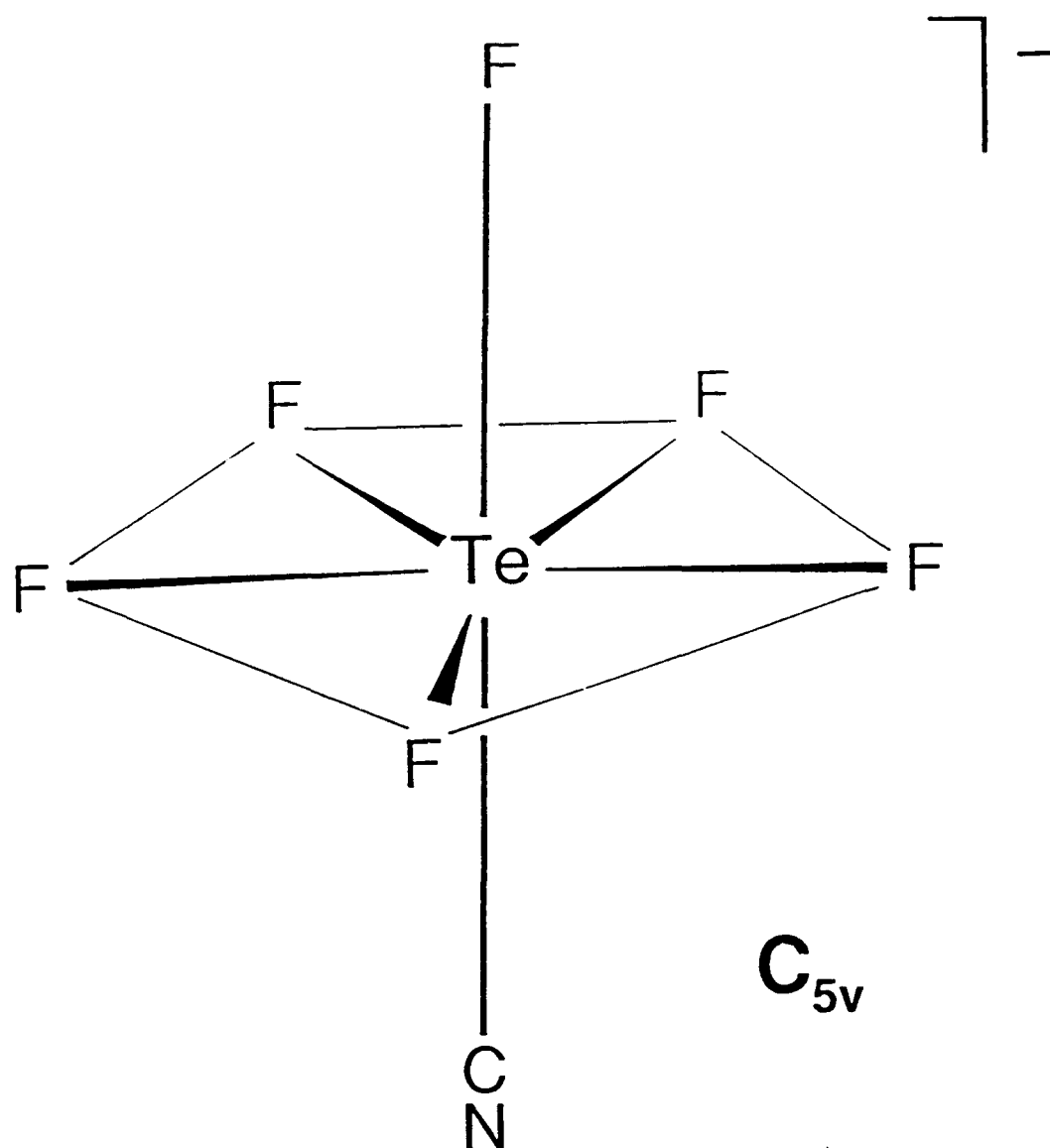
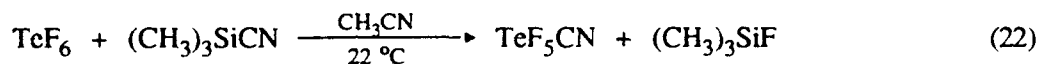
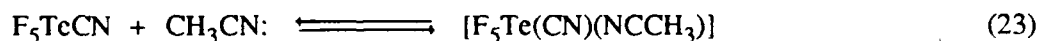


Figure 23. Expected geometry of the TeF_6CN^- anion.

a singlet with flanking satellites, in the octahedrally coordinated Te(VI) region, at -50.6 ppm (Figure 24). This resonance was due to TeF_6 , as established by comparison with the literature values and prior results. Upon warming to -22°C for 4 minutes an additional weak singlet appeared at -55.7 ppm, also in the octahedrally coordinated Te(VI) region, which was slightly broadened ($\Delta\nu_{\text{L}} = 371\text{ Hz}$) and at higher frequency relative to the TeF_6 resonance (Figure 25). In addition, there was a resonance with satellites in the F-on-Si(IV) region, which was attributed to $(\text{CH}_3)_3\text{SiF}$, as determined in previous samples. After warming briefly to 0°C , then to room temperature for 45 minutes, the resonance at -55.7 ppm had increased in intensity and now displayed ^{125}Te satellites (Figures 26 and 27). The resonance in the F-on-Si(IV) region also increased in intensity. The broadened resonance was tentatively attributed to the new mono-cyano substituted species TeF_5CN . The chemical shifts and coupling constants for these two species are listed in Table 8. The reaction to form TeF_5CN proceeded according to reaction (22)



According to integrated ^{19}F NMR data, at room temperature, TeF_5CN was produced in ca. 8 % yield. The observation of a broadened resonance in the Te(VI) region indicates that TeF_5CN is either fluxional, or exchanging, on the NMR time scale. It is not common for octahedral molecules to be fluxional on the NMR timescale, but Te(VI) compounds can readily form heptacoordinated species, as demonstrated by the syntheses of TeF_7^{2-} and TeF_6CN^- in this work. Presumably, the CH_3CN solvent, which is quite a strong donor solvent, can form a labile adduct with TeF_5CN (reaction 23), and thereby enter into the coordination sphere of Te(VI), inducing an intramolecular fluorine exchange among the ligand sites.



The ^{19}F and ^{125}Te NMR spectra of the reaction products, in SO_2ClF solvent, which is less polar compared with CH_3CN , showed that no reaction took place, neither upon warming to -45°C , nor upon warming to room temperature for 2 hours; only TeF_6 was present in the octahedrally coordinated Te(VI) region. The solubilities of $(\text{CH}_3)_3\text{SiCN}$ and TeF_6 in SO_2ClF were good, but even so no reaction was detected. Therefore, these results indicate that the reaction of $(\text{CH}_3)_3\text{SiCN}$ with TeF_6 to give TeF_5CN was solvent assisted by CH_3CN coordination. The expected geometry of TeF_5CN is given in Figure 29.

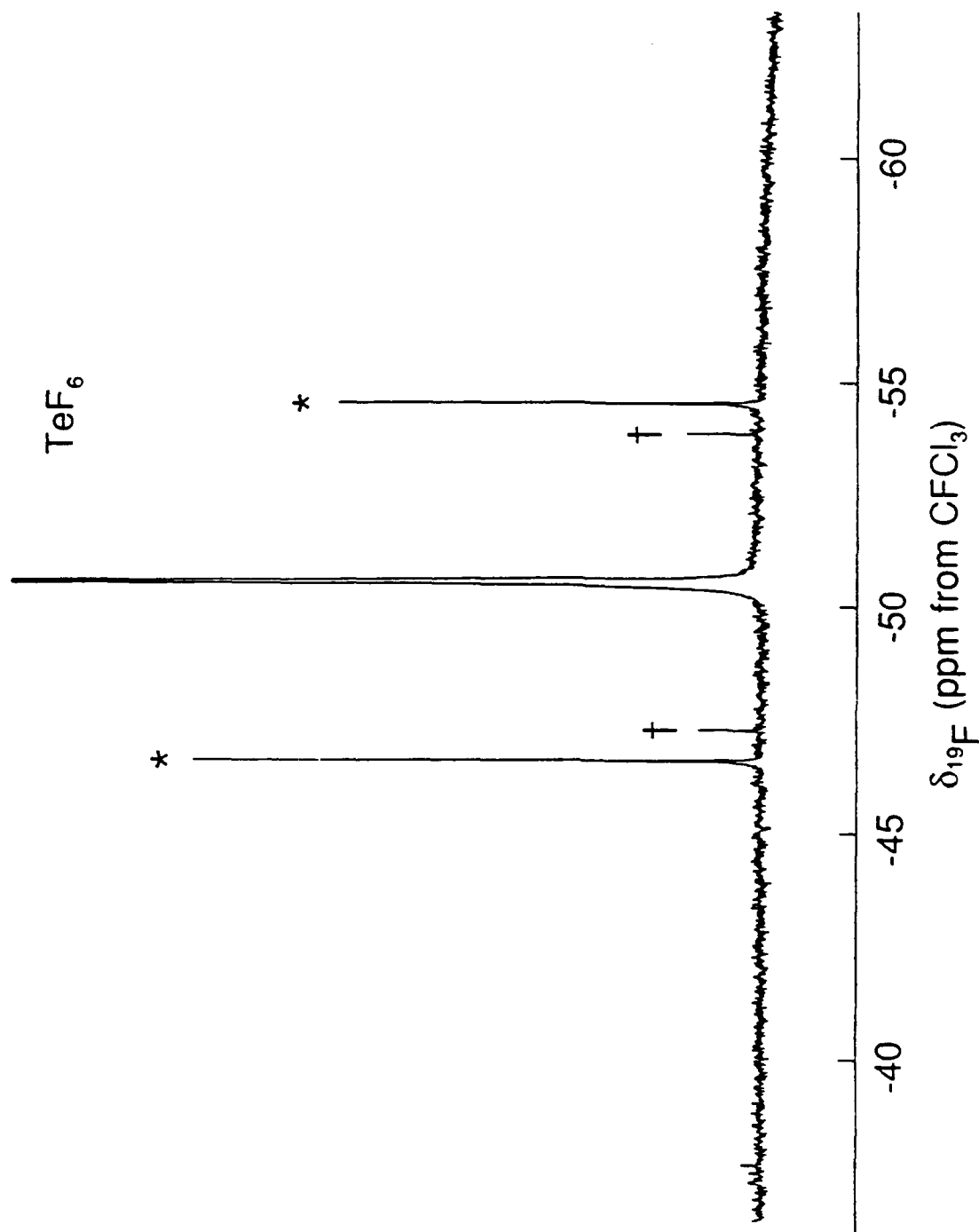


Figure 24. The ^{19}F NMR spectrum (470.599 MHz) at -45°C of the reaction mixture $\text{TeF}_6 + (\text{CH}_3)_3\text{SiCN}$ in CH_3CN after warming to -45°C . Asterisks (*) denote ^{125}Te satellites; crosses (†) denote ^{123}Te satellites.

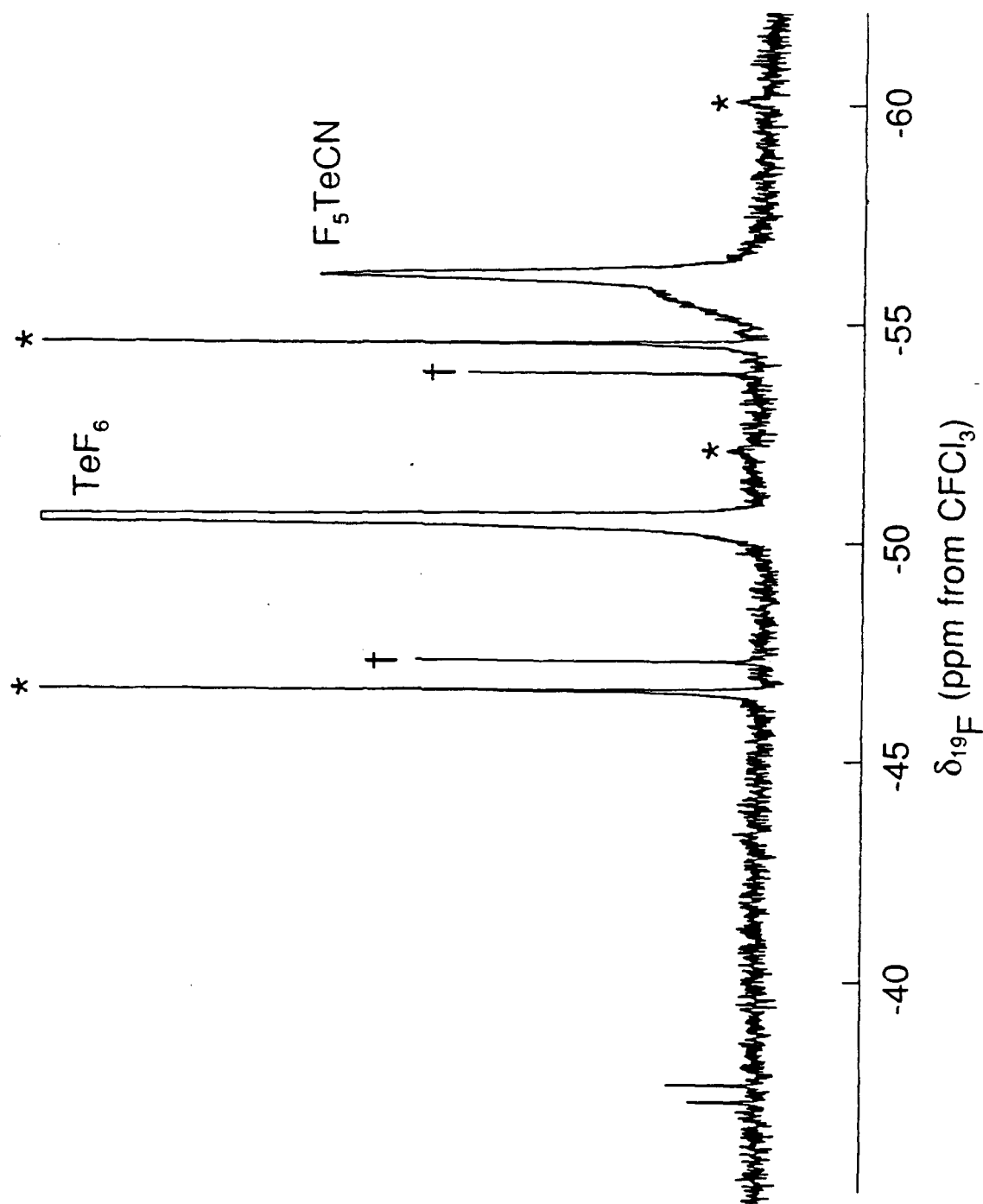


Figure 25. The ^{19}F NMR spectrum (470.599 MHz) at -45°C of the reaction mixture $\text{TeF}_6 + (\text{CH}_3)_3\text{SiCN}$ in CH_3CN after warming to -22°C . Asterisks (*) denote ^{125}Te satellites; crosses (+) denote ^{123}Te satellites.

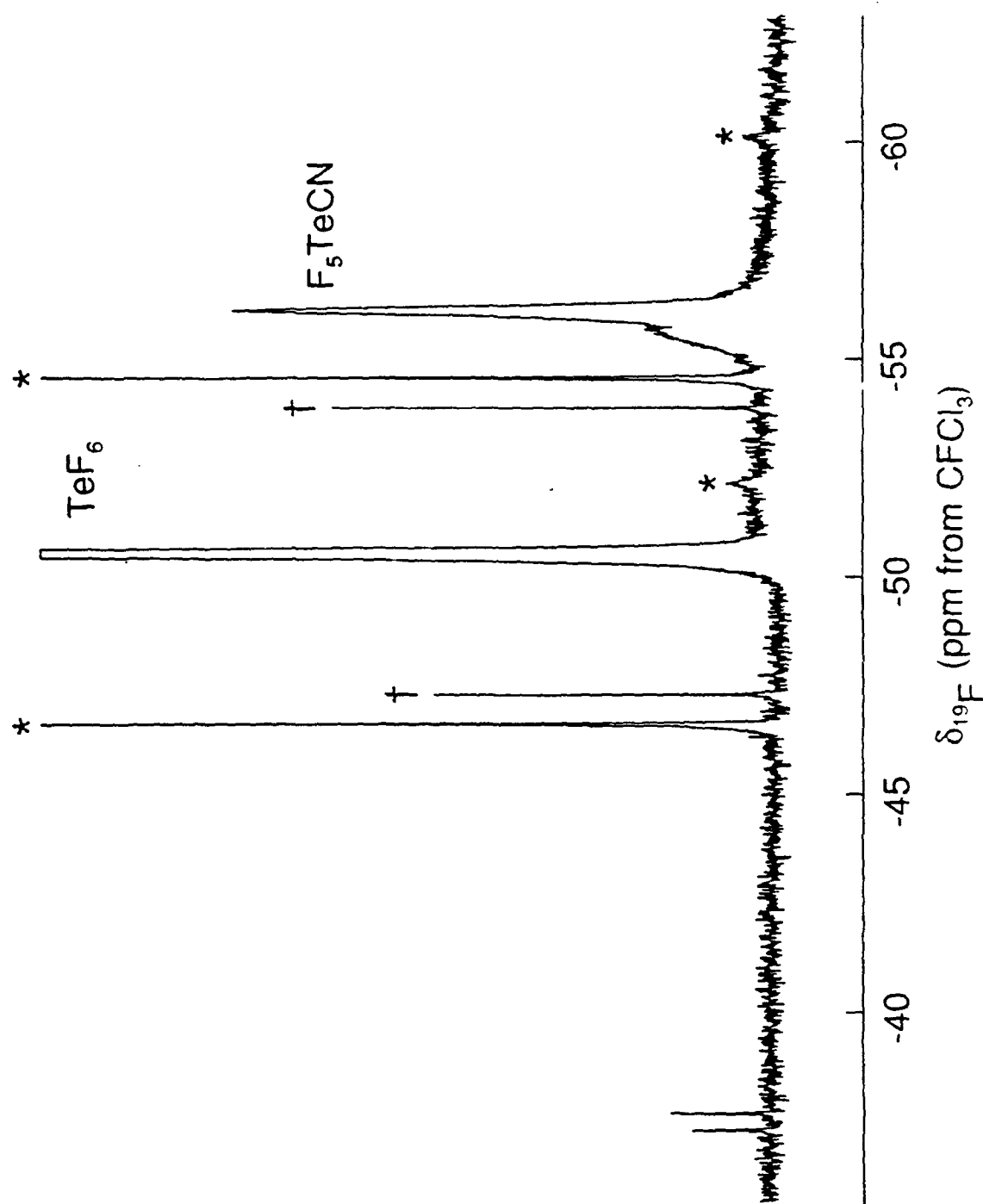


Figure 26. The ^{19}F NMR spectrum (470.599 MHz) at -45°C of the reaction mixture $\text{TeF}_6 + (\text{CH}_3)_3\text{SiCN}$ in CH_3CN after warming to 0°C . Asterisks (*) denote ^{125}Te satellites; crosses (†) denote ^{123}Te satellites.

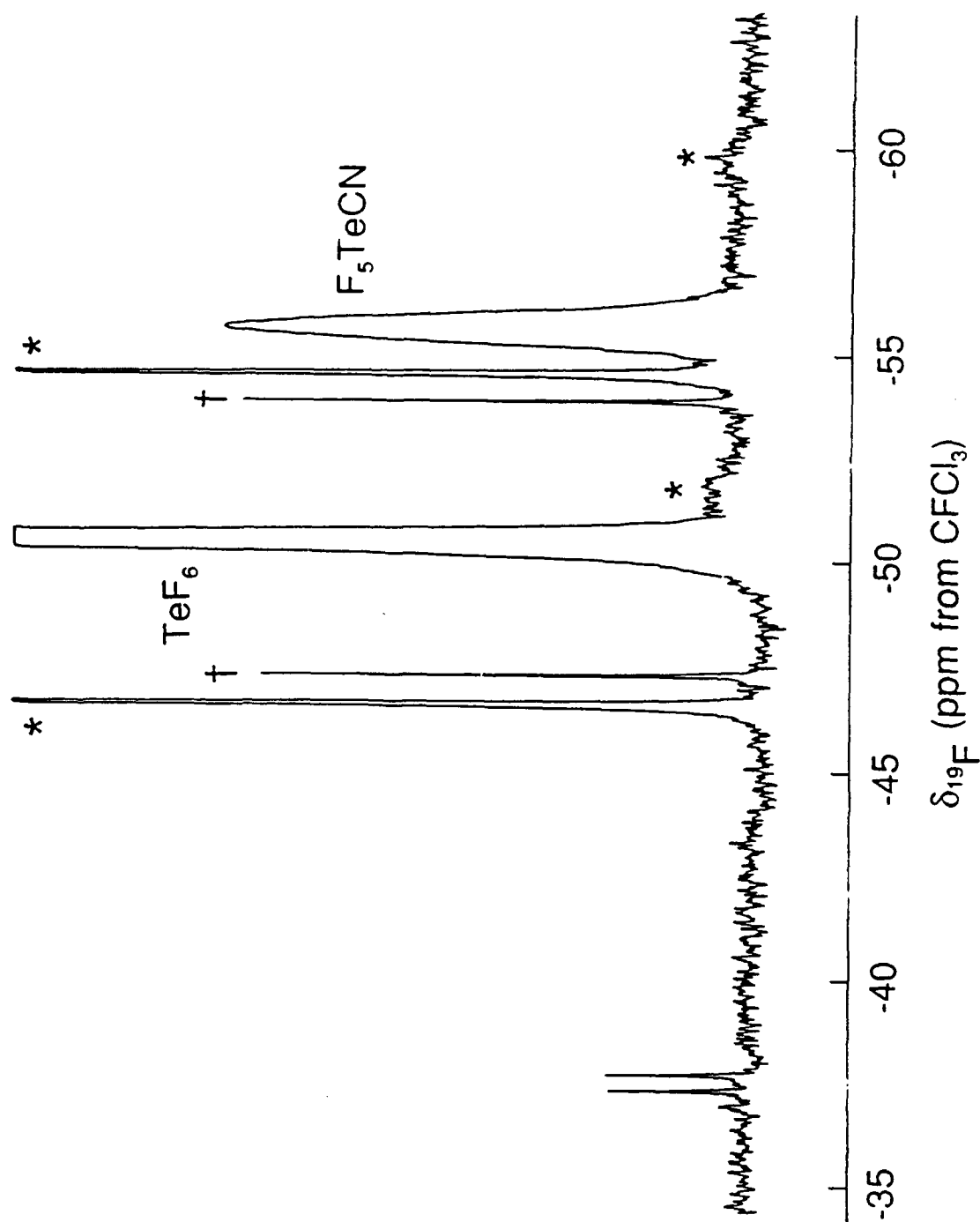


Figure 27. The ^{19}F NMR spectrum (470.599 MHz) at -45°C of the reaction mixture $\text{TeF}_6 + (\text{CH}_3)_3\text{SiCN}$ in CH_3CN after warming to 25°C . Asterisks (*) denote ^{125}Te satellites; crosses (†) denote ^{125}Te satellites.

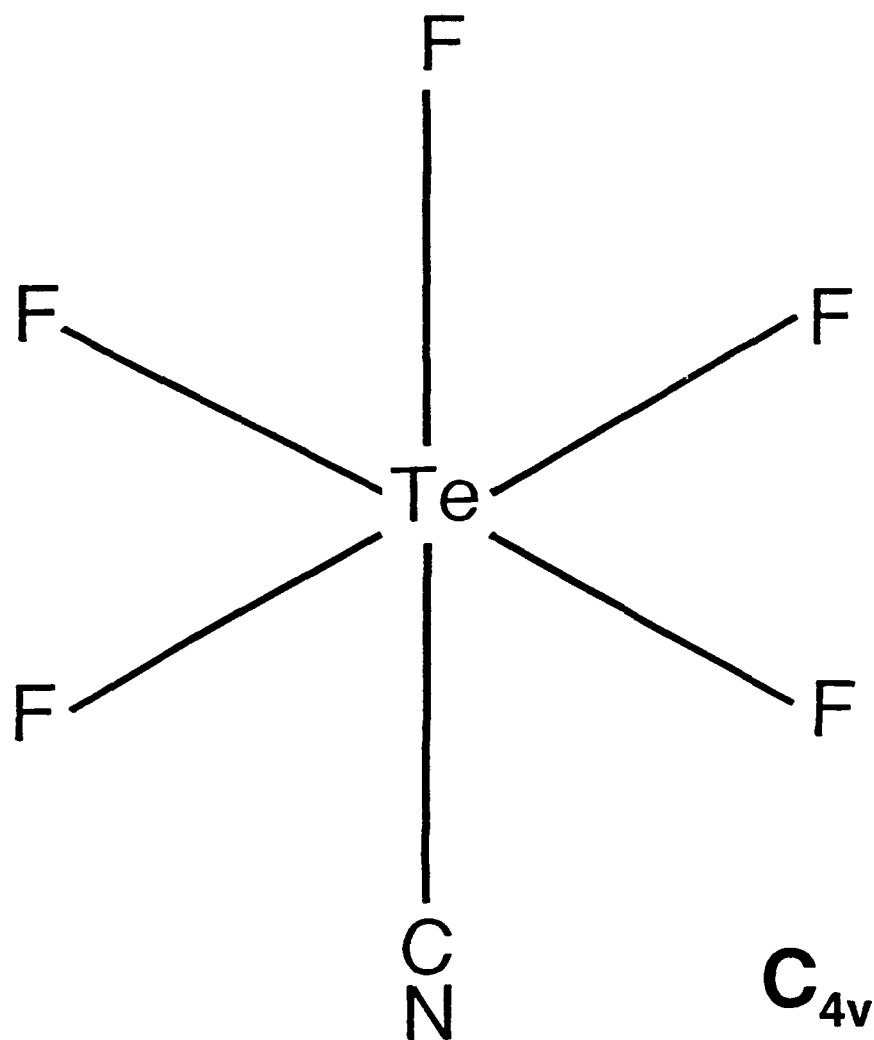


Figure 28. Expected geometry of TeF_5CN .

Table 8. ^{19}F NMR Data for Products Observed in the Reaction Between TeF_6 and $(\text{CH}_3)_3\text{SiCN}$ in CH_3CN Solvent at -45°C

Hexacoordinated-Te(VI) Environments:

	<u>δ, ppm</u>	<u>$^1\text{J}(^{19}\text{F}-^{125}\text{Te})$, Hz</u>	<u>$^1\text{J}(^{19}\text{F}-^{123}\text{Te})$, Hz</u>
TeF_6	-50.6	3754	3115
TeF_5CN	-55.7	3801	^a

F-on-Si(IV) Environment:

	<u>δ, ppm</u>	<u>$^1\text{J}(^{19}\text{F}-^{29}\text{Si})$, Hz</u>	<u>$^3\text{J}(^1\text{H}-^{19}\text{F})$, Hz</u>
$(\text{CH}_3)_3\text{SiF}$	-156.7	6.0	268

^a Too weak to be observed.

CONCLUSIONS AND FUTURE WORK

The ^{19}F NMR spectra of the attempted preparation of $\text{Te}(\text{OTeF}_5)_7^-$ showed that no reaction had occurred at either $-50\text{ }^\circ\text{C}$ or $0\text{ }^\circ\text{C}$, while the ^{19}F NMR spectra of the attempted preparation of $\text{TeF}_2(\text{OTeF}_5)_5^-$ showed only ligand exchange at $-50\text{ }^\circ\text{C}$ and $25\text{ }^\circ\text{C}$, producing a variety of pentacoordinated Te(IV) anions. The ^{19}F NMR data for the attempted preparation of $\text{TeF}_5(\text{OTeF}_5)_2^-$ suggest that there was oxidative-addition of OTeF_5 ligands to TeF_5^- , forming a labile heptacoordinated anion which decomposed to octahedrally coordinated Te(VI) species at $-50\text{ }^\circ\text{C}$. All three preparations were attempted in SO_2ClF solvent.

The attempted preparations of heptacoordinated OTeF_5 -substituted analogs of TeF_7^- have been unsuccessful, both by oxidative- and non-oxidative ligand transfer. An OTeF_5 -substituted analog of TeF_7^- would be expected to exhibit intramolecular ligand exchange and possess a pentagonal bipyramidal geometry, as does TeF_7^- . It is hypothesized that due to the steric bulk of the OTeF_5 ligand, a heptacoordinated Te(VI) anion with OTeF_5 -substitution would become labile upon pseudorotation of the bulky OTeF_5 ligand into the equatorial plane.

The preparation of $\text{TeF}_6\text{OCF}_3^-$ was abandoned due to difficulty in preparing the precursor TeF_5OCF_3 ; two attempts to prepare TeF_5OCF_3 failed, including an attempt to oxidatively add CF_3OF to TeF_4 .

The unstable TeF_6CN^- anion was produced in ca. 3.5 % yield by combining together TeF_7^- and $(\text{CH}_3)_3\text{SiCN}$ in CH_3CN solvent at $-45\text{ }^\circ\text{C}$. At $-20\text{ }^\circ\text{C}$ the anion began to decompose, yielding Te(IV) and Te(VI) products; the decomposition was complete upon warming to room temperature. The ^{19}F - ^{125}Te and ^{125}Te - ^{19}F coupling constants derived from ^{19}F and ^{125}Te NMR data, respectively, were in good agreement with each other, and also in good agreement with the TeF_7^- anion. In addition, the chemical shifts for the resonance attributed to TeF_6CN were located in the heptacoordinated Te(VI) region in both the ^{19}F and ^{125}Te NMR spectra.

In order to increase the yield of TeF_6CN^- , the logical precursor, TeF_5CN , was prepared. Initial observations indicate that this species was produced in ca. 8 % yield by reaction between TeF_6 and $(\text{CH}_3)_3\text{SiCN}$ in CH_3CN solvent. The reaction proceeded initially at $-22\text{ }^\circ\text{C}$ but was facilitated by warming to room temperature. The reaction seems to be facilitated by coordination with the CH_3CN solvent, since similar preparations using SO_2ClF solvent produced no reaction even though the solubilities of the reactants in SO_2ClF were excellent. The ability of octahedral TeF_6 to form heptacoordinated species is established, for TeF_7^- has been well characterized.

Future work could entail applying the method of preparing TeF_6CN^- to attempting the preparation of TeF_6NCO and TeF_6N_3^- by use of $(\text{CH}_3)_3\text{SiNCO}$ and $(\text{CH}_3)_3\text{SiN}_3$. The preparation of TeF_5CN needs to be further elucidated in order to optimize yields, and afford sufficient material to enable isolation of the pure substance. The pure TeF_5CN could then be utilized in the preparation of TeF_6CN^- . Further ^{13}C NMR studies need to be undertaken in order to confirm the proposed decomposition route of TeF_6CN^- to cyanogen upon warming to room temperature. Since CF_3OTeF_5 is difficult to prepare in good yield, attempts at preparing $\text{CF}_3\text{OTeF}_6^-$ are not easily facilitated. However, the analogous $\text{C}_2\text{F}_5\text{OTeF}_5$ can be prepared in quantitative yield⁴⁶ and, therefore, the synthesis of $\text{C}_2\text{F}_5\text{OTeF}_6^-$ is plausible and should be attempted.

REFERENCES

1. F.A. Cotton and G. Wilkinson, "Advanced Inorganic Chemistry", J. Wiley and Sons; Toronto, 1988, 493.
2. K.O. Christe, J.C.P. Sanders, G.J. Schrobilgen, and W.W. Wilson, *J. Chem. Soc., Chem. Commun.* 1991, 13, 837.
3. A. Mahjoub and K. Seppelt, *J. Chem. Soc., Chem. Commun.* 1991, 840.
4. K. Seppelt, *Z. Anorg. Allg. Chem.* 1977, 428, 35.
5. D. Lentz, H. Pritzkow and K. Seppelt, *Inorg. Chem.* 1978, 17, 1926.
6. K. Seppelt, *Angew. Chem. Int. Ed. Eng.* 1982, 21, 877.
7. G.W. Fraser and G.D. Meikle, *J. Chem. Soc., Chem. Commun.* 1974, 625.
8. U. Elgad and H. Selig, *Inorg. Chem.* 1975, 14, 140.
9. L. Kolditz and I. Fritz, *Z. Anorg. Allg. Chem.* 1967, 349, 175.
10. W. Tötsch and F. Sladky, *J. Chem. Soc., Chem. Commun.* 1980, 927.
11. W. Tötsch, P. Peringer and F. Sladky, *J. Chem. Soc., Chem. Commun.* 1981, 841.
12. K. Seppelt, *Angew. Chem.* 1974, 86, 104.
13. K. Seppelt, *Z. Anorg. Allg. Chem.* 1974, 406, 287.
14. M. Willert-Porada, H. Willner and K. Seppelt, *Spectrochim. Acta* 1981, 37A, 911.
15. K.O. Christe, W.W. Wilson, R.D. Wilson, R. Bau and J. Feng, *J. Am. Chem. Soc.* 1990, 112, 7619.
16. K.O. Christe, E.C. Curtis, D.A. Dixon, H.P. Mercier, J.C.P. Sanders and G.J. Schrobilgen, *J. Am. Chem. Soc.* 1991, 113, 3351.
17. (a) R.J. Gillespie and J.W. Quail, *Can. J. Chem.* 1964, 42, 2671; (b) E.L. Muetterties and K.J. Packer, *J. Am. Chem. Soc.* 1964, 86, 293.
18. R.J. Gillespie and I. Hargittai, "The VSEPR Model of Molecular Geometry", Allyn & Bacon, Boston, 1991.
19. K.O. Christe and W.W. Wilson, *Inorg. Chem.* 1982, 21, 4114.
20. K.O. Christe, W.W. Wilson, R.V. Chirakal, J.C.P. Sanders and G.J. Schrobilgen, *Inorg. Chem.* 1990, 29, 3506.
21. K.O. Christe and W.W. Wilson, *Inorg. Chem.* 1989, 28, 4172.
22. K.O. Christe and W.W. Wilson, *Inorg. Chem.* 1989, 28, 3275.

23. A. Mahjoub and K. Seppelt, *Angew. Chem. Int. Ed. Engl.* **1991**, 30, 323.
24. A. Mahjoub, A. Hoser, J. Fuchs and K. Seppelt, *Angew. Chem. Int. Ed. Engl.* **1989**, 28, 1526.
25. R.J. Gillespie, "*Molecular Geometry*", Van Nostrand Reinhold Co.; London, **1972**.
26. J.H. Burns, P.A. Argon and H.A. Levy, *Science* **1963**, 139, 1208.
27. K.O. Christie, J.C.P. Sanders, H.P. Mercier, G.J. Schrobilgen and W.W. Wilson, unpublished results.
28. S.W. Peterson, J.H. Holloway, B.A. Coyle and J.M. Williams, *Science* **1971**, 173, 1238.
29. D. Lentz and K. Seppelt, *Z. Anorg. Allg. Chem.* **1980**, 460, 5; T. Birchall, R.D. Myers, H. De Waard and G.J. Schrobilgen, *Inorg. Chem.* **1982**, 21, 1068.
30. D. Lentz and K. Seppelt, *Angew. Chem.* **1979**, 91, 68.
31. E. Jacob, D. Lentz, K. Seppelt and A. Simon, *Z. Anorg. Chem.* **1981**, 472, 7.
32. D. Lentz and K. Seppelt, *Angew. Chem.* **1978**, 90, 391.
33. W. Porcham and A. Engelbrecht, *Monatsh. Chem.* **1971**, 102, 333.
34. W. Porcham and A. Engelbrecht, *Z. Phys. Chem. (Leipzig)* **1971**, 248, 177.
35. A. Engelbrecht and F. Sladky, *Angew. Chem.* **1964**, 76, 379.
36. F. Sladky, H. Kropshofer and O. Leitzke, *J. Chem. Soc., Chem. Commun.* **1973**, 134.
37. H. Kropshofer, O. Leitzke, P. Peringer and F. Sladky, *Chem. Ber.* **1981**, 114, 2644.
38. K. Seppelt and D. Nöthe, *Inorg. Chem.* **1973**, 12, 2727.
39. F. Sladky, *Angew. Chem.* **1969**, 81, 536.
40. F. Sladky and H. Kropshofer, *J. Chem. Soc., Chem. Commun.* **1973**, 600.
41. D. Lentz, H. Pritzkow and K. Seppelt, *Angew. Chem.* **1977**, 89, 741.
42. T. Birchall, R.D. Myers, H. de Waard and G.J. Schrobilgen, *Inorg. Chem.* **1982**, 21, 1068.
43. M.J. Collins and G.J. Schrobilgen, *Inorg. Chem.* **1985**, 24, 2608.
44. W. Tötsch and F. Sladky, *Z. Naturforsch* **1983**, 38B, 1025.
45. (a) C.J. Schack and K.O. Christie, *J. Fluorine Chem.* **1984**, 24, 467; (b) C.J. Schack and K.O. Christie, *J. Fluorine Chem.* **1984**, 26, 19; (c) C.J. Schack and K.O. Christie, *J. Fluorine Chem.* **1985**, 27, 53.
46. C.J. Schack and K.O. Christie, *J. Fluorine Chem.* **1990**, 49, 79.

47. I. Agranat, M. Rabinowitz and H. Selig, *Inorg. Nucl. Chem. Lett.* **1975**, 11, 185.
48. G.W. Fraser and G.D. Meikle, *J. Chem. Soc., Dalton Trans.* **1977**, 1985.
49. K.O. Christe, C.J. Schack and W.W. Wilson, *Inorg. Chem.* **1983**, 22, 18.
50. P. Huppmann, G. Klöter, J.S. Thrasher and D.D. DesMarteau, *Inorg. Chem.* **1984**, 23, 2217;
K. Seppelt and H. Oberhammer, *Inorg. Chem.* **1985**, 24, 1227.
51. C. Lau and J. Passmore, *Inorg. Chem.* **1974**, 13, 2278.
52. L. Lawlor and J. Passmore, *Inorg. Chem.* **1979**, 18, 2921.
53. K. Seppelt, *Inorg. Chem.* **1973**, 12, 2837.
54. I.B. Gorrell, C.J. Ludman and R.S. Matthews, submitted for publication in *J. Chem. Soc., Dalton Trans.*.
55. G.W. Fraser and G.D. Meikle, *J. Chem. Soc., Perkin Trans.* **1975**, 2, 312.
56. C.J. Schack and K.O. Christe, *J. Fluorine Chem.* **1982**, 21, 393.
57. J. Mason, in, "*Multinuclear NMR*", J. Mason (Ed.), Plenum; New York, **1987**, 625.
58. K. Seppelt, personnel communications.
59. J.M. Winfield, *J. Fluorine Chem.* **1984**, 25, 91.
60. M.A. Gallop, B.F.G. Johnson, J. Lewis and A.H. Wright, *J. Chem. Soc. Dalton Trans.* **1989**, 481.
61. G.J. Schrobilgen, J.H. Holloway, P. Granger and C. Brevard, *Inorg. Chem.* **1978**, 17, 980.
62. R.G. Syvret, Ph.D. Thesis, McMaster University, **1987**.
63. G.B. Rodrigues, J.C.P. Sanders and G.J. Schrobilgen, unpublished results.
64. K. Seppelt, *Inorg. Chem.* **1980**, 20, 33.
65. M.T. Rogers, J.G. Malik and J.L. Speirs, *J. Am. Chem. Soc.* **1956**, 78, 46.
66. G.W. Fraser, R.D. Peacock and P.M. Watkins, *J. Chem. Soc. (A)*, **1971**, 1125.
67. R.J. Morris and K.C. Moss, *J. Fluorine Chem.* **1979**, 13, 551.
68. K.O. Christe, R.B. Wilson and C.J. Schack, *Inorg. Synth.* **1986**, 24, 3.
69. R.G. Syvret and G.J. Schrobilgen, *Inorg. Chem.* **1989**, 28, 1564.
70. M. Lustig, A.R. Pitochelli and J.K. Ruff, *J. Am. Chem. Soc.* **1967**, 89, 2841.
71. J.C.P. Sanders and G.J. Schrobilgen, *J. Chem. Soc., Chem. Commun.* **1989**, 1576.

72. F. Sladky, *Mh. Chem.* **1970**, 101, 1571.
73. K. Seppelt and H.H. Rupp, *Z. Anorg. Allg. Chem.* **1974**, 409, 331.
74. K. Seppelt and H.H. Rupp, *Z. Anorg. Allg. Chem.* **1974**, 409, 338.
75. K. Seppelt, *Z. Anorg. Allg. Chem.* **1973**, 399, 65.
76. P. Bladon, D.H. Brown, K.D. Crosbie and D.W.A. Sharp, *Spectrochim. Acta* **1970**, 26A, 2221.
77. K.O. Christie, J.C.P. Sanders, G.J. Schrobilgen, and W.W. Wilson, to be published.
78. G.H. Cady and L.C. Duncan, *Inorg. Chem.* **1964**, 6, 850.
79. J. Schmutzler, *J. Chem. Soc.* **1964**, 4551.
80. G.E. Maciel and D.A. Beatty, *J. Phys. Chem.* **1965**, 69, 3920.
81. G.E. Maciel, J.W. McIver, N.S. Ostland and J.A. Pople, *J. Am. Chem. Soc.* **1970**, 92, 1.
82. R.J. Morris and K.C. Moss, *J. Fluorine Chem.* **1979**, 13, 551; V.M. Afanasev, S.G. Sakharov, M.P. Sussstyakova, Yu.V. Kokunov and Yu.A. Buslaev, *Koord. Khim.* **1987**, 13, 279.
83. O. Lösing and H. Willner, *Angew. Chem. Int. Engl. Ed.* **1989**, 28, 1255.

PART VIII

THE PF_4^- ANION AND ITS HYDROLYTIC BEHAVIOR

Previous unsuccessful attempts to synthesize the PF_4^- anion had led to the belief that this species did not exist. In collaboration with Dr. K.O. Christie and Dr. W.W. Wilson at Rocketdyne, we have now prepared and characterized a salt containing the PF_4^- anion for the first time. The salt $\text{N}(\text{CH}_3)_4^+\text{PF}_4^-$ can be prepared in quantitative yield by the reaction of $\text{N}(\text{CH}_3)_4^+\text{F}^-$ with excess PF_3 in CH_3CN solvent. The anion has been characterized by vibrational and ^{19}F and ^{31}P NMR spectroscopy.

^{31}P and ^{19}F NMR Spectroscopy of the PF_4^- Anion

The ^{31}P NMR spectrum of $\text{N}(\text{CH}_3)_4^+\text{PF}_4^-$ in CH_3CN at -40°C reveals a broad singlet ($\Delta\nu_{\text{N}} = 163\text{ Hz}$) at $\delta = 42.3\text{ ppm}$. The lack of fine structure indicates that the PF_4^- anion undergoes relatively fast intermolecular exchange under these conditions. However, when a 1.5 molar excess of $\text{N}(\text{CH}_3)_4^+\text{F}^-$ is added to the sample, the intermolecular exchange is slowed down and the ^{31}P NMR spectrum at -46°C (Figure 1) reveals a triplet of triplets at $\delta = 40.5\text{ ppm}$. This is in accordance with the pseudo-trigonal bipyramidal structure expected for PF_4^- and in agreement with the structure predicted by the VSEPR model for an AX_4E type molecule.¹ The coupling pattern arises from the coupling of the phosphorus to the two inequivalent sets of fluorine ligands: $^1J(^{31}\text{P}-^{19}\text{F}_{\text{ax}}) = 660\text{ Hz}$ and $^1J(^{31}\text{P}-^{19}\text{F}_{\text{eq}}) = 1405\text{ Hz}$. The intensity pattern in the observed triplet of triplets is rather unusual in that six of the inner lines of the multiplet are broader than the central and two outer lines. This pattern is indicative of the PF_4^- anion undergoing an intramolecular ligand exchange process in which both equatorial and axial ligands interchange at the same time.² In order to confirm this, a series of variable temperature ^{31}P NMR spectra were

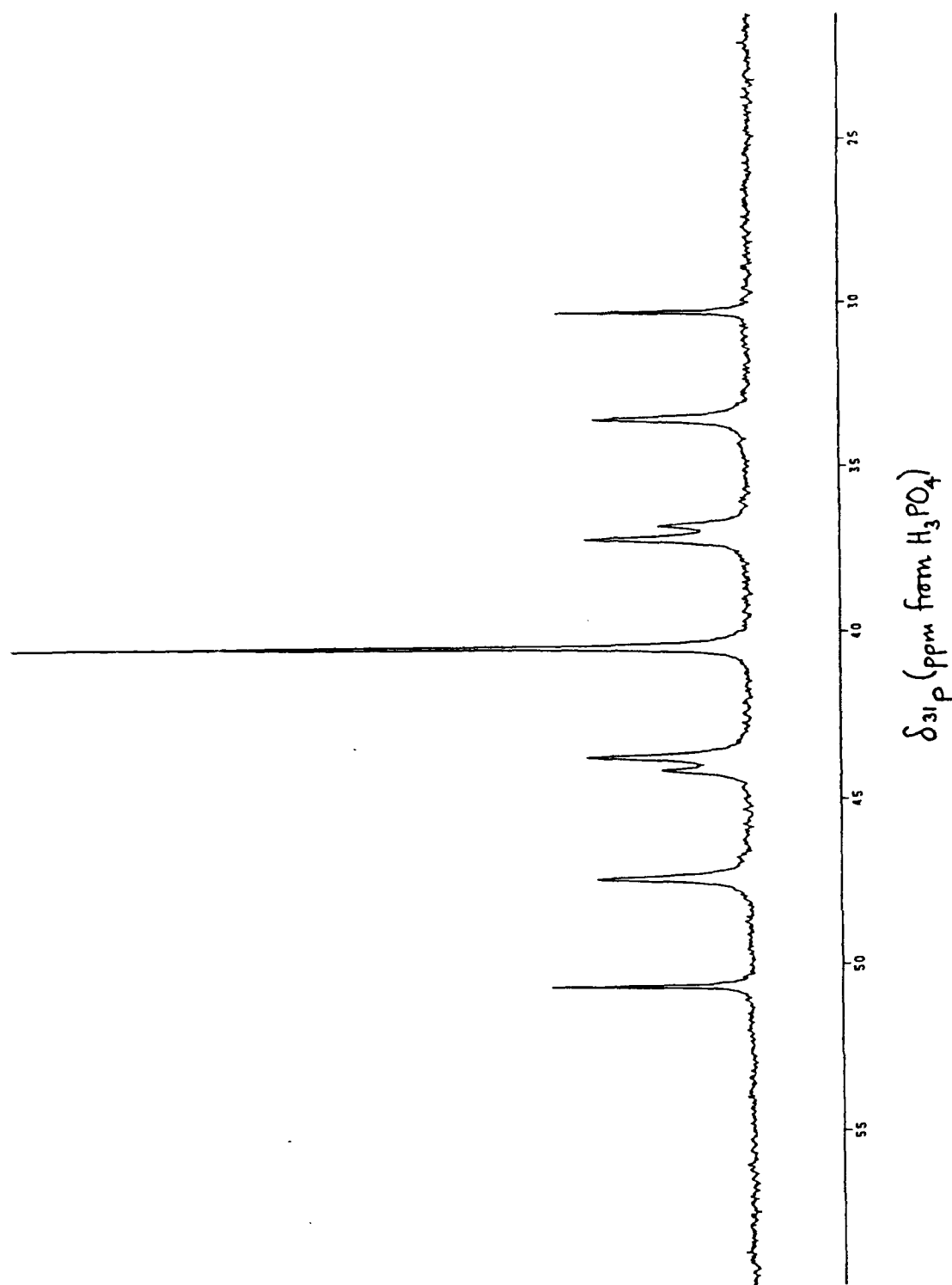


Figure 1 . The ^{31}P NMR spectrum (202.459 MHz) at -46°C of $\text{N}(\text{CH}_3)_4^+\text{PF}_6^-$ in CH_3CN containing a 2.5 molar excess of $\text{N}(\text{CH}_3)_4^+\text{F}^-$.

obtained over the range -46 to 21 °C (Figure 2). The observed changes in the multiplet pattern on going to progressively higher temperatures are analogous to those found in the XPF_4 series of molecules (where $\text{X} = \text{N}(\text{CH}_3)_2$, Cl or CH_3)³ and are consistent with a mechanism in which both equatorial and axial ligands interchange simultaneously; not one in which one axial and one equatorial ligand interchange, while the other equatorial and axial ligands remain in their positions.^{2,3} The ^{31}P NMR spectra measured at the highest temperatures reveal significant broadening of the multiplet components as a result of intermolecular fluoride exchange and, in addition, the samples turned orange in color due to attack of the excess F^- on the CH_3CN solvent.⁴ The mechanism by which the intramolecular ligand exchange process occurs in the PF_4^- anion may be the classical Berry pseudorotation mechanism, however it should be noted that NMR spectroscopy cannot distinguish between this and other mechanisms that result in the same permutation of fluorine nuclei.^{2,3} The rate constant has been determined at each temperature by visual matching of the experimental spectrum with spectra generated by the DNMR 3 simulation program⁵ for exchanging systems. The rate constant data obtained is summarized in Table 1. Using previously established equations⁶ and an Eyring plot of the rate data (Figure 3), it was possible to extract values of ΔH^\ddagger and ΔS^\ddagger as $43 \pm 2 \text{ kJ mol}^{-1}$ and $-13 \pm 2 \text{ JK}^{-1} \text{ mol}^{-1}$, respectively. These values compare well with values obtained for the intramolecular exchange process in the isoelectronic SF_4 molecule (Table 2).^{7,8} The values obtained from variable temperature ^{19}F NMR studies on purified neat liquid and gaseous samples of SF_4 are regarded as the most reliable, since they represent the highest ΔH^\ddagger and most positive ΔS^\ddagger values.⁸ The other SF_4 samples yielded smaller values for ΔH^\ddagger and negative values for ΔS^\ddagger which are thought to be due to the catalytic effect of traces of HF leading to a smaller slope and a lower intercept on the graph.^{7,9} The

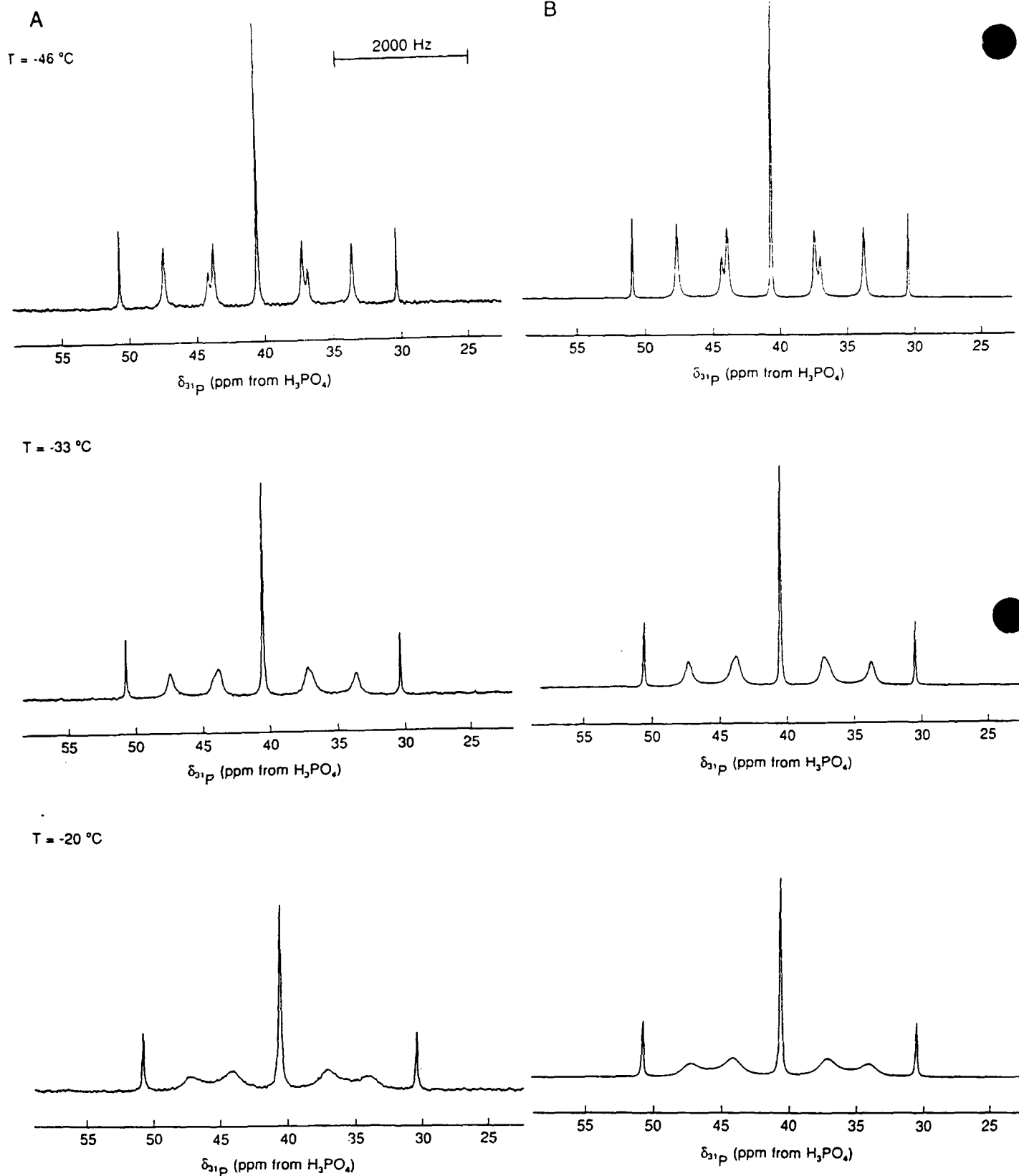


Figure 2a. Variable temperature ^{31}P NMR spectra (202.459 MHz) for $\text{N}(\text{CH}_3)_4^+\text{PF}_6^-$ in CH_3CN containing a 1.5 molar excess of $\text{N}(\text{CH}_3)_4^+\text{F}^-$. A) observed spectra; B) calculated spectra.

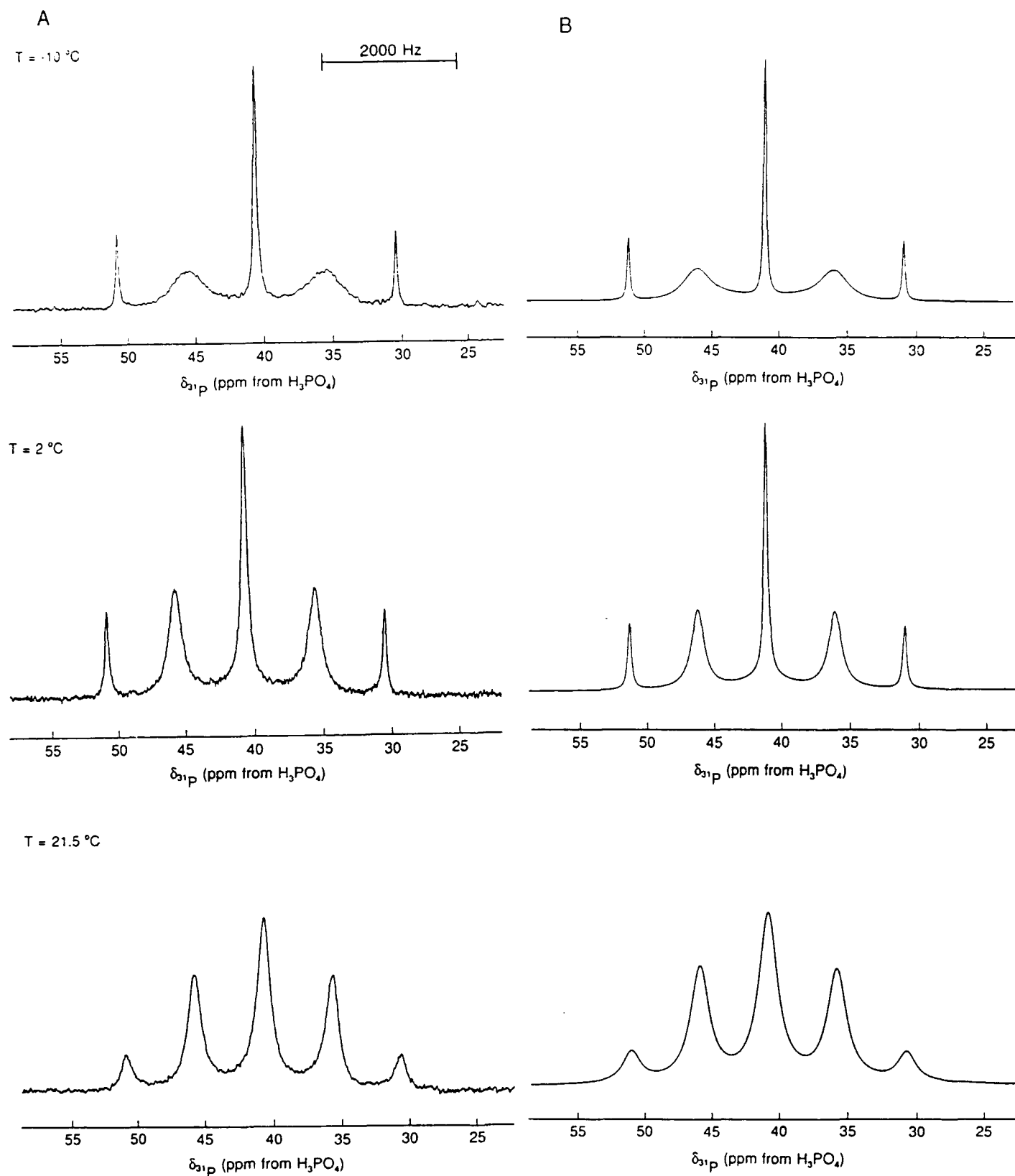


Figure 2b. Variable temperature ^{31}P NMR spectra (202.459 MHz) for $\text{N}(\text{CH}_3)_4^+\text{PF}_6^-$ in CH_3CN containing a 1.5 molar excess of $\text{N}(\text{CH}_3)_4^+\text{F}^-$. A) observed spectra; B) calculated spectra.

somewhat low values of ΔH^\ddagger and ΔS^\ddagger obtained for PF_4^- can also probably be ascribed to the effects of intermolecular fluoride exchange.

The ^{19}F NMR spectrum at -46°C of $\text{N}(\text{CH}_3)_4^+\text{PF}_4^-$ in CH_3CN containing a 2.3 molar excess of $\text{N}(\text{CH}_3)_4^+\text{F}^-$ shows, in addition to a signal due to excess F^- , resonances attributable to PF_4^- , POF_2^- and PHF_3^- . The latter two species comprised approximately 10 - 15% of the total phosphorus in the sample and are thought to have arisen from the adventitious hydrolysis of the PF_4^- anion during synthesis or storage. The reactions giving rise to these hydrolysis products are described in detail in a separate article.¹⁰ The resonances arising from the PF_4^- anion (Figure 4) comprise two doublets of triplets attributed to the axial ($\delta = 9.3$ ppm) and equatorial ($\delta = -46.7$ ppm) fluorine ligand environments, in accord with the pseudo-trigonal bipyramidal structure for PF_4^- . The doublet splittings arise from the one-bond couplings $^1J(^{31}\text{P}-^{19}\text{F}_{\text{ax}})$ and $^1J(^{31}\text{P}-^{19}\text{F}_{\text{eq}})$ and are in agreement with those measured from the ^{31}P spectrum. The smaller triplet splittings arise from $^2J(^{19}\text{F}_{\text{ax}}-^{19}\text{F}_{\text{eq}}) = 108$ Hz. The chemical shift assignments are based on the magnitudes of the $^1J(^{31}\text{P}-^{19}\text{F})$ values for each resonance and simple MO considerations. The equatorial fluorine ligands are regarded as being bonded to the phosphorus by 2-center 2-electron bonds, whereas the two axial fluorine ligands are bonded to phosphorus by a weaker 3-center 4-electron bond. As a result, the magnitude of $^1J(^{31}\text{P}-^{19}\text{F}_{\text{eq}})$ is expected to be greater than that of $^1J(^{31}\text{P}-^{19}\text{F}_{\text{ax}})$ and thus the resonance at $\delta = -46.7$ ppm with the larger $^1J(^{31}\text{P}-^{19}\text{F})$ value can be assigned to the equatorial fluorine ligands and the resonance at $\delta = 9.3$ ppm with the smaller $^1J(^{31}\text{P}-^{19}\text{F})$ value can be assigned to the axial fluorine ligands. This is also in agreement with the X-ray crystal

Table 1. Exchange Rate Data Extracted from Variable-Temperature ^{31}P NMR Spectra of $\text{N}(\text{CH}_3)_4^+\text{PF}_4^-$ Dissolved in CH_3CN Containing a 1.5 M Excess of $\text{N}(\text{CH}_3)_4^+\text{F}^-$.

T, K	T^{-1} , $\text{K}^{-1} \times 10^{-3}$	k , $\text{s}^{-1} \times 10^2$	k/T	$\ln(k/T)$
227	4.41	1.00	0.441	-0.82
233	4.29	1.60	0.687	-0.38
240	4.17	3.10	1.29	0.26
250	4.00	8.50	3.40	1.22
260	3.85	25.0	9.62	2.26
275	3.64	56.0	20.4	3.01

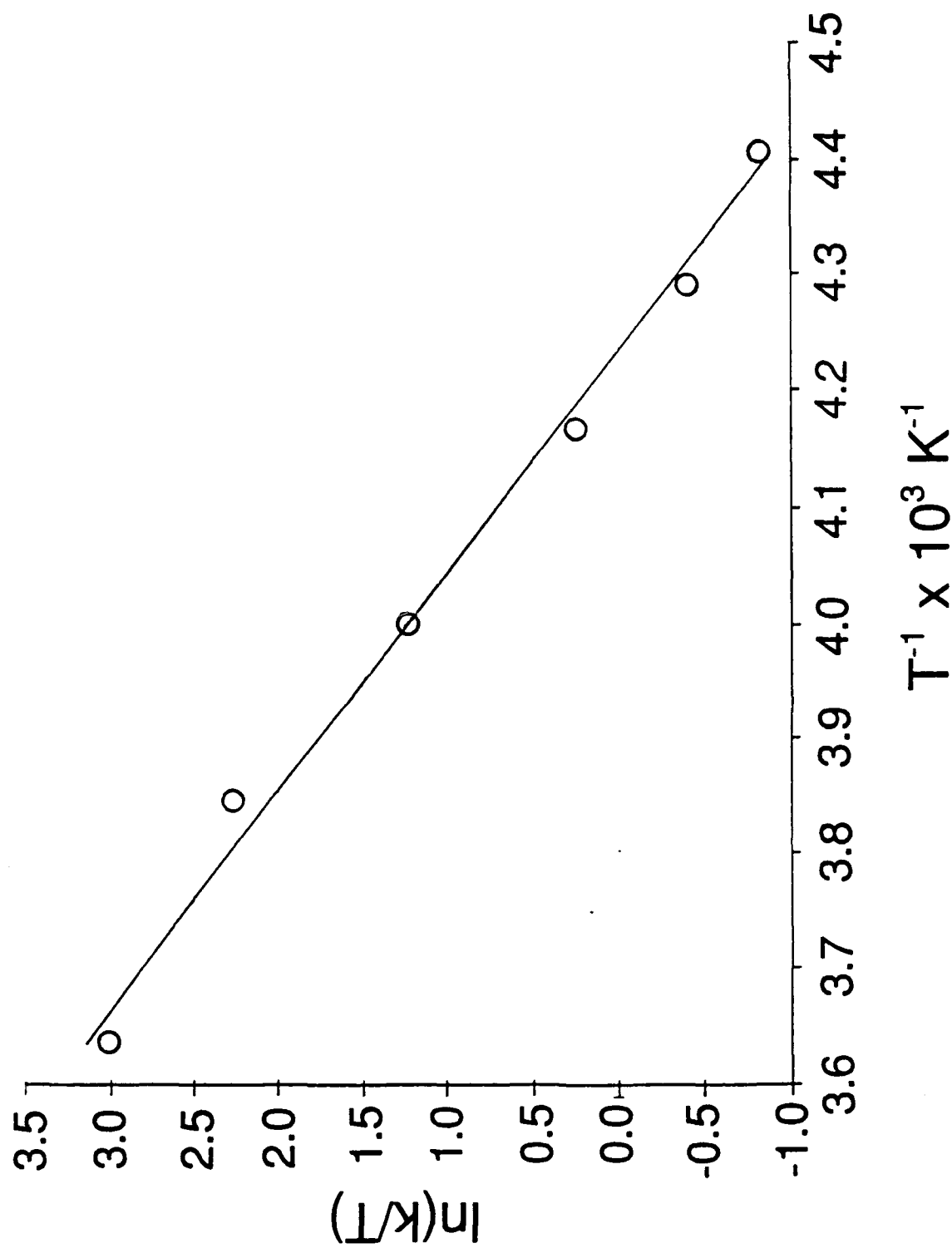


Figure 3. Eyring plot of the exchange rate data extracted from the variable temperature ^{31}P NMR spectra (202.459 MHz) for $\text{N}(\text{CH}_3)_4^+\text{PF}_6^-$ in CH_3CN containing a 1.5 molar excess of $\text{N}(\text{CH}_3)_4^+\text{F}^-$.

Table 2. Enthalpies and Entropies of Activation for Intramolecular Exchange in PF_4^- and SF_4 ^a

<u>Sample</u>	<u>$\Delta H^\ddagger/\text{kJmol}^{-1}$</u>	<u>$\Delta S^\ddagger/\text{JK}^{-1}\text{mol}^{-1}$</u>
$\text{PF}_4^-/1.5 \text{ F}^-$ in CH_3CN	43.5	-13.1
SF_4 (gas)	37.3	41.4
SF_4 (gas) ^b	61.9	9.3
SF_4 (neat liquid)	40.8	-26.9
SF_4 (neat liquid) ^b	49.2	4.4
SF_4 in CFCl_3	38.9	-30.6
$\text{SF}_4 + \text{SOF}_2$ in CFCl_3	42.9	-16.9

^a Data for SF_4 are taken from reference 8. ^b Purified free of HF.

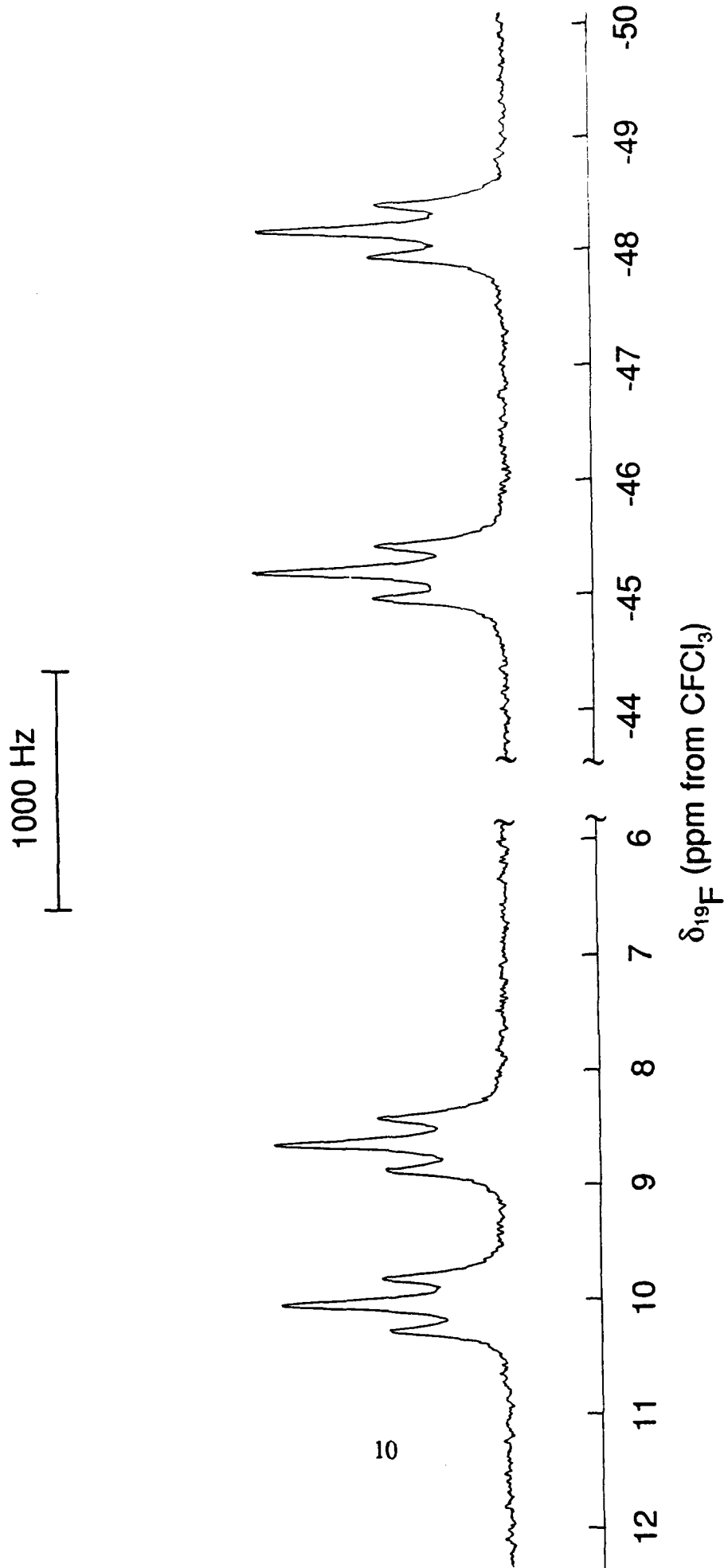


Figure 4. The ^{19}F NMR spectrum (470.599 MHz) at -46°C of $\text{N}(\text{CH}_3)_4^+\text{PF}_6^-$ in CH_3CN containing a 1.5 molar excess of $\text{N}(\text{CH}_3)_4^+\text{F}^-$.

structure of $\text{N}(\text{CH}_3)_4^+\text{PF}_4^-$ where it is found that the P-F_{eq} bond length is shorter than the P-F_{ax} bond length.

NMR Sample Preparation

Samples for ^{31}P NMR spectroscopy were prepared in 9-mm o.d. FEP NMR tubes as described previously.¹¹ Typically, the $\text{N}(\text{CH}_3)_4^+\text{PF}_4^-$ (0.0782 g, *ca.* 0.7 mmol), containing 10 - 15% $\text{N}(\text{CH}_3)_4^+\text{POF}_2^-$ and $\text{N}(\text{CH}_3)_4^+\text{PHF}_2^-$ as impurities, and $\text{N}(\text{CH}_3)_4^+\text{F}^-$ (0.1023 g, 1.0983 mmol) were weighed into the FEP tube in the dry box. The tube was closed with a Kel-F valve and attached to a glass vacuum line. Anhydrous CH_3CN (1.8 mL) was distilled *in vacuo* on to the solids at -196°C . The FEP tube was heat sealed under dynamic vacuum and stored at -196°C until the NMR spectra could be obtained. The ^{19}F NMR samples were prepared in an analogous fashion using 4-mm o.d. FEP NMR tubes and the following typical quantities: $\text{N}(\text{CH}_3)_4^+\text{PF}_4^-$ (0.0089 g, 0.083 mmol); $\text{N}(\text{CH}_3)_4^+\text{F}^-$ (0.0215 g, 0.231 mmol) and CH_3CN (0.25 mL). The sealed FEP sample tubes were inserted into 10-mm or 5-mm thin-walled precision NMR tubes (Wilmad) before being placed in the probe.

Nuclear Magnetic Resonance Spectroscopy

The ^{19}F and ^{31}P NMR spectra were recorded unlocked (field drift $<0.1\text{ Hz h}^{-1}$) on a Bruker AM-500 spectrometer equipped with an 11.744 T cryomagnet. Variable-temperature studies were carried out by using a Bruker temperature controller. Temperatures were measured with a copper-constantan thermocouple inserted directly into the sample region of the probe and were considered accurate to $\pm 1^\circ\text{C}$.

The ^{19}F spectra were obtained using a 5-mm combination $^1\text{H}/^{19}\text{F}$ probe operating at 470.599 MHz. The spectra were recorded in a 32 K memory. A spectral width setting of 50 kHz was employed, yielding a data point resolution of 3.052 Hz/data point and an acquisition time of 0.328 s. No relaxation delays were applied. Typically, 20,000 transients were accumulated. The pulse width corresponding to a bulk magnetization tip angle, θ , of approximately 90° was equal to 1 μs . A line broadening parameter of 5 Hz was used in the exponential multiplication of the free induction decays prior to Fourier transformation.

The ^{31}P NMR spectra were obtained at 202.459 MHz by using a 10-mm broad-band VSP probe tunable over the range 23-202 MHz. The spectra were recorded in a 16 K memory. The spectral width setting was 29,412 Hz, which yielded a data point resolution of 3.590 Hz/data point and an acquisition time of 0.278 s. Prior to Fourier transformation, the free induction decay was zero-filled to 32 K of memory, giving a data point resolution of 1.795 Hz/data point. No relaxation delays were applied. Typically 6000 - 20,000 transients were accumulated. The pulse width corresponding to a bulk magnetization tip angle, θ , of approximately 90° was equal to 2.5 μs . Line broadening parameters of 5 - 15 Hz were applied in the exponential multiplication of the free induction decay prior to Fourier transformation.

The spectra were referenced to neat external samples of CFCl_3 (^{19}F) and 85% H_3PO_4 (^{31}P) at ambient temperature. The chemical shift convention used is that a positive (negative) sign signifies a chemical shift to high (low) frequency of the reference compound.

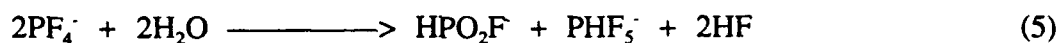
References

1. Gillespie, R.J.; Hargittai, I. *The VSEPR Model of Molecular Geometry*, Allyn and Bacon: Boston, 1991.
2. Steigel, A. in *NMR - Basic Principles and Progress*; Diel, P.; Fluck, E.; Kosfeld, R. Eds., 1978, 15, 1, and references therein.
3. Eisenhut, M.; Mitchell, H.L.; Traficante, D.D.; Kaufman, R.J.; Deutch, J.M.; Whitesides, G.M. *J. Am. Chem. Soc.* 1974, 96, 5385.
4. Christe, K.O.; Wilson, W.W. *J. Fluorine Chem.*, 1990, 46, 339.
5. a) Kleier, D.A.; Binsch, G. *Quantum Chemistry Exchange*, No. 165, Indiana University, 1969 b) Binsch, G. in *Dynamic NMR Spectroscopy*, Jackman, L.M.; Cotton, F.A. Eds.; Academic Press: New York, 1975; p 45.
6. Günther, H. *NMR Spectroscopy - An Introduction*, J. Wiley and Sons: New York, 1973; Chapter 8, p 240.
7. Seel, F.; Gombler, W. *J. Fluorine Chem.*, 1974, 4, 327; Gibson, J.A.; Ibbott, D.G.; Jansen, A.F. *Can. J. Chem.*, 1973, 51, 3203.
8. Gombler, W., Diploma Thesis, Saarbrücken, FRD, 1974.
9. Gombler, W., personal communication.
10. Christe, K.O.; Sanders, J.C.P.; Schrobilgen, G.J.; Wilson, W.W. *J. Am. Chem. Soc.*, to be submitted.
11. Christe, K.O.; Curtis, E.C.; Dixon, D.A.; Mercier, H.P.; Sanders, J.C.P.; Schrobilgen, G.J. *J. Am. Chem. Soc.*, 1991, 113, 3351.

Hydrolysis of the PF_4^- Anion

We have studied the hydrolysis of the novel PF_4^- anion using H_2O enriched in ^{17}O in order to enable the complete characterization of the products using ^{17}O as well as ^{31}P and ^{19}F NMR spectroscopy for the first time.

The ^{31}P NMR spectrum of a sample containing equimolar quantities of $\text{N}(\text{CH}_3)_4^+\text{PF}_4^-$ and H_2O (oxygen composition: ^{16}O , 35.4%; ^{17}O , 21.9%; ^{18}O , 42.7%) in CH_3CN at -45°C is shown in Figure 5 and reveals five resonances. The two most intense resonances are assigned to HPO_2F^- [$\delta = 0.7$ ppm; $^1J(^{31}\text{P}-^{19}\text{F}) = 958$ Hz; $^1J(^{31}\text{P}-^1\text{H}) = 667$ Hz] and PHF_5^- [$\delta = -140.2$ ppm; $^1J(^{31}\text{P}-^{19}\text{F}_{\text{ax}}) = 732$ Hz; $^1J(^{31}\text{P}-^{19}\text{F}_{\text{eq}}) = 819$ Hz; $^1J(^{31}\text{P}-^1\text{H}) = 941$ Hz]. The two weaker resonances at high frequency are assigned to POF_2^- [$\delta = 125.8$ ppm; $^1J(^{31}\text{P}-^{19}\text{F}) = 1221$ Hz] and PF_3 [$\delta = 103.5$ ppm; $^1J(^{31}\text{P}-^{19}\text{F}) = 1401$ Hz]. Although all the aforementioned anions have been reported previously, the data were incomplete and the anions had not been fully characterized by multi-NMR spectroscopy before. A very weak multiplet was also observed overlapping with the PHF_5^- resonance and could not be assigned unequivocally. However, since the resonance occurs in the hexacoordinate P(V) region of the spectrum, it could arise from the $\text{HPF}_4(\text{OH})^-$ anion which is a proposed intermediate in the hydrolysis reaction. The main hydrolysis reaction occurring under the conditions described above is represented by equation (5) as a disproportionation.



The POF_2^- anion observed in the sample was found to be present in the original solid $\text{N}(\text{CH}_3)_4^+\text{PF}_4^-$ used to prepare the NMR sample, and is thought to have arisen from a small amount of adventitious hydrolysis during synthesis or storage. The ^{17}O NMR spectrum (Figure

6) of the same sample at $-36\text{ }^{\circ}\text{C}$ displayed a broad doublet [$\Delta\nu_{\text{H}} = 76\text{ Hz}$; $\delta = 117\text{ ppm}$; $^1\text{J}(^{17}\text{O}-^{31}\text{P}) = 131\text{ Hz}$] assigned to the HPO_2F^- anion. A resonance ascribable to POF_2^- was not observed since this species was already present in the $\text{N}(\text{CH}_3)_4^+\text{PF}_4^-$ and had not resulted from the hydrolysis of PF_4^- with ^{17}O -enriched water.

When the ^{31}P NMR spectrum was run at $30\text{ }^{\circ}\text{C}$, the hydrolysis was observed to have gone to completion and all the PF_3 had disappeared (Figure 7). The resonance of POF_2^- had become somewhat more intense and now displayed ^{17}O satellites. Each component of the doublet of doublets (Figure 8) arising from HPO_2F^- was now resolved into a "triplet" corresponding to the $^{16,18}\text{O}$ induced secondary isotope shifts for the three isotopomers $\text{HP}^{16}\text{O}_2\text{F}^-$, $\text{HP}^{16}\text{O}^{18}\text{OF}^-$ and $\text{HP}^{18}\text{O}_2\text{F}^-$. The isotope shift $^1\Delta^{31}\text{P}(^{18,16}\text{O})$ was measured as -0.035 ppm . In addition, each component displayed well resolved, equal-intensity sextet satellites arising from coupling to ^{17}O [$I=5/2$; $^1\text{J}(^{31}\text{P}-^{17}\text{O}) = 146\text{ Hz}$]. The ^{17}O satellites are well-resolved at $30\text{ }^{\circ}\text{C}$ owing to the slower rate of quadrupolar relaxation of the ^{17}O nucleus at higher temperatures. The spectrum also reveals that the weak multiplet, which was partially obscured by the intense PHF_3^- multiplet at $-36\text{ }^{\circ}\text{C}$, has disappeared on warming, thereby indicating that it might arise from the proposed $\text{HPF}_4(\text{OH})^-$ intermediate. It is hoped that the nature of this species will be better determined by obtaining the ^{19}F NMR spectrum of a new sample. The ^{17}O NMR spectrum (Figure 9) of the same sample at $30\text{ }^{\circ}\text{C}$ shows two resonances: an intense doublet ($\delta = 131.8\text{ ppm}$; $^1\text{J}(^{17}\text{O}-^{31}\text{P}) = 144\text{ Hz}$) assigned to HPO_2F^- and a weak doublet [$\delta = 191.4\text{ ppm}$; $^1\text{J}(^{17}\text{O}-^{31}\text{P}) = 186\text{ Hz}$] assigned to POF_2^- . Each component of the doublet resonance of HPO_2F^- is further split into an overlapping doublet (Figure 10) of doublets by the two-bond couplings to ^1H and ^{19}F [$^2\text{J}(^{17}\text{O}-^1\text{H}) \approx 12\text{ Hz}$; $^2\text{J}(^{17}\text{O}-^{19}\text{F}) \approx 12\text{ Hz}$].

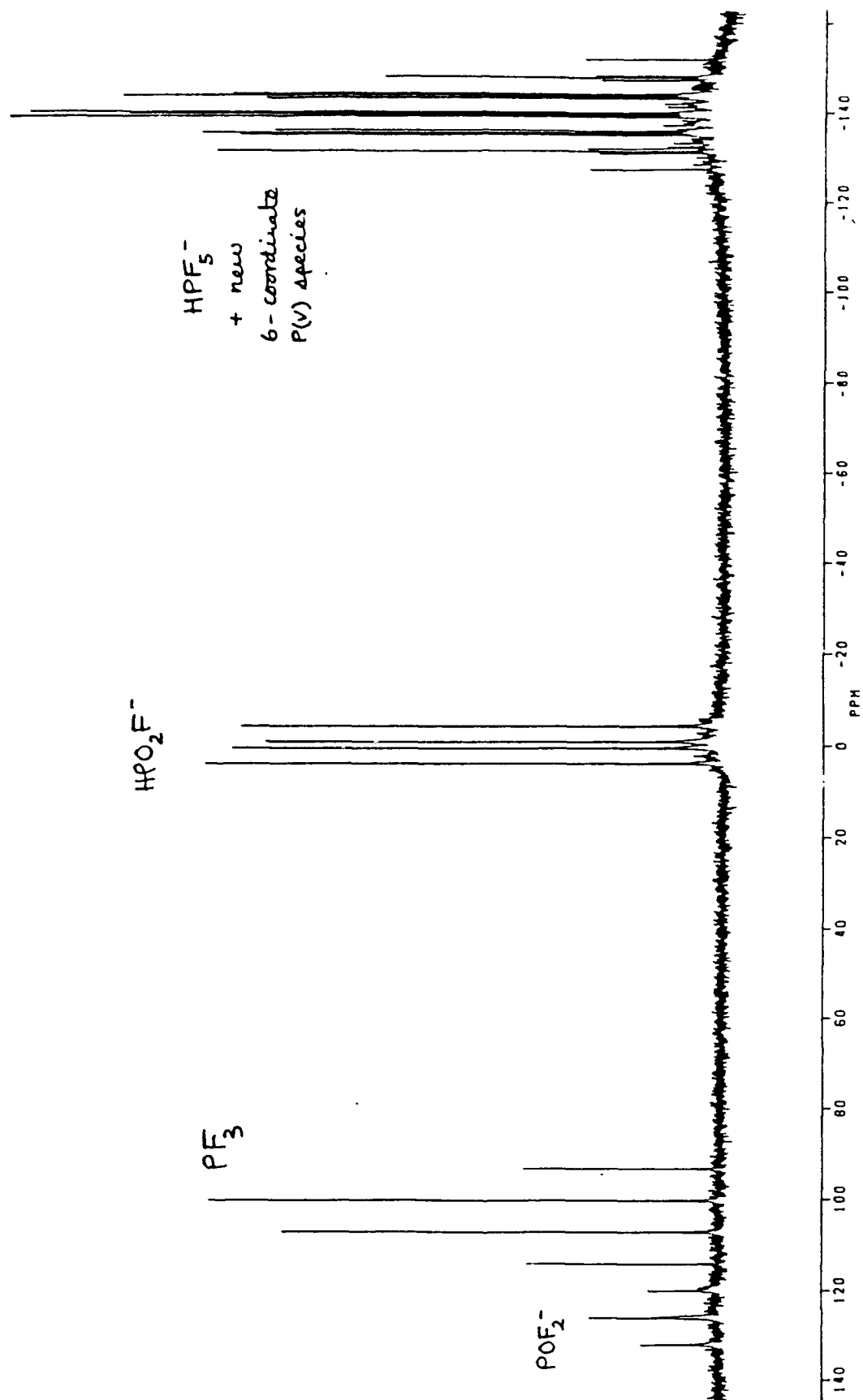


Figure 5. The ^{31}P NMR spectrum (202.459 MHz) of the products from the hydrolysis of $\text{N}(\text{CH}_3)_4^+\text{PF}_6^-$ with $\text{H}_2^{16,17,18}\text{O}$ in CH_3CN at -45°C .

HPO_2F^-

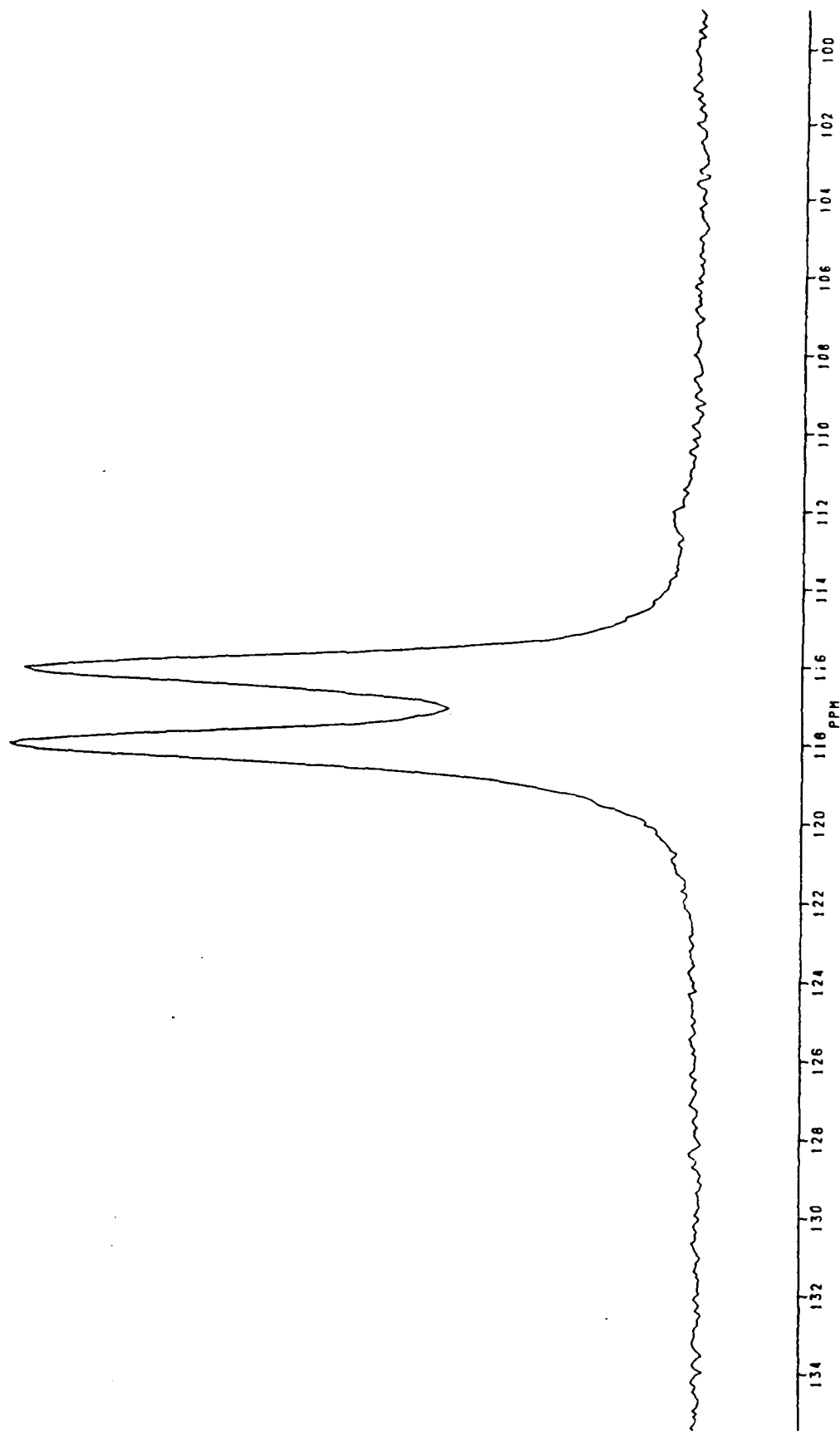
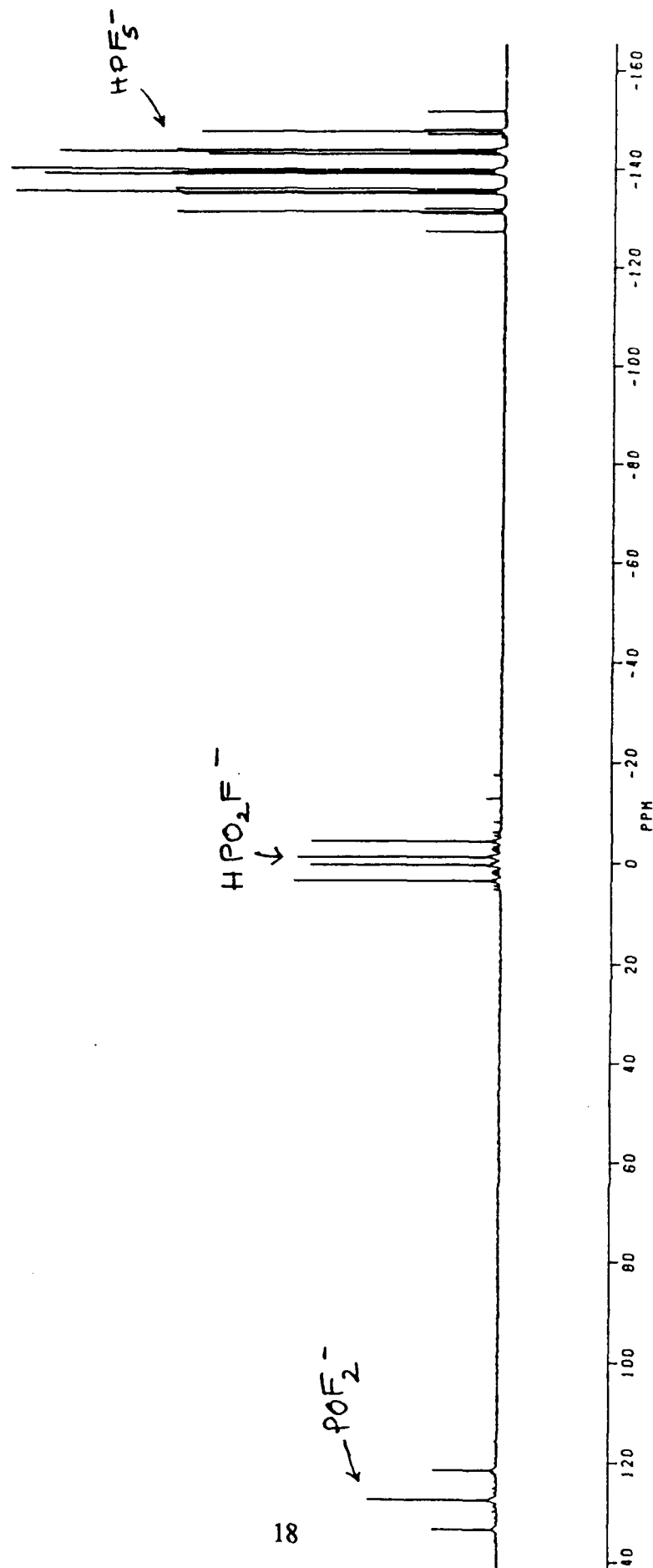


Figure 6. The ^{17}O NMR spectrum (67.801 MHz) of the products from the hydrolysis of $\text{N}(\text{CH}_3)_4^+\text{PF}_6^-$ with $\text{H}_2^{16,17,18}\text{O}$ in CH_3CN at -36°C .



18

Figure 7. The ^{31}P NMR spectrum (202.459 Mhz) of the products from the hydrolysis of

$\text{N}(\text{CH}_3)_4^+\text{PF}_6^-$ with $\text{H}_2^{16,17,18}\text{O}$ in C^{13}CN at 30 °C.

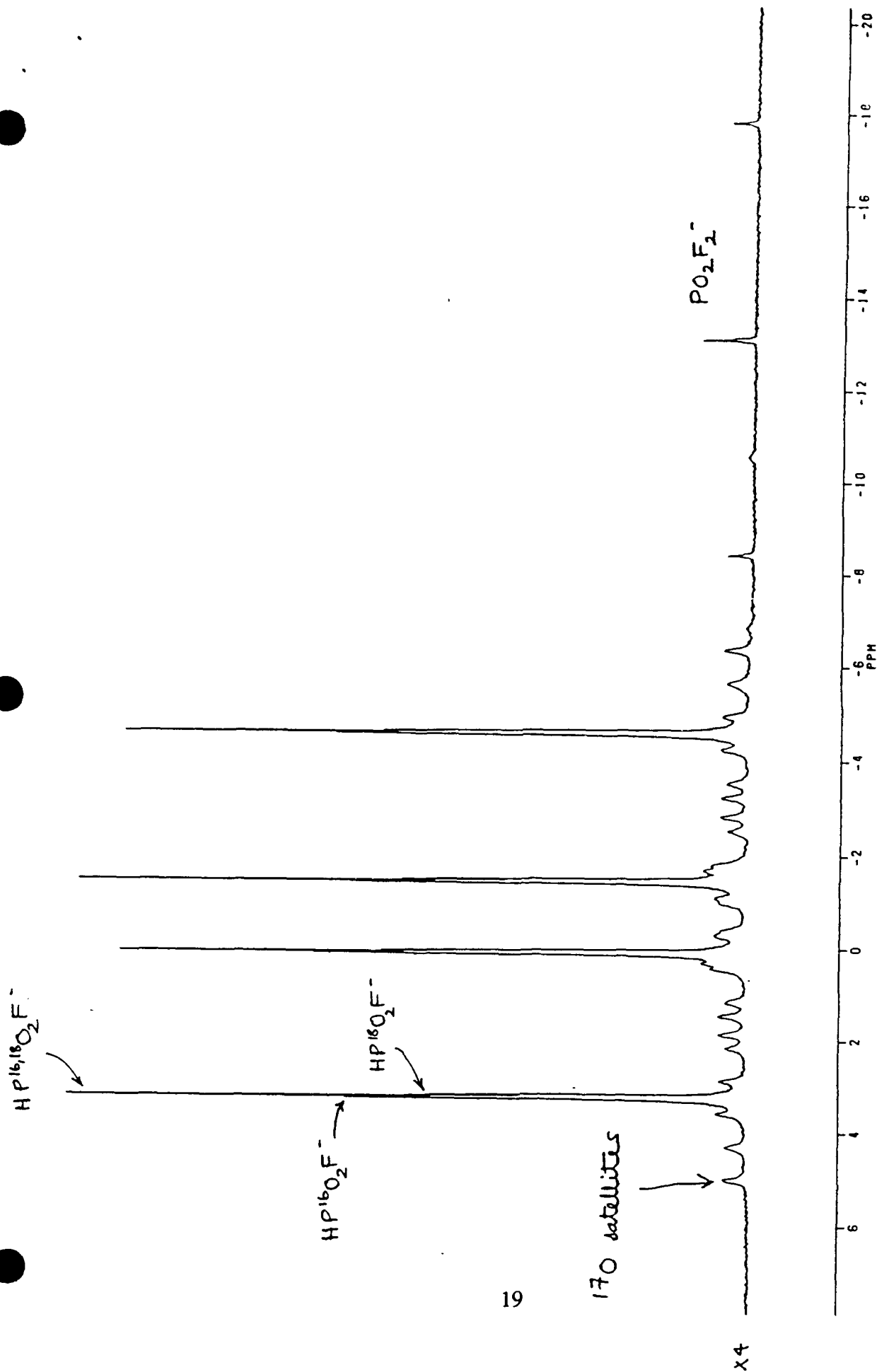


Figure 8. The ^{31}P NMR spectrum (202.459 MHz) of the products from the hydrolysis of $\text{N}(\text{CH}_3)_4^+\text{PF}_6^-$ with $\text{H}_2^{16,17,18}\text{O}$ in CH_3CN at 30°C . Expansion of the HPO_2F^- resonance.

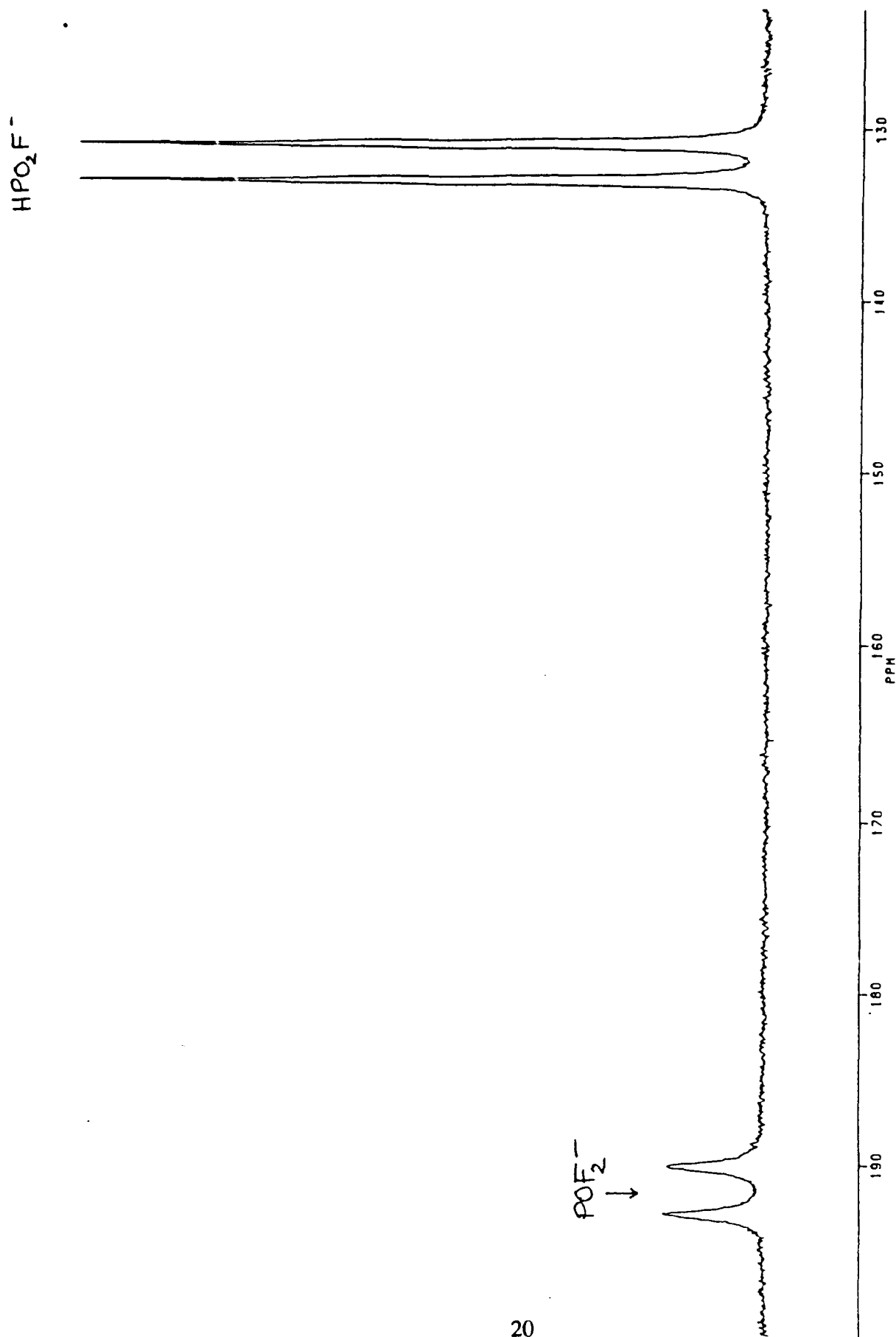


Figure 9. The ^{17}O NMR spectrum (67.801 MHz) of the products from the hydrolysis of

$\text{N}(\text{CH}_3)_4^+\text{PF}_6^-$ with $\text{H}_2^{16,17,18}\text{O}$ in CD_3CN at 30 °C.

HPO_2F^-

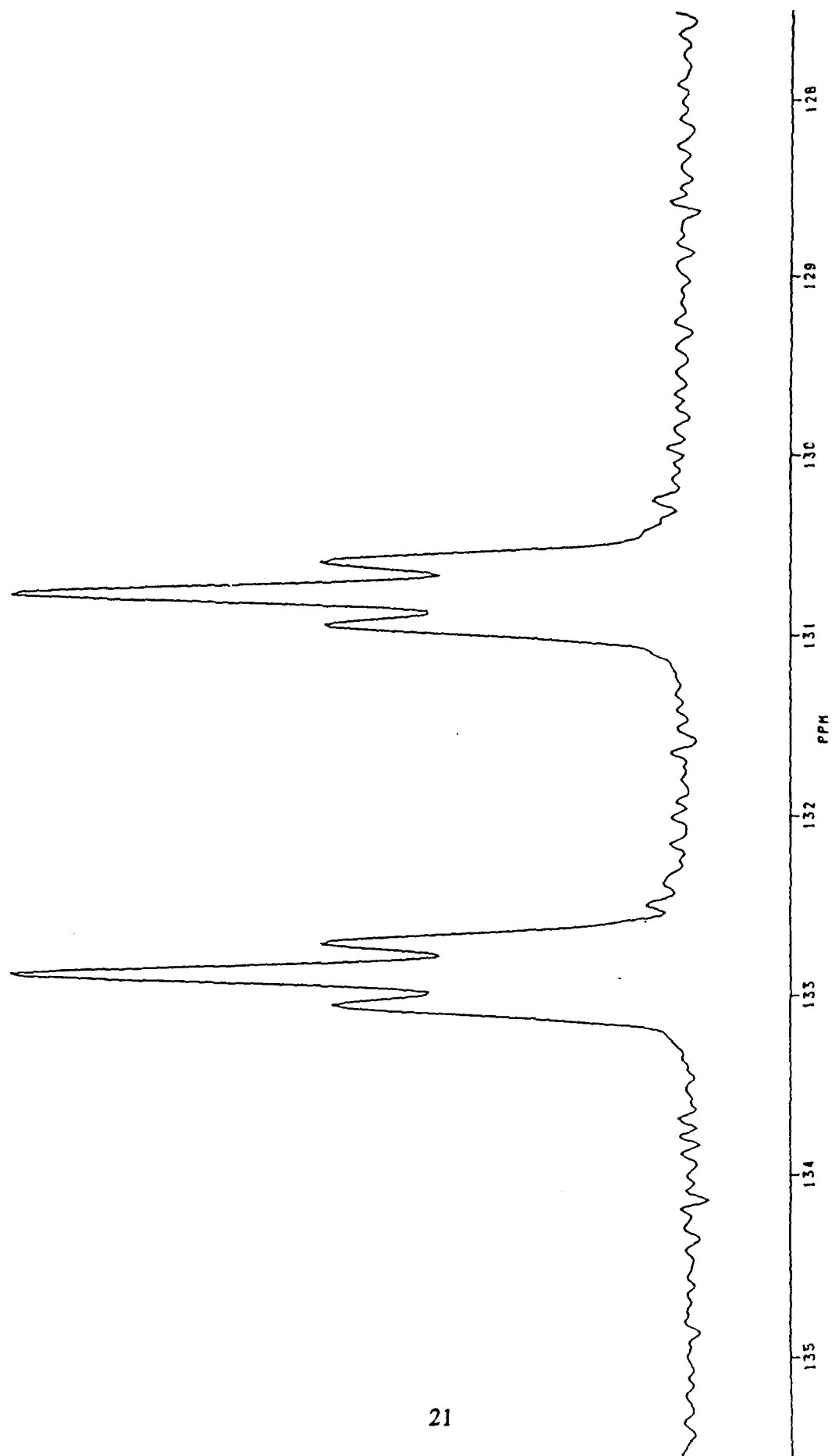


Figure 10. The ^{17}O NMR spectrum (67.801 Mhz) of the products from the hydrolysis of $\text{N}(\text{CH}_3)_4^+\text{PF}_6^-$ with $\text{H}_2^{16,17,18}\text{O}$ in CH_3CN at 30°C . Expansion of HPO_2F^- resonance.

The hydrolysis of $\text{N}(\text{CH}_3)_4^+\text{PF}_4^-$ with an equimolar quantity of $^{17,18}\text{O}$ -enriched H_2O in the presence of a 2.5 molar excess of $\text{N}(\text{CH}_3)_4^+\text{F}^-$ in CH_3CN proceeds differently to the above hydrolysis reaction. The ^{31}P NMR spectrum of this sample at -45°C reveals three resonances attributable to PF_4^- , PHF_3^- and POF_2^- (Figure 11). The HPF_3^- was present as an impurity in the $\text{N}(\text{CH}_3)_4^+\text{PF}_4^-$ used to prepare the NMR sample. The triplet due to POF_2^- was significantly more intense than that in the sample of $\text{N}(\text{CH}_3)_4^+\text{PF}_4^-$ in CH_3CN alone; furthermore the resonance exhibited a small "doublet" splitting due to the $^{16,18}\text{O}$ secondary isotope shift, thereby providing conclusive proof that the POF_2^- had arisen from the hydrolysis of $\text{N}(\text{CH}_3)_4^+\text{PF}_4^-$ with the $^{17,18}\text{O}$ -enriched H_2O . On warming the sample to -10°C , the amount of POF_2^- increased further and after warming to room temperature complete hydrolysis of PF_4^- to POF_2^- had taken place with the $\text{N}(\text{CH}_3)_4^+\text{F}^-$ acting to complex the HF produced according to equation (2).



The ^{31}P NMR spectrum (Figure 12) of the sample at 30°C shows two triplets [$^1J(^{31}\text{P}-^{19}\text{F}) = 1183$ Hz] ascribed to the two isotopomers $\text{P}^{16}\text{OF}_2^-$ and $\text{P}^{18}\text{OF}_2^-$ [$^1\Delta^{31}\text{P}(^{18,16}\text{O}) = -0.068$ ppm]. In addition, each component of the triplet is flanked by equal-intensity sextet satellites arising from coupling to ^{17}O . These satellites are highly resolved [$^1J(^{31}\text{P}-^{17}\text{O}) = 189$ Hz] and demonstrate that there is a fortuitously small electric field gradient at the ^{17}O nucleus and consequently the quadrupolar relaxation of the ^{17}O nucleus is very slow. Correspondingly, the ^{17}O NMR spectrum (Figure 13) displays a very sharp doublet [$\Delta\nu_{\text{K}} = 5$ Hz; $^1J(^{31}\text{P}-^{17}\text{O}) = 189$ Hz] at $\delta = 211.9$ ppm due to the $\text{P}^{17}\text{OF}_2^-$ anion. A weak resonance attributable to the HPO_2F^- anion was observed at $\delta = 137$ ppm.

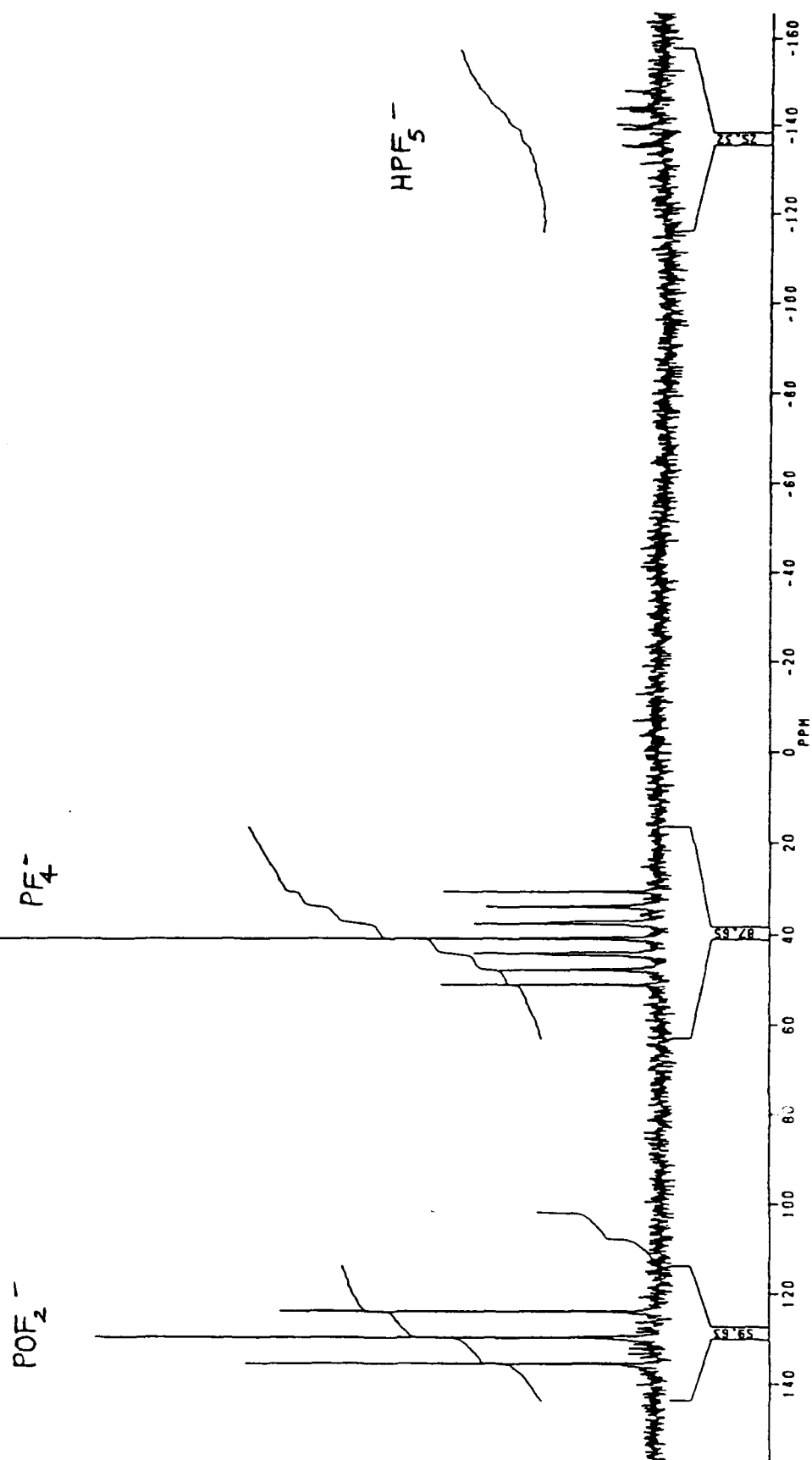


Figure 11. The ^{31}P NMR spectrum (202.459 Mhz) of the products from the hydrolysis of $\text{N}(\text{CH}_3)_4^+\text{PF}_6^-$ with $\text{H}_2^{16,17,18}\text{O}$ in the presence of a 2.5 molar excess of $\text{N}(\text{CH}_3)_4^+\text{F}^-$ in CH_3CN at -45°C .

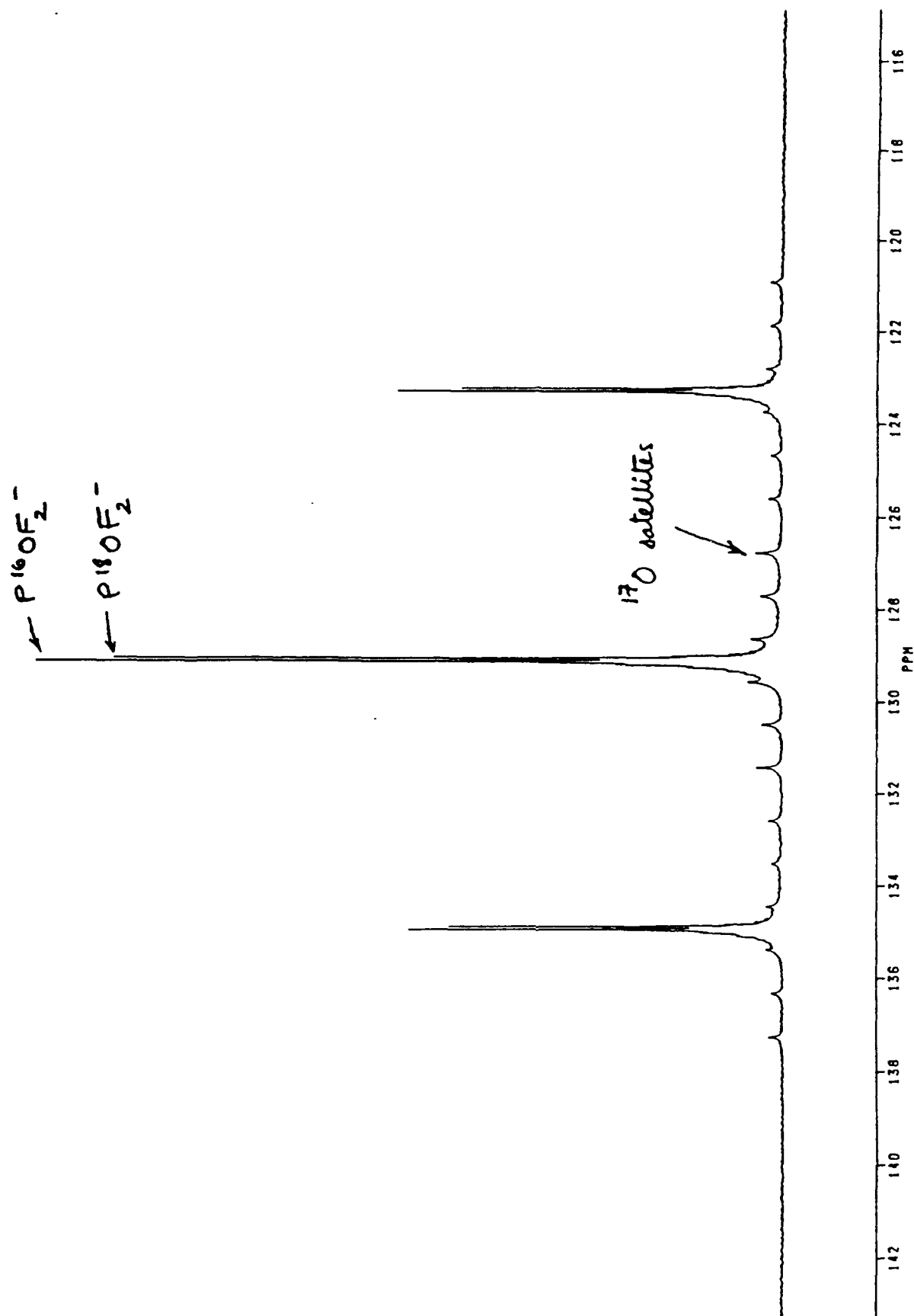


Figure 12. The ^{31}P NMR spectrum (202.459 Mhz) of the POF_2^- anion produced in the hydrolysis of $\text{N}(\text{CH}_3)_4^+\text{PF}_4^-$ with $\text{H}_2^{16,17,18}\text{O}$ in the presence of a 2.5 molar excess of $\text{N}(\text{CH}_3)_4^+\text{F}^-$ in CH_3CN 0°C .

POF_2^-

HPO_2F^-

25

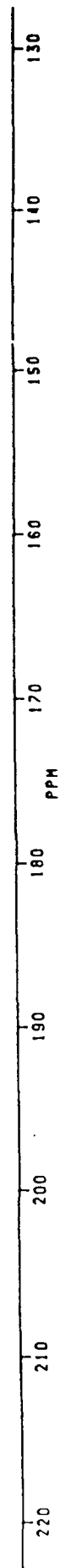


Figure 13. The ^{17}O NMR spectrum (67.801 Mhz) of the products formed in the hydrolysis of $\text{N}(\text{CH}_3)_4^+\text{PF}_6^-$ with $\text{H}_2^{16,17,18}\text{O}$ in the presence of a 2.5 molar excess of $\text{N}(\text{CH}_3)_4^+\text{F}^-$ in CH_3CN at 30 $^\circ\text{C}$.

Crystal Structure Determination of $\text{N}(\text{CH}_3)_4^+\text{PF}_6^-$

Crystal Growing. The purity of the starting material, $\text{N}(\text{CH}_3)_4^+\text{PF}_6^-$, was checked by ^{31}P and ^{19}F NMR spectroscopy, and only small amounts of the hydrolysis products, i.e. HPO_2F and POF_2 , were observed. The crystals were obtained from a saturated solution of $\text{N}(\text{CH}_3)_4^+\text{PF}_6^-$ at 50°C in acetonitrile in an FEP sample tube by allowing the sample to cool slowly to room temperature. This was accomplished by placing the tube near the surface of a 2-L glass dewar filled with warm water.

A first set of large transparent crystals was obtained when the solution was allowed to stand over a warm bath for 24 hours. The crystals were square plates and grew as clusters. Several of these crystals were mounted in 0.3 Lindemann glass capillaries. A second set of very thin transparent crystals also grew as clusters and was obtained when the solution was allowed to stand for only 8 hours. These crystals were mounted in 0.1 and 0.2 Lindemann glass capillaries. Several crystals from each crop were studied by Raman spectroscopy and were shown to contain only the PF_6^- anion.

A preliminary observation of the crystals under a polarized microscope revealed that some of the thin and thick plates were single crystals. The crystal used in this study was a plate with dimensions $0.3 \times 0.3 \times 0.05$ mm.

Collection and Reduction of X-Ray Data. The crystal was centered on a Syntex P2₁ diffractometer. This crystal was a single crystal which only diffracted at low angles. Accurate cell dimensions were determined at $T = -100^\circ\text{C}$ from a least-squares refinement of the setting angles (χ , ϕ and 2θ) obtained from 14 accurately centered reflections (with $5.35^\circ \leq 2\theta \leq 12.77^\circ$) chosen from a variety of points in reciprocal space.

Integrated diffraction intensities were collected using a $\theta - 2\theta$ scan technique with scan rates varying from 1.5 to $14.65^\circ/\text{min}$ (in 2θ) and a scan range of $\pm 0.6^\circ$ so that the weaker reflections were examined most slowly to minimize counting errors. The data were collected with $0 \leq h \leq 10$, $0 \leq k \leq 10$ and $0 \leq l \leq 6$ and $3 \leq 2\theta \leq 40^\circ$ using silver radiation monochromatized with a graphite crystal ($\lambda = 0.56087 \text{ \AA}$). During data collection the intensities of the three standard reflections were monitored every 97 reflections to check for crystal stability and alignment; no decay was observed. A total of 472 reflections were collected out of which 10

were standard reflections. A total of 270 unique reflections remained after averaging of equivalent reflections of which 163 satisfied the condition $I \geq 2\sigma(I)$ and were used for structure solution. No decay was observed. These reflections exhibited systematic absences corresponding to $0\ k\ 0$: $k = 2n$. An empirical absorption correction was applied to the data by using the ϕ scan method ($\Delta\phi = 10^\circ$), the indices of the principal face being $0\ 0\ 1$. Corrections were made for Lorentz and polarization effects.

Crystal Data. The compound, $C_4H_{12}NPF_4$ ($f_w = 181.11\text{ g mol}^{-1}$), crystallizes in the tetragonal system, space group $P4_2/m$; $a = 8.465(3)\text{ \AA}$, $c = 5.674(2)\text{ \AA}$; $V = 407\text{ \AA}^3$; $D_{calc} = 1.48\text{ g cm}^{-3}$ for $Z = 2$. $Ag(K_\alpha)$ radiation ($\lambda = 0.56087\text{ \AA}$, $\mu (AgK_\alpha) = 1.8\text{ cm}^{-1}$) was used.

Solution and Refinement of the Structure. The XPREP program was used for determining the correct cell and space group and first confirmed the original cell and that the lattice was tetragonal primitive ($R\text{-int} = 0.026$). The three space groups which were consistent with the systematic absences were the non-centrosymmetric space group $P4_2/m$ and the two centrosymmetric space groups $P4_2/2$ and $P4_2/2_12$. The structure was shown to be non-centrosymmetric by examination of the E-statistics (calc: 0.751, theor: 0.736) and consequently the structure was solved in the space group $P4_2/m$. The solution was obtained by direct methods, which located the positions of all atoms for both the anion and the cation. The carbon atoms were located on general positions, while the phosphorus, the equatorial and axial fluorine atoms and the nitrogen atoms were located on special positions, i.e., $2.m\bar{m}$, $2.m\bar{m}$, $..m$ and $-4..$. The model implied a two-fold disorder in the equatorial plane consisting of a superposition of two molecules with identical P, axial F and one equatorial F position. Consequently, the site occupancy factors of the remaining equatorial fluorine atoms were set equal to 0.25 instead of 0.50. The full matrix least-squares refinement of the positions and isotropic thermal parameters of all atoms gave a conventional agreement index $R (= \sum |F_o| - |F_c| / \sum |F_o|)$ of 0.17. The introduction of anisotropic thermal parameters for the P and N atoms produced a very slight change in the R factor (0.14) and almost no change occurs by introducing anisotropic thermal parameters for the carbon atoms and calculated values of the positions of the hydrogen atoms ($R = 0.13$). A significant improvement in the structure was achieved by introducing anisotropic thermal

parameters for all the fluorine atoms, dropping the R-factor to 4.8%. The introduction of a weighting factor ($\text{weight} = 1/\sigma^2(\text{F}) + 0.00283\text{F}^2$) gave a final solution with $R = 4.7\%$ ($R_w = 4.8\%$).

This solution was obtained with a small number of reflections and consequently the ratio of the number of reflections over the number of parameters was rather small (4.5), and may have had some impact on the final values of the structural parameters. At the moment we are waiting for diffractometer time in order to obtain better data. The data will be recorded on the same crystal using a diffractometer equipped with a $\text{Mo(K}\alpha\text{)}$ rotating anode so that weaker, higher angle reflections can be recorded.

All calculations were performed on a 486 computer, using the SHELXTL PLUS determination package for structure solution, refinement, structure determination and molecular graphics.

X-Ray Crystal Structure of $\text{N}(\text{CH}_3)_4^+\text{PF}_6^-$. Important bond lengths and angles for the PF_4^- anion are listed in Table 3. The crystal structure consists of well-separated $\text{N}(\text{CH}_3)_4^+$ and PF_4^- ions in which the anion displays a two-fold disorder in the equatorial plane (Figures 14a and 14b). The geometric structure of the PF_4^- anion can be described as a pseudo-trigonal bipyramidal structure with the lone electron pair occupying one equatorial position and the axial P-F bonds being longer than the equatorial P-F bonds (Figure 15). The structure is in agreement with the structure predicted by the VSEPR model for an AX_4E type molecule. It is interesting to note that

Table 3. Interatomic distances (Å) and Angles (deg) for $\text{N}(\text{CH}_3)_4^+\text{PF}_4^-$, $\text{N}(\text{CH}_3)_4^+\text{PF}_6^-$, $\text{NaPF}_6 \cdot \text{H}_2\text{O}$ and SF_4 .

$\text{N}(\text{CH}_3)_4^+\text{PF}_4^-$		$\text{N}(\text{CH}_3)_4^+\text{PF}_6^-$		$\text{NaPF}_6 \cdot \text{H}_2\text{O}$		SF_4	
P-F1(ax)	1.714 (1.725) ^a	P-F1(ax)	1.591	P-F(ax)	1.73	S-F(ax)	1.646
		-F2(ax)	1.585				
-F2(eq)	1.496 (1.532) ^a	-F3(eq)	1.569	-F(eq)	1.58	-F(eq)	1.545
-F3(eq)	1.372 (1.413) ^a						
F2-P-F3	108.2					F _(eq) -S-F _(eq)	101
F1-P-F1A	178.2					F _(ax) -S-F _(ax)	173
F1-P-F2	89.2	F-P-F	90 or 180	F-P-F	90 or 180		
F1-P-F3	90.3						

a. Corrected for libration

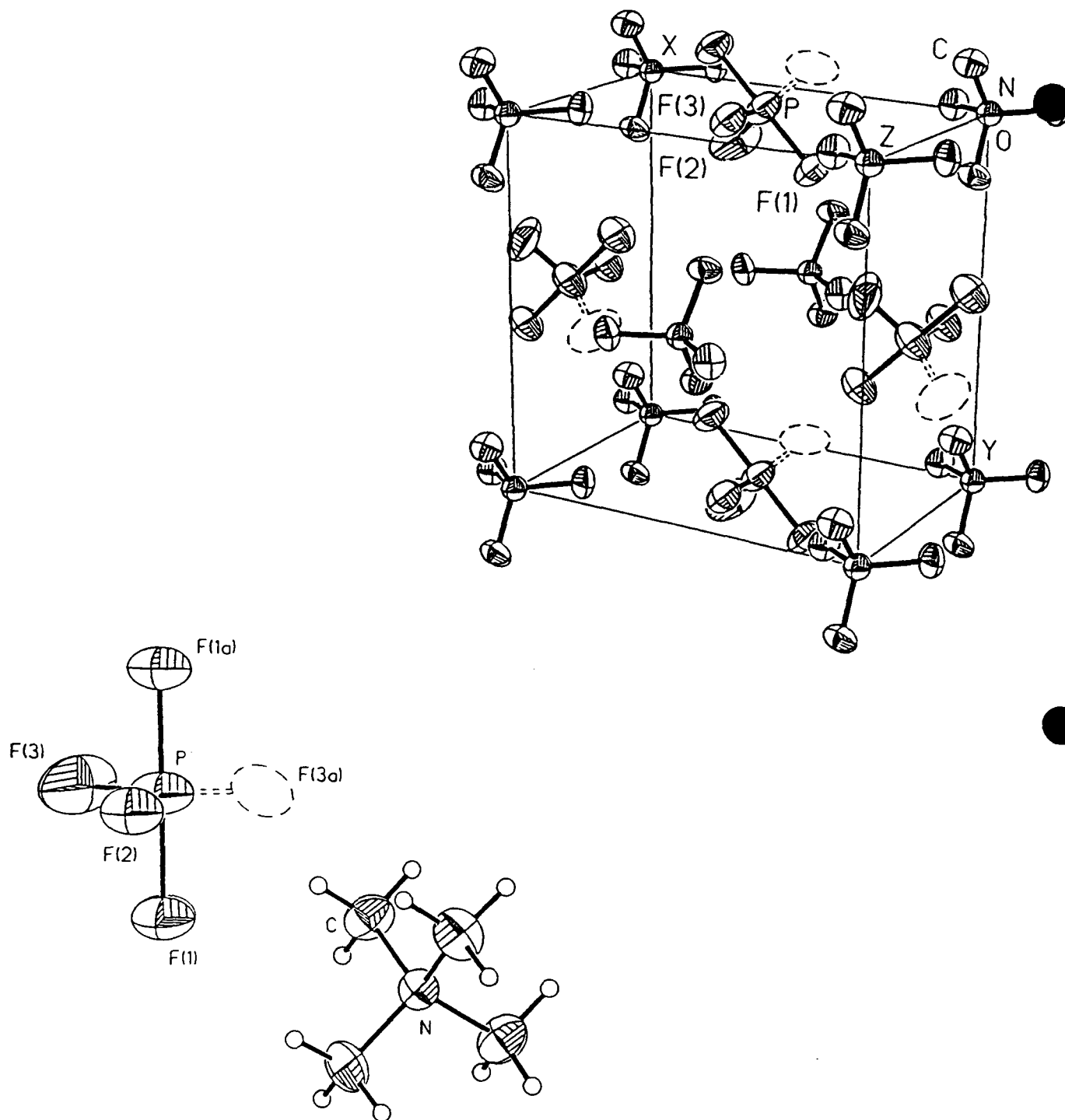


Figure 14. (a) The structural units for $N(CH_3)_4^+PF_4^-$ and (b) The unit cell of $N(CH_3)_4^+PF_4^-$.

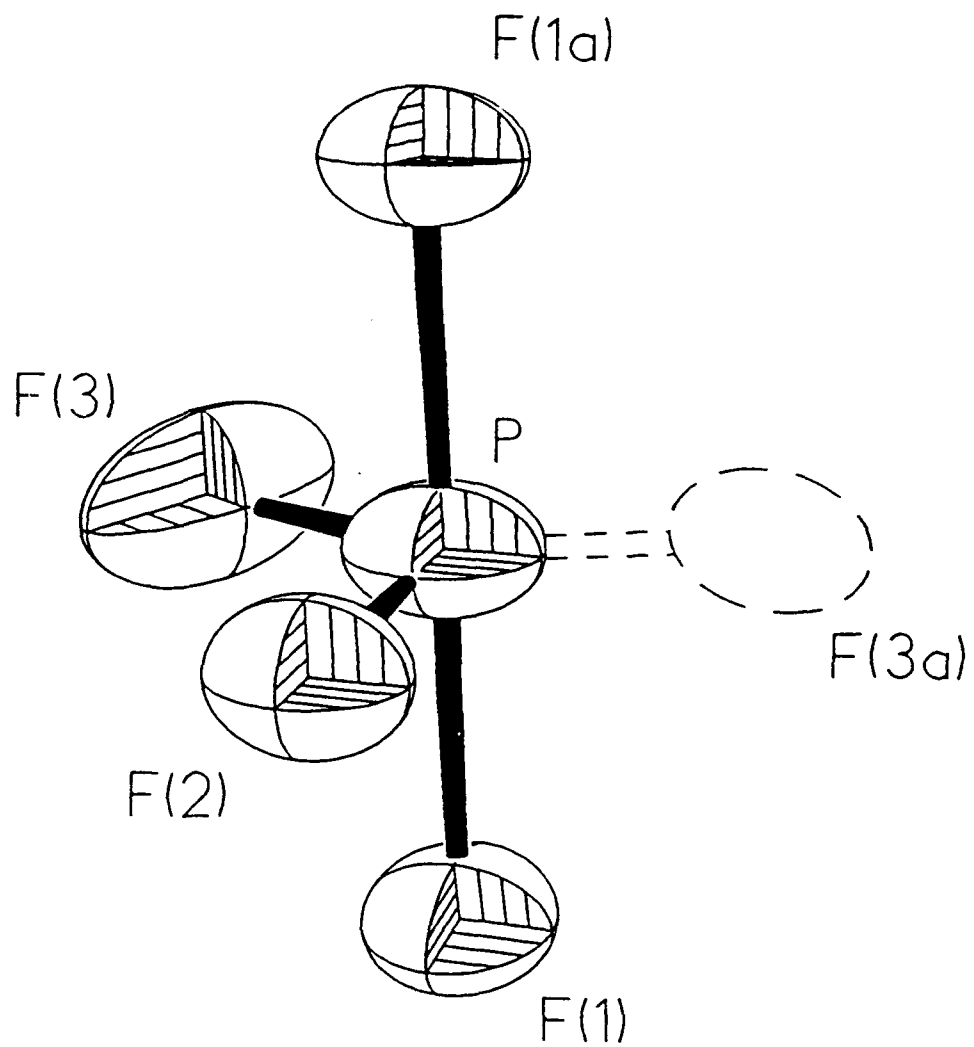


Figure 15. View of the PF_4^- anion showing the two-fold disorder in the equatorial plane.

the volume of the unit cell ($V = 406 \text{ \AA}^3$) is significantly smaller than that determined for $\text{N}(\text{CH}_3)_4^+\text{PF}_6^-$ ($V = 433 \text{ \AA}^3$) at the same temperature.¹ It is generally accepted that the effective volume of a lone pair is approximately the same as for a fluorine atom (i.e., 20 \AA^3).² Consequently, the expected volume difference between $\text{N}(\text{CH}_3)_4^+\text{PF}_6^-$ and $\text{N}(\text{CH}_3)_4^+\text{PF}_4^-$ should be close to 20 \AA^3 and is comparable to the observed difference of 27 \AA^3 .

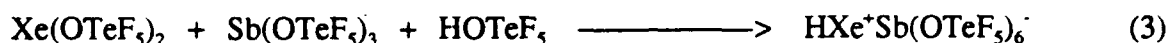
The axial bond lengths (1.725 \AA) are similar to those found in the PF_6^- anion in $\text{NaPF}_6 \cdot \text{H}_2\text{O}$ (1.73 \AA)³ where two sets of P-F bond lengths were found. The equatorial bond lengths are shorter than expected even after correction for librational motion (Table 1). A more accurate correction will be applied when a better data set becomes available. Also, and contrary to what was previously observed in $\text{PBr}_4^-/\text{PBr}_3$ and $\text{PCl}_4^-/\text{PCl}_3$, the equatorial bond lengths of PF_4^- shorter than the P-F bonds found in PF_3 (1.57 \AA).⁴ The P-F2 equatorial bond length (1.532 \AA) is similar to the axial bond lengths found in the PF_6^- anion in both $\text{N}(\text{CH}_3)_4^+\text{PF}_6^-$ (1.57 \AA) and $\text{NaPF}_6 \cdot \text{H}_2\text{O}$ (1.58 \AA). The P-F3 bond lengths arising from the two-fold positional disorder, even when corrected for libration, are too short. In this structure, the two-fold positionally disordered fluorine atom (F3) exhibits relatively large amplitude in its thermal motion ($U_{\text{eq}}(\text{F3}) = 0.096 \text{ \AA}^2$) despite the low temperature at which the data set was collected. As expected in such a case, the P-F3 bond lengths, even corrected for libration, are too small. The F2-P-F3 angle (108.2°) can be compared with the equivalent angle in the isoelectronic SF_4 molecule ($\text{F}_{\text{ax}}-\text{S}-\text{F}_{\text{ax}} = 101^\circ$).⁵ Similarly, the F1-P-F1A angle (178°) is comparable to the $\text{F}_{\text{eq}}-\text{P}-\text{F}_{\text{eq}}$ angle (173°) in SF_4 . As expected, in both cases the axial fluorines point toward the two equatorial F atoms owing to lone pair-axial fluorine bond pair repulsions. In fact, the $\text{F}_{\text{ax}}-\text{P}-\text{F}_{\text{ax}}$ angle in PF_4^- should be even smaller, but this angle is probably related to a steric problem induced by the shortening of the $\text{P}-\text{F}_{\text{eq}}$ bond length. The same trend, but even more pronounced, has been observed in the PBr_4^- anion⁶ where the angle defined by the axial fluorine atoms and Br actually point toward the lone electron pair.

References

1. Wang, Y.; Calvert, L.D.; Brownstein, S.K. *Acta Cryst*, 1980, B36, 1523.
2. Zachariasen, W.H., *J. Am. Chem. Soc.*, 1948, 70, 2147; Edwards, A.J.; Sills, R.J.C., *J. Chem. Soc. A*, 1971, 942.
3. Teufer, B. and G. *Acta Cryst.* 1956, 9, 825.
4. Morino, Y.; Kuchitsu, K.; Moritani T. *Inorg. Chem.*, 1969, 8, 867.
5. Tolles W.M.; Gwinn, W.D. *J. Chem. Phys.*, 1962, 36, 825.
6. Sheldrick, W.S.; Schmidpeter, A.; Zwaschka, F.; Dillon, K.B.; Platt, A.W.; Waddington, T.C. *J. Chem. Soc., Dalton* 1981, 413.

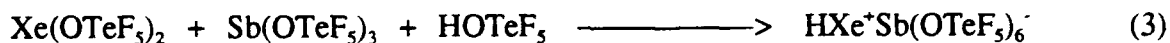
PART IX
LEAST COORDINATING ANIONS

The Group 5 (15) anions $\text{As}(\text{OTeF}_6)_6^-$, $\text{Sb}(\text{OTeF}_6)_6^-$ and $\text{Bi}(\text{OTeF}_6)_6^-$ have been prepared and characterized in this laboratory previously by ^{19}F , ^{75}As , ^{125}Te , ^{121}Sb and ^{209}Bi NMR spectroscopy. All of these anions are expected, unlike their fluorine analogs, AsF_6^- , SbF_6^- and BiF_6^- , to be weakly coordinating anions. For example, $\text{XeF}^+\text{SbF}_6^-$ is strongly fluorine-bridged in the solid state, i.e., $\text{F-Xe}^+\cdots\text{F-SbF}_5^-$, whereas the cation and anion in the OTeF_5 -analog, $\text{XeOTeF}_5^+\text{Sb}(\text{OTeF}_5)_6^-$, are only weakly interacting. It is anticipated that these anions hold considerable promise for the preparation of novel and unusual species by virtue of their weakly coordinating natures. Toward this end, we have laid the groundwork attempt to protonate xenon by carrying out reaction (1) in a solvent (Freon 114) having a proton affinity lower than that of Xe.



We have now prepared and characterized the $\text{As}(\text{OTeF}_6)_6^-$, $\text{Sb}(\text{OTeF}_6)_6^-$ and $\text{Bi}(\text{OTeF}_6)_6^-$ anions as their tetra-alkylammonium salts using X-ray crystallography. These findings are summarized in the present report:

These large weakly basic anions may also be useful in stabilizing the methyl analog, XeCH_3^+ . The XeH^+ , XeCH_3^+ and KrCH_3^+ cations are spectroscopically well characterized in the gas phase and the other NgH^+ cations are also stable gas phase species and one might anticipate using these weakly coordinating anions to protonate lighter noble gases. The isolation of the first salts of the heavy and light noble-gas cations, NgH^+ and NgCH_3^+ , could be of general interest to the development and storage of monopropellants and fuels. In addition to their potential applications, several of the proposed $\text{Te}(\text{VI})$ anions exhibit the coordination number seven, and promise to exhibit novel geometries if they can be synthesized. As part of our proposal, we are attempting to protonate xenon by carrying out reaction (1) in a solvent (Freon 114) having a proton affinity lower than that of Xe.



These large weakly basic anions may also be useful in stabilizing the methyl analog, XeCH_3^+ . The XeH^+ , XeCH_3^+ and KrCH_3^+ cations are spectroscopically well characterized in the gas phase

and the other NgH^+ cations are also stable gas phase species and one might anticipate using these weakly coordinating anions to protonate lighter noble gases. The isolation of the first salts of the heavy and light noble-gas cations, NgH^+ and NgCH_3^+ , could be of general interest to the development and storage of monopropellants and fuels. In addition to their potential applications, several of the proposed Te(VI) anions exhibit the coordination number seven, and promise to exhibit novel geometries if they can be synthesized.

X-Ray Crystal Structures of $\text{N(CH}_3)_4^+\text{Bi(OTeF}_5)_6^-$ (1), $\text{N(CH}_3)_4^+\text{As(OTeF}_5)_6^-$ (2) and $\text{N(CH}_3\text{CH}_2)_4^+\text{Sb(OTeF}_5)_6^-$ (3)

Important bond lengths and angles for the $\text{Bi(OTeF}_5)_6^-$ (1), $\text{As(OTeF}_5)_6^-$ (2) and $\text{Sb(OTeF}_5)_6^-$ (3) anions, together with bond lengths and angles for the $\text{N(CH}_3)_4^+$ (1) and (2) and $\text{N(CH}_3\text{CH}_2)_4^+$ (3) cations are listed in Table I. Details of the data collection parameters and other crystallographic information for the respective $\text{P}\bar{1}$, $\text{R}\bar{3}$ and C2/c space groups are given in Table II. Figures 1, 2 and 3 show the environments around the Bi, As and Sb atoms, respectively.

$\text{N(CH}_3)_4^+\text{Bi(OTeF}_5)_6^-$ (1). The crystal structure consists of well separated $\text{N(CH}_3)_4^+$ and $\text{Bi(OTeF}_5)_6^-$ ions. The required crystallographic symmetry of the molecule is $\bar{1}$ with the central bismuth atom on the inversion center, but the actual symmetry is approximately $\bar{3}$. While the anion is perfectly ordered, the cation is subject to a positional disorder and gives rise to the superposition of two cations in which the central N atoms occupy identical positions. Each cation is tetrahedral with the expected bond lengths. The central bismuth atom of the anion is bonded octahedrally to the six oxygen atoms and each of the six tellurium atoms octahedrally bonded to an oxygen and five fluorines. Consequently, the structure can be described as composed of an octahedron of octahedra. Average bond distances are $\text{Bi-O} = 2.057(6) \text{ \AA}$ (range $2.052(6) - 2.064(5) \text{ \AA}$), $\text{Te-O} = 1.851(6) \text{ \AA}$ (range $1.846(6) - 1.860(6) \text{ \AA}$) and $\text{Te-F} = 1.820(7) \text{ \AA}$ ($\text{Te-F}_{\text{ax}} = 1.822(7) \text{ \AA}$ and $\text{Te-F}_{\text{eq}} = 1.819(7) \text{ \AA}$) with no correction for thermal motion. The angles around the central Bi atoms and the tellurium atoms deviate by a maximum of 5° from the octahedral angles. The angles at the three crystallographic independent oxygen atoms have approximately the same value ranging from $135.3(3)^\circ$ to $137.1(3)^\circ$ (Table I). The Te-O and Te-F bond distances are comparable to those found in many OTeF_5 compounds such as $\text{Te(OTeF}_5)_6$ ($\text{Te-O} = 1.896(4) \text{ \AA}$; $\text{Te-F} = 1.817(4) \text{ \AA}$)¹ or $\text{B(OTeF}_5)_3$ ($\text{Te-O} = 1.874(6) \text{ \AA}$; $\text{Te-F} = 1.816(5) \text{ \AA}$).² Little or no

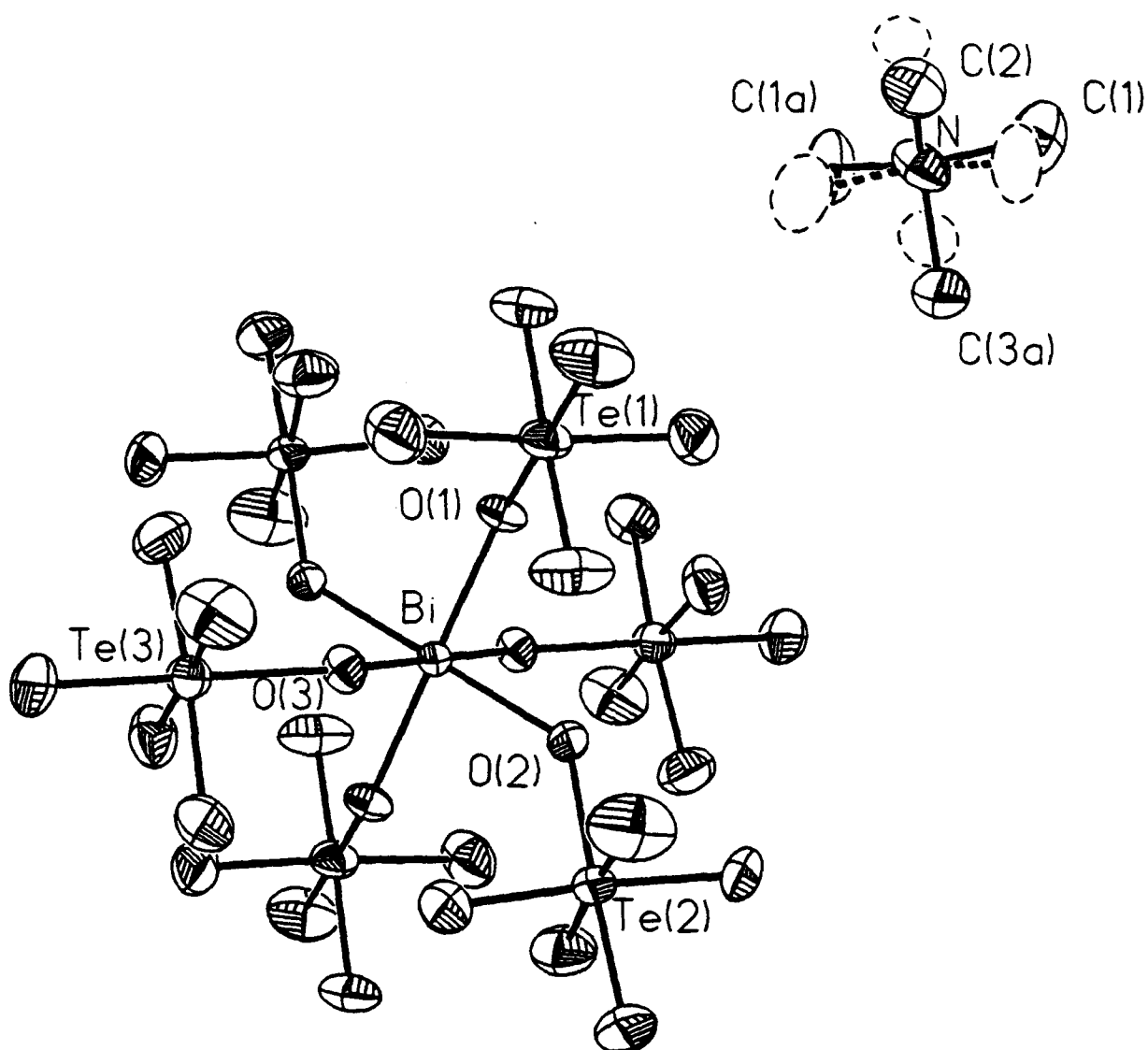


Figure 1: ORTEP view of $\text{N}(\text{CH}_3)_4^+\text{Bi}(\text{OTeF}_5)_6^-$; thermal ellipsoids are shown at the 50% probability level.

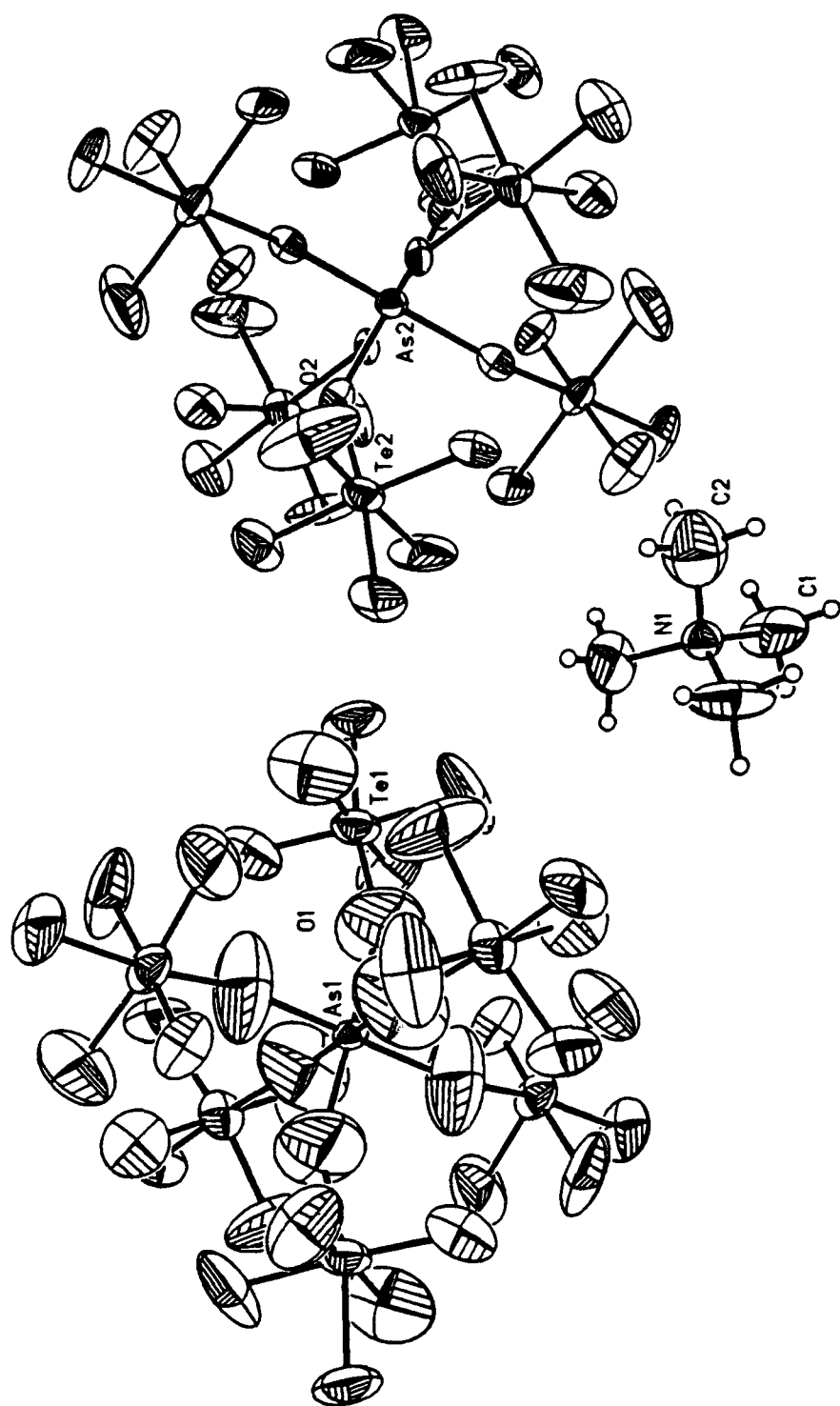


Figure 2: ORTEP view of $\text{N}(\text{CH}_3)_4^+\text{As}(\text{OTeF}_5)_6^-$; thermal ellipsoids are shown at the 30% probability level.

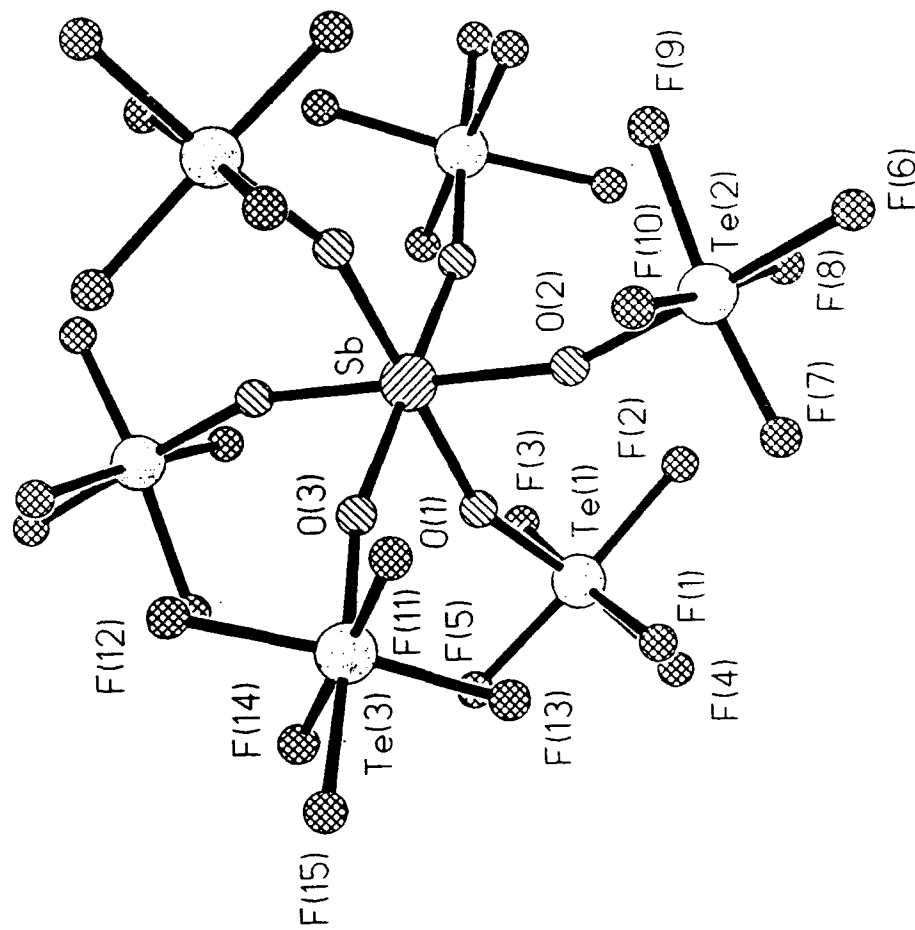
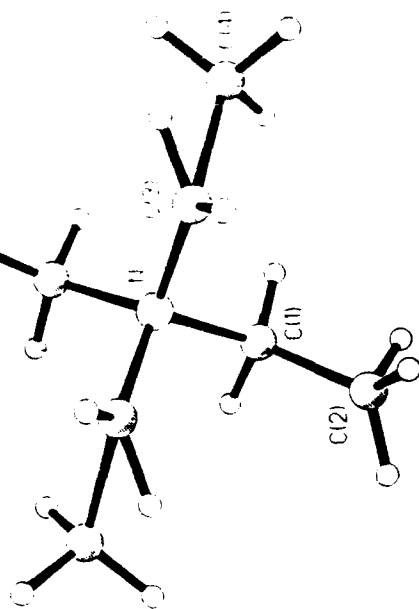


Figure 3: Representation of the Sb and N atoms environments in $\text{N}(\text{CH}_3\text{CH}_2)_4^+\text{Sb}(\text{OTeF}_5)_6^-$; the size of the atoms is arbitrary.



information is available in the literature regarding Bi-O bond distances, and to our knowledge, the $\text{Bi}(\text{OTeF}_5)_6^-$ anion is the first compound where a Bi(V)-O bond length has been determined. Only very few examples of Bi(III)-O bonds are known. In fact, many of the known Bi(III) compounds have Bi---O contacts which are greater than the sum of the van der Waals radii. The compound $\text{Bi}_6\text{O}_4(\text{HO})_4(\text{ClO}_4)_6 \cdot 7\text{H}_2\text{O}$ with a mean Bi(III)-O bond length of 2.15(3) Å, is the only example available.³

$\text{N}(\text{CH}_3)_4^+ \text{As}(\text{OTeF}_5)_6^-$ (2) and $\text{N}(\text{CH}_3\text{CH}_2)_4^+ \text{Sb}(\text{OTeF}_5)_6^-$ (3). The crystal structures of the title compounds consist of well separated anions and cations. The central arsenic atom lies on the rotary inversion center and the molecule has $\bar{3}$ symmetry imposed on it by the lattice. For the antimony compound, the required crystallographic symmetry of the anion is 2/m with the central antimony atom on the inversion center, but the actual symmetry is almost $\bar{3}$ as in the bismuth compound. The cations have the expected bond lengths and angles (Table I). The central arsenic and antimony atoms are bonded octahedrally to the six oxygen atoms of the OTeF_5 groups, which are almost octahedral (Table I). The average bond distances are Sb-O = 1.89(2) Å (range 1.87(2) - 1.91(2) Å), Te-O = 1.73(2) Å (range 1.71(2) - 1.75(2) Å), Te-F = 1.73(3) Å (Te-F_{ax} = 1.75(2) Å and Te-F_{eq} = 1.72(2) Å) with no correction for thermal motion and the Sb-O-Te angle is 162.2(1.3)° (range 160(1) - 166(1)°). As previously observed in the case of the $\text{U}(\text{OTeF}_5)_6$ molecule,⁴ the fluorine atoms, but also the oxygen atoms have exceptionally large thermal parameters showing the fluorotellurate groups are undergoing angular motions of large amplitudes. Consequently, the Te-O and Te-F distances are significantly affected by this thermal motion (see below for the values obtained after corrections for libration). However, the Sb-O distances are less affected by this thermal motion, and indeed, the 1.89(2) Å value found can be compared with the Sb(V)-O distances of 1.92 Å in $\text{Cs}_3\text{Sb}_3\text{F}_{12}\text{O}_3$,⁵ and 1.91 Å in $\text{Rb}_2(\text{Sb}_2\text{F}_{10}\text{O})$,⁶ where the Sb atoms are also octahedrally coordinated by O atoms.

For the arsenic compound, there are two crystallographically independent anions and interestingly, the amplitudes of the oxygen and fluorine atom parameters are quite different. For the anion which exhibits smaller thermal parameters, the average bond distances are As(2)-O(2) = 1.80(1) Å, Te(2)-O(2) = 1.858(7) Å, Te(2)-F = 1.81(1) Å (Te-F_{ax} = 1.84(1) Å and Te-F_{eq} = 1.80(1) Å) and the As(2)-O(2)-Te(2) angle is 139.7(6)° with no correction for thermal motion. In the second anion, all the bond lengths are shorter [As(1)-O(1) = 1.74(4) Å, Te(1)-O(1) = 1.80(4) Å, Te(1)-F = 1.78(2) Å (Te-F_{ax} = 1.81(2) Å and Te-F_{eq} = 1.78(2) Å) and the angle As(1)-

O(1)-Te(1) is larger (151(2)°)]. The values obtained after correction for libration are discussed below. The As-O bond lengths are comparable to normal As(V)-O bond lengths found in $M_2(As_2F_{10}O).H_2O$ (M = Rb: As-O = 1.75 Å; M = K: As-O = 1.74 Å),⁷ and $M_2(As_2F_8O_2)$ (M = K: As-O = 1.816 Å; M = Rb: As-O = 1.811 Å; M = Cs: As-O = 1.790 Å),⁸ in which As is hexacoordinated.

A standard rigid-body librational analysis was performed for all compounds. The corrections were expected to be largest for the light atoms, but as a check, a calculation was also carried out for the heavy atoms. Only minor corrections were obtained for the M-O distances, the order of magnitude being about one estimated standard deviation.

As expected, for the bismuth anion and one of the arsenic anions, the corrections are not significant (Table I). For the second arsenic anion and the antimony anion, the Te-O and Te-F distances are significantly affected by thermal motion and, as expected, the librationaly corrected Te-O and Te-F bond distances are longer than the uncorrected distances (Table I) and are consistent with other known values.^{1,2}

In all structures, the Te-O distances [1.849(5), 1.858(7), 1.73(2)] are slightly longer than the Te-F distances [1.820(7), 1.81(1), 1.73(x)], but the difference lies in the range of the standard deviations and is not significant. The $OTeF_5^-$ anion is the only compound where the Te-O bond [1.803 Å] has been found significantly smaller than the Te-F bond [1.871 Å].⁹ As already observed in many other structures containing the $OTeF_5$ moiety, the $Te-F_{eq}$ and $Te-F_{ax}$ bond lengths are very similar. However, this seems to be true not only in the solid state, but also in solution where the resonances associated with the F_{eq} and F_{ax} environments in the ^{19}F NMR spectra are generally very strongly coupled and exhibit severe second order effects.

One of the most interesting aspects of these three related anions is concerned with the variations of the M-O bond lengths and the M-O-Te angles. As expected, the M-O bond values increase in the order As-O < Sb-O < Bi-O [1.814 Å < 1.929 Å < 2.065 Å], and are in good agreement with the sum of the ionic radii [$As^{5+} \approx 0.47$ Å, $Sb^{5+} \approx 0.62$ Å, $Bi^{5+} \approx 0.74$ Å, $O^{2-} = 1.40$ Å].¹⁰ However, and contrary to what had been speculated by Seppelt and co-workers,¹¹ there is no simple trend in the variation of the M-O-Te angle and, in fact, the Sb-O-Te angle is the larger angle : Bi-O-Te < As-O-Te < Sb-O-Te.

In the bismuth compound, the closest anion-cation distance occurs between F7 and C2A [2.77(3) Å] and F14 and C4A [2.75(2) Å] whereas the remaining closest F---C distances occur

at 3.228 (F4---C1), 3.134 (F10---C3) and 3.229 Å (F5---C1). The sum of the van der Waals radii of CH₃ (2.00 Å)¹⁰ and F (1.35¹⁰ - 1.40¹² Å) is 3.35 - 3.40 Å. The F7---C2A and F14---C4A distances consequently suggest a significant degree of hydrogen bonding between the C2A and C4A methyl groups and F7 and F14 atoms.

In the arsenic and antimony compounds, the closest anion-cation distances occurs between F4 and C1 [3.243 Å] and F7 and C4 [3.295 Å], respectively, which are at the limit of the van der Waals distance [3.35 - 3.40 Å].

EXPERIMENTAL

Syntheses of N(CH₃)₄⁺Bi(OTeF₅)₆⁻ (1), N(CH₃)₄⁺As(OTeF₅)₆⁻ (2) and N(CH₃CH₂)₄⁺Sb(OTeF₅)₆⁻ (3) and Crystal Growing. Compound (1). In the dry box, Bi(OTeF₅)₅ (0.4776 g, 0.3407 mmol) and N(CH₃)₄⁺OTeF₅⁻ (0.1078 g, 0.3447 mmol) were loaded into separate limbs of a two-limb vessel equipped with J. Young stopcocks. The vessel was attached to a glass vacuum line and SO₂ClF solvent (ca. 5 mL) distilled *in vacuo* on to the Bi(OTeF₅)₅ at -78 °C. The mixture was allowed to warm to 0 °C and the resulting solution poured on to the N(CH₃)₄⁺OTeF₅⁻ in the other limb. The reaction mixture was left stirring at room temperature overnight. A very pale yellow solution containing a small amount of white insoluble material resulted. The solution was warmed to 35 °C, however the white material remained insoluble. The pale yellow supernatant solution was decanted into the other limb of the vessel. An equal volume of Freon 114 was distilled into the limb containing the white solid. The Freon 114 vapor was allowed to diffuse into the SO₂ClF solution over a period of 48 hours. This resulted in the formation of clusters of large, pale yellow crystals or prisms of N(CH₃)₄⁺Bi(OTeF₅)₆⁻ (0.3283g, 53.8%). The vessel was then transferred to a dry box equipped with a microscope. The crystals were sealed in 0.3-0.4 mm Lindemann glass capillaries and stored at room temperature prior to mounting on the diffractometer. A preliminary observation of the sealed crystals under a polarizing microscope revealed that most of them were single crystals.

Compound (2). The As(OTeF₅)₅ (0.9050 g, 0.7138 mmol) and N(CH₃)₄⁺OTeF₅⁻ (0.2238 g, 0.7158 mmol) were loaded into separate limbs of a two-limb Pyrex vessel equipped with J. Young stopcocks in the dry box. The vessel was attached to a glass vacuum line and SO₂ClF (ca. 4 mL) distilled on to the As(OTeF₅)₅ at -78 °C. On warming to room temperature, the

$\text{As}(\text{OTeF}_5)_3$ dissolved in the SO_2ClF and the resulting solution was then poured on to the $\text{N}(\text{CH}_3)_4^+\text{OTeF}_5^-$. The other limb was rinsed three times with SO_2ClF in order to ensure that all the $\text{As}(\text{OTeF}_5)_3$ had transferred. The $\text{N}(\text{CH}_3)_4^+\text{OTeF}_5^-$ rapidly dissolved giving a clear colorless solution. Freon 114 was distilled *in vacuo* into the empty limb of the vessel while keeping the stopcock between the two limbs closed. When the Freon 114 had warmed to room temperature, the interconnecting stopcock was opened, allowing the Freon 114 vapor to diffuse into the SO_2ClF solution. Clusters of large colorless plate-like crystals as well as isolated cubic prisms formed over a period of 24 hours. The supernatant liquid comprised two layers which were decanted away from the crystals. The latter were rinsed with Freon 114 and pumped dry in dynamic vacuum (0.6760 g, 60%) before being transferred in a dry box. Some of the crystals were cut with a scalpel and mounted in 0.3, 0.4 and 0.5 mm Lindemann glass capillaries and stored at room temperature prior to mounting on the diffractometer since they proved to undergo a phase transition when kept at -65°C . The crystal used in this study was a thick plate with dimensions $0.2 \times 0.5 \times 0.55$ mm.

Compound (3). Freshly sublimed $\text{Sb}(\text{OTeF}_5)_3$ (2.0974 g, 2.5043 mmol) was loaded into one limb of a two-limbed vessel equipped with J. Young stopcocks. The $\text{N}(\text{CH}_2\text{CH}_3)_4^+\text{OTeF}_5^-$ (0.9314 g, 2.5252 mmol) was added on top of the $\text{Sb}(\text{OTeF}_5)_3$. Into the empty limb of the vessel, $\text{Xe}(\text{OTeF}_5)_2$ (1.5553 g, 2.5561 mmol) was added. The vessel was removed from the dry box and attached to a glass vacuum line. Sulphuryl chloride fluoride (ca. 5 mL) was distilled *in vacuo* on to the $\text{Sb}(\text{OTeF}_5)_3/\text{N}(\text{CH}_2\text{CH}_3)_4^+\text{OTeF}_5^-$ mixture at -78°C . The solids dissolved on warming to room temperature giving a clear colorless solution of $\text{N}(\text{CH}_2\text{CH}_3)_4^+\text{Sb}(\text{OTeF}_5)_4^-$. The SO_2ClF was distilled off the $\text{N}(\text{CH}_2\text{CH}_3)_4^+\text{Sb}(\text{OTeF}_5)_4^-$ and condensed on to the $\text{Xe}(\text{OTeF}_5)_2$ at -78°C . The $\text{Xe}(\text{OTeF}_5)_2$ dissolved in the SO_2ClF ; this solution was poured through the side arm on to the $\text{N}(\text{CH}_2\text{CH}_3)_4^+\text{Sb}(\text{OTeF}_5)_4^-$ held at -78°C . On warming the mixture to 0°C , evolution of Xe gas was observed and a clear colorless solution resulted. The solution was allowed to warm to room temperature and the SO_2ClF slowly distilled off until a significant quantity of crystals had formed and did not redissolve on agitating the mixture. The solution was warmed in order to redissolve the crystalline material and then allowed to stand at room temperature for 48 hours. A crop of hexagonal plates was obtained, but they proved to be unsuitable for an X-ray crystallography study. Consequently, the mother liquor was decanted off and the crystals were redissolved in a small quantity of fresh SO_2ClF (ca. 1 mL). Freon 114 (ca. 1 mL) was carefully distilled on top

of the SO_2ClF solution at 0°C . The two-phase system was allowed to stand at room temperature for 48 hours resulting in the formation of large, colorless plate-like crystals of $\text{N}(\text{CH}_2\text{CH}_3)_4^+\text{Sb}(\text{OTeF}_5)_6^-$; some of them presenting triangular edges. The solvents were drained away from the crystals which were then pumped dry in dynamic vacuum. The crystals were finally rinsed with a small amount of Freon 114 and dried in dynamic vacuum before being transferred in a dry box where they were mounted and sealed in 0.4 - 0.5 mm Lindemann glass capillaries. The crystals were kept at room temperature prior to mounting on the diffractometer since they appeared to undergo a phase transition when kept in solid dry ice. The crystals, observed under a polarizing microscope, appeared to be single or perfectly twined. The crystal used in this study was triangular with dimensions 1.2 x 0.9 x 0.45 mm.

Crystal Structure Determination of $\text{N}(\text{CH}_3)_4^+\text{Bi}(\text{OTeF}_5)_6^-$ (1), $\text{N}(\text{CH}_3)_4^+\text{As}(\text{OTeF}_5)_6^-$ (2) and $\text{N}(\text{CH}_3\text{CH}_2)_4^+\text{Sb}(\text{OTeF}_5)_6^-$ (3)

Collection and Reduction of X-Ray Data. All the crystals were centered on a Syntex P2₁ diffractometer, using silver radiation monochromatized with a graphite crystal ($\lambda = 0.56086 \text{ \AA}$). During data collection the intensities of three standard reflections were monitored every 97 reflections to check for crystal stability and alignment. The experimental values for the antimony compound (3), when they differ from those of the bismuth one (1), are given in square brackets. Accurate cell dimensions were determined at -62°C [24°C] from a least-squares refinement of the setting angles (χ , ϕ and 2θ) obtained from 25 [18] accurately centered reflections (with 21.09° [12.44°] $\leq 2\theta \leq 35.23^\circ$ [29.06°]) chosen from a variety of points in reciprocal space. The examination of the peak profiles revealed single peaks. Integrated diffraction intensities were collected using a $\theta - 2\theta$ scan technique with scan rates varying from 1.5 to $14.65^\circ/\text{min}$ (in 2θ) so that the weaker reflections were examined most slowly to minimize counting errors. The data were collected with $0 [0] \leq h \leq 13 [12]$, $-13 [0] \leq k \leq 13 [20]$ and $-14 [-22] \leq l \leq 14 [22]$ and with $3^\circ [3^\circ] \leq 2\theta \leq 45^\circ [35^\circ]$. For compound (1), the intensities of the standards changed regularly to about 89% of their original values during the course of the data collection; this decomposition was later corrected by scaling the data linearly between each set of standards. Only a 4.7% decay was observed for compound (3). A total of 4643 [5837]¹³ reflections were collected out of which 144 [180] were standard reflections. 4217 [2536] unique reflections

remained after averaging of equivalent reflections. A total of 3610 [1660], satisfying the condition $I \geq 2.5 \sigma(I)$, were used for structure solution.

For the arsenic compound (2), accurate cell dimensions were determined at 24 °C from a least-squares refinement of the setting angles (χ , ϕ and 2θ) obtained from 22 accurately centered reflections (with $14.54^\circ \leq 2\theta \leq 29.36^\circ$) chosen from a variety of points in reciprocal space. Integrated diffraction intensities were collected using an ω scan technique with scan rates varying from 1.5 to 14.65 °/min (in 2θ). Data were collected in three steps, and only the reflexions ($-h+k+l=3n$) were collected since the system was known to be rhombohedral R. In the first step, the data were collected with $0 \leq h \leq 13$, $0 \leq k \leq 13$ and $0 \leq l \leq 68$ and with $3^\circ \leq 2\theta \leq 40^\circ$. When the system was confirmed to be trigonal, second and third set (in brackets) of data were collected with $0 [0] \leq h \leq 13 [13]$, $-13 [-13] \leq k \leq 13 [0]$ and $-68 [0] \leq l \leq 0 [68]$. A decay of 7% was observed for compound (2). A total of 7149 reflexions were collected out of which 225 were standard reflections. 2107 unique reflections remained after averaging of equivalent reflections. A total of 1328 reflections, satisfying the condition $I \geq 2 \sigma(I)$ were used for structure solution.

For all three compounds, corrections were made for Lorentz and polarization effects. Absorption corrections were applied by using the program DIFABS.¹⁴

Crystal Data. Compound (1) ($f_w = 1714.73 \text{ g mol}^{-1}$), crystallizes in the triclinic system, space group $P\bar{1}$; $a = 8.945(2) \text{ \AA}$, $b = 9.217(2) \text{ \AA}$, $c = 10.029(2) \text{ \AA}$, $\alpha = 100.03(3)^\circ$, $\beta = 99.95(3)^\circ$, $\gamma = 98.06(3)^\circ$; $V = 789.5 \text{ \AA}^3$; $D_{\text{calc}} = 3.606 \text{ g cm}^{-3}$ for $Z = 1$. $\text{Ag}(K\alpha)$ radiation ($\lambda = 0.56086 \text{ \AA}$, $\mu(\text{Ag}K\alpha) = 60.4 \text{ cm}^{-1}$) was used. Compound (2) ($f_w = 1580.67 \text{ g mol}^{-1}$), crystallizes in the trigonal system, space group $R\bar{3}$; $a = 10.109(2) \text{ \AA}$, $c = 55.443(18) \text{ \AA}$; $V = 4907.0 \text{ \AA}^3$; $D_{\text{calc}} = 3.209 \text{ g cm}^{-3}$ for $Z = 6$. $\text{Ag}(K\alpha)$ radiation ($\lambda = 0.56086 \text{ \AA}$, $\mu(\text{Ag}K\alpha) = 34.2 \text{ cm}^{-1}$) was used. Compound (3) ($f_w = 1683.6 \text{ g mol}^{-1}$), crystallizes in the monoclinic system, space group $C2/c$; $a = 10.506(3) \text{ \AA}$, $b = 18.370(6) \text{ \AA}$, $c = 20.352(7) \text{ \AA}$, $\beta = 91.23(2)^\circ$; $V = 3926.9 \text{ \AA}^3$; $D_{\text{calc}} = 2.848 \text{ g cm}^{-3}$ for $Z = 4$. $\text{Ag}(K\alpha)$ radiation ($\lambda = 0.56086 \text{ \AA}$, $\mu(\text{Ag}K\alpha) = 27.7 \text{ cm}^{-1}$) was used.

Solution and Refinement of the Structures. Compound (1). The program XPREP¹⁵ was used for determining the correct cell and space group and confirmed that the lattice was triclinic primitive ($R\text{-int} = 0.018$). The structure was shown to be centrosymmetric by an examination of

the E-statistics (calc., 0.875, theor., 0.968), and consequently the structure was solved in the space group $P\bar{1}$. A first solution was obtained without absorption corrections and it was achieved by direct methods which located the positions of the bismuth and tellurium atoms on special ($d\bar{1}$) and general positions, respectively. The full matrix least-squares refinement of the bismuth and tellurium atom positions and isotropic thermal parameters gave a conventional agreement index R ($=\sum|F_o| - |F_c|/\sum|F_o|$) of 0.165. A difference Fourier synthesis revealed the remaining oxygen and fluorine atoms of the anion (both on general positions), as well as the nitrogen and carbon atoms of the cation on special ($g\bar{1}$) and general positions, respectively. The presence of the carbon atoms on general positions implied a positional disorder of the cation and consequently the site occupancy factors (s.o.f.) of the carbon atoms were set equal to 0.5 instead of 1.00. Refinement of positional and isotropic temperature parameters for all atoms converged at $R = 0.109$. A significant improvement of the structure was achieved by introducing anisotropic positions for the hydrogen atoms ($d(C-H) = 0.96 \text{ \AA}$, $U(H)$ fixed to 0.08, s.o.f. fixed to 0.5), reducing R to 0.046. The structure was solved a second time using data that had been corrected empirically for absorption. The initial model used the atomic coordinates and isotropic thermal parameters defined previously for the Bi, Te, O, F, N, C and H atoms. The solution obtained ($R = 0.094$) indicated a small improvement over that obtained without absorption corrections ($R = 0.109$). The final refinement was obtained by introducing a weight factor ($w = 1/\sigma^2(F) + 0.002266\sigma F^2$) and an isotropic correction for secondary extinction, and gave rise to a residual, R , of 0.0456 ($R_w = 0.0516$). In the final difference map, the maximum and the minimum electron densities were 3.52 and -2.22 e\AA^{-3} .

Compound (2). The program XPREP¹⁵ was used for determining the correct cell and space group and confirmed that the lattice was trigonal ($R\text{-int} = 0.059$). The two space groups, which were consistent with the systematic absences, were the centrosymmetric $R\bar{3}$ and the chiral $R3$ space groups. The structure was shown to be centrosymmetric by an examination of the E-statistics (calc., 0.993, theor., 0.968), and consequently the structure was solved in the space group $R\bar{3}$. A first solution was obtained without absorption corrections and it was achieved by using the Patterson function which located the arsenic and nitrogen atoms on special, $a\bar{3}$ (As1) and $b\bar{3}$ (As2) and $c3$ (N), respectively, and the tellurium atoms on general positions. The full matrix least-squares refinement of the arsenic, tellurium and nitrogen atom positions and isotropic thermal parameters gave a conventional agreement index R of 0.228. Successive difference

Fourier syntheses revealed the positions of one carbon atom and all the remaining oxygen and fluorine atoms on general positions as well as that of the other carbon atom on the special position (c3). Refinement of positional and isotropic temperature parameters for all atoms (the calculated positions for the hydrogen atoms with $d(\text{C-H}) = 0.96 \text{ \AA}$, $U(\text{H})$ fixed to 0.08 were also introduced) converged at $R = 0.135$, and revealed somewhat large thermal parameters for the oxygen and fluorine atoms associated with one of the anions. The structure was considerably improved by introducing anisotropic thermal parameters for the As, Te, O and N atoms, giving a residual R of 0.0768. The structure was solved a second time using data that had been corrected empirically for absorption. The initial model used the atomic coordinates and isotropic thermal parameters defined previously for the Sb, Te, O, F, N, C and H atoms. The final refinement was obtained by introducing a weight factor ($w = 1/\sigma^2(F) + 0.000689F^2$) and gave rise to a residual, R , of 0.0559 ($R_w = 0.0605$). In the final difference map, the maximum and the minimum electron densities were 1.28 and -1.02 e\AA^{-3} .

Compound (3). The program XPREP¹⁵ was used for determining the correct cell and space group and confirmed that the lattice was monoclinic C ($R_{\text{int}} = 0.022$). The two space groups, which were consistent with the systematic absences, were the centrosymmetric $C2/c$ and the non-centrosymmetric Cc space groups. The structure was shown to be centrosymmetric by an examination of the E -statistics (calc., 0.907, theor., 0.968), and consequently the structure was solved in the space group $C2/c$. A first solution was obtained without absorption corrections and it was achieved by direct methods which located the positions of the antimony and tellurium atoms on special ($a\bar{1}$) and general positions, respectively. The full matrix least-squares refinement of the antimony and tellurium atom positions and isotropic thermal parameters gave a conventional agreement index R of 0.215. Successive difference Fourier syntheses revealed the positions of all the remaining oxygen, fluorine and carbon atoms on general positions as well as that of the nitrogen atom on the special position ($e2$). Refinement of positional and isotropic temperature parameters for all atoms converged at $R = 0.162$. Introduction of anisotropic thermal parameters for all the atoms markedly improved the crystallographic residual, since the anisotropies of all the light atoms as well as tellurium atom were very large (Table xx), reducing R to 0.0528 (the calculated positions for the hydrogen atoms ($d(\text{C-H}) = 0.96 \text{ \AA}$, $U(\text{H})$ fixed to 0.10) were also included). The anisotropies of the carbon atoms were also high. The final refinement was obtained by introducing a weight factor ($w = 1/\sigma^2(F) + 0.000876F^2$) and gave rise

to a residual, R , of 0.055 ($R_w = 0.062$). In the final difference map, the maximum and the minimum electron densities were 0.95 and $-0.55 \text{ e}\text{\AA}^3$.

All calculations were performed on a 486 personal computer using the SHELXTL PLUSTM (Sheldrick, 1990)¹⁵ determination package for structure solution and refinement as well as structure determination molecular graphics.

REFERENCES

1. Lentz, D.; Pritzkow, H.; Seppelt, K. *Inorg. Chem.* 1978, 17, 1926.
2. Sawyer, J.F.; Schrobilgen, G.J. *Acta Crystallogr.* 1982, B38, 1561.
3. Sundvall, B. *Inorg. Chem.* 1983, 22, 1906.
4. Templeton, L.K.; Templeton, D.H.; Bartlett, N.; Seppelt, K. *Inorg. Chem.* 1976, 15, 2720.
5. Haase, von W. *Acta Crystallogr.* 1974, B30, 2465.
6. Haase, von W. *Acta Crystallogr.* 1974, B30, 2508.
7. Haase, von W. *Acta Crystallogr.* 1974, B30, 1722.
8. Haase, von W. *Chem. Ber.* 1974, 107, 1009.
9. Miller, P.K.; Abney, K.D.; Rappé, A.K.; Anderson, O.P.; Strauss, S.H. *Inorg. Chem.* 1988, 27, 2255.
10. Pauling, L. "The Nature of the Chemical Bond, 3rd ed.; Cornell University Press: Ithaca, NY, 1960; p260.
11. Turowsky, L.; Seppelt, K. *Z. Anorg. Allg. Chem.* 1990, 590, 23.
12. Bondi, A. J. *Phys. Chem.* 1964, 68, 441.
13. For compound (3), the strongest reflections at very low angles could not be recorded in normal conditions of data acquisition (i.e. maximum intensity, 1.5 kW Ag X-rays, without attenuation); the power had to be decreased to 900 kW, and another set of data was collected with $0 \leq h \leq 0$, $0 \leq k \leq 7$ and $-7 \leq l \leq 4$.
14. Walker, N.; Stuart, D. *Acta Crystallogr.* 1983, A39, 158.
15. Sheldrick, G.M. (1990); SHELXTL PLUS™ Release 4.21/V. Siemens Analytical X-Ray Instruments. Inc., Madison, Wisconsin.

Table I. Bond Lengths and Bond Angles in $\text{N}(\text{CH}_3)_4^+\text{Bi}(\text{OTeF}_5)_6^-$ (**1**), $\text{N}(\text{CH}_3)_4^+\text{As}(\text{OTeF}_5)_6^-$ (**2**) and $\text{N}(\text{CH}_3\text{CH}_2)_4^+\text{Sb}(\text{OTeF}_5)_6^-$ (**3**).

Bond Lengths (Å)					
	(1)	(*)		(2)	(*)
Bi-O(1)	2.052(6)	2.058	Sb-O(1)	1.91(2)	1.960
Bi-O(2)	2.054(6)	2.066	Sb-O(2)	1.87(2)	1.900
Bi-O(3)	2.064(5)	2.072	Sb-O(3)	1.89(2)	1.927
Te(1)-O(1)	1.848(5)	1.854	Te(1)-O(1)	1.72(2)	1.746
Te(2)-O(2)	1.860(6)	1.864	Te(2)-O(2)	1.75(2)	1.770
Te(3)-O(3)	1.846(6)	1.852	Te(3)-O(3)	1.71(2)	1.720
Te(1)-F(1)	1.815(6)	1.826	Te(1)-F(1)	1.70(3)	1.862
-F(2)	1.826(7)	1.840	-F(2)	1.75(2)	1.881
-F(3)	1.826(7)	1.838	-F(3)	1.70(2)	1.846
-F(4)	1.824(7)	1.838	-F(4)	1.79(3)	1.833
-F(5)	1.818(6)	1.824	-F(5)	1.68(3)	1.817
Te(2)-F(6)	1.815(7)	1.833	Te(2)-F(6)	1.77(3)	1.790
-F(7)	1.825(7)	1.844	-F(7)	1.61(2)	1.657
-F(8)	1.819(9)	1.837	-F(8)	1.79(2)	1.857
-F(9)	1.818(6)	1.836	-F(9)	1.77(2)	1.831
-F(10)	1.818(7)	1.822	-F(10)	1.79(2)	1.852

Table I. Continued

	(1)	(*)		(2)	(*)
Te(3)-F(11)	1.807(7)	1.821	Te(3)-F(11)	1.72(2)	1.837
-F(12)	1.819(5)	1.835	-F(12)	1.74(2)	1.872
-F(13)	1.814(7)	1.828	-F(13)	1.68(2)	1.802
-F(14)	1.824(6)	1.840	-F(14)	1.62(3)	1.734
-F(15)	1.830(8)	1.836	-F(15)	1.77(2)	1.795
Mean Te-F	1.820(7)	1.833	Mean Te-F	1.73(x)	1.818
N-C(1)	1.53(3)		N-C(1)	1.50(3)	
N-C(2)	1.46(2)		N-C(3)	1.45(2)	
N-C(3)	1.63(4)		C(1)-C(2)	1.38(4)	
N-C(4)	1.35(2)		C(3)-C(4)	1.58(3)	

Table I. Continued

	(3)	(*)		(3)	(*)
As(1)-O(1)	1.74(4)	1.739	As(2)-O(2)	1.80(1)	1.814
Te(1)-O(1)	1.80(4)	1.800	Te(2)-O(2)	1.858(7)	1.865
-F(1)	1.76(3)	1.791	-F(6)	1.82(1)	1.857
-F(2)	1.76(1)	1.805	-F(7)	1.80(1)	1.834
-F(3)	1.83(2)	1.870	-F(8)	1.81(2)	1.843
-F(4)	1.75(2)	1.794	-F(9)	1.78(1)	1.817
-F(5)	1.81(2)	1.814	-F(10)	1.84(1)	1.845
Mean Te-F	1.78(2)	1.815	Mean Te-F	1.81(1)	1.839
N(1)-C(1)	1.45(2)				
N(1)-C(2)	1.56(5)				

Table 1. Continued

Bond Angles (°) in (1)

Bi-O(1)-Te(1)	137.1(3)	Bi-O(2)-Te(2)	135.7(3)	Bi-O(3)-Te(3)	135.3(3)
O(1)-Bi-O(2)	89.4(2)	O(2)-Bi-O(3)	89.7(2)	O(1)-Bi-O(3)	90.0(2)
O(1)-Te(1)-F(1)	91.1(2)	O(2)-Te(2)-F(6)	94.6(3)	O(3)-Te(3)-F(11)	91.3(3)
-F(2)	93.8(3)	-F(7)	91.3(3)	-F(12)	95.1(3)
-F(3)	94.1(3)	-F(8)	89.8(3)	-F(13)	93.4(3)
-F(4)	92.0(3)	-F(9)	94.0(3)	-F(14)	89.0(3)
-F(5)	178.9(3)	-F(10)	177.6(3)	-F(15)	177.3(3)
F(5)-Te(1)-F(1)	88.0(3)	F(10)-Te(2)-F(6)	87.0(3)	F(15)-Te(3)-F(11)	88.0(3)
-F(2)	86.9(3)	-F(7)	86.9(4)	-F(12)	87.5(3)
-F(3)	86.8(3)	-F(8)	88.7(4)	-F(13)	87.3(3)
-F(4)	87.4(3)	-F(9)	87.7(3)	-F(14)	88.3(3)
F(1)-Te(1)-F(2)	90.6(3)	F(6)-Te(2)-F(7)	89.8(3)	F(11)-Te(3)-F(12)	90.9(3)
F(2)-Te(1)-F(3)	89.6(3)	F(7)-Te(2)-F(8)	90.4(4)	F(12)-Te(3)-F(13)	90.4(3)
F(3)-Te(1)-F(4)	91.5(3)	F(8)-Te(2)-F(9)	89.0(4)	F(13)-Te(3)-F(14)	89.2(3)
F(4)-Te(1)-F(1)	88.4(3)	F(9)-Te(2)-F(6)	90.4(3)	F(14)-Te(3)-F(11)	89.2(3)
C(1)-N-C(2)	105(2)	C(1)-N-C(3A)	105(2)	C(1)-N-C(1A)	114(1)
C(2)-N-C(3A)	104(1)	C(2)-N-C(4A)	118(1)	C(3A)-N-C(4A)	110(1)

Table I. Continued

Bond Angles (°) in (2)

As(1)-O(1)-Te(1)	151(2)	As(2)-O(2)-Te(2)	139.7(6)
O(1)-Te(1)-F(5)	171.2(9)	O(2)-Te(2)-F(10)	175.1(5)
-F(1)	91(1)	-F(6)	93.4(4)
-F(2)	102(1)	-F(6)	96.9(5)
-F(3)	97(1)	-F(6)	88.3(5)
-F(4)	86(1)	-F(6)	92.6(5)
F(5)-Te(1)-F(1)	89(1)	F(10)-Te(2)-F(6)	86.3(5)
-F(1)	86.6(7)	-F(6)	88.0(5)
-F(1)	84.1(9)	-F(6)	86.8(6)
-F(1)	85.2(9)	-F(6)	88.0(5)
F(1)-Te(1)-F(2)	89.4(9)	F(6)-Te(2)-F(7)	86.9(7)
-F(4)	93(1)	-F(8)	89.9(7)
F(3)-Te(1)-F(2)	87.4(8)	F(7)-Te(2)-F(9)	90.0(7)
-F(4)	90(1)	F(8)-Te(1)-F(9)	92.7(8)
C(1)-N(1)-C(2)	106(1)	C(1)-N(1)-C(1b)	113(1)
C(1)-N(1)-C(1a)	113(1)		

Table I. Continued

Bond Angles (°) in (3)					
Sb-O(1)-Te(1)	160.0(1.3)	Sb-O(1)-Te(1)	160.1(1.3)	Sb-O(1)-Te(1)	166.4(1.3)
O(1)-Sb-O(2)	88.4(9)	O(2)-Sb-O(3)	90.6(9)	O(1)-Sb-O(3)	88.1(9)
O(1)-Te(1)-F(1)	90.9(1.3)	O(2)-Te(2)-F(6)	93.3(1.0)	O(3)-Te(3)-F(11)	93.1(1.2)
-F(2)	96.1(1.0)	-F(7)	92.7(1.0)	-F(12)	89.0(1.2)
-F(3)	94.5(1.1)	-F(8)	92.5(9)	-F(13)	95.5(1.2)
-F(4)	86.2(1.3)	-F(9)	96.5(9)	-F(14)	91.8(1.3)
-F(5)	172.4(1.1)	-F(10)	177.9(1.0)	-F(15)	175.9(1.1)
F(5)-Te(1)-F(1)	83.3(1.6)	F(10)-Te(2)-F(6)	86.2(1.0)	F(15)-Te(3)-F(11)	90.8(1.2)
-F(2)	89.0(1.1)	-F(7)	89.4(1.0)	-F(12)	89.3(1.3)
-F(3)	91.7(1.4)	-F(8)	87.9(1.0)	-F(13)	86.2(1.2)
-F(4)	89.5(1.4)	-F(9)	81.5(9)	-F(14)	84.4(1.4)
F(1)-Te(1)-F(2)	90.5(1.5)	F(6)-Te(2)-F(7)	88.9(1.1)	F(11)-Te(3)-F(12)	90.3(1.5)
F(2)-Te(1)-F(3)	84.2(1.3)	F(7)-Te(2)-F(8)	94.3(1.1)	F(12)-Te(3)-F(14)	86.8(1.7)
F(3)-Te(1)-F(4)	88.6(1.7)	F(8)-Te(2)-F(9)	87.7(1.0)	F(14)-Te(3)-F(13)	91.8(1.6)
F(4)-Te(1)-F(1)	96.6(1.9)	F(9)-Te(2)-F(6)	88.2(1.0)	F(13)-Te(3)-F(11)	90.7(1.4)
C(1)-N-C(1A)	107.2(2.4)	C(1)-N-C(3)	109.8(1.4)	C(1)-N-C(3A)	112.8(1.4)
C(3)-N-C(3A)	104.6(2.0)				

(°) Distances after corrections for thermal motion by the riding model.

Table II. Summary of Crystal Data and Refinement Results for $N(CH_3)_4^+Bi(OTeF_5)_6^-$ (1), $N(CH_3)_4^+As(OTeF_5)_6^-$ (2) and $N(CH_3CH_2)_4^+Sb(OTeF_5)_6^-$ (3).

	(1)	(2)	(3)
chemical formula	$C_4H_{12}NO_6F_{30}Te_6Bi$	$C_4H_{12}NO_6F_{30}Te_6As$	$C_8H_{20}F_{30}NO_6Te_6Sb$
space group	$P\bar{1}$	$R\bar{3}$	$C2/c$
a (Å)	8.945(2)	10.109(2)	10.506(3)
b (Å)	9.217(2)	10.109(2)	18.370(6)
c (Å)	10.029(2)	55.443(17)	20.352(7)
α (°)	100.03(3)	90	90
β (°)	99.95(3)	90	91.23(2)
γ (°)	98.06(3)	120	90
V (Å ³)	789.5	4908	3926.9
molecules/unit cell	1	6	4
molecular wt (g mol ⁻¹)	1714.7	1580.7	1683.6
calcd density (g cm ⁻³)	3.606	3.209	2.848
T (°C)	-62	24	24
μ (cm ⁻¹)	60.4	34.2	27.7
λ (Å)	0.56086	0.56086	0.56086
final agreement factors	$R = 0.0456$ $R_w = 0.0516$	$R = 0.0586$ $R_w = 0.0647$	$R = 0.055$ $R_w = 0.0618$

PART X

^{18}F EXCHANGE STUDIES OF F_2 ACTIVATION BY
LEWIS ACIDS AND HYDROGEN FLUORIDE

Background of the Application of Fluorine-18 as a Radiotracer

Fluorine-18 has proven to be a powerful tool in inorganic chemistry and organic synthesis. Its application to the field of nuclear medicine through the use of Positron Emission Tomography (PET) has allowed image reconstruction to produce images of the brain with a typical spatial resolution of a few millimeters.

Inorganic applications include the determination of labilities of element-fluorine bonds and the identification of hypervalent reaction intermediates. The ^{18}F containing precursors used in exchange studies have included F_2 , NOF , HF , HF_2 .

Production and Decay of Fluorine-18

Until recently, ^{18}F has been produced in our linear (van de Graaff) accelerator at McMaster by means of the nuclear reaction $^{20}\text{Ne}(\text{d},\alpha)^{18}\text{F}$. This method produces pure $[\text{F}^{18}]\text{-F}_2$, which provides specific activities and a radiochemical yields that are dependent upon the energy of the deuteron beam and the target conditions. The $[\text{F}^{18}]\text{-F}_2$ produced within the target tends to adhere to the walls of the target and therefore must be extracted from the target with the use of F_2 carrier gas.

The method of ^{18}F production used in the present work uses a cyclotron and the nuclear reaction $^{18}\text{O}(\text{p},\text{n})^{18}\text{F}$. Within the cyclotron, H^+ ions are accelerated until they reach the desired energy. They then pass through a strip of carbon foil which strips off two electrons producing a proton beam which can be focused on the target.

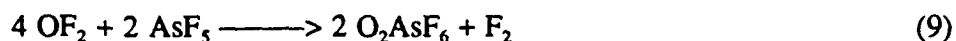
Fluorine has five isotopes, four of which are found to be radioactive. Fluorine-20 and 21 are both β -emitters with 11 and 5 second half-lives, respectively. Fluorine-17 is a positron emitter which decays to ^{17}O in 66 seconds. Fluorine-18 is also a positron emitter decaying to ^{18}O and having a half-life of 110 minutes. The emitted positron has an energy of 0.64 MeV and will

immediately annihilate with an electron to emit two 0.511 MeV gamma rays in almost opposite directions. It is believed that a certain amount of ^{17}F may be produced within the target and can usually be detected as a rapid drop in the initial activity.

Properties and Reactivity of OF_2

The high pressures and elevated temperatures present within the target during the irradiation produce oxygen radicals which can react with the fluorine atoms to produce oxygen fluorides. Several oxygen fluorides are known and their properties and structures are well characterized. The radicals $\text{OF}\cdot$ and $\text{O}_2\text{F}\cdot$ will generally react with fluorine atoms to produce the compounds OF_2 and O_2F_2 . The formation of the higher, unstable oxygen fluorides, such as O_3F_2 , requires an electrical discharge at low temperatures. These compounds, with the exception of OF_2 , readily decompose to O_2 and F_2 upon warming to ambient temperatures and therefore are not factors in the present work. Oxygendifluoride is found to be thermally stable at room temperature and therefore is suspected as a possible by-product in the formation of $^{18}\text{F}\text{-F}_2$. In the present work, fluorine exchange with Lewis acids has been studied, therefore the impurity $^{18}\text{F}\text{-OF}_2$ and reactivity of OF_2 with Lewis acid species must also be considered.

It has been shown that OF_2 decomposes at high temperatures to F atoms and $\text{OF}\cdot$ radicals and then to O_2 and F_2 , however, it is the radical species that most likely reacts with inorganic compounds. At 200 °C and 250 atm., OF_2 and AsF_5 react in a 1:1 ratio to form the dioxygenyl salt, $\text{O}_2^+\text{AsF}_6^-$

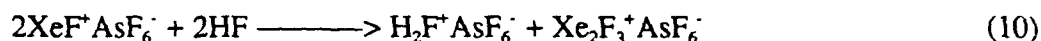


At ambient temperatures and pressures, however, a mixture of the two compounds is known to

be stable with only a trace of the dioxygenyl salt is formed.

Lewis Acid Assisted Oxidation of Xenon at Low Temperatures

One of the main goals of the present work has been to gain some insight into the work currently being done by Bartlett and coworkers at Berkeley and the activation of F_2 under low-temperature and ambient conditions. It has been found that fluorine is a more potent oxidizer of xenon in the presence of the Lewis acids AsF_5 and HF . This can be seen from the enthalpy changes $\Delta H^\circ (e^- + \frac{1}{2}F_2 + AsF_5 \longrightarrow AsF_6^-) = -723 \text{ kJ mol}^{-1}$, compared to $\Delta H^\circ (e^- + \frac{1}{2}F_2 \longrightarrow F^-) = -259 \text{ kJ mol}^{-1}$. A mixture of Xe , F_2 and liquid AsF_5 has been shown to react rapidly at -60°C to produce the salt $XeF^+AsF_6^-$ and, similarly, HF , F_2 and Xe react, although more slowly, in the dark to form XeF_2 . These reactions were only found to take place when the Lewis acids, HF and AsF_5 , were in the liquid phase, or when the reaction was carried out in WF_6 solvent. It was also found that AsF_5 , Xe and F_2 reacted in anhydrous HF to form $Xe_2F_3^+AsF_6^-$ and not $XeF^+AsF_6^-$, and is most likely the result of the solvolytic action of HF .



None of the mixtures were found to interact in the gas phase, even under pressures as high as 10 atm.

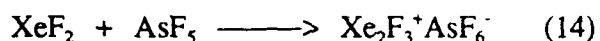
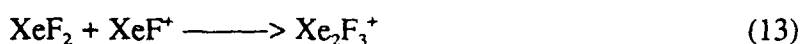
Xenon difluoride is routinely prepared by exposing a mixture of xenon and fluorine to ultraviolet light



and reacts with AsF_5 in BrF_3 or HF solvents to produce the salt $\text{XeF}^+\text{AsF}_6^-$



It has also been shown that the cation, Xe_2F_3^+ , can be formed by allowing XeF^+ to react with an additional mole of XeF_2 , i.e., a 2 : 1 molar ratio of the reactants $\text{XeF}_2 : \text{AsF}_5$



In the prior work of the group at Berkeley, ternary systems were studied. It would seem that the Lewis acids are in some way activating the F-F bond of F_2 fluorine, while at the same time, the xenon is acting as an electron donor, the result being a concerted interaction which breaks the F-F bond heterolytically.

Production of ^{18}F - F_2 and Activity Measurements

Fluorine-18 as ^{18}F - F_2 was produced using the nuclear reaction $^{18}\text{O}(p,n)^{18}\text{F}$ on the Siemens RDS 112 Cyclotron in the Nuclear Medicine Department at McMaster University which produces protons with an energy of 10 MeV. A thick target environment was used having target pressures between 550 and 600 psi during irradiation. With 10 MeV protons, 150 mCi of activity was produced per μA . The amount of activity actually extracted is dependent upon several factors including the amount of carrier gas and the length of a second irradiation in the presence of $^{19}\text{F}_2$ carrier, both of which can be varied to maximize the yield of carrier-added ^{18}F - F_2 .

Initially the F_2 target was pressurized to 250 psi with ^{18}O - O_2 gas (Isotech Inc., min.

99.99% chemical purity). The target was then irradiated at a specific beam current and for a predetermined length of time dependent on the quantity of activity desired. After the first irradiation, the target was pumped off, swept once with Ne and then repressurized to 140 psi with a 1% F₂ in Ne mixture. The target was further pressurized to 300 psi with 100% Ne and then irradiated for 10 minutes at 10 A (EOB₂). The recovery line was pumped and then the [¹⁸F]-F₂/Ne mixture condensed into a 40 mL 304 stainless steel Whitey cylinder at -196 °C. The number of moles of F₂ recovered from the target is calculated to be 0.074 mmol.

Activities were measured using a radioisotope calibrator Model CRC-12 manufactured by Capintec Inc. having a reported efficiency of 97%.

Preparation of [¹⁸F]-HF

Fluorine-18 labelled HF was prepared by condensing a Ne/[¹⁸F]-F₂ mixture into a 40.0 mL stainless steel cylinder containing H₂ (2.28 mmol) and anhydrous HF (1.14 mmol) at -196 °C. The mixture was allowed to react for 30 min. followed by pumping off the excess H₂ and Ne at -196 °C. Finally, the vessel was pumped at -94 °C to remove any OF₂ (vapor pressures; 1 Torr and 760 Torr at -196 °C and -144.5 °C). The activity was assayed before proceeding.

Preparation of [¹⁸F]-AsF₅

Fluorine-18 labelled AsF₅ was prepared by condensing a Ne/[¹⁸F]-F₂ mixture into a 40 mL stainless steel cylinder containing H₂ (2.40 mmol) and AsF₅ (1.10 mmol) at -196 °C. The vessel was warmed to -70 °C and allowed to react for 32 minutes after which the excess Ne and H₂ were pumped off at -196 °C. The vapor pressures of AsF₅ are 1 Torr at -117.9 °C and 760 Torr - 52.8 °C, making it possible to separate [¹⁸F]-OF₂ and [¹⁸F]-AsF₅ using standard vacuum techniques. The vessel was assayed and then warmed to -124 °C in a pentane slush bath in order

to pump off the $[^{18}\text{F}]\text{-OF}_2$ without loss of any of the $[^{18}\text{F}]\text{-AsF}_5$. In separate experiments, the above procedure was repeated, but the vessel was assayed to account for ^{18}F loss due to absorption on the walls of the steel cylinder, thus allowing a determination of the activity lost due to $[^{18}\text{F}]\text{-OF}_2$. The cylinder was warmed to -94°C in a methanol slush and connected to U-trap cooled to -196°C . The $[^{18}\text{F}]\text{-AsF}_5$ was slowly pumped into the U-trap under a dynamic vacuum and upon completion the U-trap and steel cylinder were assayed separately. Generally between 4 - 12% of the activity initially produced consisted of $[^{18}\text{F}]\text{-OF}_2$ impurity.

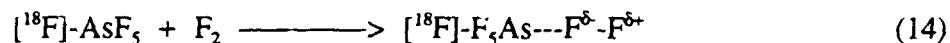
In order to confirm the presence of OF_2 in the cyclotron product, we will also run a ^{19}F NMR spectrum on the target gases in HF. The ^{19}F NMR shift for gaseous OF_2 is found at 248 ppm. The OF_2 molecule has been shown by microwave spectroscopy to be a symmetrical bent AX_2E_2 species with a 103° angle, therefore, the two fluorine environments are identical and thus give rise to a singlet in the ^{19}F spectrum. In addition, the F_2 singlet should be found at 422 ppm.

Mechanistic Evidence for $\text{F}_5\text{As} \rightleftharpoons \text{F-F}$

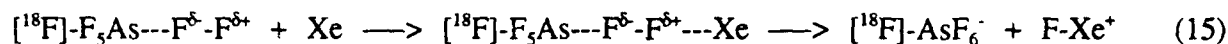
Considering the AsF_5/F_2 and HF/F_2 systems, the theoretical relative equilibrium distributions of activity would be 71.4% on the AsF_5 and 28.6% on the F_2 and, in the HF exchange, 66.6% would be on the F_2 and 33.3% on the HF. This assumes, however, that the exchange is fast and within the time constraints of the experiment, which are, in turn, determined by the 110 min half-life of ^{18}F .

To date, we have determined that $\text{F}_2/\text{H}^{18}\text{F}$, $\text{F}_2/\text{H}^{18}\text{F}/\text{AsF}_5$, $\text{F}_2/\text{As}^{18}\text{F}_5$ and $\text{F}_2/\text{H}^{18}\text{F}/\text{Xe}$ mixtures do not undergo exchange with F_2 in the dark in an FEP vessel after 0.5 to 0.75 hrs when HF is present as a liquid phase and the pressure of "cold" F_2 is 4 atm. However, we have determined that Xe is rapidly fluorinated (significant activities were detected after 0.5 hr.) when an equimolar amount of AsF_5 was added to the mixture or when liquid F_2 /liquid As^{18}F_5 mixtures

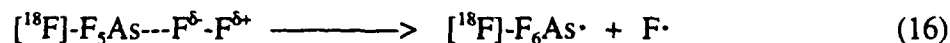
are used at -60 °C. Moreover, the salt, $\text{XeF}^+\text{AsF}_6^-$, was isolated from both systems and found to contain the radioactive label. Interestingly, ^{18}F was also not found in the unreacted F_2 of the reactions involving xenon. The latter fact provides the clearest evidence for the proposed F_2 activation mechanism (equations (14) and (15)). In a related experiment, we have shown that H^{18}F and AsF_5 undergo rapid fluorine exchange to produce $[\text{}^{18}\text{F}]\text{-AsF}_5$. Thus, in HF solutions of AsF_5 and in the preparation of $[\text{}^{18}\text{F}]\text{-AsF}_5$, AsF_5 clearly contains ^{18}F -label and forms a ^{18}F -labelled activated donor-acceptor complex with F_2 according to equation (14)

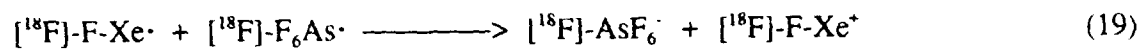
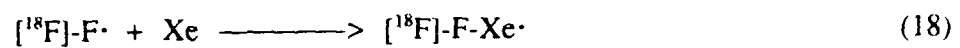
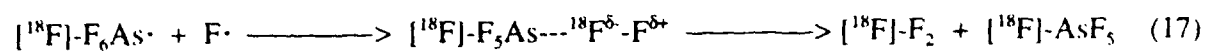


The activated complex is expected to be a strong electrophile. At the same time, xenon is expected to behave as a nucleophile towards the activated complex, leading to homolytic cleavage of the F-F bond



According to this mechanism, no cold/hot fluorine exchange can occur unless the activated complex actually reacts with xenon, that is to say, the unreacted complex simply dissociates according to the reverse of equation (14) resulting in no exchange of ^{18}F onto cold F_2 . The alternative mechanism would also involve a radical mechanism and homolytic cleavage of the F-F bond (equation 16), and would be expected to result in $^{18}\text{F}/^{19}\text{F}$ scrambling according to equations (17) - (19).





PART XI

GENERATION OF A MICROWAVE-EXCITED DISCHARGE IN A
LIQUID-NITROGEN COOLED DIELECTRIC TUBE

BACKGROUND

We have sought to develop new low-temperature synthetic methods which yield significant quantities of novel oxidant materials. Although methods such as matrix isolation and/or gas phase spectroscopic characterizations may indicate the existence of suitable novel species, these techniques generally do not produce isolable products that may be studied in an applied setting. Two such examples which are targeted by the present contract are ArF^+ and XeH^+ , both of which have been characterized in the gas phase but have not been isolated. Towards this end we have designed and built a microwave resonator which is capable of exciting a gas discharge in a dielectric enclosure that is immersed in liquid nitrogen.

Due to the corrosive gas mixtures employed, e.g., F_2 and OF_2 , DC excitation and other methods that require electrodes are completely unsuitable. The proposed technique uses high-power microwave (2.45-GHz) radiation, and accordingly does not require electrodes to be in contact with the discharge. The location of all reactive materials away from direct contact with the plasma helps alleviate problems such as gas clean-up and alternative chemistry resulting from electrode attack by the aggressive oxidants we are proposing to study. Lower frequency RF techniques share this advantage, but there are differences between these methods and microwave excitation.

Electronic wall collisions become less probable as the frequency of the applied field is increased. This can be seen by examining the excursion of a free electron in a sinusoidal electric field that has peak field E and frequency f . The excursion amplitude is

$$A = \frac{Ee}{m(2\pi f)^2} \quad (1)$$

where the electronic mass is $m = 9.1 \times 10^{-31}$ kg, and its charge is $e = 1.6 \times 10^{-19}$ C. The dielectric strength of dry air is 3 MV/m, which represents a useful upper limit for E. For $f = 2.45$ GHz, the maximum travel ($2A$) for a single electron is only 4.5 mm. Of course, under most circumstances the value of E will be orders of magnitude lower, and the value of A will be reduced still further by electronic collisions. For example, if E is now taken as 30 kV/m (which is easily attainable in a practical cavity), then the maximum travel is reduced to 45 μ m. Examination of equation (1) indicates that wall collisions are of sharply increasing importance as the frequency is decreased, and of little importance at microwave frequencies.

By creating a suitable discharge cavity, electric fields may be created that are large enough to excite a gas sample that is enclosed (in a dielectric envelope) within the cavity. The provision of liquid-nitrogen cooling for the discharge tube is possible because the loss tangent for liquid nitrogen is low enough at 2.45 GHz that microwave absorption is insignificant. A transmission line is used to couple the discharge cavity to the oscillator.

The problems of microwave leakage can be controlled by sensible design of the microwave components of the system. It is usually advisable to make all resonant and transmission structures closed so that there is no need for external EMI shielding. In particular, extensive use of waveguides operating below cutoff can allow visual and physical access to internal regions of the apparatus.

MICROWAVE GENERATION

The microwave radiation is generated by a 2M209A magnetron. A magnetron is

essentially a high-power vacuum-tube diode that is operated in forward bias. Because of this, the I-V curve has a very steep slope, and stable DC operation is difficult to achieve. Therefore, the magnetron is powered by a half-wave voltage doubler circuit, as is usually found in a microwave oven. In this method, the power is applied in a train of pulses at a rate of 60 Hz. A schematic diagram of the power supply is given in Figure 1.

As is the case with almost all high-power vacuum tubes, magnetron operation requires a hot cathode in order to allow electrons to be ejected easily via thermionic emission. For this purpose, a low-voltage (3-V) high-current (12-A) AC winding is provided on the core of the main transformer to heat the cathode filament. The main power supply uses the high voltage secondary winding that is on the same core. The high-voltage that is generated on that winding is AC coupled to the cathode of the magnetron. The diode is used to clamp the anode potential to ground. Note that the filament circuit is at high-voltage with respect to ground, and that the cathode heater cannot be powered independently of the main circuit.

With this configuration, the 2M209A magnetron is capable of delivering nearly 2-kW peak power in 8-ms pulses, with an average power in excess of 500 W. It is possible to use a variable transformer to adjust the line supply and modify the magnetron output. The fact that the filament power is taken from the main core is a complication. If there is insufficient power to the filament, the magnetron will not operate. However, once magnetron oscillation is initiated, secondary emission and electronic collisions with the cathode allow the microwave output to be reduced to a stable power level of approximately 50% before the filament cools intolerably and oscillation is terminated.

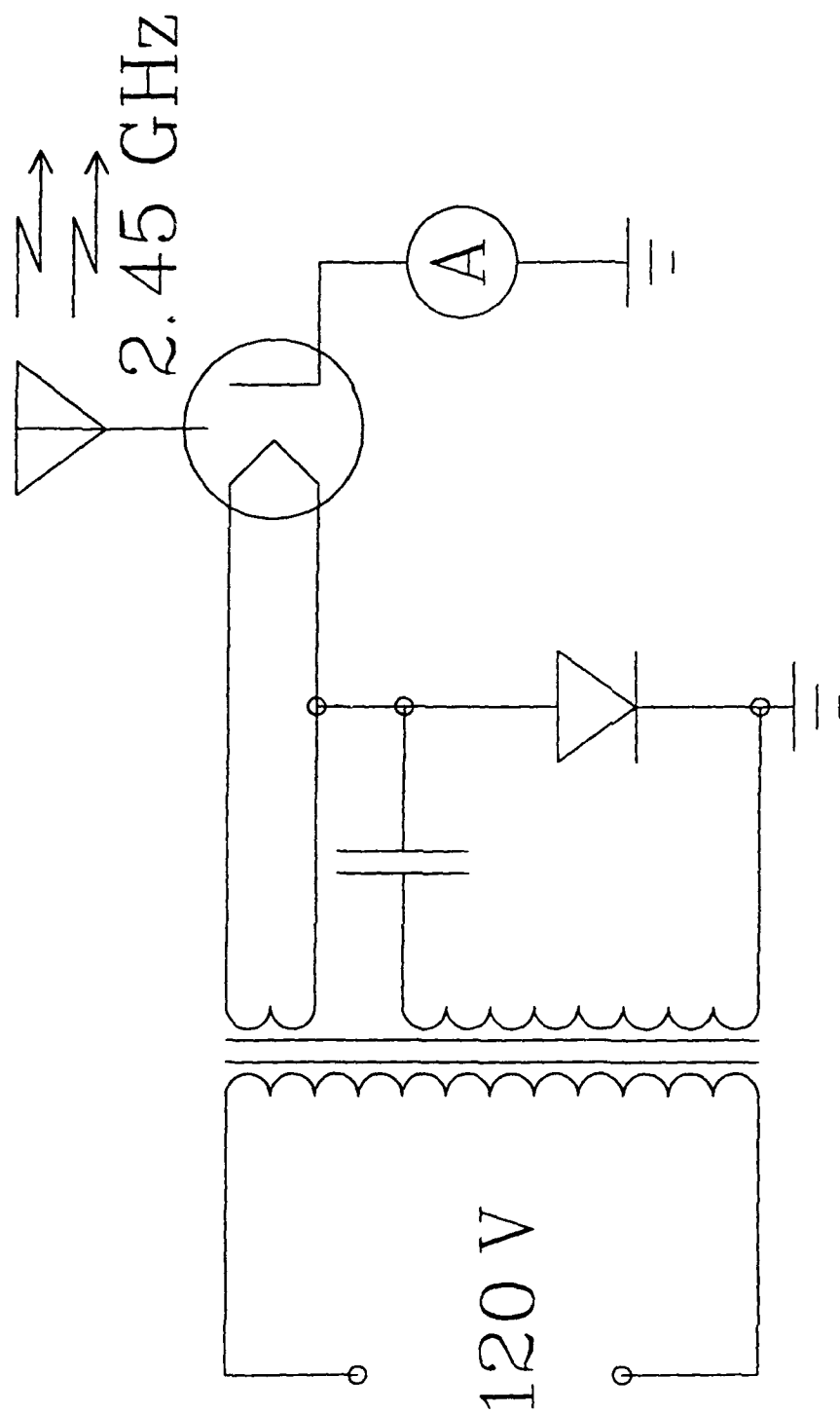


Figure 1. Half-wave voltage-doubler power-supply circuit used to drive the magnetron. Note that operation of the filament heater is tied to the main circuit.

EXCITATION CAVITY DESIGN AND OPERATION

A cross-section of the microwave structure is shown in Figure. 2. A co-axial transmission line is used to deliver the magnetron output to the discharge cavity, which is kept submerged in liquid nitrogen. The discharge is excited in a dielectric tube (not shown) positioned within this cavity. A small probe couples the discharge to the inner conductor of the transmission line. The outer conductor by itself is a waveguide below cutoff; it cannot support propagating waves. The same is true of the discharge cavity. Any microwave radiation that is launched into such a structure is exponentially attenuated. Quantitatively, the power attenuation for a length L is given (in decibels) by

$$\text{Total Power Attenuation} = 8.6864\pi \frac{L}{\lambda \lambda_{co}} \sqrt{\lambda^2 - \lambda_{co}^2} \text{ dB} \quad (2)$$

where λ is the free space microwave wavelength and λ_{co} is the cutoff wavelength, which only depends on the width and geometry of the conductor. As an example, a circular tube of 3-cm diameter and 8-cm length provides over 140 dB attenuation for 2.45-GHz radiation.

Positioning an inner conductor within the outer conductor creates a coaxial transmission line. The inner conductor is supported at each end by a "shorting" pin. This metal pin is electrically connected to both conductors and so forms a near short circuit (actually, the termination is slightly inductive). However, these short circuits are located a quarter of a wavelength from the magnetron antenna and the discharge antenna, and so they act as an open circuit at those junctions. The distance between the inner conductor and the magnetron antenna can be adjusted by loosening a set screw and sliding the inner conductor along the shorting pin.

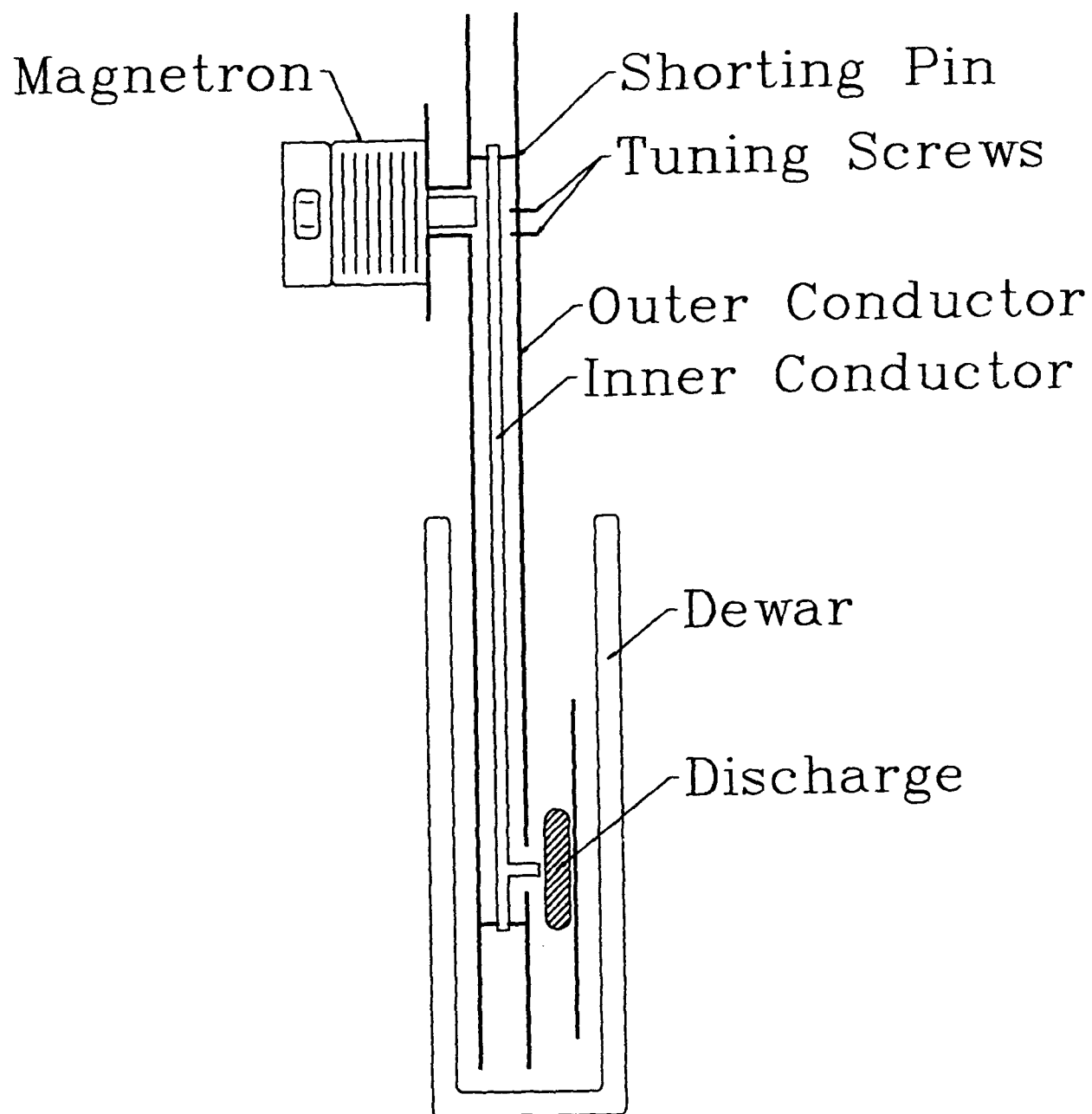


Figure 2. Cross-section of microwave apparatus. The heavy lines indicate the outer conductor and discharge cavity.

This adjustment varies the amount of capacitive coupling between the magnetron and the discharge. A similar adjustment can be made at the other end of the apparatus. Further tuning (in the form of variable shunting capacitances) is provided by the two screws indicated in Figure 2. Provided that dielectric tools are used, all of these adjustments can be safely made during full-power operation.

The electrical equivalent of this apparatus is shown in Figure 3. Note that the quarter-wave shorted stubs are omitted for the reasons given above. By making suitable tuning adjustment, microwave coupling efficiencies in excess of 80% should be possible. Similarly, it should be possible to generate low-power discharges by detuning the apparatus.

The mechanical design of the apparatus is extremely well suited to its purpose. The open-ended structure will allow a low-pressure path for the escape of gaseous nitrogen from the discharge cavity. In addition, ample visual access of all interior portions of the apparatus allows the rapid detection unwanted discharges and similar problems. Furthermore, the arrangement of the discharge cavity allows the use of different discharge-tube designs to be examined.

The method will be initially assessed by carrying out discharge experiments on gaseous fluorine and solid krypton mixtures in $\frac{1}{4}$ " and $\frac{1}{2}$ " o.d. sapphire tubes with the tube axis parallel to the conductors. These experiments will allow us to assess the viability of using this method to produce fluorine atoms at low temperature, which will be quantified by the KrF_2 yields in these experiments. If these preliminary experiments are successful, our efforts will be directed towards achieving the synthetic goals using microwave discharges outlined in our proposal.

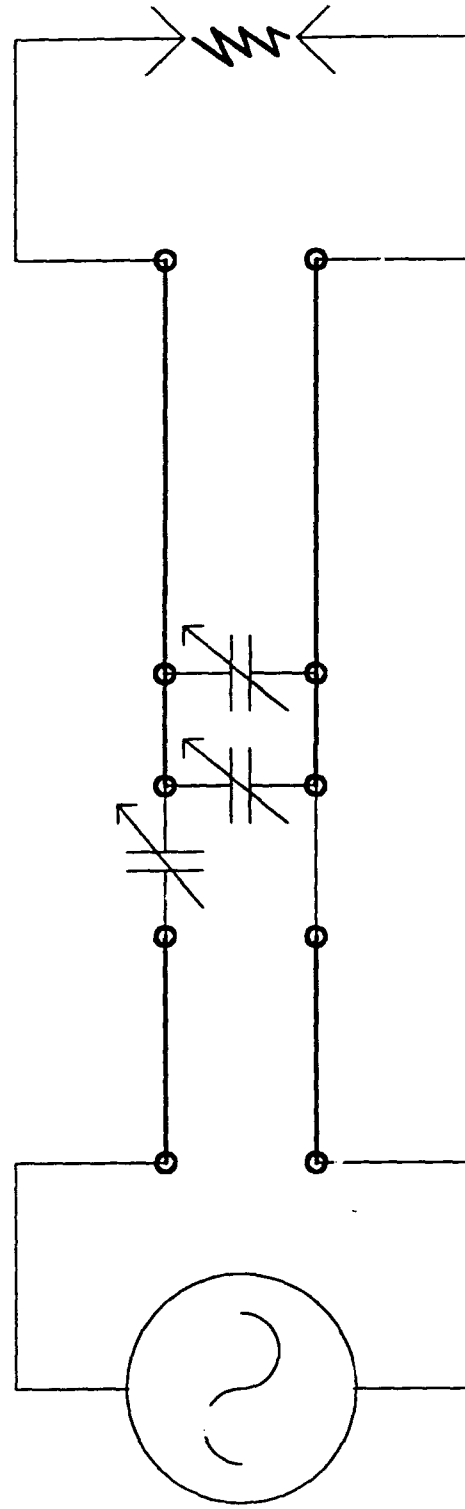


Figure 3. Equivalent electrical circuit of the microwave apparatus. The quarter-wave shorted stubs are omitted from this schematic because they have no electrical effect.